

***Novel Inhibitors of Phosphate-Binding Enzymes as Potential
Human Therapeutics***

Cyrus M. Lacbay

Department of Chemistry, McGill University

Montreal, QC, Canada

October 2016

*A thesis submitted to McGill University in partial fulfillment of the requirements
of the degree of Doctor of Philosophy*

© Cyrus M. Lacbay, 2016

*To my family,
Without whom none of my success would be possible*

Abstract

Studies on the discovery and development of small-molecule enzyme inhibitors are continuously growing due to their application as drugs for essentially every type of human disease, including cancer, metabolic, cardiovascular, neurodegenerative, and infectious diseases. However, the design of high affinity and membrane permeable inhibitors for phosphate- or pyrophosphate-binding enzymes with highly charged and metal-dependent active site pockets, such as the HIV-1 reverse transcriptase (HIV-1 RT) and the human geranylgeranyl pyrophosphate synthase (hGGPPS), poses a significant challenge in medicinal chemistry. In the past, the problems associated with this class of biological targets have been overcome with the development of effective phosphate or pyrophosphate bioisosteres and prodrugs or through the discovery of allosteric inhibitors.

Guided by several successful incorporations of phosphate and pyrophosphate mimics, our studies were dedicated to the following: (1) identification and development of *bona fide* active site inhibitors of HIV-1 RT with a mechanism of action that is uniquely different from the currently known anti-HIV/AIDS drugs, and (2) discovery of potent and selective inhibitors of hGGPPS that can be used as molecular probes to investigate the role of hGGPPS in human diseases. The design, synthesis, and preliminary biological profiling of these novel compounds will be discussed.

Résumé

Les études portant sur la découverte et le développement de petites molécules jouant le rôle d'inhibiteurs enzymatiques ne cessent de s'accroître en raison de leurs applications en tant que médicaments pour un large spectre de maladies humaines telles que le cancer ou encore les maladies métaboliques, cardiovasculaires, neurodégénératives et infectieuses. Cependant, la conception d'inhibiteurs enzymatiques perméables aux membranes cellulaires ayant une grande affinité pour le site actif, qui lui-même est dépendant d'un métal hautement chargé qui est normalement lié à des substrats comportant des groupements phosphates et pyrophosphates, représente un défi très important en chimie médicinale. Nous nous sommes particulièrement intéressés aux inhibiteurs de la transcriptase inverse du VIH-1 (VIH-1 RT) et à la géranylgeranyl pyrophosphate synthétase humaine (GGPPSh). Dans le passé, les problèmes associés à cette classe de cibles biologiques ont pu être surmontés soit avec le développement de bioisostères de type phosphate ou pyrophosphate, de promédicaments efficaces ou par la découverte d'inhibiteurs allostériques.

Guidés par plusieurs implémentations à nos inhibiteurs de groupements imitant les groupes fonctionnels phosphates et pyrophosphates, nos études ont été consacrées à: (1) l'identification et le développement d'inhibiteurs du site actif du VIH-1 RT *bona fide* avec un mécanisme d'action unique en comparaison aux médicaments actuels prescrits pour le traitement VIH/SIDA; et, (2) la découverte d'inhibiteurs puissants et sélectifs de GGPPSh qui peuvent être utilisés comme sondes moléculaires pour étudier les différents rôles de l'enzyme GGPPSh dans le traitement des maladies humaines. La conception ainsi que la synthèse et le profilage biologique préliminaire de ces nouveaux composés seront discutés dans ce manuscrit de thèse de doctorat.

Preface

Parts of the material included in the following thesis is adapted from published papers and is under copyright.

Material in Chapter 2 is adapted from:

Lacbay, C.M.; Mancuso, J.; Lin, Y.-S.; Bennett, N.; Götte, M.; and Tsantrizos, Y.S. “Modular assembly of purine-like bisphosphonates as inhibitors of HIV-1 reverse transcriptase.” *J. Med. Chem.* 2014, 57, 7435-7449. © American Chemical Society (2014). Used in this thesis with permission.

Portions of Chapters 3 and 5 will be submitted for publication as part of a collaborative paper.

Other manuscripts (published or *in preparation*) that are not included in this thesis, but to which the candidate has key contributions are the following:

Park, J; Leung, C.Y.; Matralis, A.; Lacbay, C.M.; Tsakos, M.; Berghuis, A.M.; Tsantrizos, Y.S. Pharmacophore mapping of thienopyrimidine-based monophosphonate (ThP-MP) inhibitors of the human farnesyl pyrophosphate synthase. Submitted to *J. Med. Chem.*

Gritzalis, D.; Park, J.; Chiu, W.; Cho, H.; Lin, Y.-S.; De Schutter, J.W.; Lacbay, C.M.; Zielinski, M.; Berghuis, A.M.; Tsantrizos, Y.S. Probing the molecular and structural elements of ligands binding to the active site versus an allosteric pocket of the human farnesyl pyrophosphate synthase. *Bioorg. Med. Chem. Lett.* 2015, 25, 1117-1123.

Acknowledgements

I would like to begin by expressing my sincerest gratitude to my PhD supervisor, Prof. Youla S. Tsantrizos for a truly outstanding support and tutelage throughout my graduate studies. I am also very grateful to the many opportunities she has provided me, especially the chance to work on exciting research and multidisciplinary projects that equipped me with valuable scientific knowledge and skills.

I am also very fortunate to have worked with and exchanged ideas with a team of collaborators of the finest caliber. I thank Prof. Mathias Götte (Department of Medical Microbiology and Immunology, University of Alberta) and his team for the biochemical studies in the HIV-1 project. I especially thank Michael Menni and Dr. Hsiao-Wei Liu for the fruitful discussions in the interpretation of the bioassay results. I also thank Dr. Jaeok Park and Prof. Albert Berghuis (Department of Biochemistry, McGill University); Xian Fang Huang, Dr. Daniel Waller, and Dr. Michael Sebag (Division of Haematology, McGill University Health Center); and Dr. Sandra Pelleieux and Dr. Judes Poirier (Douglas Mental Health University Institute) for sharing their expertise and enthusiasm in the hFPPS and hGGPPS projects.

I extend my gratitude to the faculty and staff of the Department of Chemistry, McGill University. The impressive research and resources, friendly, and multi-cultural environment in the department have helped greatly with my transition to graduate studies as an international student. I thank the members of my review committee: Prof. Anthony Mittermaier, Prof. C.J. Li, Prof. Masad Damha, and Prof. Karine Auclair for the constructive feedback on my research progress; Chantal Marotte, our graduate studies coordinator, is also very much appreciated for all the assistance with the paperwork throughout my studies; many thanks as well to Jean-Philippe Guay, Rick Rossi, and

Weihua Huang for extending their help every time we need repairs of the instruments in the lab; an enormous thanks too to Dr. Fred Morin, Dr. Tara Sprules, and Dr. Robin Stein for the NMR training and for the well-managed NMR facility; and Nadim Saade and Dr. Alexander Wahba for the time and expertise in obtaining HRMS data. I am also very grateful to McGill and the Chemistry department for the fellowships and travel awards that allowed me to pursue my studies and present the results in conferences.

I have been very privileged to have worked alongside and surrounded with a talented group of young scientists throughout the graduate program. I am very thankful to the post-docs, fellow graduate students, and undergraduates from our group and other research groups for the help and support, prolific scientific conversations, and good times inside and outside the lab. I thank Dr. John Mancuso, Dr. Joris de Schutter, Dr. Yih-Shyan Lin, and Dr. Nicolas De Rycke, who have been a great source of information during my early years in the PhD program. I especially thank John and Yih-Shyan for their contributions in the synthesis of pyridopyrimidines. I also thank Carlos Leung, Dimitrios Gritzalis, Hyungjun Cho, Viviane Ta, Weiling Chiu, Mark Sasson, Dr. Alexios Matralis, Eleni Ladopoulou, Dr. Guillermo Fernandez De Troconiz, Dr. Michail Tsakos, Dimitrios Xanthopoulos, Benita Kapuku, Dr. Shiguang Li, Dr. Zhi Zhou, Kristina Wolf, Chris Hegde, Hugo de Vries, Linda Do, Xue Bin, Sebastian Draxler, Alejandra Dominguez Huerta, Ryan Barrett, Peter Viereck, and Félix Vincent, for the meaningful discussions (whether about science or life, in general), for the company during late-night hours and week-ends in the lab, and more especially, for making my graduate experience and stay at McGill, a truly memorable one.

A special thanks to Dr. Nicolas De Rycke for translating the abstract in French and to Félix Vincent for proofreading it.

I am also very grateful to having met families and friends in Montreal who welcomed me into their homes, shared delicious home-cooked meals, and made sure I am doing well outside the lab. I thank the Negrana family (*Ate* Amy and *Ate* Jessie), Dayang-Mallannao family (Mark and Criscelle), team Aylmer 3472, especially my Montreal “siblings” (Thomas Raissi and Justina Sebastian), and the Blanco family (Ruben, Berna, Giovanni and our extended Drummond 3445 family: Saanchla and Alberto). I also appreciate their interest listening to my lab adventures and for reminding me of the other things that are really important in life.

I have been also blessed with great people who’d been an important influence in my life before flying halfway around the world to pursue my scientific aspirations. I thank my mentors, friends, and former colleagues from Wyeth/Pfizer Philippines who have helped me grow and mature professionally: Dr. Norriel S. Nipales, Tina Dichoso-Domer, Guada Tongco, and Celine Remo; my friends from the Institute of Chemistry, University of the Philippines Los Baños, whom I shared the interest of either pursuing PhD studies or medicine when we were just starting out as young chemistry instructors: Dr. Crisita Atienza-Mann, Dr. Allan Jay Cardenas, Dr. Leslie Moises, and Dr. Rufie Gravador; and my good friends since high school: Dr. Remil Galay, Richel Sandoval, Rein Alfonso, and Liezel Añonuevo-Banag. I may have missed many travel adventures, weddings, and other special occasions but I would like you to know that I treasure our friendships despite the distance.

Finally, I will not be able to reach this far without the unwavering support of my family. I thank my “*nanay*” who taught me valuable life skills that guided me in surpassing the challenges of graduate school and living abroad. I also thank my brothers: Kiel and Jeng, and the new members of the family: Kyle, Prince, Dylan, Empress, and Grey for being a constant source of motivation

and inspiration. The last five years and so have been quite a journey to all of us but I would like to assure you that any success that I may enjoy in the future is your success as well.

Once again, Thank you very much/*Merci beaucoup/Maraming salamat!!!*

Cyrus Lacbay

Table of Contents

Abstract.....	i
Résumé.....	ii
Preface.....	iii
Acknowledgements.....	iv
Table of Contents.....	viii
List of Figures.....	xi
List of Schemes.....	xiii
List of Tables.....	xiv
Frequently Used Symbols and Abbreviations.....	xv
CHAPTER 1: Introduction.....	1
1.1. Phosphate-Binding Enzymes as Therapeutic Targets.....	1
1.2. Phosphate and Pyrophosphate Bioisosteres.....	2
1.3. Phosphate and Phosphonate Prodrugs.....	7
1.4. The HIV Life Cycle.....	12
1.5. HIV-1 RT Structure and Function.....	14
1.6. Examples of Clinically Approved Inhibitors of HIV-1 RT.....	17
1.7. NRTI Drug Resistance.....	19
1.8. New Class of Active Site Inhibitors Targeting the Translocation of HIV-1 RT.....	21
1.9. Research Goals (Part 1).....	26
1.10. References.....	27
CHAPTER 2: Modular Assembly of Purine-Like Bisphosphonates as Inhibitors of HIV-1 Reverse Transcriptase.....	39
2.1. Preface.....	39
2.2. Abstract.....	39
2.3. Introduction.....	40
2.4. Chemistry.....	44
2.5. Results and Discussion.....	52
2.6. Conclusions.....	54
2.7. Experimental Section.....	55
2.8. Associated Content.....	94

2.9. Author Information	95
2.10. Acknowledgements	95
2.11. Abbreviations Used	95
2.12. References	95
Chapter 2: Supporting Information	105
CHAPTER 3: Diketo Acid Bioisosteres and Structure-Activity Relationship Studies of Mechanistically Unique Inhibitors of HIV-1 Reverse Transcriptase	116
3.1. Preface	116
3.2. Abstract	116
3.3. Introduction	117
3.4 Chemistry	121
3.5 Results and Discussion	129
3.6 Conclusions	135
3.7 Experimental Section	135
3.8. Associated Content	160
3.9. Author Information	161
3.10. Acknowledgments	161
3.11 References	161
Chapter 3: Supporting Information	166
CHAPTER 4: The Mevalonate Pathway and the Human Geranylgeranyl Pyrophosphate Synthase (hGGPPS)	176
4.1. Preface	176
4.2. Regulatory Enzymes of the Mevalonate Pathway as Drug Targets	176
4.3. Isoprenoids and Alzheimer's Disease	178
4.4. Isoprenylation and Multiple Myeloma	180
4.5. Targeting the Prenyltransferases: Farnesyl and Geranylgeranyl Transferases	181
4.6. Targeting the Prenylsynthases: Farnesyl and Geranylgeranylpyrophosphate Synthases. 183	
4.6.1. The human FPPS	183
4.6.2. The human GGPPS	188
4.6.3. Inhibitors of hGGPPS	190
4.7. Research Goals (Part 2)	192
4.8. References	193

CHAPTER 5: Potent and Selective Thieno[2,3-<i>d</i>]pyrimidine-Based Inhibitors of the Human Geranylgeranyl Pyrophosphate Synthase (hGGPPS): Implications for Drug Discovery	201
5.1. Preface	201
5.2. Abstract	202
5.3. Introduction	202
5.4. Chemistry	207
5.5. Results and Discussion	210
5.6. Conclusions and Outlook	221
5.7. Experimental Section	222
5.8. Associated Content	248
5.9. Author Information	248
5.10. Acknowledgments	248
5.11. References	248
Chapter 5: Supporting Information	256
CHAPTER 6: Contributions to Knowledge	265
6.1 Claims to Original Knowledge	265
6.2 Papers and Conference Presentations	266
6.2.1 Papers Published	266
6.2.2 Manuscripts in Preparation	266
6.2.3 Conference Proceedings	267

List of Figures

Figure 1.1. General representation of the active site interaction of an enzyme recognizing a pyrophosphate group.....	1
Figure 1.2. Ionization states and pKa values for phosphate and pyrophosphate moieties.....	3
Figure 1.3. Examples of phosphates and pyrophosphate bioisosteres.	5
Figure 1.4. Structure of raltegravir bound to the prototype foamy virus IN <i>via</i> metal-chelation. .	5
Figure 1.5. Examples of HIV-IN inhibitors (FDA-approved or in clinical trials).	6
Figure 1.6. Examples of clinically-approved and exploratory prodrugs.....	9
Figure 1.7. Representation of the life cycle of HIV-1 (as described in the text) and examples of drugs currently used to intervene some key steps.....	13
Figure 1.8. Representation of RT-catalyzed DNA polymerization cycle described in the text..	16
Figure 1.9. Two-metal ion mechanism of RT polymerase. The active site is located in the middle of the palm, fingers, and thumb subdomains.	16
Figure 1.10. Examples of clinically approved NRTIs.	18
Figure 1.11. Mechanism of action of NRTIs.	18
Figure 1.12. Examples of NNRTIs that bind at the allosteric pocket in the palm domain.	19
Figure 1.13. Illustration of the ATP-mediated excision of the drug AZT leading to the release of AZT-ATP (5',5'-adduct) and availability of 3'-OH at the primer terminus to continue with DNA synthesis.....	21
Figure 1.14. Representation of North and South sugar pucker conformations.....	21
Figure 1.15. New classes of inhibitors that target the translocation status of HIV-1 RT.	24
Figure 1.16. Representation of the iron-mediated site specific footprinting used to investigate the mechanism of action.	25
Figure 2.1. Oligonucleotide polymerization reaction.	42
Figure 3.1. Examples of inhibitors of nucleic acid processing enzymes.	118
Figure 3.2. Representative examples of HIV-1 RT inhibitors from our compound library.	128
Figure 3.3. Representation of the translocation step in the DNA polymerization cycle catalyzed by HIV-1 RT polymerase.....	129
Figure 3.4. Structure of β -thujaplicinol.....	132
Figure 3.5. Inhibition of HIV-1 RT DNA synthesis by PFA and compounds 3.17h and 3.17i . 134	

Figure 3.6. Investigation of the mechanism of action <i>via</i> site-specific footprinting assay performed using the previously described protocol.	134
Figure 4.1. Representative inhibitors of prenyl transferases.....	183
Figure 4.2. Crystal structure of hFPPS in complex with RIS (PDB: 1YV5).....	185
Figure 4.3. Examples of active site and allosteric inhibitors of hFPPS.....	187
Figure 4.4. (a) Crystal structure of human GGPPS (PDB: 2Q80) revealing a homohexameric organization; (b) Inter dimer contact between two α -helices.	190
Figure 4.5. Examples of hGGPPS inhibitors.	192
Figure 5.1. Examples of PAINS.....	203
Figure 5.2. Thienopyrimidines structural isomers.	204
Figure 5.3. Examples of bioactive thieno[2,3- <i>d</i>]pyrimidines.	205
Figure 5.4. Proposed mechanism on the role of CuTC in the Liebeskind–Srogl cross-coupling of heteroaromatic thioether with boronic acid under base-free condition.	209
Figure 5.5. Representative examples from compound library.....	212
Figure 5.6. (A) <i>In vitro</i> wild-type hGGPPS inhibition data of ThP-BPs screened at a fixed concentration of 100 nM, average values of three determinations, standard deviation of $\leq 10\%$; the known hGGPPS inhibitor, 4.15 was used as the positive control; (B) Highlights of the SAR as discussed in the text.	213
Figure 5.7. MTT reduction to formazan.	214
Figure 5.8. Chemical structure of velcade.	216
Figure 5.9. Cell viability analysis using CD138 as the marker and detection of Annexin V positive apoptotic MM RPMI-8226 cells via flow cytometry.....	218
Figure 5.10. Western blot analysis to detect non-geranylgeranylated Rap1A.....	219
Figure 5.11. Add-back experiments using GGOH.....	220

List of Schemes

Scheme 1.1. Proposed mechanism of activation of (A) ProTides and (B) POC prodrug.	11
Scheme 2.1. Synthesis of substituted 2-aminonicotinitriles; (a) Classical Hantzsch synthesis; (b) Modified Teague synthesis.	46
Scheme 2.2. Two common approaches for the synthesis of 2-aminonicotinitriles that are not substituted at C-4.	47
Scheme 2.3. Modular synthesis of C-6/C-7 substituted pyrido[2,3- <i>d</i>]pyrimidin-4-amines.	48
Scheme 2.4. Cyclization mechanism (*incorporation of ¹⁵ N from ¹⁵ NH ₄ Cl).	50
Scheme 3.1. Route 1 synthetic approach for the preparation of analogs of 3.17	121
Scheme 3.3. Proposed formation of 3.23 involving a polar radical pair mechanism.	123
Scheme 3.4. Synthesis of adenine-based compounds.	125
Scheme 3.5. Synthesis of pyridopyrimidine-based compounds.	127
Scheme 4.1. Representation of the mevalonate pathway and examples of drugs that intervene some key enzymes.	178
Scheme 4.2. Proposed mechanism for hFPPS catalysis.	185
Scheme 5.1. (A) Synthetic approaches for 5.16 ; (B) Gewald reaction mechanism leading to 2-aminothiophene-precursor (5.14) of thieno[2,3- <i>d</i>]pyrimidines.	206
Scheme 5.2. Synthesis of C-5 and/or C-6 substituted thienopyrimidines via a modified Gewald approach.	207
Scheme 5.3. General synthesis of C-2 and/or C-6 substituted ThP-BP.	209
Scheme 5.4. Synthesis of expanded ThP-BP analogs.	210

List of Tables

Table 2.1. Compound library	51
Table 2.2. Activity data of key compounds	53
Table 2.3. Activity data of key compounds in HIV-1 wild-type vs HIV mutants	54
Table 3.1. Bioactivity of some literature polyoxygenated compounds shown in Fig. 3.1	119
Table 3.2. Preliminary results on the use of CuBr as additive in the synthesis of 3.29a from 3.27a ^[a] as depicted in Scheme 3.4	125
Table 3.3. Inhibition data in HIV-1 RT polymerase and RNase H.....	131
Table 5.1. Activity of selected compounds in MM tumor cell lines.....	215
Table 5.2. Modulation of P-Tau levels in immortalized human neurons.....	221

Frequently Used Symbols and Abbreviations

AD	Alzheimer's disease
AZT	1-[(2 <i>R</i> ,4 <i>S</i> ,5 <i>S</i>)-4-Azido-5-(hydroxymethyl)oxolan-2-yl]-5-methylpyrimidine-2,4-dione; Zidovudine
BP	Bisphosphonate
br	broad
°C	Degree Celsius
Cdc4	Cell division cycle 4
CPHM	4-chlorophenylhydrazone of mesoxalic acid
α -CNP	α -carboxy nucleoside phosphonate
CuTC	Copper(I) thiophene-2-carboxylate
DCM	Dichloromethane
DKA	α,γ -diketo acid
DMAPP	Dimethylallyl pyrophosphate
DMF	<i>N,N</i> -dimethylformamide
DMSO	Dimethylsulfoxide
dNTP	Deoxynucleoside triphosphate
DNA	Deoxyribonucleic acid
Dppf	(diphenylphosphino)ferrocene
EC ₅₀	Effective concentration for 50% inhibition
eq.	Molar equivalence
Et	Ethyl
EtOAc	Ethyl acetate
EtOH	Ethanol
FPP	Farnesyl pyrophosphate
GGPP	Geranylgeranyl pyrophosphate
GPP	Geranyl pyrophosphate
GSK-3 β	Glycogen synthase kinase 3 beta
GTPases	Small guanine triphosphate binding proteins
h	Hours
HAART	Highly active antiretroviral therapy

HBTU	<i>N,N,N',N'</i> -Tetramethyl-O-(1H-benzotriazol-1-yl)uranium hexafluorophosphate
DIPEA	<i>N,N</i> -Diisopropylethylamine
HCMV	Human cytomegalovirus
HCV	Hepatitis C virus
hFPPS	Human farnesyl pyrophosphate synthase
hGGPPS	Human geranylgeranyl pyrophosphate synthase
HIV-1	Human immunodeficiency virus type 1
HPLC	High-performance liquid chromatography
IC ₅₀	Inhibitor concentration causing 50% inhibition
IN	Integrase
INDOPY-1	indolopyridone-1
IPP	Isopentenyl pyrophosphate
LCMS	Liquid Chromatography-Mass Spectrometry
LDH	Lactate dehydrogenase
M	Molar
m/z	Mass-to-charge ratio
MeOH	Methanol
MHz	Megahertz
min	Minutes
MM	Multiple Myeloma
MS	Mass spectrometry
MTT	3-(4,5-dimethylthiazol-2-yl)-2,5-diphenyltetrazolium bromide
μW	Microwave
<i>N</i> -BPs	Nitrogen-containing Bisphosphonates
NBS	N-bromosuccinimide
NcRTI	Nucleotide-competing reverse transcriptase inhibitors
NMR	Nuclear Magnetic Resonance
NNRTI	Non-Nucleoside Reverse Transcriptase Inhibitors
NRTI	Nucleoside Reverse Transcriptase Inhibitors
N-site	Nucleotide binding site
PAINS	Pan Assay Interference Compounds

P/T	Primer/Template
PFA	Phosphonoformic acid; Foscarnet
PFV	Prototype foamy virus
Ph	Phenyl
POM	Pivaloyloxymethyl
PPh ₃	Triphenylphosphine
PP _i	Inorganic pyrophosphate
P-site	Priming site
P-Tau	Phosphorylated tau
Py	Pyridine
PYPY-BP	Pyrido[2,3- <i>d</i>]pyrimidine bisphosphonate
RIS	Risedronic acid
RNA	Ribonucleic acid
RNase H	Ribonuclease H
RT	Reverse transcriptase
rt	Room temperature
SAR	Structure-activity relationship
SPA	Scintillation proximity assay
3TC	4-amino-1-[(2 <i>R</i> ,5 <i>S</i>)-2-(hydroxymethyl)-1,3-oxathiolan-5-yl]-1,2-dihydropyrimidin-2-one; Lamivudine
TBAF	Tetrabutylammonium fluoride
TCEP	Tris(2-carboxyethyl)phosphine
ThP-BP	Thieno[2,3- <i>d</i>]pyrimidine bisphosphonate
TMS	Trimethylsilyl
T-Tau	Total tau protein
ZOL	Zoledronic acid

CHAPTER 1: Introduction

1.1. Phosphate-Binding Enzymes as Therapeutic Targets

Enzymes that bind phosphate, diphosphate (also known as pyrophosphate) or triphosphate natural substrates are involved in numerous biological processes.

The active site of these enzymes also typically bind two to three divalent metal cations as their

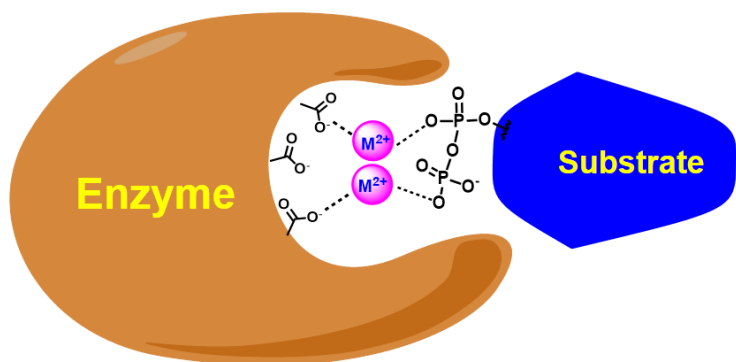


Figure 1.1. General representation of the active site interaction of an enzyme recognizing a pyrophosphate group.

cofactors that interact with a number of highly conserved acidic residues within the active site cavity (**Fig. 1.1**).¹⁻³ Nucleic acid processing enzymes (e.g. DNA/RNA polymerases, integrase, Ribonuclease H and other nucleases) belong to this large family of enzymes. For example, DNA polymerases bind substrates bearing a triphosphate group and catalyze the oligonucleotide synthesis essential for DNA replication.^{2,4} Virally-encoded DNA/RNA polymerases, in particular are important therapeutic targets for many infectious diseases, including HIV/AIDS,^{5,6} influenza,⁷ and hepatitis.^{8,9} Regulatory enzymes of the mevalonate pathway, such as the human farnesyl pyrophosphate synthase (hFPPS) and human geranylgeranyl pyrophosphate synthase (hGGPPS) also interact with their natural substrates bearing a pyrophosphate moiety and control the biosynthesis of FPP and GGPP, respectively. These human metabolites are essential for the post-translational modification of small GTPase proteins, which are associated with a plethora of cellular processes.^{3,10,11} Given their important biological roles, a number of human diseases can result from their dysregulation; therefore, it is not surprising that these enzymes have been targets

for drug discovery for over 30 years with the goal of finding effective therapeutics against cancer, infectious diseases, cardiovascular, and neurological disorders. However, due to their highly charged active site cavity, these enzymes are extremely challenging drug targets and are often labeled as “undruggable” since small molecules with complementary size, shape and electrostatic surface must also be charged in order to bind tightly and, consequently, suffer from poor drug-like properties. Nonetheless, several productive advances in targeting the active site have been reported, particularly by incorporating effective phosphate and pyrophosphate bioisosteres or prodrugs and also by targeting a catalytically relevant allosteric pocket of these enzymes.

1.2. Phosphate and Pyrophosphate Bioisosteres

Bioisosteres are structural moieties that are able to elicit similar biological effect with the key pharmacophore due to resemblance in properties (e.g. size, shape, pKa, polarity, electronic distribution, lipophilicity, etc.). The term was coined by Harris Friedman in 1950¹² and while it has broad applications in drug discovery, bioisosteric replacements are typically done in order to improve the “drug-like” properties of a compound, including its cell-membrane permeability, pharmacokinetic and toxicity profile.¹³ Phosphates and pyrophosphates are highly versatile functional groups that are widespread in biological molecules. However, the application of these functionalities in drug design is limited due their highly polar and charged nature at physiological pH¹⁴ (**Fig. 1.2**) that render them chemically unstable and unable to cross cell membranes.

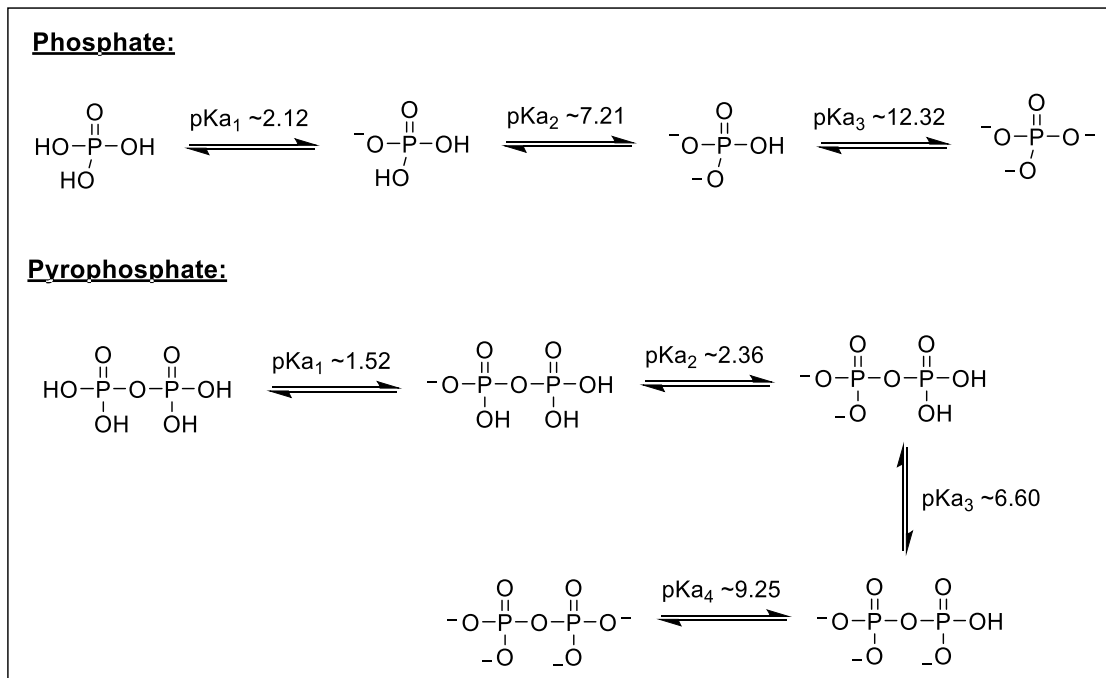


Figure 1.2. Ionization states and pKa values for phosphate and pyrophosphate moieties. At physiological pH, these functionalities are both negatively charged.

As would be expected, there have been significant efforts focusing on the design of effective phosphate/pyrophosphate bioisosteres with enhanced drug-like physicochemical properties. Examples of the traditional and more recent mimics that have been explored are shown in **Figures 1.3** and **1.5**.¹³⁻¹⁶ A phosphonic acid (also referred as phosphonate when in salt form; **1.1**, **Fig. 1.3**) typically serves as a starting point, as it represents a chemically stable phosphate mimic (where the oxygen atom that links the phosphate group to the rest of the molecule is replaced with a carbon) that can be further improved by introduction of a halogen (e.g. fluorine) at the C α to more closely match the acidity of the phosphate moiety.¹⁷ Carboxylic acids (e.g. oxoacetic acid **1.2**)¹⁸ are also potentially useful carbon-based phosphate mimics even though their planar trigonal shape differs from the tetrahedral geometry of the phosphate moiety. Nonetheless, in principle, any negatively charged group can engage with a basic amino acid residue, such as lysine or arginine

via electrostatic interactions. Sulfur-based mimetics (with their nearly tetrahedral shape in the fully oxidized state; e.g. *N*-acyl sulfamate **1.3**)¹⁹ have the ability to be fully ionized at physiological pH are also potential replacements of a phosphate. Other examples include cyclic motifs, such as the isothiazolidinone (**1.4**)²⁰ scaffold, which was used in the development of protein tyrosine phosphatase 1B (PTP1B) inhibitors. Isothiazolidinone **1.4** acts as a mimic of phosphotyrosine (pTyr) and binds competitively to the active site of PTP1B,²¹ an enzyme that is being pursued as a therapeutic target for obesity and diabetes.²² Successful use of tetramic acids (**1.5**) in inhibiting undecaprenyl pyrophosphate synthase (UPPS), a target of potential antibacterial agents has also been reported.²³ The design of **1.5** was inspired by the binding mode of the natural substrate, farnesyl pyrophosphate at the active site of UPPS.²³ One major milestone in the metal-chelation strategy, particularly in the context of HIV-1 integrase (IN) was the incorporation of the hydroxylated pyrimidinone **1.7** in the drug raltegravir, Isentress® (**Fig. 1.5**), which has good oral bioavailability in humans.²⁴ Crystal structure of full-length IN from the prototype foamy virus (PFV) in complex with raltegravir revealed that the pyrimidinone moiety binds to the aspartate-rich IN active site *via* coordination with the two Mg²⁺ ions (**Fig. 1.4**).²⁵ The metal-chelating pharmacophore (hydroxypyrimidinone moiety **1.7**) was designed as a more stable and “drug-like” substitute of α,γ -diketo acids (DKAs; **1.6**).^{26, 27} DKAs inhibit a variety of viral integrases, polymerases, and endonucleases by acting as a pyrophosphate mimic.^{8, 13} Since the discovery of raltegravir and its FDA approval in 2007, several other DKA-like motifs that bind to the active site of HIV- IN have been investigated. These initiatives led to the development of other HIV- IN drugs, such as elvitegravir (approved in 2012)^{28, 29} and dolutegravir (approved in 2013)³⁰ (**Fig. 1.5**) and those in different stages of clinical development (e.g. bictegravir, cabotegravir, and MK-2048).^{16, 31}

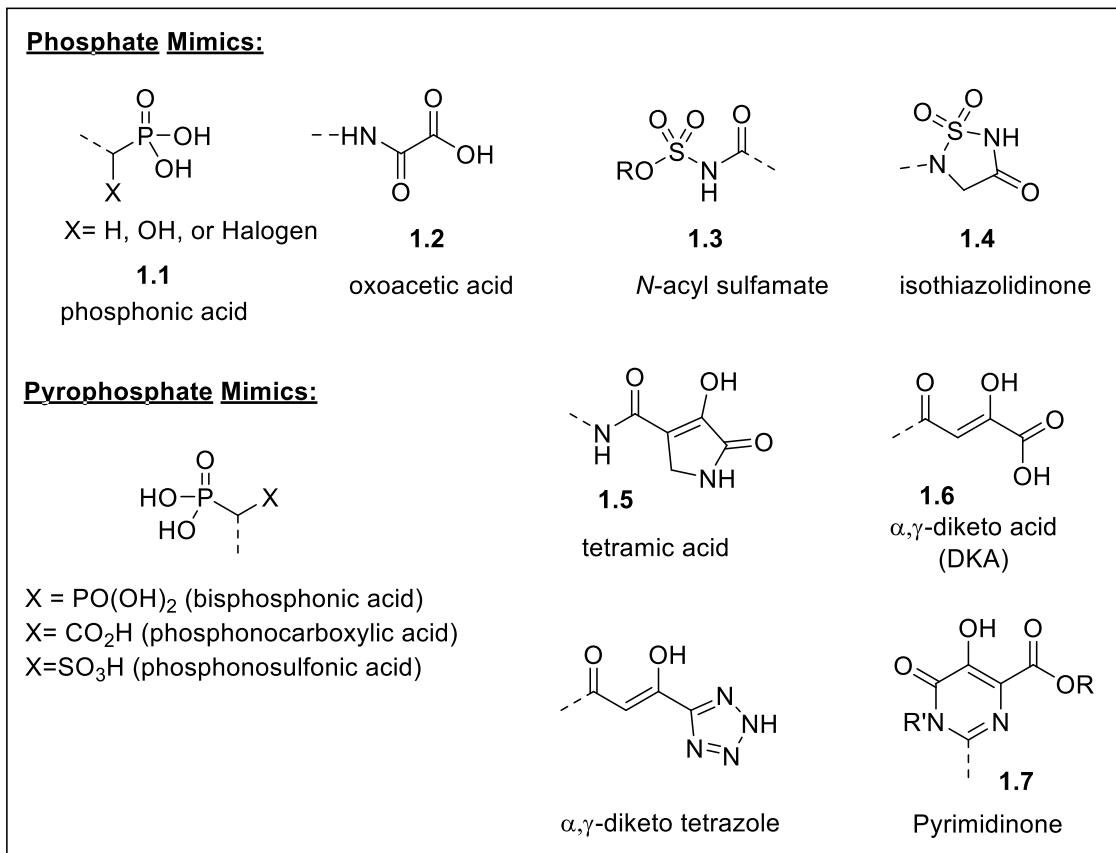


Figure 1.3. Examples of phosphates and pyrophosphate bioisosteres.

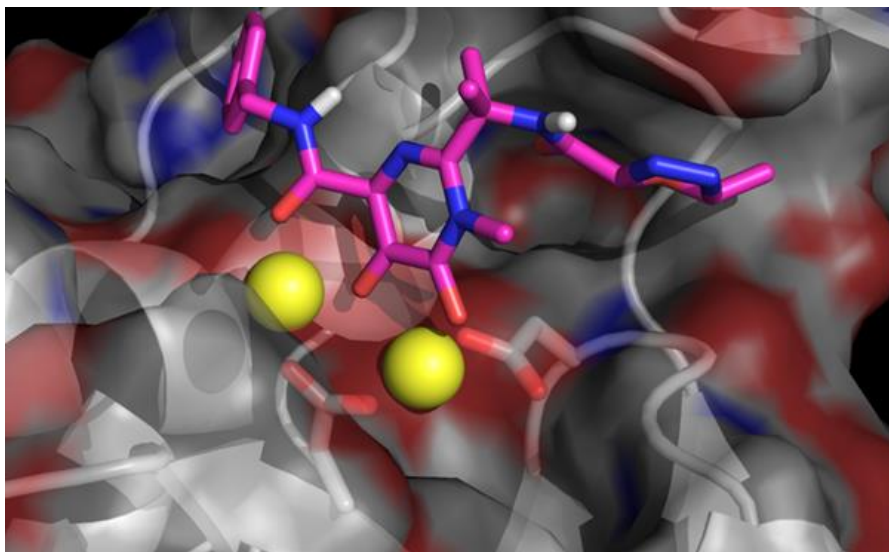


Figure 1.4. Structure of raltegravir bound to the prototype foamy virus IN *via* metal-chelation. The yellow spheres represent Mg²⁺ ions (PDB: 3OYA).

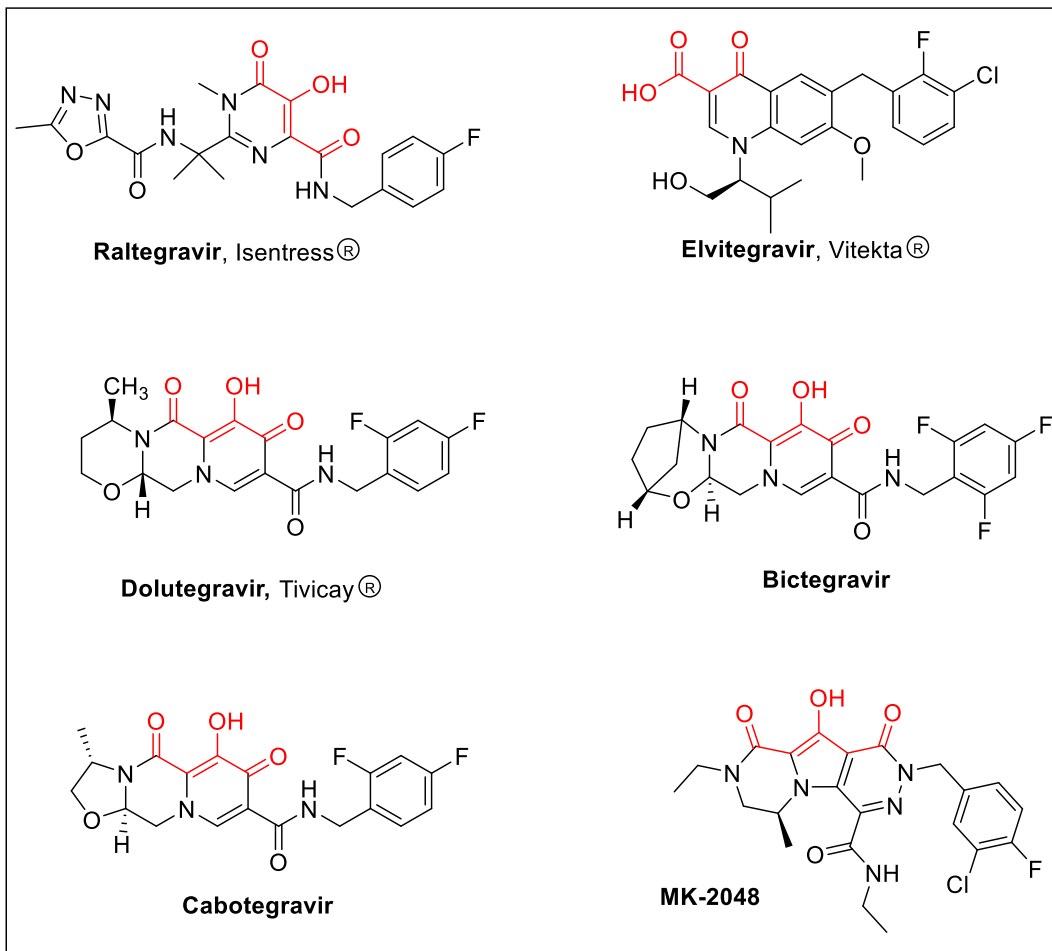


Figure 1.5. Examples of HIV-IN inhibitors (FDA-approved or in clinical trials). The metal-binding motif for each inhibitor is highlighted in red.

While there have been few successes in the use of phosphate and pyrophosphate bioisosteres, it is still acknowledged that these functionalities are amongst the most difficult pharmacophores to mimic when designing biologically active compounds. In situations where phosphates or phosphonates are the only option in mimicking a specific drug-target interaction, prodrug strategies have been also explored.

1.3. Phosphate and Phosphonate Prodrugs

Use of a prodrug that incorporates various protecting groups to mask the negative charges of a phosphate, phosphonate or diphosphate moieties have been developed and investigated.³²⁻³⁴ Over the past decades, the design and development of effective prodrugs have faced substantial challenges. A prodrug has to survive the gastrointestinal tract and be absorbed into the systemic circulation, remain stable until reaching the desired biological target, and when activated, release by-products that are considered innocuous. Nonetheless, examples of clinically validated nucleoside monophosphate and monophosphonate prodrugs with improved oral bioavailability and cellular uptake for the treatment of viral infections are now known.

The “aryloxyphosphoramidate” approach or ProTide technology developed by Christopher McGuigan (Cardiff University, UK) in the early 1990s³⁴ has been successfully employed for sofosbuvir³⁵ and tenofovir alafenamide (TAF, **1.8a**)³⁶ (**Fig. 1.6**). Sofosbuvir (Sovaldi®) was approved by FDA in 2013 for the treatment of chronic hepatitis C infection. This prodrug is given orally in combination with other antiviral medicines and metabolized to the active antiviral agent through the action of enzymes in the human liver.³⁷ TAF was the most recent ProTide approved by the FDA (November 2015) that is being used as part of a combination therapy to treat HIV-I infection. TAF was shown to have improved anti-HIV activity and better *in vivo* stability than the parent nucleotide drug, tenofovir and can be given at a much lower dose than the other FDA-approved tenofovir disoproxil prodrug (**1.8b**).³⁸ It is also under evaluation as a possible treatment for hepatitis B.³⁹ Other examples of monophosphate ProTides in clinical development include GS-5734 and NUC-1031 (also known as acelarin) (**Fig. 1.6**). The C-nucleoside derivative, GS-5734 displayed antiviral activity against Zika virus and other pathogenic RNA viruses, but has shown more promise against Ebola. In a rhesus monkey model of Ebola virus infection, treatment with

GS-5734 showed significant suppression of viral replication and protected the infected animals against the fatal disease.⁴⁰ This prodrug, which is being developed by Gilead Sciences, Inc. is now in phase I clinical trials. NUC-1031 is the ProTide of the anticancer drug, gemcitabine, which displayed encouraging clinical efficacy in Phase I/II studies. For instance, the addition of the phosphoramidate motif to gemcitabine was reported to not only enhanced its cellular uptake but also overcame the key cancer resistance mechanisms observed for the parent nucleoside-based drug.^{41, 42} NUC-1031 has entered phase III clinical trials in 2015 as a potential treatment for pancreatic cancer. Additionally, it is being evaluated in two different combination studies to assess both safety and potency along with (1) carboplatin (for patients with ovarian cancer) and (2) with cisplatin (for patients with biliary cancers).⁴³

Aside from the ProTide technology, successful use of alkoxycarbonyloxyalkyl esters (e.g. POC; **Fig. 1.6 ii**) and acyloxyalkyl esters (e.g. POM; **Fig. 1.6 iii**) prodrugs have also been shown to have clinical value. The first tenofovir prodrug that was developed against HIV-1 infection contains a bis-POC moiety (**1.8b**) and marketed under the trade name Viread.⁴⁴ The drug adefovir, on the other hand, is formulated as a bis-POM prodrug (**1.8c**) to enhance its oral absorption and is currently used to treat hepatitis B infection.⁴⁵ In the case of bisphosphonates, tris-POM approach was applied for squalene synthase (SQS) inhibitor **1.10**, which has been shown to reduce plasma cholesterol levels in rhesus monkeys.⁴⁶ Tetra-POM modification have also been explored with several inhibitors of hFPPS⁴⁷ and hGGPPS.^{48, 49} The hGGPPS inhibitor **1.9**, for instance exhibited enhanced potency in inhibiting cellular protein geranylgeranylation in comparison to its free acid (~25-fold);⁴⁸ however, in contrast to the success of monophosphonate prodrugs, none of the bisphosphonate prodrugs have been validated clinically.

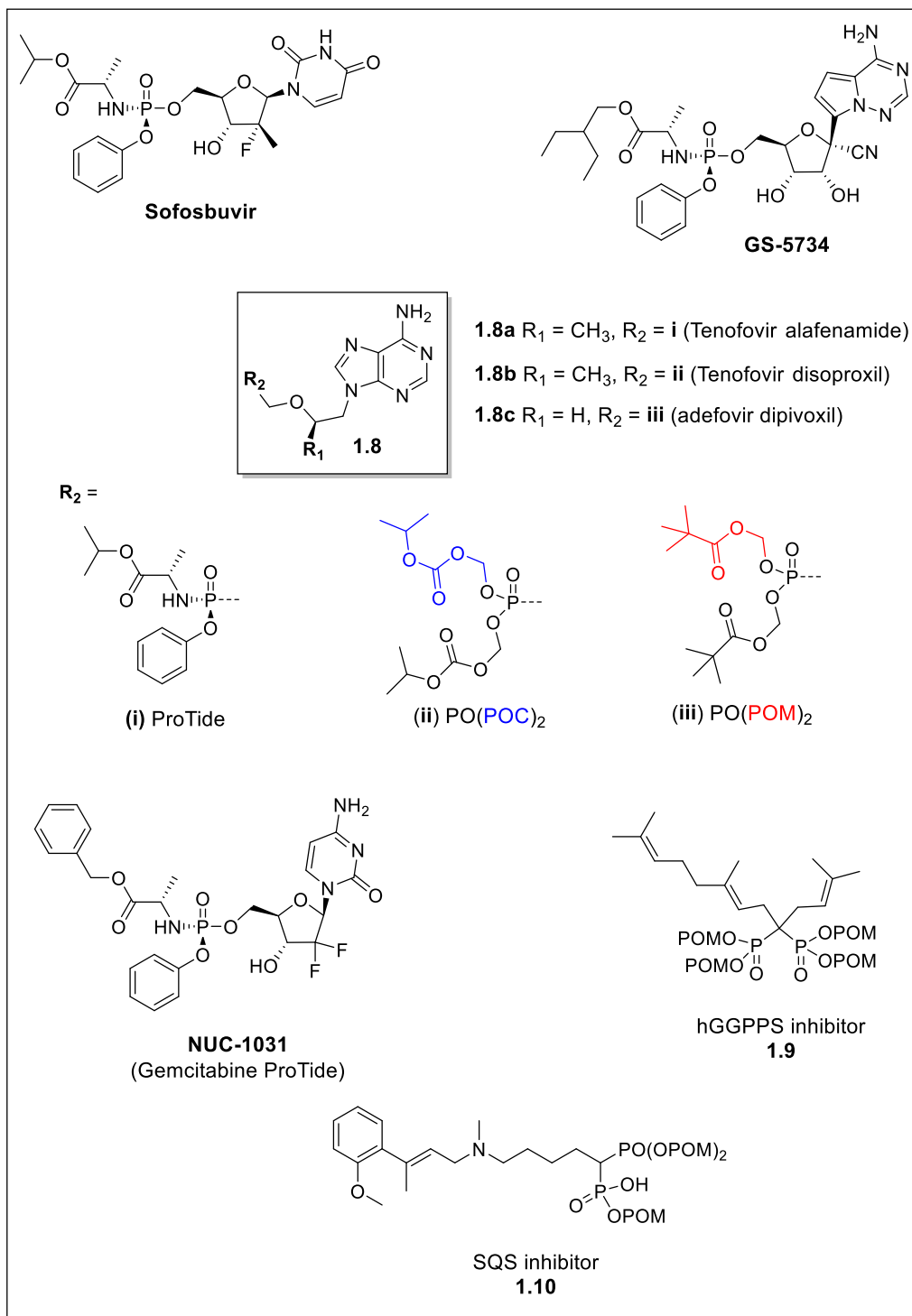
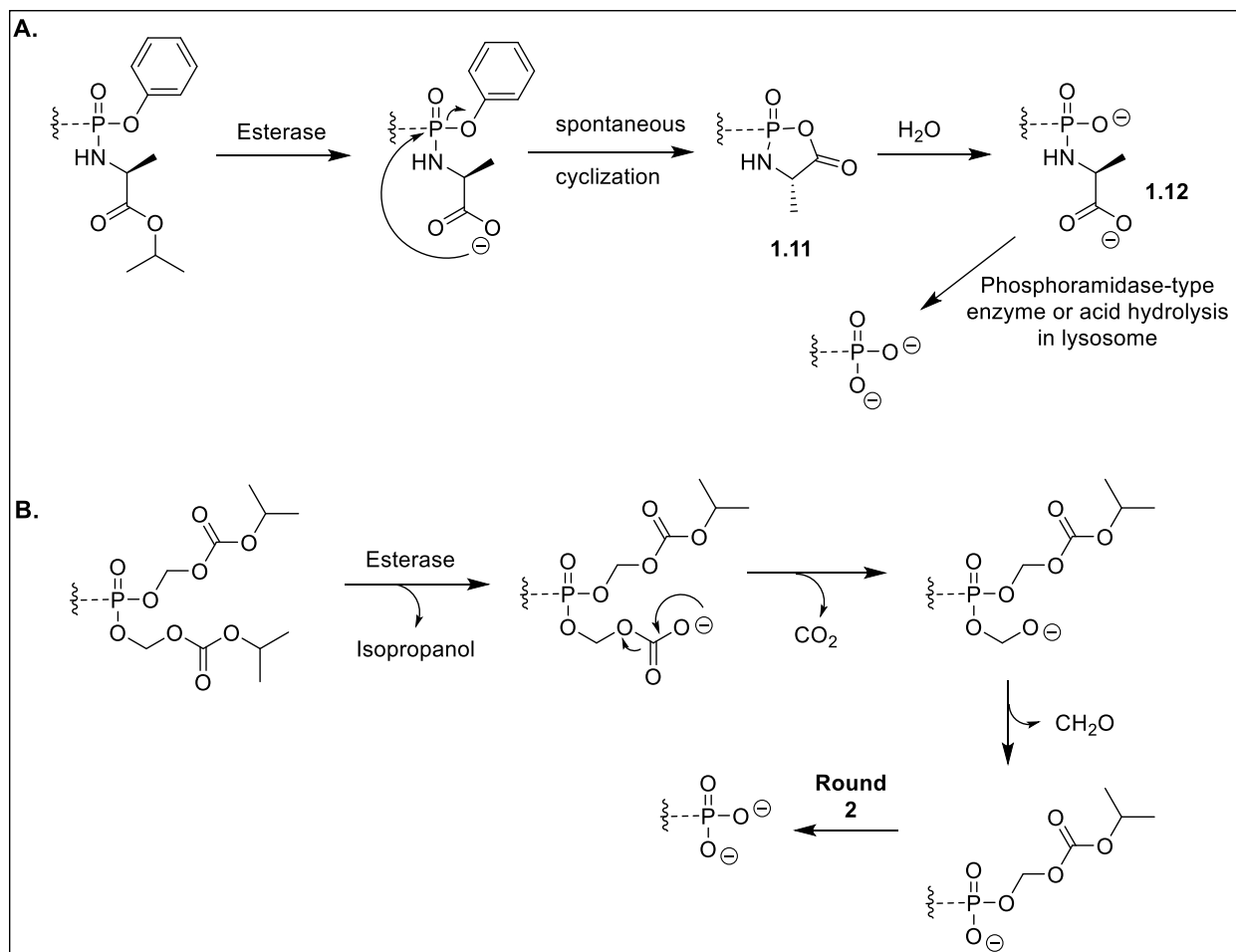


Figure 1.6. Examples of clinically-approved and exploratory prodrugs.

The mechanism of activation of aryloxyphosphoramidates involves release of the monophosphate (e.g. in the case of sofosbuvir) or monophosphonate (e.g. in the case of TAF) species, and has been

proposed to proceed *via* enzyme-mediated and spontaneous reactions (**Scheme 1.1A**).^{34, 50, 51} The first cleavage is initiated by esterases (e.g. cathepsin A)⁵² followed by an intramolecular cyclization that is accompanied by the release of the phenoxy group. This results in the formation of a short-lived cyclic mixed anhydride **1.11** that is subject to ring opening *via* hydrolysis. The final step, which is the cleavage of the P-N bond of intermediate **1.12** leading to the release of the monophosphate or monophosphonate analog was proposed to be mediated by intracellular phosphoramidase-type enzyme⁵³ or through spontaneous hydrolysis due to the acidic pH in the lysosomes.⁵⁴ The monophosphate or monophosphonate species then undergo further activation to exert the desired pharmacological effects. The cleavage of POM and POC-based prodrugs are also triggered by esterases. In the case of POC, this process is followed by spontaneous fragmentation to release the parent phosphate or phosphonate, in addition to carbon dioxide and formaldehyde as by-products (**Scheme 1.1B**).^{33, 55} The POM prodrug undergoes similar cleavage as POC except that upon release of pivalic acid *via* the action of esterases, only formaldehyde and the parent species are generated by the spontaneous cleavage.³³

The increasing selection and clinical success of prodrug technology has reignited interest in the development of phosphate or phosphonate-containing drugs. However, finding the right balance of achieving good pharmacokinetics, optimal chemical and metabolic stability of the protecting group, and effective delivery of the parent drug to a particular tissue remains as a highly challenging task depending on the target. Furthermore, the safety issues of the cleavage by-products (e.g. phenol, formaldehyde, pivalic acid) especially in long-term treatment and high dosage of the prodrug constitute another major concerns of this approach.



Scheme 1.1. Proposed mechanism of activation of (A) ProTides and (B) POC prodrug.

This thesis describes our efforts toward the discovery and development of active site inhibitors of two important targets belonging to the group of enzymes that bind natural substrates containing a diphosphate or a triphosphate moiety. Specifically, the first part of the thesis (**Chapters 1.4 to 3**) gives a background on HIV and the current antiretroviral therapy used to treat this infection and our own studies toward the synthesis and evaluation of HIV-1 RT inhibitors with a novel mechanism of action. The second part (**Chapters 4 to 5**) provides an overview of the key enzymes of the mevalonate pathway as drug targets and our efforts toward inhibiting the human GGPPS, a promising but yet virtually underexplored biological target.

1.4. The HIV Life Cycle

The human immunodeficiency virus type 1 (HIV-1), the causative agent of the acquired immune deficiency syndrome (AIDS), remains as a major public health problem worldwide. Since the first reports of the infection in 1981 and the subsequent discovery and isolation of the virus two years later, around 35 million people have died of AIDS-related illnesses. As of 2015, approximately 36.7 million people are living with HIV with the number of new infections reaching 2.1 million globally.⁵⁶

HIV is a member of the lentivirus family of retroviruses that replicates *via* reverse transcription. The viral life cycle (illustrated in **Fig. 1.7**)^{5,57} starts by the binding of the HIV virion to the surface of the host's immune cell receptors known as CD4. This is followed by membrane fusion, a process that allows entry of the virion to the cell. Once inside the cell's cytoplasm, the viral capsid is uncoated and the reverse transcriptase (RT) enzyme converts the viral genomic RNA into proviral double-stranded DNA through the action of its polymerase and RNase H catalytic activities. The proviral DNA then enters the cell's nucleus and becomes incorporated with the host's genetic material through the action of another virally-encoded enzyme, the integrase (IN). The integrated viral genome then undergoes transcription and translation using the host's machinery to form long chains of precursor proteins that are cleaved by HIV protease generating the smaller "immature" form of the virus. Finally, the smaller HIV virus assemble into mature and infectious particles, which are later released from the cell *via* budding.

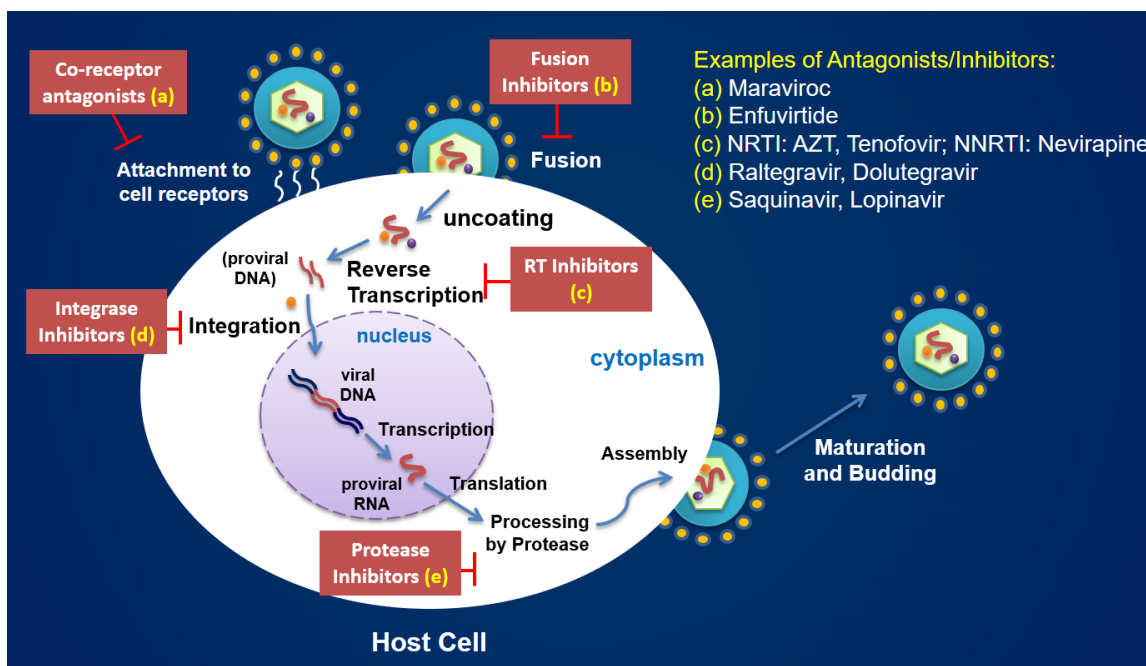


Figure 1.7. Representation of the life cycle of HIV-1 (as described in the text) and examples of drugs currently used to intervene some key steps.

Many of the key steps in the HIV life cycle have been targeted by medicinal chemists. For example, entry inhibitors, such as maraviroc was developed to prevent the attachment of the HIV virion to the cell surface receptors and thereby blocks viral multiplication and cell infection.^{58, 59} Another drug called enfuvirtide (a short peptide originally known as T-20) is a pharmaceutical agent that disrupts HIV fusion with the host cell and also prevents entry of the virus to the cell.⁶⁰ The RT enzyme, on the other hand, is the target of many important therapeutic agents, the nucleoside (NRTI) drugs that act as substrate mimics and the non-nucleoside (NNRTI) drugs that bind to a catalytically relevant allosteric pocket of the enzyme.⁵ A more detailed discussion regarding RT inhibitors is provided in the succeeding sections. Clinically-validated integrase inhibitors that block the strand-transfer reaction include raltegravir (RAL), elvitegravir (EVG), and dolutegravir (DTG). The second generation drug DTG was reported to have higher genetic barrier to resistance selection than RAL and EVG.⁶¹ Lastly, inhibitors of the HIV protease enzyme have also been

developed and marketed since the mid-1990s. One example is lopinavir⁶² (approved in September 2000), which is usually administered in combination with another protease inhibitor, the drug ritonavir. Interestingly, ritonavir inhibits cytochrome P450-3A4 (CYP3A4) enzyme, which is known to deactivate protease inhibitors; hence, its main value in the treatment of HIV is by blocking the metabolic breakdown of other drugs, such as lopinavir by acting as a booster drug.^{63,64}

Drug combinations using three or more inhibitors that target different viral enzymes or stages in the HIV life cycle (known as the highly active antiretroviral therapy, HAART) turned HIV/AIDS into a manageable chronic disease.⁶⁵ However, in spite of the success of the HAART therapy, HIV/AIDS remains incurable. Additionally, due to the long duration of treatment (that also results in poor compliance of patients), the current regimen is still plagued with problems, such as the emergence of drug-resistant viral strains and adverse side effects. Hence, there is a continued interest in developing new therapeutic agents with different mechanisms of action from those currently in use that would help address drug resistance and complement the existing regimens.

It is noteworthy that of the nearly 30 antiretrovirals approved for use in HIV therapy, the majority of these drugs are directed toward HIV-1 reverse transcriptase (HIV-1 RT), underscoring the importance of this virally-encoded enzyme as an important therapeutic target. The following sections of this chapter will focus on HIV-1 RT and its polymerase catalytic mechanism as the target for the development of new therapies against HIV infection.

1.5. HIV-1 RT Structure and Function

RT is a heterodimeric, multifunctional enzyme composed of a 66 kDa (p66) and 51 kDa (p51) subunit. The p66 accommodates both the catalytically active polymerase and the RNase H domains whereas the p51 only provides structural support for the enzyme.^{66, 67} Similar with other nucleic

acid processing enzymes, the polymerase domain resembles a right hand that traps the nucleic acid substrate through its fingers, palm, and thumb subdomains.⁶⁸ The synthesis of proviral DNA is mediated by both the RNA- and DNA-dependent DNA polymerase activities starting from a viral genomic RNA as the template. On the other hand, the C-terminal RNase H domain, which is about 60 Å away from the polymerase active site catalyzes the specific cleavage of the RNA portion of the RNA:DNA duplex formed during the reverse transcription process. Both the polymerase and RNase H active sites are characterized by having a number of highly conserved acidic residues within their pockets that coordinate two divalent metal cofactors that are critical for catalysis.^{68,69}

The mechanism of DNA polymerization mediated by RT polymerase proceeds in a similar fashion as with other polymerases. Once RT binds to the primer/template (P/T) hybrid, DNA synthesis starts by binding of an incoming nucleotide (dNTP) to the nucleotide binding site (N-site) forming a ternary complex (**Fig. 1.8**). Through a conformational change (*via* closing of the fingers domain), a stabilized ternary complex results, which is followed by the catalytic reaction. During catalysis, two Mg²⁺ ions coordinate to the active site aspartate residues (D110, D185, and D186) and with the phosphate groups of dNTP, and assist in the correct positioning of the 3'-OH group of the primer terminus for nucleophilic attack (**Fig. 1.9**).^{66,70} A new phosphodiester bond is formed that is accompanied by the release of inorganic pyrophosphate (PPi). The final stage is translocation. When the N-site is occupied, the RT P/T complex is in the pre-translocation conformation and in order to incorporate the next dNTP, the enzyme must slide by a single nucleotide from the N-site to the adjacent priming site (P-site) resulting to the post-translocation state. At this stage, the N-site is available again to accept the next dNTP to continue with the elongation of viral DNA.^{71,72}

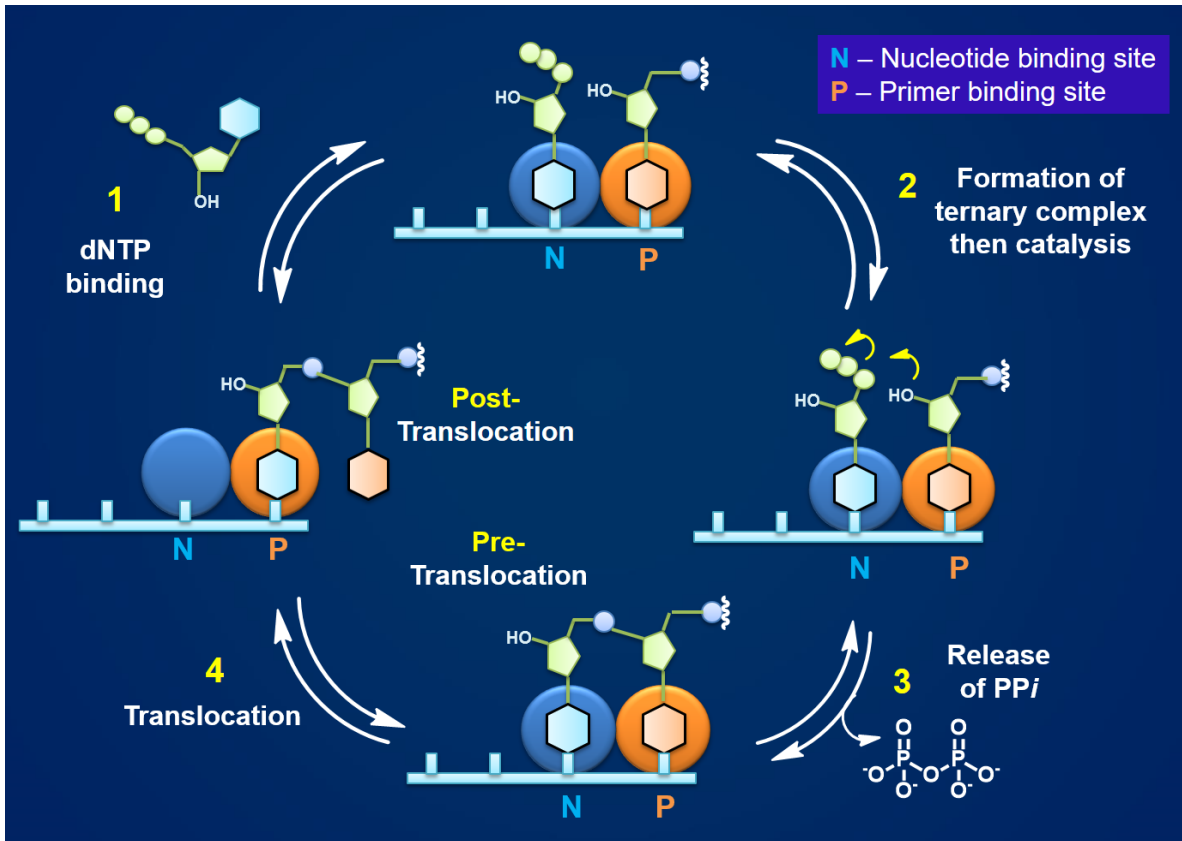


Figure 1.8. Representation of RT-catalyzed DNA polymerization cycle described in the text.

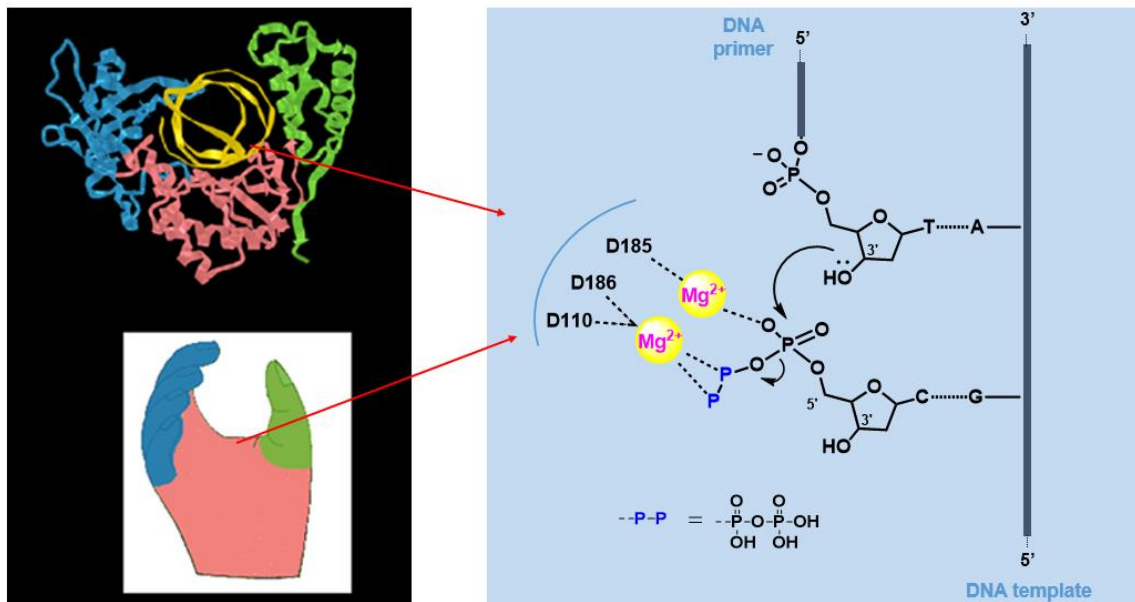


Figure 1.9. Two-metal ion mechanism of RT polymerase. The active site is located in the middle of the palm, fingers, and thumb subdomains. Left image was from: <http://www.psc.edu/science>.

1.6. Examples of Clinically Approved Inhibitors of HIV-1 RT

Approximately half of the currently available drugs for HIV are inhibitors of RT polymerase. Although some inhibitors of the RNase H function of RT have also been reported, none of these compounds have reached clinical development. The two main classes of RT antivirals are the nucleosides/nucleotides (NRTIs) and the non-nucleosides (NNRTIs) drugs; the latter are allosteric inhibitors of RT. Two NRTIs, in combination with either an NNRTI or inhibitors targeting another virally-encoded enzyme, such as a protease or integrase inhibitor are the typical compositions of HAART.

The NRTIs (examples shown in **Fig. 1.10**) are structural mimics of the natural dNTP substrates but lack the 3'-hydroxyl group on the sugar ring or differ in conformation from the natural dNTPs. These compounds are incorporated into the growing viral oligonucleotide chain, but then act as “chain terminators.”^{5,73} The nucleoside analogs AZT and 3TC are the early members of this class of RT inhibitors, and more recently, the nucleotide analog, tenofovir was developed (**Fig. 1.10**). These NRTIs have to be converted to their corresponding triphosphate derivatives by cellular kinases in order to inhibit reverse transcription (illustrated in **Fig. 1.11**).⁵ Tenofovir was designed to bypass the first kinase phosphorylation, which is believed to be the rate limiting step of the bioactivation, but has to be administered as a prodrug (as mentioned previously) in order to improve oral bioavailability and cellular uptake.⁴⁴

While use of NRTIs is central in HAART, one of the main problems, in addition to drug resistance is their relatively low selectivity between viral and host polymerase enzymes (e.g. mitochondrial polymerase γ) that can lead to toxic side effects.⁷⁴

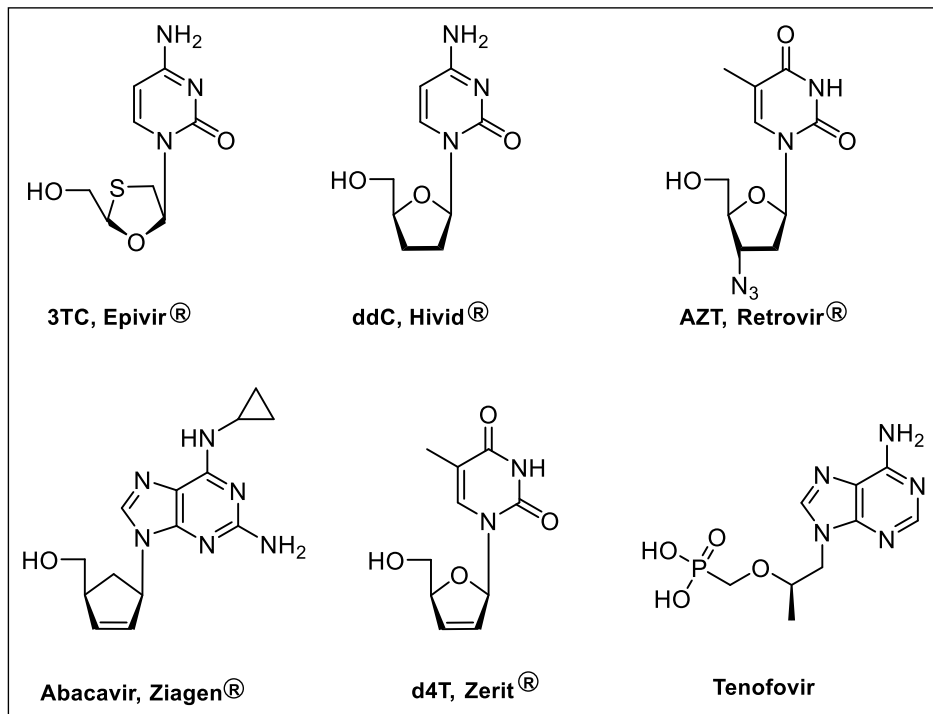


Figure 1.10. Examples of clinically approved NRTIs.

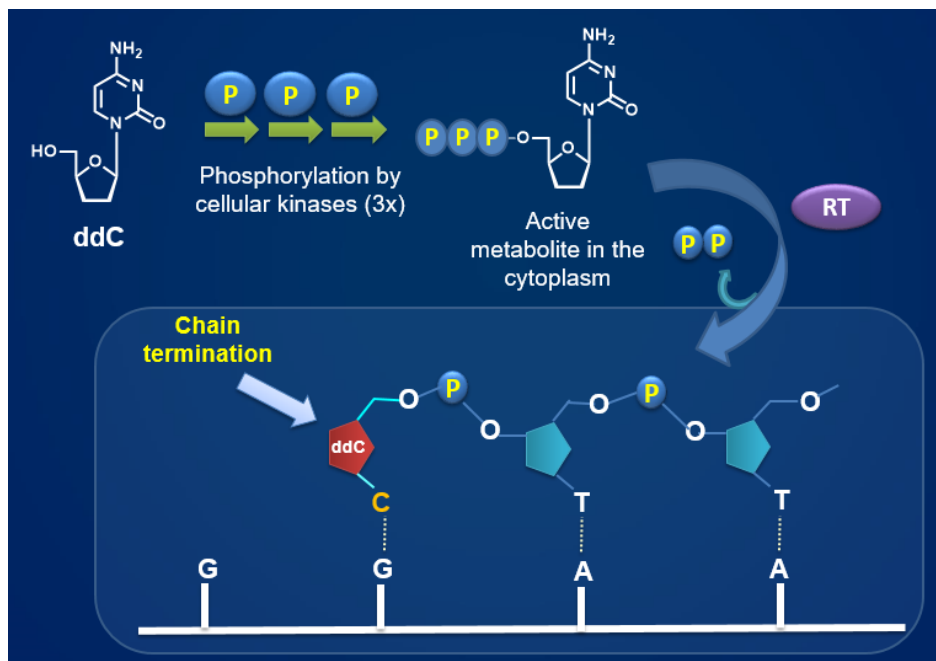


Figure 1.11. Mechanism of action of NRTIs. Upon phosphorylation, these compounds are incorporated as substrates of the growing oligonucleotide but the absence of 3'-OH leads to chain termination.

The second class of RT inhibitors, NNRTIs are more structurally and chemically diverse compounds (examples are given in **Fig. 1.12**) that bind to an allosteric pocket of the enzyme (about 10 Å away from the polymerase active site) and function as non-competitive inhibitors of the polymerase activity.⁷⁵ Through crystallographic and modeling studies, the early generation NNRTIs (e.g. nevirapine; **Fig. 1.12**) have been proposed to adopt a “butterfly-like” conformation that interact with the allosteric pocket *via* hydrophobic, π stacking, and H-bonding interactions.⁷⁶ However, these compounds are more susceptible to inducing drug-resistant mutations, such as Y181C and Y188C that disrupt their key hydrophobic interactions with the binding pocket. New generation NNRTIs, such as etravirine have been shown to exhibit an increased barrier to resistance (*i.e.* multiple mutations must be present before resistance is observed).⁷³

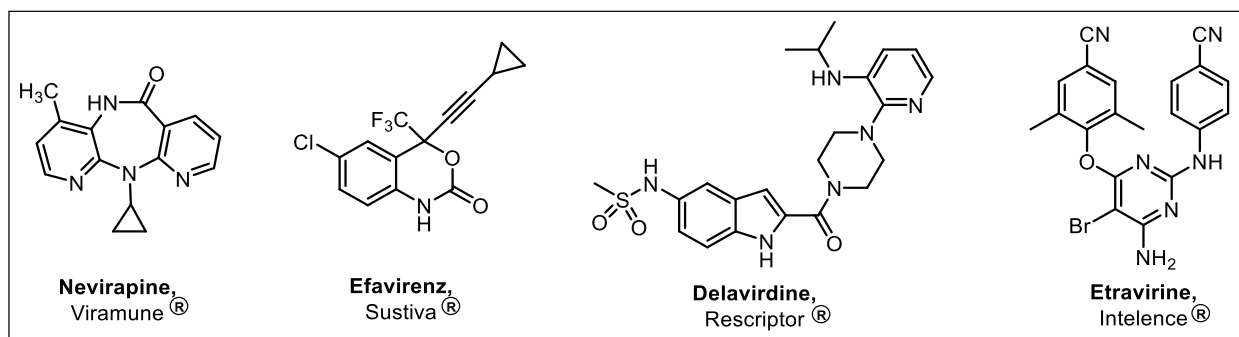


Figure 1.12. Examples of NNRTIs that bind at the allosteric pocket in the palm domain.

1.7. NRTI Drug Resistance

Drug resistance, which occurs rapidly with monotherapy and even during a long-term use of combination drugs with varied mechanism of action, is one of the major setbacks in the treatment of HIV infection. The high genetic drift, low proofreading ability, and poor fidelity of RT in incorporating its substrate contribute to the rapid emergence of viral clones and drug resistance.^{77,78}

Resistance to NRTIs can involve two distinct mechanisms: (1) discrimination in substrate binding and (2) excision.⁷⁹ Discrimination reduces the incorporation of the NRTI drug in favor of the natural dNTPs. For example, the M184I/V mutation that confers resistance towards 3TC and FTC has been explained using *in silico* studies showing that the branched side chain of an isoleucine or a valine residue inside the binding site and at the location of methionine 184 creates a steric clash with the sulfur atom of the oxathiolane ring, blocking the binding of the mentioned drugs.⁸⁰ Similarly, another mutation, K65R also discriminates against the incorporation of NRTIs, such as tenofovir, abacavir, and 3TC. K65 is believed to interact with the γ phosphate of the nucleotide for proper positioning and incorporation into the growing DNA chain.⁸¹ Substitution with arginine at residue 65 results in restricted conformational adaptability of the polymerase protein (due to the interaction between R65 and R72) and compromise the positioning and binding of the susceptible drugs.⁸² The second mechanism of resistance, known as thymidine analogue mutations (TAMs) facilitates the phosphorolytic excision of the incorporated drug at the 3'-end of the DNA primer strand. TAMs confer high-level of resistance to AZT.^{83, 84} The phosphorolysis is thought to be mediated by PP_i ⁸⁵ or a PP_i donor, such as ATP⁸³ and occurs when the AZT chain-terminated primer occupies the N-site or when RT is in the pre-translocated state (illustrated in **Fig. 1.13**).^{71,72} It has been also reported that the conformation of the sugar moiety (*i.e.* the pucker preference) of the nucleotide can influence excision. For example, North-puckered nucleotides prefer to occupy the P-site and are resistant to excision, whereas South-puckered nucleotides favor the N-site and are efficiently excised (**Fig. 1.14**).⁸⁶ NRTI excision ultimately lead to the rescue of the elongation of viral DNA.

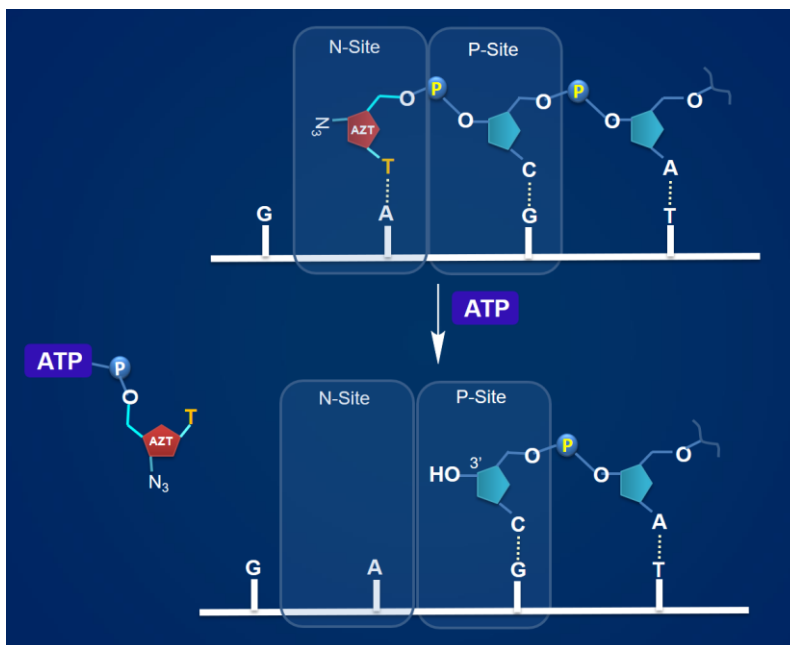


Figure 1.13. Illustration of the ATP-mediated excision of the drug AZT leading to the release of AZT-ATP (5',5'-adduct) and availability of 3'-OH at the primer terminus to continue with DNA synthesis.

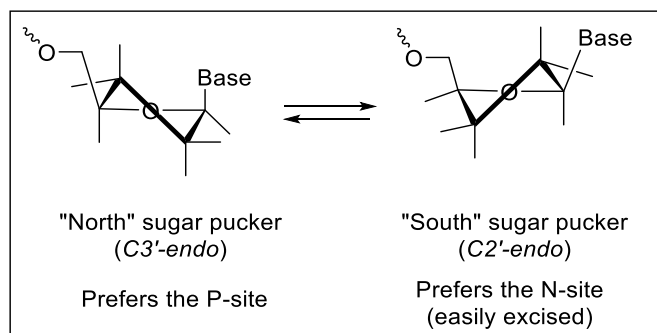


Figure 1.14. Representation of North and South sugar pucker conformations. DNA primers containing South-puckered nucleotide at the 3'-terminus tend to occupy the N-site and are susceptible to undergo phosphorolytic excision.⁸⁶

1.8. New Class of Active Site Inhibitors Targeting the Translocation of HIV-1 RT

Potent HIV-1 RT polymerase inhibitors that operate *via* an alternative mode of inhibition are likely to evade the current clinically relevant drug-resistant HIV mutants and/or elicit better resistance

profile, thus providing new therapeutic options in treating this infection. It should be noted that there are no true polymerase active site inhibitors of HIV-1 RT that are currently approved for clinical use; NRTIs are substrate mimics that act as chain terminators and are not considered “true” active site inhibitors of the enzyme.

Chemically distinct compounds have been reported that target the translocation stage of the RT-catalyzed DNA polymerization cycle and are potential *bonafide* active site inhibitors. The pyrophosphate analog, phosphonoformic acid (PFA, foscarnet; **Fig. 1.15**) is a broad-spectrum antiviral that has been shown to inhibit the DNA polymerases of herpes viruses and retroviruses.^{87,88} A long time ago, PFA was used to treat cytomegalovirus (CMV) retinitis and viral diseases caused by herpes simplex viruses (*via* intravenous administration). However, due to its poor selectivity and high toxicity, its use as a therapeutic agent has been mainly discontinued. In extremely exceptional cases, PFA may be used only as part of salvage therapy when all other alternative forms of treatment are found to be unsuccessful. PFA inhibits DNA polymerases by acting as a mimic of the pyrophosphate by-product of the nucleotide transfer reaction. The crystal structure of chimeric human cytomegalovirus (HCMV) polymerase in complex with its nucleic acid substrates and PFA⁸⁹ and the recent crystal structure of HIV-1 RT/DNA aptamer in complex with PFA⁹⁰ corroborate with this type of inhibition. In-depth mechanistic investigations by the group of Mathias Götte revealed that PFA inhibits RT by freezing the RT pre-translocation conformation (*via* metal-mediated interactions), which prevent the binding of the next dNTP and consequently, terminate viral DNA synthesis.⁹¹ Interest in the mechanism of action of PFA stems from reports indicating that the majority of currently known NRTI and NNRTI mutations do not alter its efficacy in inhibiting the HIV-1 RT polymerase.^{92, 93} Moreover, biochemical data have also shown that mutations leading to PFA resistance diminish the phosphorolytic removal of AZT

from the 3'-end of the oligonucleotide chain, thus providing therapeutic compensation when PFA is used in combination with AZT.⁹⁴ Additionally, bisphosphonate compounds have been also reported to prevent excision of AZT.^{95,96}

With the aim of identifying new molecules that exhibit a PFA-like mechanism in inhibiting the HIV-1 RT polymerase catalytic activity, derivatives of 4-chlorophenylhydrazone of mesoxalic acid (CPHM; **Fig. 1.15**) were recently reported.⁹⁷ Mechanistic investigations with this compound provided further support for targeting specifically the pre-translocation complex as a novel mechanism of RT inhibitors. Although CPHM was previously described as an inhibitor of HIV-1 RT associated RNase H activity,^{98,99} later studies found that the observed activity in RNase H was an indirect consequence of the stable complex that forms when CPHM binds to the polymerase active site.^{97,100} In addition, CPHM was reported to exhibit some target selectivity towards HIV-1 RT and was found to be inactive toward inhibiting the human cytomegalovirus (HCMV) polymerase.⁹⁷ However, CPHM is also not a “drug-like” compound and lacks chemical stability and cell-based antiviral activity. Nevertheless, compounds, such as PFA and CPHM have served as prototype compounds in investigating the mechanism of RT translocation and could be considered as “hits” for further optimization into highly potent inhibitors with good biopharmaceutical properties.

Compounds that trap the post-translocated state of RT have also been identified. The indolopyridone-based compound, INDOPY-1 (**Fig 1.15**) discovered in 2006 through high-throughput screening was the first compound to display this mode of inhibition.¹⁰¹ In spite of the significant difference in the chemical structure from natural dNTPs, INDOPY-1 has been suggested to compete with natural dNTPs for binding at the N-site of the post-translocated

complex, hence also referred as nucleotide competing reverse transcriptase inhibitors (NcRTIs). In 2013, researchers from Boehringer Ingelheim reported a new series of NcRTIs with optimized antiviral activity and distinct resistance profile. For example, compound **1.13** was found to be a very potent inhibitor of HIV-1 replication in cell-based assays with an EC₅₀ of 1.5 nM that remains active against viruses encoding M184V mutation (unlike INDOPY-1).¹⁰² In a separate study, Balzarini and co-workers disclosed a new generation of NcRTIs that are more reminiscent of natural nucleotides.¹⁰³ Analogs of α -carboxy nucleoside phosphonates (α -CNPs; **Fig. 1.15**) were reported to function as universal mimics of nucleoside triphosphate that do not require metabolic activation (*i.e.* phosphorylation) and inhibit a variety of DNA polymerases.^{103,104} For example, compound **1.14** was also found to operate by stabilizing the RT post-translocated state *via* metal-mediated interactions. Similar to NRTIs, α -CNPs are sensitive to RT mutations adjacent to its pseudo sugar ring, such as M184V. However, enhanced target selectivity and cell-membrane permeability must be achieved before analogs, such as **1.14**, can be considered as leads for drug discovery.

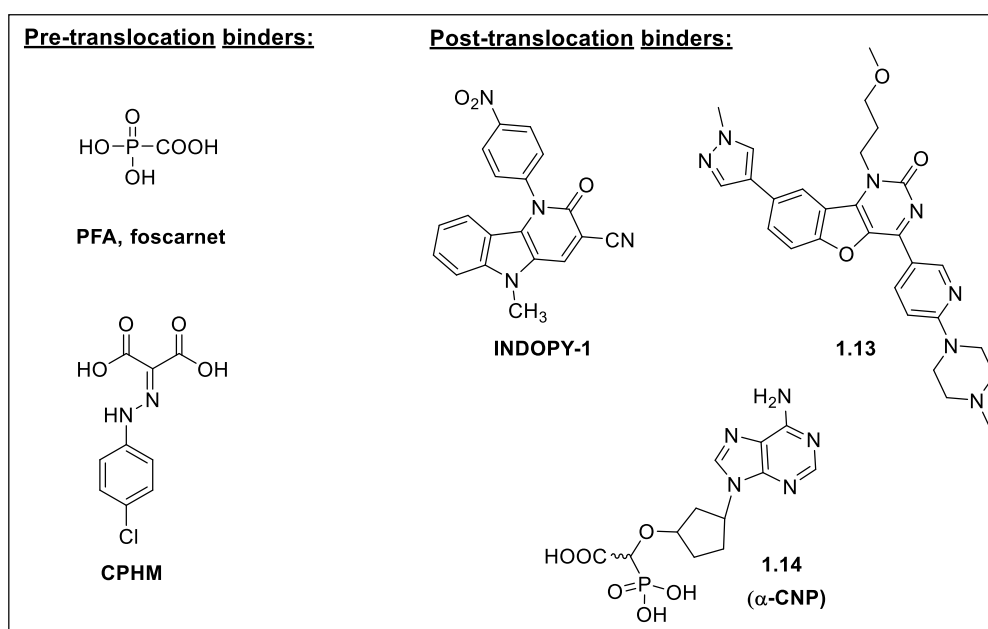


Figure 1.15. New classes of inhibitors that target the translocation status of HIV-1 RT.

The mechanistic information relating to the inhibition of RT translocation was elucidated through an established site-specific footprinting technique that generate radicals and produce site-specific cuts to the oligonucleotide, which allows tracking of the position of RT on its nucleic acid substrate through single-nucleotide resolution.^{71, 91} The iron-mediated method is one way to do such studies wherein Fe^{2+} ions are incubated with the RT/oligonucleotide complex and bind in close proximity to the RNase H active site of RT. Fenton-like chemistry is used to generate a local concentration of hydroxyl radicals. These radicals lead to a specific cleavage of the template strand 18 nucleotides away from the N-site (in the case of pre-translocation) or 17 nucleotides away (in the case of post-translocation). The oligonucleotide products of these radical-mediated cleavage can be resolved by gel electrophoresis. As depicted in **Fig. 1.16**, in the absence of an inhibitor (lane 2), two bands of almost equal intensity are typically observed, representing the equilibrium between the pre- and post-translocation complexes (a minor cut at -19 is also typically seen as an artefact of the iron-mediated method). In the presence of an inhibitor that stabilizes the pre-translocation complex (e.g. PFA; **Fig. 1.16** lane 4), only the band that corresponds to the “trapped” pre-translocation complex is primarily visible.

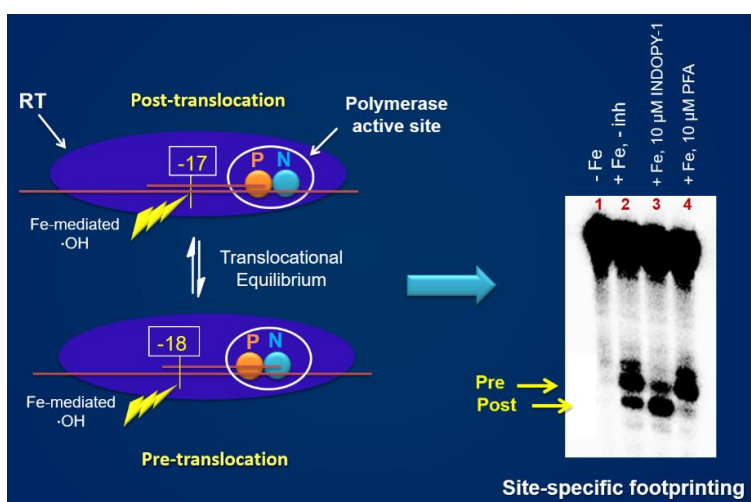


Figure 1.16. Representation of the iron-mediated site specific footprinting used to investigate the mechanism of action. The gel image shows the cleavage fragments corresponding to pre- and post-

translocation complexes in the absence of inhibitor (lane 2). Addition of INDOPY-1 and PFA, resulted to the “freezing” of post- (lane 3) and pre- (lane 4) translocated states, respectively.

1.9. Research Goals (Part 1)

The increasing knowledge and understanding of the pathogenesis of HIV infection has opened tremendous opportunities in the management of the disease. The function of HIV-1 RT, in particular has proven to be central in the development of antiviral agents with clinical efficacy. RT continues to be an indispensable target, specifically of novel small molecules with innovative modes of inhibition that can provide added benefits in the current therapies.

To date, clinically validated “true” active site inhibitors of HIV-1 RT polymerase are not available. NRTIs act primarily as chain terminators that require both metabolic activation and covalent bond formation in the growing viral oligonucleotide chain. The underexplored translocation inhibitors that can bind directly and reversibly in the polymerase active site without being incorporated into the nucleic acids are promising active site inhibitors of HIV-1 RT. Specifically, pyrophosphate analogs that can “freeze” RT pre-translocation or post-translocation selectively are of current interest given their potential application in combination therapy and their anticipated high potential to overcome the resistance observed with the current drugs.

Our goals for the first part of the thesis are to develop HIV-1 RT inhibitors with PFA- or CPHM-like mechanism of action. In **Chapter 2**, we explored the potential of pyrido[2,3-*d*]pyrimidine bisphosphonates (PYPY-BPs) in inhibiting the function of HIV-1 RT. The bisphosphonate moiety is a more stable mimic of pyrophosphate and the purine-like pyridopyrimidines can serve as the specificity domain. Unlike PFA which lacks drug-like properties, PYPY-BPs are highly elaborated compounds that can be further optimized into novel antiviral agents. The modular synthesis,

preliminary SAR studies, and biochemical evaluation of PYPY-BPs using a primer extension scintillation proximity assay (SPA), both in wild-type and mutant enzymes are presented. Preliminary characterization of the mode of inhibition showed that the PYPY-BPs exhibit a mixed-type of inhibition and their main mechanism of action appears to be different from that of PFA and CPHM. In our subsequent studies, compounds containing the diketo acid (DKA) bioisostere, pyrimidinol carboxylic acid as the metal-chelating pharmacophore were discovered to display the desired mechanism. These compounds are of primary interest because unlike PFA and CPHM, they have significantly better drug-like properties. The synthesis, preliminary SAR, selectivity studies (against RT-associated RNase H), and other biochemical profiling studies, including the evaluation of mechanism of action *via* iron-mediated site specific footprinting, are detailed in **Chapter 3**.

1.10. References

1. Cowan, J. A. Metal activation of enzymes in nucleic acid biochemistry. *Chem. Rev.* **1998**, 98, 1067-1088.
2. Rogolino, D.; Carcelli, M.; Sechi, M.; Neamati, N. Viral enzymes containing magnesium: Metal binding as a successful strategy in drug design. *Coord. Chem. Rev.* **2012**, 256, 3063-3086.
3. Park, J.; Matralis, A.; Berghuis, A. M.; Tsantrizos, Y. S. Human isoprenoid synthase enzymes as therapeutic targets. *Front. Chem.* **2014**, 2, 1-21.
4. Loeb, L. A.; Monnat, R. J. DNA polymerases and human disease. *Nat. Rev. Genet.* **2008**, 9, 594-604.
5. Clercq, E. D. The design of drugs for HIV and HCV. *Nat. Rev. Drug Discov.* **2007**, 6, 1001-1018.
6. Zhan, P.; Pannecouque, C.; De Clercq, E.; Liu, X. Anti-HIV drug discovery and development: Current innovations and future trends. *J. Med. Chem.* **2016**, 59, 2849-2878.

7. te Velthuis, A. J. W.; Fodor, E. Influenza virus RNA polymerase: insights into the mechanisms of viral RNA synthesis. *Nat. Rev. Micro.* **2016**, 14, 479-493.
8. De Francesco, R.; Tomei, L.; Altamura, S.; Summa, V.; Migliaccio, G. Approaching a new era for hepatitis C virus therapy: inhibitors of the NS3-4A serine protease and the NS5B RNA-dependent RNA polymerase. *Antiviral Res.* **2003**, 58, 1-16.
9. Beaulieu, P. L.; Bös, M.; Cordingley, M. G.; Chabot, C.; Fazal, G.; Garneau, M.; Gillard, J. R.; Jolicoeur, E.; LaPlante, S.; McKercher, G.; Poirier, M.; Poupart, M.-A.; Tsantrizos, Y. S.; Duan, J.; Kukulj, G. Discovery of the first thumb pocket 1 NS5B polymerase inhibitor (BILB 1941) with demonstrated antiviral activity in patients chronically infected with genotype 1 hepatitis C virus (HCV). *J. Med. Chem.* **2012**, 55, 7650-7666.
10. Oldfield, E. Targeting isoprenoid biosynthesis for drug discovery: Bench to bedside. *Acc. Chem. Res.* **2010**, 43, 1216-1226.
11. Holstein, S. A. Chapter 12 - The isoprenoid biosynthetic pathway and statins. In *The Enzymes*, Christine A. Hrycyna, M. O. B.; Fuyuhiko, T., Eds. Academic Press: 2011; Vol. 30, pp 279-299.
12. Friedman, H. L. Influence of isosteric replacements upon biological activity. In *First Symposium on Chemical-biological Correlation, May 26-27, 1950*. National Academy of Sciences, National Research Council Publication No. 206, Washington, D.C., pp. 295-362: 1951.
13. Meanwell, N. A. Synopsis of some recent tactical application of bioisosteres in drug design. *J. Med. Chem.* **2011**, 54, 2529-2591.
14. Nottbohm, A. C.; Hergenrother, P. J.; Begley, T. P. Phosphate mimics: Cyclic compounds. In *Wiley Encyclopedia of Chemical Biology*, John Wiley & Sons, Inc.: 2008., pp 1-16.
15. Elliott, T. S.; Slowey, A.; Ye, Y.; Conway, S. J. The use of phosphate bioisosteres in medicinal chemistry and chemical biology. *Med. Chem. Commun.* **2012**, 3, 735-751.
16. Di Santo, R. Inhibiting the HIV integration process: Past, present, and the future. *J. Med. Chem.* **2014**, 57, 539-566.
17. Romanenko, V. D.; Kukhar, V. P. Fluorinated phosphonates: Synthesis and biomedical application. *Chem. Rev.* **2006**, 106, 3868-3935.
18. Holmes, C. P.; Li, X.; Pan, Y.; Xu, C.; Bhandari, A.; Moody, C. M.; Miguel, J. A.; Ferla, S. W.; De Francisco, M. N.; Frederick, B. T.; Zhou, S.; Macher, N.; Jang, L.; Irvine, J. D.;

- Grove, J. R. PTP1B inhibitors: Synthesis and evaluation of difluoromethylenephosphonate bioisosteres on a sulfonamide scaffold. *Bioorg. Med. Chem. Lett.* **2008**, 18, 2719-2724.
19. Branchini, B. R.; Murtiashaw, M. H.; Carmody, J. N.; Mygatt, E. E.; Southworth, T. L. Synthesis of an N-acyl sulfamate analog of luciferyl-AMP: A stable and potent inhibitor of firefly luciferase. *Bioorg. Med. Chem. Lett.* **2005**, 15, 3860-3864.
 20. Combs, A. P. Recent advances in the discovery of competitive protein tyrosine phosphatase 1B inhibitors for the treatment of diabetes, obesity, and cancer. *J. Med. Chem.* **2010**, 53, 2333-2344.
 21. Yue, E. W.; Wayland, B.; Douty, B.; Crawley, M. L.; McLaughlin, E.; Takvorian, A.; Wasserman, Z.; Bower, M. J.; Wei, M.; Li, Y.; Ala, P. J.; Gonneville, L.; Wynn, R.; Burn, T. C.; Liu, P. C. C.; Combs, A. P. Isothiazolidinone heterocycles as inhibitors of protein tyrosine phosphatases: Synthesis and structure–activity relationships of a peptide scaffold. *Bioorg. Med. Chem.* **2006**, 14, 5833-5849.
 22. Cho, H. Chapter 17 - Protein tyrosine phosphatase 1B (PTP1B) and obesity. In *Vitamins & Hormones*, Gerald, L., Ed. Academic Press: 2013; Vol. Volume 91, pp 405-424.
 23. Peukert, S.; Sun, Y.; Zhang, R.; Hurley, B.; Sabio, M.; Shen, X.; Gray, C.; Dzink-Fox, J.; Tao, J.; Cebula, R.; Wattanasin, S. Design and structure–activity relationships of potent and selective inhibitors of undecaprenyl pyrophosphate synthase (UPPS): Tetramic, tetric acids and dihydropyridin-2-ones. *Bioorg. Med. Chem. Lett.* **2008**, 18, 1840-1844.
 24. Summa, V.; Petrocchi, A.; Bonelli, F.; Crescenzi, B.; Donghi, M.; Ferrara, M.; Fiore, F.; Gardelli, C.; Gonzalez Paz, O.; Hazuda, D. J.; Jones, P.; Kinzel, O.; Laufer, R.; Monteagudo, E.; Muraglia, E.; Nizi, E.; Orvieto, F.; Pace, P.; Pescatore, G.; Scarpelli, R.; Stillmock, K.; Witmer, M. V.; Rowley, M. Discovery of raltegravir, a potent, selective orally bioavailable HIV-integrase inhibitor for the treatment of HIV-AIDS infection. *J. Med. Chem.* **2008**, 51, 5843-5855.
 25. Hare, S.; Gupta, S. S.; Valkov, E.; Engelman, A.; Cherepanov, P. Retroviral intasome assembly and inhibition of DNA strand transfer. *Nature* **2010**, 464, 232-236.
 26. Summa, V.; Petrocchi, A.; Pace, P.; Matassa, V. G.; De Francesco, R.; Altamura, S.; Tomei, L.; Koch, U.; Neuner, P. Discovery of α,γ -diketo acids as potent, selective and

- reversible inhibitors of Hepatitis C virus NS5b RNA-dependent RNA polymerase. *J. Med. Chem.* **2004**, 47, 14-17.
27. Summa, V.; Petrocchi, A.; Matassa, V. G.; Taliani, M.; Laufer, R.; De Francesco, R.; Altamura, S.; Pace, P. HCV NS5b RNA-dependent RNA polymerase inhibitors: From α,γ -diketoacids to 4,5-dihydropyrimidine- or 3-methyl-5- hydroxypyrimidinonecarboxylic acids. Design and synthesis. *J. Med. Chem.* **2004**, 47, 5336-5339.
28. Sato, M.; Motomura, T.; Aramaki, H.; Matsuda, T.; Yamashita, M.; Ito, Y.; Kawakami, H.; Matsuzaki, Y.; Watanabe, W.; Yamataka, K.; Ikeda, S.; Kodama, E.; Matsuoka, M.; Shinkai, H. Novel HIV-1 integrase inhibitors derived from quinolone antibiotics. *J. Med. Chem.* **2006**, 49, 1506-1508.
29. Sato, M.; Kawakami, H.; Motomura, T.; Aramaki, H.; Matsuda, T.; Yamashita, M.; Ito, Y.; Matsuzaki, Y.; Yamataka, K.; Ikeda, S.; Shinkai, H. Quinolone carboxylic acids as a novel monoketo acid class of human immunodeficiency virus type 1 integrase inhibitors. *J. Med. Chem.* **2009**, 52, 4869-4882.
30. Johns, B. A.; Kawasuji, T.; Taishi, T.; Taoda, Y. Polycyclic carbamoylpyridone derivative having HIV integrase inhibitory activity. US 2009/0318421 A1.
31. Agrawal, A.; DeSoto, J.; Fullagar, J. L.; Maddali, K.; Rostami, S.; Richman, D. D.; Pommier, Y.; Cohen, S. M. Probing chelation motifs in HIV integrase inhibitors. *Proc. Natl. Acad. Sci.* **2012**, 109, 2251-2256.
32. Pradere, U.; Garnier-Amblard, E. C.; Coats, S. J.; Amblard, F.; Schinazi, R. F. Synthesis of nucleoside phosphate and phosphonate prodrugs. *Chem. Rev.* **2014**, 114, 9154-9218.
33. Thornton, P. J.; Kadri, H.; Miccoli, A.; Mehellou, Y. Nucleoside phosphate and phosphonate prodrug clinical candidates. *J. Med. Chem.* **2016**, ASAP, doi: 10.1021/acs.jmedchem.6b00523.
34. Mehellou, Y.; Balzarini, J.; McGuigan, C. Aryloxy phosphoramidate triesters: A technology for delivering monophosphorylated nucleosides and sugars into cells. *ChemMedChem* **2009**, 4, 1779-1791.
35. Sofia, M. J.; Bao, D.; Chang, W.; Du, J.; Nagarathnam, D.; Rachakonda, S.; Reddy, P. G.; Ross, B. S.; Wang, P.; Zhang, H.-R.; Bansal, S.; Espiritu, C.; Keilman, M.; Lam, A. M.; Steuer, H. M. M.; Niu, C.; Otto, M. J.; Furman, P. A. Discovery of a β -d-2'-Deoxy-2'- α -

- fluoro-2'- β -C-methyluridine nucleotide prodrug (PSI-7977) for the treatment of hepatitis C virus. *J. Med. Chem.* **2010**, *53*, 7202-7218.
36. Lee, W. A.; He, G.-X.; Eisenberg, E.; Cihlar, T.; Swaminathan, S.; Mulato, A.; Cundy, K. C. Selective intracellular activation of a novel prodrug of the human immunodeficiency virus reverse transcriptase inhibitor tenofovir leads to preferential distribution and accumulation in lymphatic tissue. *Antimicrob. Agents Chemother.* **2005**, *49*, 1898-1906.
37. Bhatia, H.; Singh, H.; Grewal, N.; Natt, N. Sofosbuvir: A novel treatment option for chronic hepatitis C infection. *J. Pharmacol. Pharmacother.* **2014**, *5*, 278-284.
38. Callebaut, C.; Stepan, G.; Tian, Y.; Miller, M. D. In vitro virology profile of tenofovir alafenamide, a novel oral prodrug of tenofovir with improved antiviral activity compared to that of tenofovir disoproxil fumarate. *Antimicrob. Agents Chemother.* **2015**, *59*, 5909-5916.
39. Murakami, E.; Wang, T.; Park, Y.; Hao, J.; Lepist, E.-I.; Babusis, D.; Ray, A. S. Implications of efficient hepatic delivery by tenofovir alafenamide (GS-7340) for hepatitis B virus therapy. *Antimicrob. Agents Chemother.* **2015**, *59*, 3563-3569.
40. Warren, T. K.; Jordan, R.; Lo, M. K.; Ray, A. S.; Mackman, R. L.; Soloveva, V.; Siegel, D.; Perron, M.; Bannister, R.; Hui, H. C.; Larson, N.; Strickley, R.; Wells, J.; Stuthman, K. S.; Van Tongeren, S. A.; Garza, N. L.; Donnelly, G.; Shurtleff, A. C.; Retterer, C. J.; Gharaibeh, D.; Zamani, R.; Kenny, T.; Eaton, B. P.; Grimes, E.; Welch, L. S.; Gomba, L.; Wilhelmsen, C. L.; Nichols, D. K.; Nuss, J. E.; Nagle, E. R.; Kugelman, J. R.; Palacios, G.; Doerffler, E.; Neville, S.; Carra, E.; Clarke, M. O.; Zhang, L.; Lew, W.; Ross, B.; Wang, Q.; Chun, K.; Wolfe, L.; Babusis, D.; Park, Y.; Stray, K. M.; Trancheva, I.; Feng, J. Y.; Barauskas, O.; Xu, Y.; Wong, P.; Braun, M. R.; Flint, M.; McMullan, L. K.; Chen, S.-S.; Fearn, R.; Swaminathan, S.; Mayers, D. L.; Spiropoulou, C. F.; Lee, W. A.; Nichol, S. T.; Cihlar, T.; Bavari, S. Therapeutic efficacy of the small molecule GS-5734 against Ebola virus in rhesus monkeys. *Nature* **2016**, *531*, 381-385.
41. McGuigan, C.; Murziani, P.; Slusarczyk, M.; Gonczy, B.; Vande Voorde, J.; Liekens, S.; Balzarini, J. Phosphoramidate ProTides of the anticancer agent FUDR successfully deliver the preformed bioactive monophosphate in cells and confer advantage over the parent nucleoside. *J. Med. Chem.* **2011**, *54*, 7247-7258.

42. Slusarczyk, M.; Lopez, M. H.; Balzarini, J.; Mason, M.; Jiang, W. G.; Blagden, S.; Thompson, E.; Ghazaly, E.; McGuigan, C. Application of ProTide technology to gemcitabine: A successful approach to overcome the key cancer resistance mechanisms leads to a new agent (NUC-1031) in clinical development. *J. Med. Chem.* **2014**, *57*, 1531-1542.
43. Acelarin. <http://www.nucanabiomed.com/acelarin.html>. September 2016.
44. Kearney, B. P.; Flaherty, J. F.; Shah, J. Tenofovir disoproxil fumarate. *Clinical Pharmacokinetics* **2004**, *43*, 595-612.
45. Annaert, P.; Tukker, J. J.; Van Gelder, J.; Naesens, L.; De Clercq, E.; Van den Mooter, G.; Kinget, R.; Augustijns, P. In vitro, ex vivo, and in situ intestinal absorption characteristics of the antiviral ester prodrug adefovir dipivoxil. *J. Pharm. Sci.* **2000**, *89*, 1054-1062.
46. Hiyoshi, H.; Yanagimachi, M.; Ito, M.; Ohtsuka, I.; Yoshida, I.; Saeki, T.; Tanaka, H. Effect of ER-27856, a novel squalene synthase inhibitor, on plasma cholesterol in rhesus monkeys: comparison with 3-hydroxy-3-methylglutaryl-CoA reductase inhibitors. *J. Lipid Res.* **2000**, *41*, 1136-1144.
47. Zhang, Y.; Leon, A.; Song, Y.; Studer, D.; Haase, C.; Koscielski, L. A.; Oldfield, E. Activity of nitrogen-containing and non-nitrogen-containing bisphosphonates on tumor cell lines. *J. Med. Chem.* **2006**, *49*, 5804-5814.
48. Wiemer, A. J.; Yu, J. S.; Shull, L. W.; Barney, R. J.; Wasko, B. M.; Lamb, K. M.; Hohl, R. J.; Wiemer, D. F. Pivaloyloxymethyl-modified isoprenoid bisphosphonates display enhanced inhibition of cellular geranylgeranylation. *Bioorg. Med. Chem.* **2008**, *16*, 3652-3660.
49. Foust, B. J.; Allen, C.; Holstein, S. A.; Wiemer, D. F. A new motif for inhibitors of geranylgeranyl diphosphate synthase. *Bioorg. Med. Chem.* **2016**, *24*, 3734-3741.
50. Birkus, G.; Bam, R. A.; Willkom, M.; Frey, C. R.; Tsai, L.; Stray, K. M.; Yant, S. R.; Cihlar, T. Intracellular activation of tenofovir alafenamide and the effect of viral and host protease inhibitors. *Antimicrob. Agents Chemother.* **2016**, *60*, 316-322.
51. Balzarini, J.; Karlsson, A.; Aquaro, S.; Perno, C. F.; Cahard, D.; Naesens, L.; De Clercq, E.; McGuigan, C. Mechanism of anti-HIV action of masked alaninyl d4T-MP derivatives. *Proc. Natl. Acad. Sci.* **1996**, *93*, 7295-7299.

52. Birkus, G.; Wang, R.; Liu, X.; Kutty, N.; MacArthur, H.; Cihlar, T.; Gibbs, C.; Swaminathan, S.; Lee, W.; McDermott, M. Cathepsin A is the major hydrolase catalyzing the intracellular hydrolysis of the antiretroviral nucleotide phosphonoamidate prodrugs GS-7340 and GS-9131. *Antimicrob. Agents Chemother.* **2007**, *51*, 543-550.
53. Congiatu, C.; Brancale, A.; McGuigan, C. Molecular modelling studies on the binding of some protides to the putative human phosphoramidase Hint1. *Nucleos. Nucleot. Nucl.* **2007**, *26*, 1121-1124.
54. Birkus, G.; Kutty, N.; Frey, C. R.; Shribata, R.; Chou, T.; Wagner, C.; McDermott, M.; Cihlar, T. Role of cathepsin A and lysosomes in the intracellular activation of novel antipapillomavirus agent GS-9191. *Antimicrob. Agents Chemother.* **2011**, *55*, 2166-2173.
55. Yuan, L.-C.; Dahl, T. C.; Oliyai, R. Degradation kinetics of oxycarbonyloxymethyl prodrugs of phosphonates in solution. *Pharm. Res.* **2001**, *18*, 234-237.
56. UNAIDS. Fact Sheet 2016. www.unaids.org. April 2016.
57. Engelman, A.; Cherepanov, P. The structural biology of HIV-1: mechanistic and therapeutic insights. *Nat. Rev. Micro.* **2012**, *10*, 279-290.
58. Kramer, V. G.; Schader, S. M.; Oliveira, M.; Colby-Germinario, S. P.; Donahue, D. A.; Singhroy, D. N.; Tressler, R.; Sloan, R. D.; Wainberg, M. A. Maraviroc and other HIV-1 entry inhibitors exhibit a class-specific redistribution effect that results in increased extracellular viral load. *Antimicrob. Agents Chemother.* **2012**, *56*, 4154-4160.
59. Dorr, P.; Westby, M.; Dobbs, S.; Griffin, P.; Irvine, B.; Macartney, M.; Mori, J.; Rickett, G.; Smith-Burchnell, C.; Napier, C.; Webster, R.; Armour, D.; Price, D.; Stammen, B.; Wood, A.; Perros, M. Maraviroc (UK-427,857), a potent, orally bioavailable, and selective small-molecule inhibitor of chemokine receptor CCR5 with broad-spectrum anti-human immunodeficiency virus type 1 activity. *Antimicrob. Agents Chemother.* **2005**, *49*, 4721-4732.
60. Matthews, T.; Salgo, M.; Greenberg, M.; Chung, J.; DeMasi, R.; Bolognesi, D. Enfuvirtide: the first therapy to inhibit the entry of HIV-1 into host CD4 lymphocytes. *Nat. Rev. Drug Discov.* **2004**, *3*, 215-225.
61. Hightower, K. E.; Wang, R.; DeAnda, F.; Johns, B. A.; Weaver, K.; Shen, Y.; Tomberlin, G. H.; Carter, H. L.; Broderick, T.; Sigethy, S.; Seki, T.; Kobayashi, M.; Underwood, M. R. Dolutegravir (S/GSK1349572) exhibits significantly slower dissociation than

- raltegravir and elvitegravir from wild-type and integrase inhibitor-resistant HIV-1 integrase-DNA complexes. *Antimicrob. Agents Chemother.* **2011**, *55*, 4552-4559.
62. Sham, H. L.; Kempf, D. J.; Molla, A.; Marsh, K. C.; Kumar, G. N.; Chen, C.-M.; Kati, W.; Stewart, K.; Lal, R.; Hsu, A.; Betebenner, D.; Korneyeva, M.; Vasavanonda, S.; McDonald, E.; Saldivar, A.; Wideburg, N.; Chen, X.; Niu, P.; Park, C.; Jayanti, V.; Grabowski, B.; Granneman, G. R.; Sun, E.; Japour, A. J.; Leonard, J. M.; Plattner, J. J.; Norbeck, D. W. ABT-378, a highly potent inhibitor of the human immunodeficiency virus protease. *Antimicrob. Agents Chemother.* **1998**, *42*, 3218-3224.
63. Kempf, D. J.; Marsh, K. C.; Kumar, G.; Rodrigues, A. D.; Denissen, J. F.; McDonald, E.; Kukulka, M. J.; Hsu, A.; Granneman, G. R.; Baroldi, P. A.; Sun, E.; Pizzuti, D.; Plattner, J. J.; Norbeck, D. W.; Leonard, J. M. Pharmacokinetic enhancement of inhibitors of the human immunodeficiency virus protease by coadministration with ritonavir. *Antimicrob. Agents Chemother.* **1997**, *41*, 654-60.
64. Li, F.; Lu, J.; Ma, X. CPY3A4-mediated lopinavir bioactivation and its inhibition by ritonavir. *Drug Metab. Dispos.* **2012**, *40*, 18-24.
65. Arts, E. J.; Hazuda, D. J. HIV-1 antiretroviral drug therapy. *Cold Spring Harb. Perspect. Med.* **2012**, *2*, 1-23.
66. Esposito, F.; Corona, A.; Tramontano, E. HIV-1 reverse transcriptase still remains a new drug target: structure, function, classical inhibitors, and new inhibitors with innovative mechanisms of actions. *Mol. Biol. Int.* **2012**, *2012*, 1-23.
67. Sarafianos, S. G.; Marchand, B.; Das, K.; Himmel, D. M.; Parniak, M. A.; Hughes, S. H.; Arnold, E. Structure and function of HIV-1 reverse transcriptase: molecular mechanisms of polymerization and inhibition. *J. Mol. Biol.* **2009**, *385*, 693-713.
68. Huang, H.; Chopra, R.; Verdine, G. L.; Harrison, S. C. Structure of a covalently trapped catalytic complex of HIV-1 reverse transcriptase: Implications for drug resistance. *Science* **1998**, *282*, 1669-1675.
69. Klumpp, K.; Hang, J. Q.; Rajendran, S.; Yang, Y.; Derosier, A.; Wong Kai In, P.; Overton, H.; Parkes, K. E. B.; Cammack, N.; Martin, J. A. Two-metal ion mechanism of RNA cleavage by HIV RNase H and mechanism-based design of selective HIV RNase H inhibitors. *Nucleic Acids Res.* **2003**, *31*, 6852-6859.

70. Steitz, T. A. DNA polymerases: Structural diversity and common mechanisms. *J. Biol. Chem.* **1999**, 274, 17395-17398.
71. Marchand, B.; Götte, M. Site-specific footprinting reveals differences in the translocation status of HIV-1 reverse transcriptase: Implications for polymerase translocation and drug resistance. *J. Biol. Chem.* **2003**, 278, 35362-35372.
72. Sarafianos, S. G.; Clark, A. D.; Das, K.; Tuske, S.; Birktoft, J. J.; Iankumaran, P.; Ramesha, A. R.; Sayer, J. M.; Jerina, D. M.; Boyer, P. L.; Hughes, S. H.; Arnold, E. Structures of HIV-1 reverse transcriptase with pre- and post-translocation AZTMP-terminated DNA. *EMBO J.* **2002**, 21, 6614-6624.
73. Asahchop, E. L.; Wainberg, M. A.; Sloan, R. D.; Tremblay, C. L. Antiviral drug resistance and the need for development of new HIV-1 reverse transcriptase inhibitors. *Antimicrob. Agents Chemother.* **2012**, 56, 5000-5008.
74. Brinkman, K.; Kakuda, T. N. Mitochondrial toxicity of nucleoside analogue reverse transcriptase inhibitors: a looming obstacle for long-term antiretroviral therapy? *Curr. Opin. Infect. Dis.* **2000**, 13, 5-11.
75. Kohlstaedt, L.; Wang, J.; Friedman, J.; Rice, P.; Steitz, T. Crystal structure at 3.5 Å resolution of HIV-1 reverse transcriptase complexed with an inhibitor. *Science* **1992**, 256, 1783-1790.
76. Ding, J.; Das, K.; Moereels, H.; Koymans, L.; Andries, K.; Janssen, P. A. J.; Hughes, S. H.; Arnold, E. Structure of HIV-1 RT/TIBO R 86183 complex reveals similarity in the binding of diverse nonnucleoside inhibitors. *Nat. Struct. Mol. Biol.* **1995**, 2, 407-415.
77. Preston, B.; Poiesz, B.; Loeb, L. Fidelity of HIV-1 reverse transcriptase. *Science* **1988**, 242, 1168-1171.
78. Coffin, J. HIV population dynamics in vivo: implications for genetic variation, pathogenesis, and therapy. *Science* **1995**, 267, 483-489.
79. Menéndez-Arias, L. Molecular basis of human immunodeficiency virus drug resistance: An update. *Antiviral Res.* **2010**, 85, 210-231.
80. Sarafianos, S. G.; Das, K.; Clark, A. D.; Ding, J.; Boyer, P. L.; Hughes, S. H.; Arnold, E. Lamivudine (3TC) resistance in HIV-1 reverse transcriptase involves steric hindrance with β -branched amino acids. *Proc. Natl. Acad. Sci.* **1999**, 96, 10027-10032.

81. Tuske, S.; Sarafianos, S. G.; Clark, A. D.; Ding, J.; Naeger, L. K.; White, K. L.; Miller, M. D.; Gibbs, C. S.; Boyer, P. L.; Clark, P.; Wang, G.; Gaffney, B. L.; Jones, R. A.; Jerina, D. M.; Hughes, S. H.; Arnold, E. Structures of HIV-1 RT-DNA complexes before and after incorporation of the anti-AIDS drug tenofovir. *Nat. Struct. Mol. Biol.* **2004**, *11*, 469-474.
82. Das, K.; Bandwar, R. P.; White, K. L.; Feng, J. Y.; Sarafianos, S. G.; Tuske, S.; Tu, X.; Clark, A. D.; Boyer, P. L.; Hou, X.; Gaffney, B. L.; Jones, R. A.; Miller, M. D.; Hughes, S. H.; Arnold, E. Structural basis for the role of the K65R mutation in HIV-1 reverse transcriptase polymerization, excision antagonism, and tenofovir resistance. *J. Biol. Chem.* **2009**, *284*, 35092-35100.
83. Meyer, P. R.; Matsuura, S. E.; So, A. G.; Scott, W. A. Unblocking of chain-terminated primer by HIV-1 reverse transcriptase through a nucleotide-dependent mechanism. *Proc. Natl. Acad. Sci.* **1998**, *95*, 13471-13476.
84. Meyer, P. R.; Matsuura, S. E.; Mian, A. M.; So, A. G.; Scott, W. A. A mechanism of AZT resistance: An increase in nucleotide-dependent primer unblocking by mutant HIV-1 reverse transcriptase. *Mol. Cell* **1999**, *4*, 35-43.
85. Rigourd, M.; Lanchy, J.-M.; Le Grice, S. F. J.; Ehresmann, B.; Ehresmann, C.; Marquet, R. Inhibition of the initiation of HIV-1 reverse transcription by 3'-azido-3'-deoxythymidine: Comparison with elongation *J. Biol. Chem.* **2000**, *275*, 26944-26951.
86. Yamada, K.; Wahba, A. S.; Bernatchez, J. A.; Ilina, T.; Martínez-Montero, S.; Habibian, M.; Deleavey, G. F.; Götte, M.; Parniak, M. A.; Damha, M. J. Nucleotide sugar pucker preference mitigates excision by HIV-1 RT. *ACS Chem. Biol.* **2015**, *10*, 2024-2033.
87. Öberg, B. Antiviral effects of phosphonoformate (PFA, foscarnet sodium). *Pharmacol. Ther.* **1982**, *19*, 387-415.
88. Crumpacker, C. S. Mechanism of action of foscarnet against viral polymerases. *Am. J. Med.* **1992**, *92*, S3-S7.
89. Zahn, K. E.; Tchesnokov, E. P.; Götte, M.; Doublie, S. Phosphonoformic acid inhibits viral replication by trapping the closed form of the DNA polymerase. *J. Biol. Chem.* **2011**, *286*, 25246-25255.
90. Das, K.; Balzarini, J.; Miller, M. T.; Maguire, A. R.; DeStefano, J. J.; Arnold, E. Conformational states of HIV-1 reverse transcriptase for nucleotide incorporation vs

- pyrophosphorolysis—binding of foscarnet. *ACS Chem. Biol.* ASAP, doi: 10.1021/acscchembio.6b00187 **2016**.
91. Marchand, B.; Tchesnokov, E. P.; Götte, M. The pyrophosphate analogue foscarnet traps the pre-translocational state of HIV-1 reverse transcriptase in a brownian ratchet model of polymerase translocation. *J. Biol. Chem.* **2007**, 282, 3337-3346.
 92. Canestri, A.; Ghosn, J.; Wirden, M.; Marguet, F.; Ktorza, N.; Boubezari, I.; Dominguez, S.; Bossi, P.; Caumes, E.; Calvez, V. Foscarnet salvage therapy for patients with late-stage HIV disease and multiple drug resistance. *Antivir. ther.* **2006**, 11, 561-566.
 93. Schmit, J.-C.; Cogniaux, J.; Hermans, P.; Van Vaeck, C.; Sprecher, S.; Van Remoortel, B.; Witvrouw, M.; Balzarini, J.; Desmyter, J.; De Clercq, E.; Vandamme, A.-M. Multiple drug resistance to nucleoside analogues and nonnucleoside reverse transcriptase inhibitors in an efficiently replicating human immunodeficiency virus type 1 patient strain. *J. Infect. Dis.* **1996**, 174, 962-968.
 94. Arion, D.; Sluis-Cremer, N.; Parniak, M. A. Mechanism by which phosphonoformic acid resistance mutations restore 3'-azido-3'-deoxythymidine (AZT) sensitivity to AZT-resistant HIV-1 reverse transcriptase. *J. Biol. Chem.* **2000**, 275, 9251-9255.
 95. Song, Y.; Chan, J. M. W.; Tovian, Z.; Secrest, A.; Nagy, E.; Krysiak, K.; Bergan, K.; Parniak, M. A.; Oldfield, E. Bisphosphonate inhibitors of ATP-mediated HIV-1 reverse transcriptase catalyzed excision of chain-terminating 3'-azido, 3'-deoxythymidine: A QSAR investigation. *Bioorg. Med. Chem.* **2008**, 16, 8959-8967.
 96. Cruchaga, C.; Ansó, E.; Rouzaut, A.; Martínez-Irujo, J. J. Selective excision of chain-terminating nucleotides by HIV-1 reverse transcriptase with phosphonoformate as substrate. *J. Biol. Chem.* **2006**, 281, 27744-27752.
 97. Bernatchez, J. A.; Paul, R.; Tchesnokov, E. P.; Ngure, M.; Beilhartz, G. L.; Berghuis, A. M.; Lavoie, R.; Li, L.; Auger, A.; Melnyk, R. A.; Grobler, J. A.; Miller, M. D.; Hazuda, D. J.; Hecht, S. M.; Götte, M. Derivatives of mesoxalic acid block translocation of HIV-1 reverse transcriptase. *J. Biol. Chem.* **2015**, 290, 1474-1484.
 98. Davis, W. R.; Tomsho, J.; Nikam, S.; Cook, E. M.; Somand, D.; Peliska, J. A. Inhibition of HIV-1 reverse transcriptase-catalyzed DNA strand transfer reactions by 4-chlorophenylhydrazone of mesoxalic acid. *Biochemistry* **2000**, 39, 14279-14291.

99. Gabbara, S.; Davis, W. R.; Hupe, L.; Hupe, D.; Peliska, J. A. Inhibitors of DNA strand transfer reactions catalyzed by HIV-1 reverse transcriptase. *Biochemistry* **1999**, *38*, 13070-13076.
100. Shaw-Reid, C. A.; Munshi, V.; Graham, P.; Wolfe, A.; Witmer, M.; Danzeisen, R.; Olsen, D. B.; Carroll, S. S.; Embrey, M.; Wai, J. S.; Miller, M. D.; Cole, J. L.; Hazuda, D. J. Inhibition of HIV-1 ribonuclease H by a novel diketo acid, 4-[5-(benzoylamino)thien-2-yl]-2,4-dioxobutanoic acid. *J. Biol. Chem.* **2003**, *278*, 2777-2780.
101. Jochmans, D.; Deval, J.; Kesteleyn, B.; Van Marck, H.; Bettens, E.; De Baere, I.; Dehertogh, P.; Ivens, T.; Van Ginderen, M.; Van Schoubroeck, B.; Ehteshami, M.; Wigerinck, P.; Götte, M.; Hertogs, K. Indolopyridones inhibit human immunodeficiency virus reverse transcriptase with a novel mechanism of action. *J. Virol.* **2006**, *80*, 12283-12292.
102. Rajotte, D.; Tremblay, S.; Pelletier, A.; Salois, P.; Bourgon, L.; Coulombe, R.; Mason, S.; Lamorte, L.; Sturino, C. F.; Bethell, R. Identification and characterization of a novel HIV-1 nucleotide-competing reverse transcriptase inhibitor series. *Antimicrob. Agents Chemother.* **2013**, *57*, 2712-2718.
103. Balzarini, J.; Das, K.; Bernatchez, J. A.; Martinez, S. E.; Ngure, M.; Keane, S.; Ford, A.; Maguire, N.; Mullins, N.; John, J.; Kim, Y.; Dehaen, W.; Vande Voorde, J.; Liekens, S.; Naesens, L.; Götte, M.; Maguire, A. R.; Arnold, E. Alpha-carboxy nucleoside phosphonates as universal nucleoside triphosphate mimics. *Proc. Natl. Acad. Sci.* **2015**, *112*, 3475-3480.
104. Keane, S. J.; Ford, A.; Mullins, N. D.; Maguire, N. M.; Legigan, T.; Balzarini, J.; Maguire, A. R. Design and synthesis of α -carboxy nucleoside phosphonate analogues and evaluation as HIV-1 reverse transcriptase-targeting agents. *J. Org. Chem.* **2015**, *80*, 2479-2493.

CHAPTER 2: Modular Assembly of Purine-Like Bisphosphonates as Inhibitors of HIV-1 Reverse Transcriptase

2.1. Preface

This chapter was adapted from an article authored by C.M. Lacbay, J. Mancuso, Y.-S. Lin, N. Bennett, M. Götte, and Y. S. Tsantrizos, *J. Med. Chem.* **2014**, 57, 7435-7449 and presented in this thesis with permission. I completed the synthesis of the majority of inhibitors described in this chapter (~90%), including the mechanistic investigation leading to the formation of compound **2.22** from **2.21a** (**Scheme 2.3**). I also conducted most of the *in vitro* inhibition assays to evaluate selectivity using the human FPPS and GGPPS enzymes; these enzymes bind substrates bearing a diphosphate moiety *via* metal-mediated interactions, and are therefore reasonable candidates for preliminary evaluation of target selectivity. The synthesis of intermediate **2.12c** (**Scheme 2.1**) was initially explored by Dr. J. Mancuso. Y.-S. Lin prepared the inhibitors substituted at C-7. Biochemical evaluation for inhibition of HIV-1 RT was carried out by Dr. N. Bennet (PDF in Prof. Götte's group) using a primer extension scintillation proximity assay (SPA).

2.2. Abstract

Bisphosphonates can mimic the pyrophosphate leaving group of the nucleotidyl transfer reaction and effectively inhibit RNA/DNA polymerases. In a search of HIV-1 reverse transcriptase (RT) inhibitors, a new chemotype of non-hydrolysable purine diphosphate mimic was synthesized. A modular synthetic protocol was developed, utilizing 2-amino-6-(methylthio)-4-(trimethylsilyl)nicotinonitrile as the key synthon in the preparation of highly substituted 2-aminonicotinonitriles. These building blocks were subsequently elaborated to the pyrido[2,3-

d]pyrimidine bisphosphonates (PYPY-BPs). Biochemical screening identified analogs of PYPY-BPs that inhibit HIV-1 RT-catalyzed DNA synthesis.

2.3. Introduction

Virally-encoded nucleic acid processing enzymes are essential for viral replication and represent a large family of validated therapeutic targets. Important examples include the hepatitis C virus (HCV) NS5B RNA-dependent RNA polymerase, and both the reverse transcriptase (RT) and integrase (IN) of the human immunodeficiency virus type 1 (HIV-1). Nucleoside analogues were the first antiviral agents developed to bind at the polymerase active site, thus blocking DNA or RNA chain elongation. Examples include the purine bioisosteres MK-0608 (**2.1c**) and abacavir (**2.2**), which inhibit HCV NS5B¹ and HIV-1 RT,² respectively. Abacavir (**2.2**) is one of seven currently approved nucleoside drugs (NRTIs) for the treatment of AIDS.² These compounds are metabolized to their corresponding 5'-triphosphates, thus mimicking the natural substrates (e.g. **2.1a** is converted to **2.1b**). Additionally, allosteric inhibitors targeting virally-encoded polymerases and integrases are also clinically validated. However, identification and development of *bona fide* active site inhibitors for these targets, with good biopharmaceutical properties, is a significant challenge. This is mainly due to the highly charged nature of the protein surface inside the active sites of these enzymes. Despite the uniqueness of the catalytic function of each nucleic acid processing enzyme, all of the active site cavities are characterized by having a cluster of highly conserved aspartic acid residues that bind their substrates *via* metal-mediated interactions.

Inorganic pyrophosphate (PP_i; **2.3a**) is the phosphorolysis by-product formed during each catalytic cycle of nucleotide triphosphate incorporation into a growing oligonucleotide biopolymer (**Fig. 2.1**). Numerous biochemical and crystallographic studies have provided evidence that polymerases

undergo a large conformational change (from an “open” to a “closed” conformation) upon binding of a nucleotide triphosphate (NTP, e.g. **2.1b**) in the active site, resulting in the formation of a stable complex with the primer and template (P/T) nucleic acid strands. Interestingly, studies have also shown that the same conformational change can be induced upon binding of either the NTP substrate or the PPi byproduct to the active site; it is presumed that stabilization of this complex by a small molecule can be an effective, novel mechanism of inhibiting HIV-1 RT. Several crystal structures of polymerase/P/T/PPi complexes for both DNA and RNA polymerases have been reported.^{3,4,5,6}

A number of PPi bioisosteres have been previously investigated, including phosphonoformates and α,γ -diketo acids (e.g. **2.3b** and **2.4**, respectively), and shown to inhibit virally-encoded nucleic acid processing enzymes (e.g. HCV-NS5B,⁷ HIV-1 RT-dependent RNase H and HIV-1 IN⁸). Although the main pharmacophores of compounds such as **2.3b** and **2.4** are clearly not desirable to have in a therapeutic agent, replacement of these motifs with other bioisosteres of PPi has provided drugs with significant clinical value, such as the HIV-1 IN inhibitor raltegravir (**2.6**).⁹ The 5-hydroxy-6-oxo-1,6-dihydropyrimidine-4-carboxamide core of **2.6** (a structural mimic of an α,γ -diketo acid) binds to aspartate-rich active site of the HIV-1 IN *via* bifurcated Mg²⁺-mediated interactions. Raltegravir represents the first clinically validated, *true* active site inhibitor of a nucleic acid processing enzyme.

Chart 1

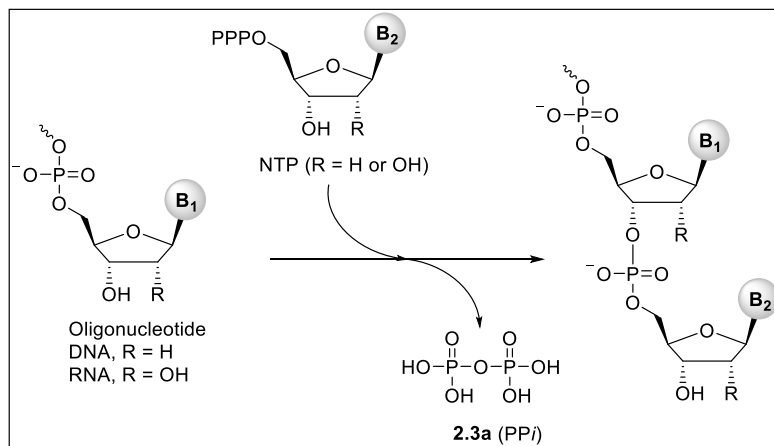
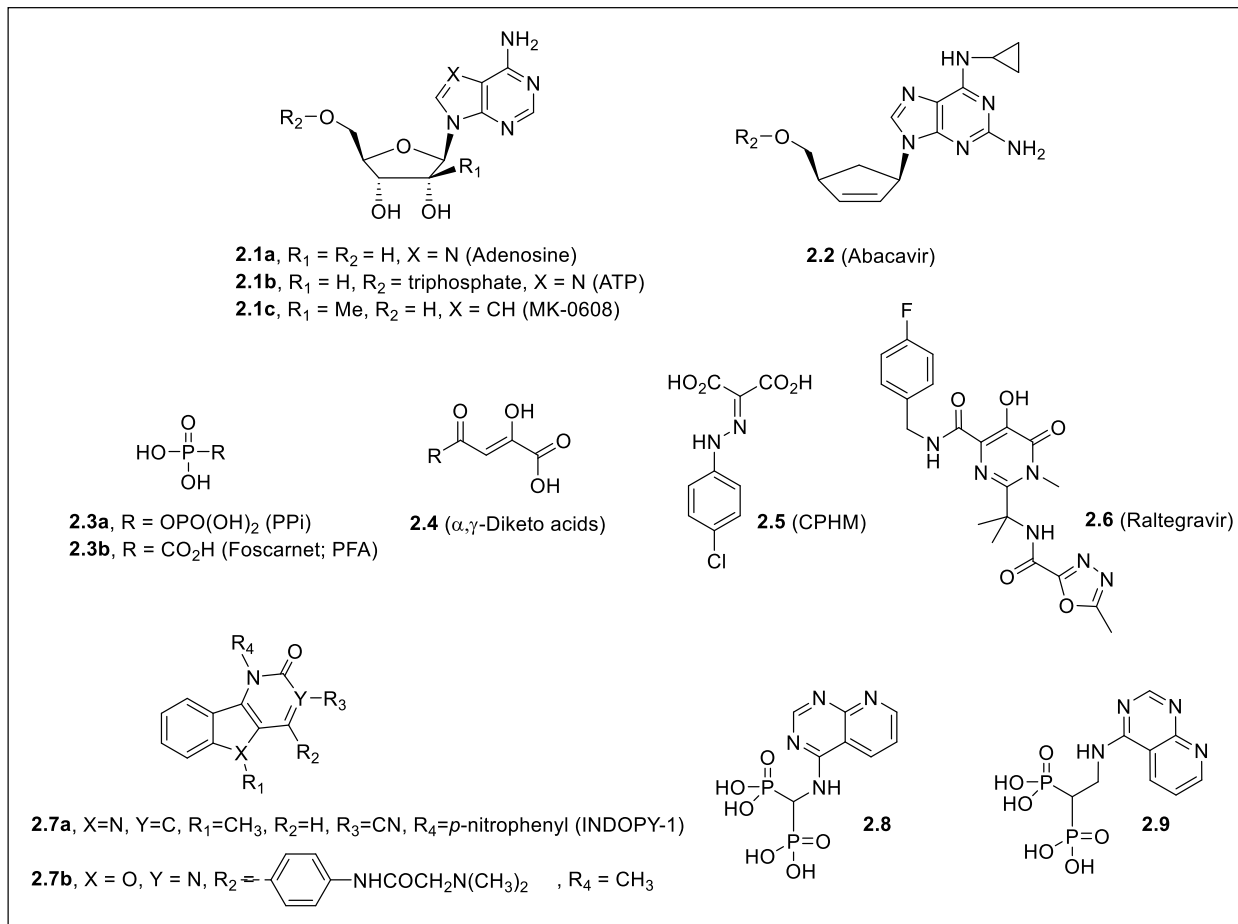


Figure 2.1. Oligonucleotide polymerization reaction.

Foscarnet (PFA, **2.3b**) is the simplest bioisostere of PPi that has been extensively investigated. It exhibits broad spectrum antiviral activity against *Herpesviridae* and *Retroviridae* and has been used for the treatment of herpes simplex (HSV-1 and HSV-2) and human cytomegalovirus (HCVM)¹⁰ infections, in second line drug regimens. Stable complexes of HIV-1 RT-P/T-**2.3b** have been observed.¹¹ Recently, it was shown that **2.3b** can trap the HIV-1 RT/DNA complex at the pre-translocational state, in which the ultimate nucleoside monophosphate of the primer occupies the substrate binding site.¹² Similar results were previously reported for the mesoxalic acid derivative **2.5**, which presumably can also bind Mg²⁺ *via* the dicarboxylate anions.¹³ These compounds inhibit HIV-1 *via* a mechanism that is uniquely different from that of the NRTIs and NNRTIs and have been labeled as nucleotide competitive RT inhibitors (NcRTIs). Non-pyrophosphate mimics, such as the pyridoindolone analog **2.7a** (INDOPY-1)¹⁴ and benzofuroprymidinone analog **2.7b**¹⁵ have also been described as NcRTIs. Interestingly, these compounds appear to form RT-DNA/RNA ternary complexes that “freeze” the post-translocation state, in a similar manner to the natural nucleotide substrate.

Our group has had a long-standing interest in designing inhibitors for enzymes that typically bind phosphate, diphosphate (pyrophosphate) or triphosphate substrates using divalent metal ions as co-factors. We previously designed bisphosphonate (BP) inhibitors of the human farnesyl pyrophosphate synthases (hFPPS), the gate-keeper enzyme of isoprenoid biosynthesis in mammalian cells.¹⁶ Currently, bisphosphonates are clinically validated drugs for the treatment of skeletal diseases targeting the human farnesyl pyrophosphate synthase.¹⁷ These drugs have high affinity for bone, are potent inhibitors of osteoclastic activity and are widely used for the treatment of bone-related diseases.¹⁸

BPs have also been described to bind to HIV-1 RT and block the excision of 3'-azido,3'-deoxythymidine (AZT) from the 3'-end of an oligonucleotide.^{19,20} However, the BPs described so far exhibited little or no activity at inhibiting RT-catalyzed RNA-templated DNA synthesis.²⁰ Recently, BPs were also reported to be weak inhibitors of DNA 3'-processing and strand transfer reactions catalyzed by HIV-1 IN; however, the potency of these compounds was found to be even weaker in the presence of the biologically relevant co-factor (Mg^{2+}) than other divalent metals.²¹ BPs have also been reported as very weak inhibitors of HCV NS5B (IC_{50} values $>100 \mu M$).²² In this study, we report the synthesis of pyrido[2,3-*d*]pyrimidine bisphosphonates (PYPY-BPs) with general structure **2.8** and **2.9** as potential bioisosteres of purine-based nucleotide diphosphates (NDPs). A modular synthetic protocol was developed, utilizing 2-amino-6-(methylthio)-4-(trimethylsilyl)nicotinonitrile (**2.14b**) as the key synthon, to prepare highly substituted pyrido[2,3-*d*]pyrimidine bisphosphates (PYPY-BPs). *In vitro* biochemical screening led to the identification of several "hits" that block HIV-1 RT-catalyzed DNA synthesis at low micromolar concentrations, with IC_{50} values of 1-5 μM range. A preliminary structure-activity relationship (SAR) was established that suggests a promising path forward for the optimization of this chemotype into novel antiviral agents.

2.4. Chemistry

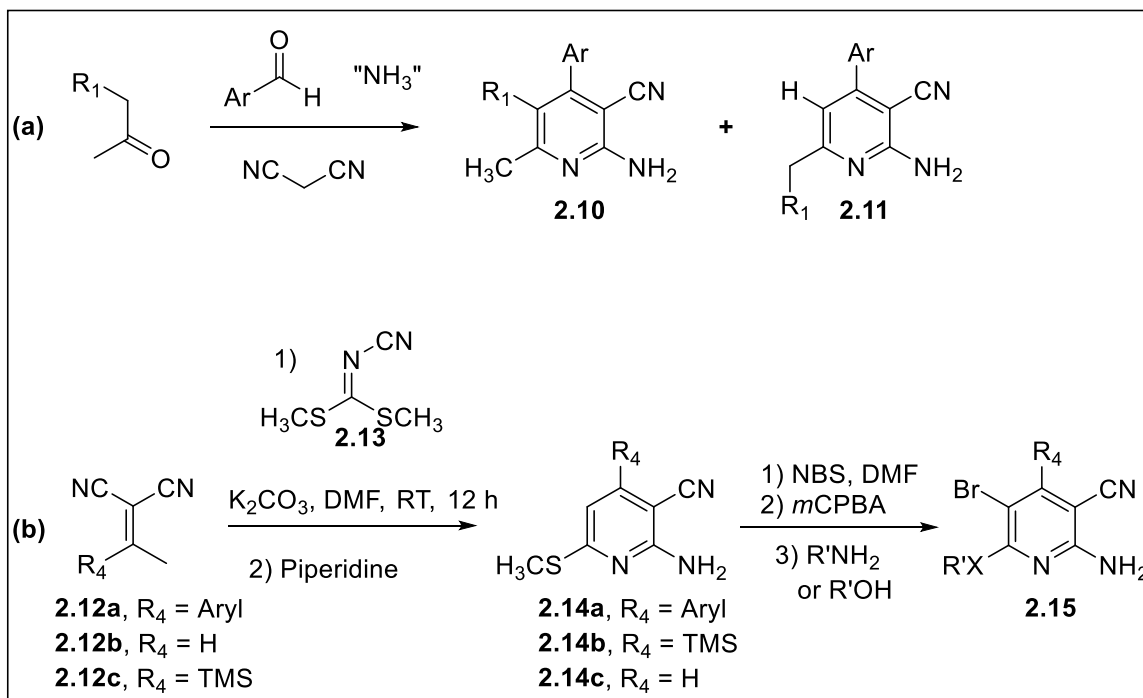
Substituted 2-aminonicotinonitriles (e.g. **2.10**, **2.11**; **Scheme 2.1**) are common synthetic precursors to the pyrido[2,3-*d*]pyrimidine scaffold, which is a privileged bioisostere of the purine nucleobase core. In recent years, pyrido[2,3-*d*]pyrimidin-4-amine-based molecules have received significant attention in drug discovery. Pre-clinical/clinical exploratory therapeutics of this class include antiviral agents targeting the HCV NS5A,²³ agents for the treatment of cardiovascular diseases,²⁴ acetylcholinesterase inhibitors,²⁵ and anticancer agents.²⁶ The 2-aminonicotinonitrile precursor to

these compounds is also an important structural motif of pharmaceutical interest; examples include P2Y₁₂ inhibitors as anti-thrombotic agents,²⁷ antitumor agents,²⁸ A_{2A} adenosine receptor antagonists,²⁹ potential prion disease therapeutics³⁰ and IKK- β kinase inhibitors.³¹

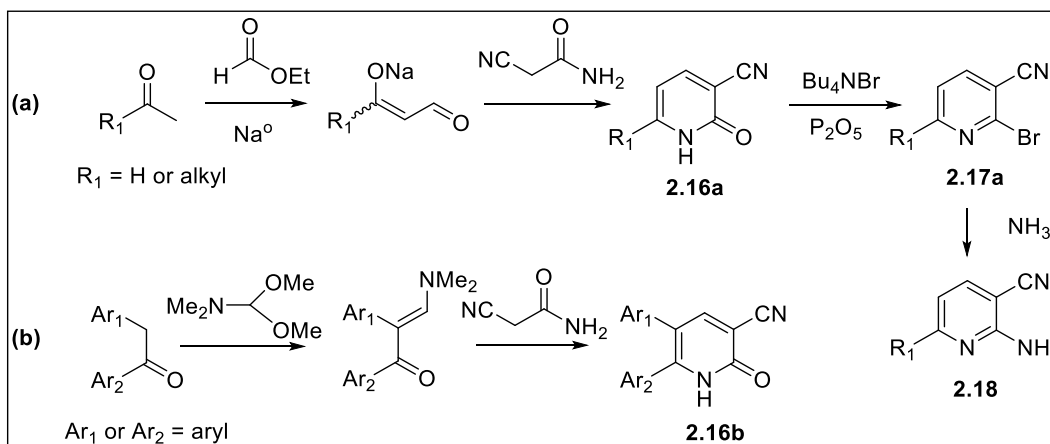
In the past, a number of useful methodologies were reported for the construction of substituted 2-aminonicotinonitriles and their conversion to pyridopyrimidines. Most of these approaches employed the classical three-component Hantzsch-type condensation/dehydrogenation reaction of ketones with aryl aldehydes, malononitrile and ammonia (or ammonium acetate) under thermal or microwave conditions (**Scheme 2.1a**).³² This methodology often suffers from poor yields, particularly in the case of non-symmetrical aliphatic ketones, which lead to mixtures of regioisomers (e.g. **2.10** and **2.11**; **Scheme 2.1**). Several modifications have been reported,³³ including the ytterbium perfluorooctanoate [Yb(PFO)₃] catalyzed one-pot synthesis, which provides higher yields under more favorable reaction conditions.³⁴ In 2008, Teague reported a modification that proved to be particularly relevant to our work.³⁵ This method involves condensation of 2-(1-arylethylidene)propanedinitriles (**2.12a**) with dimethyl *N*-cyanodithioiminocarbonate (**2.13**) under basic conditions to give the 2-amino-6-(methylthio)-4-arylnicotinonitriles (**2.14a**; **Scheme 2.1b**). This intermediate can be selectively brominated at C-5, even in the presence of an electron-rich aryl substituent at C-4, and the C-6 thiomethyl group can be oxidized to sulfoxide, before displacement with various nucleophiles to give highly substituted pyridines.³⁵ However, this methodology is limited by the requirement of an arylethylidene precursor (**2.12a**) in order for the reaction to proceed efficiently (**Scheme 2.1b**).

Our goal was to explore pyrido[2,3-*d*]pyrimidine bisphosphonates (PYPY-BPs) as potential bioisosteres of purine-like NDPs. Based on structural and conformational considerations, we

anticipated that a large aromatic substituent at C-5 of the pyridopyrimidine scaffold (originating from the C-4 substituent of the 2-aminonicotinonitrile precursor) was likely to hinder proper binding of the bisphosphonate moiety in the active site of the enzyme. For this purpose, we required the synthesis of 2-aminonicotinonitriles that were unsubstituted at C-4 and could be easily modified at C-5 and C-6 in a modular synthesis, library mode. Preparation of 2-aminonicotinonitriles from a 2-oxo-1,2-dihydropyridine-3-carbonitrile precursor (e.g. **Scheme 2.2a/b**; **2.16a**^{23a} or **2.16b**³⁶) has been previously reported. Conversion of the pyridone to the corresponding C-2 halo derivative (e.g. **2.17a**) provides access to the desired 2-aminonicotinonitrile (e.g. **2.18**). Although this approach allows the preparation of the desired compounds, the synthetic protocol is linear, making the preparation of libraries of structurally diverse pyridopyrimidines challenging.



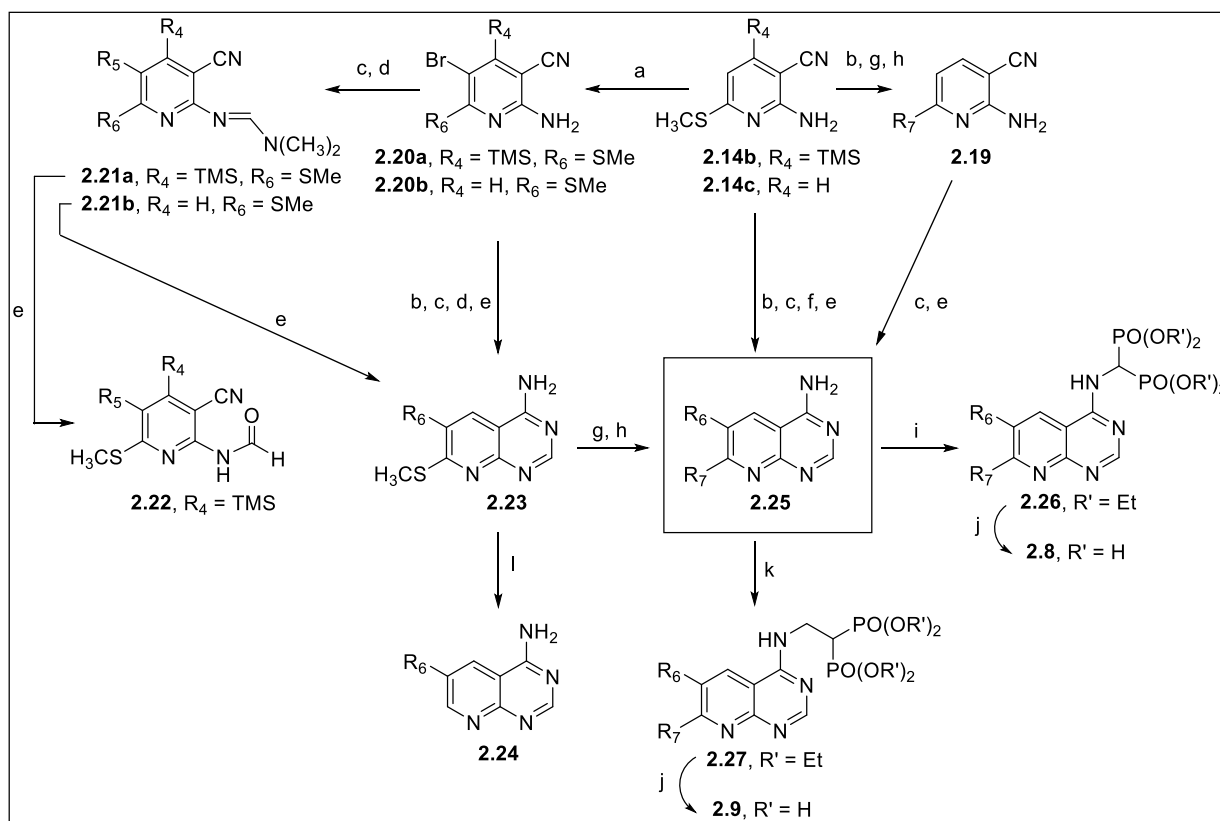
Scheme 2.1. Synthesis of substituted 2-aminonicotinonitriles; (a) Classical Hantzsch synthesis; (b) Modified Teague synthesis.³⁵



Scheme 2.2. Two common approaches for the synthesis of 2-aminonicotinonitriles that are not substituted at C-4.

Initially, we attempted to optimize the reaction shown in **Scheme 2.1b**.³⁵ We explored the removal of the aromatic substituent from this ylide (*i.e.* **2.12b**), which had a dramatic effect on the reactivity of the olefin, flipping this reagent from a Michael donor into a Michael acceptor even superior to compound **2.13** (**Scheme 2.1b**). For example, we prepared ylide **2.12b** (*via* condensation of malononitrile with acetaldehyde in the presence of a catalytic amount of diethylamine) and found that this ylide was prone to self-condensation in the presence of base. In an attempt to enhance the electrophilicity of the iminithiocarbonate **2.13**, we also added various alkyl iodides or TMS triflate to the reaction mixture, however, only polymerization of **2.12b** was observed. We then modified the ylide with a TMS substituent (*i.e.* ylide **2.12c**; **Scheme 2.1b**), as a masking moiety at C-4 of the desired 2-aminonicotinonitrile intermediate (**2.14b**). Knoevenagel condensation of acetyltrimethylsilane and malononitrile provided the stable ylide building block **2.12c**, as we previously reported.³⁷ A one-pot, two step condensation of **2.12c** with the iminithiocarbonate **2.13** under basic conditions led to good overall conversion of the starting material to a mixture of 2-aminonicotinonitriles **2.14b** and the desilylated product **2.14c** in 2:1

ratio (**Scheme 2.1b**). Separation of **2.14b** from **2.14c** can be easily achieved by chromatography, although for our purposes this step was not required and the mixture was treated with TBAF to give exclusively intermediate **2.14c** in ~60%-70% isolated yield. Bromination of **2.14b** or **2.14c** with NBS proceeded selectively at C-5, giving **2.20a** or **2.20b**, respectively, in good to excellent yields (70%-80%). Pd-catalyzed cross coupling of **2.20a** or **2.20b** with various boronic acids or boronate esters under typical Suzuki conditions proceeded in good yield (average yields of 45-70%), although a small amount of the corresponding desilylated product was usually formed when using **2.20a** (~10%). These observations suggest that replacing the TMS group of ylidene **2.12c** with a more stable silyl group may further improve this synthetic protocol (such optimization was unnecessary for our objectives).



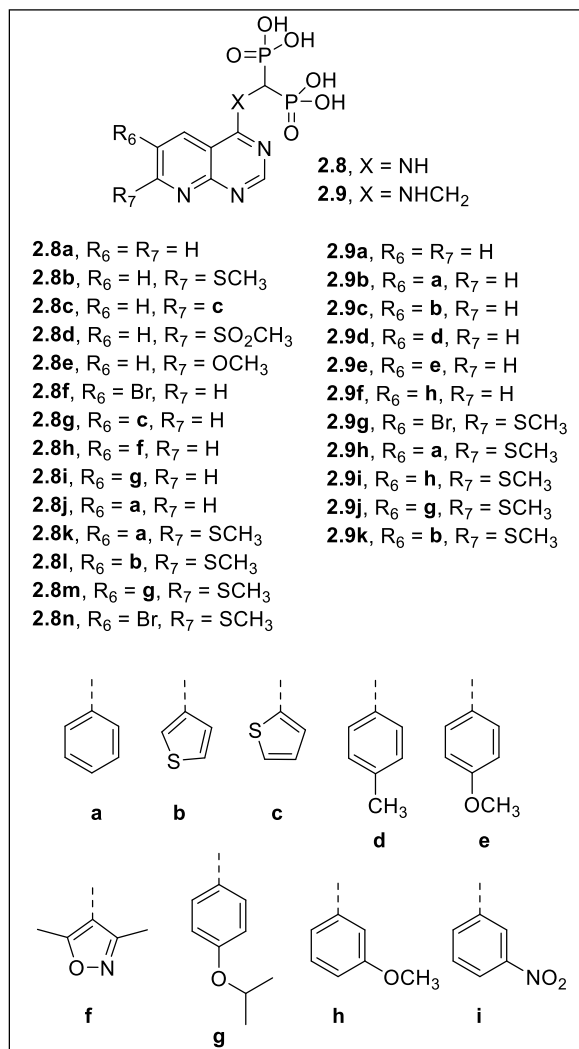
Scheme 2.3. Modular synthesis of C-6/C-7 substituted pyrido[2,3-d]pyrimidin-4-amines. Conditions: (a) NBS in acetonitrile, 4h, rt, 78%; (b) TBAF, THF, rt, 12h, 90-98%; (c) *N,N*-

dimethylformamide dimethylacetal DMF-DMA, DMF, 4-12h, rt, 70-95%; (d) Pd-catalyzed Suzuki cross coupling, 40-90% yield; (e) NH₄OAc, AcOH, 100 °C, 1-2h, 50-98%; (f) ArZnI·LiCl, Pd(OAc)₂, S-Phos, THF, 25-50°C, 15h, 40-45%; (g) *m*CPBA, DCM, 40 min, rt, 80%; (h) NaOR' or HNR'R'', EtOH, 10-15 h, 80°C, 70-80%; (i) diethyl phosphite, triethyl orthoformate, toluene or DMF, 150°C (microwave), 1.5h; (j) i. TMSBr, 2-3 days, rt; ii MeOH; (k) tetraethyl ethane-1,1-diylbis(phosphonate), THF, rt 16h; (l) Et₃SiH, Pd/C, 0°C to rt, ~35%.

Intermediates **2.20a** and **2.20b** were converted to their corresponding *N,N*-dimethylformamidine derivatives **2.21a** and **2.21b**, respectively, prior to cyclization. Surprisingly, whereas cyclization of **2.21b** with ammonium acetate in acetic acid gave the expected pyrido[2,3-*d*]pyrimidin-4-amine product **2.23**, cyclization of **2.21a** under the same conditions produced mainly the formamide intermediate **2.22** (60-70% isolated yield). It appears that the steric bulk of the TMS group at C-4 disfavors formation the exocyclic imine intermediate **2.28** (Scheme 2.4, Path I), leading to formation of **2.22** via nucleophilic attack by water present in AcOH (Scheme 2.4, Path II). Cyclization of **2.21b** in the presence of ¹⁵NH₄Cl in AcOH provided the expected ¹⁵N-labeled product **2.23** (*i.e.* specifically labeled at N-3), whereas cyclization of **2.21a** under the same conditions did not lead to incorporation of the ¹⁵N-label; the structures of compounds **2.22a** and **2.22b** were confirmed by 2D NMR, IR and HRMS. The nitro intermediate **2.21s** (R₄= TMS, R₅=3-nitrophenyl, R₆=SMe) leading to **2.22b** was only prepared to test any electronic contributions in the formation of **2.22** vs the cyclized pyridopyrimidine **2.23** and was not pursued further to a final inhibitor.

formation of the tetraethyl bisphosphonate esters **2.26** and **2.27**, respectively (**Scheme 2.3**). The ethyl esters were treated with TMSBr followed by methanolysis to obtain the final phosphonic acids **2.8** and **2.9** in good yield (isolated yields of ~50% for the two steps). It is noteworthy that the overall synthetic protocol outlined in **Scheme 2.3** is fairly robust and amenable to library synthesis. For example, intermediate **2.20b** could be converted directly to the bisphosphonate tetra esters **2.26** or **2.27** before replacing the C-6 bromo moiety *via* a Pd-catalyzed cross coupling reaction. To validate the chemistry and the amenability of this protocol for parallel synthesis, a mini-library of compounds was synthesized; representative compounds are shown in **Table 2.1**.

Table 2.1. Compound library



2.5. Results and Discussion

Preliminary biochemical profiling of our pyridopyrimidine bisphosphonates (PYPY-BPs) focused on the identification of low micromolar “hits” that could inhibit HIV-1 RT-catalyzed DNA synthesis. It is noteworthy that at very high concentrations, bisphosphonates may appear to be inhibiting the enzyme (*i.e.* giving a false positive result) due to their ability to chelate the divalent metal ion required for catalytic activity (*e.g.* the Mg^{2+} cofactor of HIV-1 RT). Mindful of this property, we initiated *in vitro* screening of our PYPY-BP analogs (**Table 2.1**) at a fixed concentration of 10 μM inhibitor and 6 mM $MgCl_2$ using a modified scintillation proximity assay (SPA) and purified HIV-1 RT.⁴⁰ Significant inhibition of primer extension (>50% inhibition) was observed with several analogs. A full dose response inhibition curve (IC_{50}) was subsequently determined for the most promising of these compounds (**Table 2.2**).

Initial evidence of a structure-activity relationship (SAR) indicated that while neither parent compounds PYPY-BPs **2.8a** and **2.9a**, nor their corresponding C-7 thiomethyl ethers (*e.g.* **2.8d**), exhibited any significant activity in inhibiting HIV-1 RT, some of the C-6 substituted analogs inhibited RT with an IC_{50} value in the 10-25 μM range. Further increased in potency was observed with analogs having the thiomethyl ether moiety at C-7. For example, the potency (IC_{50}) of analogs **2.8i** and **2.9f** was approximately 10-fold lower than that of the corresponding derivatives **2.8m** and **2.9i**, respectively (**Table 2.2**). The same trend in SAR was observed when analog **2.9b** (data not shown) was compared to **2.9h** (**Table 2.2**). Interestingly, the longer linker between the pyridopyrimidine core and the bisphosphonate moiety (*i.e.* analogs **2.8** vs **2.9**) was well tolerated for our SAR purposes. In line with our objective to identify selective inhibitors for HIV-1 RT, the most potent HIV-1 RT inhibitors identified (**Table 2.1**; IC_{50} of 1-5 μM) were also tested in our *in vitro* hFPPS and hGGPPS inhibition assays.^{16c} Interestingly, analogs **2.9h** and **2.9i** were found to

also exhibit considerable potency in inhibiting hFPPS, but not hGGPPS. In contrast, inhibitor **2.8m** was selective in inhibiting HIV-1 RT and showed no activity in our hFPPS and hGGPPS inhibition assays even at concentration of 50 μ M.

The active site of the RT enzyme is the target of the current nucleoside drugs (NRTIs), although these compounds are substrate mimics that lead to chain termination and are not true inhibitors of the RT enzyme. Preliminary evaluation of our most potent compounds in HIV mutants that are typically associated with resistance to the current nucleoside drugs, such as K65R (*e.g.* tenofovir) and M184V (*e.g.* lamivudine and emtricitabine),⁴⁵ as well as the forcarment resistant E89K mutant,¹² were carried out. The K65R mutant appears to confer low level resistance to all compounds tested (**Table 2.3**), whereas, the M184V mutant leads to a small decrease (<3-fold) in sensitivity to analog **2.9i**; these results are summarized in **Table 2.3**.

Table 2.2. Activity data of key compounds

Compound	IC ₅₀ (μ M) ¹	Compound	IC ₅₀ (μ M) ¹
2.3b	2.5 \pm 1.3	2.9a	>50
2.5	1.5 \pm 0.9	2.9c	9.0 \pm 1.4
2.8a	>50	2.9f	20.0 \pm 4.8
2.8b	>50	2.9h ²	1.1 \pm 0.3
2.8c	10.4 \pm 1.4	2.9i ²	2.4 \pm 1.5
2.8i	10.0 \pm 1.5	2.9j	7.1 \pm 0.8
2.8m	1.8 \pm 0.8 ³	2.9k	8.3 \pm 1.3

¹Inhibition of DNA primer extension catalyzed by HIV-1 RT; average IC₅₀ value of three determinations. ²Compounds also inhibit hFPPS (75-95% inhibition at 10 μ M), but not hGGPPS.

³Less than 10% inhibition was observed in the hFPPS and hGGPPS inhibition assay at 50 μ M.

Table 2.3. Activity data of key compounds in HIV-1 wild-type vs HIV mutants

	Foscarnet		2.8m		2.9h		2.9i	
	IC ₅₀ ¹ (μ M)	Fold Change						
RT WT	1.2	1.0	0.8	1.0	2.0	1.0	1.5	1.0
RT K65R	2.8	2.4	1.8	2.1	5.2	3.4	3.3	2.1
RT E89K	5.2	4.5	0.8	1.0	1.0	0.6	2.1	1.3
RT M184V	0.8	0.7	1.4	1.6	0.6	0.4	4.2	2.7

¹Inhibition of DNA primer extension catalyzed by HIV-1 RT; average IC₅₀ values from an assay run in triplicates; all compounds were run in parallel with the wild-type RT and three mutants (the IC₅₀ values for WT are the average from this one assay run in triplicate and within the variability of the data shown in **Table 2.2**).

2.6. Conclusions

HIV/AIDS remains a major global public health problem, but manageable with highly active antiretroviral therapy (HAART), which provides a combination of drugs with different mechanisms of action that target various virally-encoded enzymes. The current clinically validated RT inhibitors include nucleosides/nucleotides (NRTIs) and allosteric inhibitors (NNRTIs). The triphosphates of NRTIs bind to the active site of RT and mimic the natural dNTP substrates, leading to incorporation into the viral DNA and chain termination. Resistance to an NRTI drug can emerge due to mutation(s) in the active site of RT that introduce electronic or steric effects, thus hindering the binding of the drug. Alternatively, mutations can create a new binding site for cellular ATP, which promotes the excision of the incorporated nucleotide monophosphate drug. For example, resistance to AZT or d4T is mediated through this type of mechanism, where ATP acts like a PP_i-donor and removes the incorporated AZT monophosphate. This reaction can be seen as the reverse of the nucleotide incorporation (**Fig. 2.1**), however, the affinity of PP_i for the RT complex is presumed to be inefficient, thus disfavoring the reversibility of this reaction.

Recently, a novel class of RT inhibitors, referred to as nucleotide-competing RT inhibitors (NcRTIs), was identified.^{14,15,41} Biochemical studies suggest that these compounds compete with the nucleotide substrate for binding to the RT active site, blocking translocation of HIV-1 RT at the pre- or post-translocation DNA/RT complex. Included in this mechanism-based category is the pyrophosphate bioisosteres **2.3b**, which traps the RT/DNA pre-translocation complex.¹² In an effort to identify better “drug-like” molecules for further optimization into novel antiviral agents with NcRTI-like mechanism of action, we explored the ability of pyridopyrimidine-based bisphosphonates (PYPY-BPs) to inhibit the HIV-1 RT-catalyzed DNA polymerization. We developed a modular protocol that is amenable to high throughput parallel synthesis of compound libraries. In the course of our methodology development, we prepared a mini-library of analogs and identified several hits of low micromolar inhibitors, such as compound **2.8m** ($IC_{50} = \sim 1.8 \mu M$), which exhibits equivalent potency to foscarnet (**2.3b**; $IC_{50} = \sim 2.5 \mu M$) in inhibiting HIV-1 RT-catalyzed DNA synthesis. Preliminary SAR and biochemical evidence also suggests that the structural/molecular recognition can be fine-tuned to provide molecules that are selective in inhibiting HIV-1 RT versus other biological targets that are more commonly associated with bisphosphonate inhibitors, such as the human FPPS.

2.7. Experimental Section

General Procedures for Characterization of Compounds:

All compounds were purified by normal phase flash column chromatography on silica gel using a CombiFlash instrument and a solvent gradient from 5% EtOAc in hexanes to 100% EtOAc and then to 20% MeOH in EtOAc, unless otherwise indicated. The homogeneity of all final compounds was confirmed to be $\geq 95\%$ by reverse-phase HPLC. Only phosphonate esters with

homogeneity $\geq 90\%$ were processed further to the final phosphonic acid inhibitors. HPLC analysis was performed using a Waters ALLIANCE[®] instrument (e2695 with 2489 UV detector and 3100 mass spectrometer). Final compounds were fully characterized by ¹H, ¹³C and ³¹P NMR, and HRMS. Chemical shifts (δ) are reported in ppm relative to the internal deuterated solvent (¹H, ¹³C) or external H₃PO₄ (δ 0.00 ³¹P), unless indicated otherwise. The NMR spectra of all final bisphosphonate inhibitors were acquired in D₂O with 0.15% ND₄OD. In many cases, the C α to the bisphosphonate of intermediates **2.26** and final inhibitors **2.8** was broad and overlapped with the solvent peak, as confirmed by the HSQC data; the HSQC data of key compounds are provided. The high resolution MS spectra of final products were recorded using electrospray ionization (ESI^{+/-}) and Fourier transform ion cyclotron resonance mass analyzer (FTMS).

Method (homogeneity analysis using a Waters Atlantis T3 C18 5 μ m column):

Solvent A: H₂O, 0.1% formic acid

Solvent B: CH₃CN, 0.1% formic acid

Mobile phase: linear gradient from 95%A and 5%B to 0%A and 100%B in 13 min

Library Synthesis

General Synthetic Protocols: Suzuki cross-coupling reactions and deprotection of the phosphonate esters to the phosphonic acids were carried out using the general protocols previously reported.^{16a} Reductive scission of the thioether was performed using the protocol of Graham and co-workers.³⁹ Selective bromination at C-5 of the 2-aminonicotinonitrile scaffolds was carried out using 1.1 eq. of *N*-bromosuccinimide in acetonitrile for 4 h in the dark at rt.⁴² The 2-amino moieties of intermediates **2.20** were converted to the corresponding *N,N*-dimethyl formamidine derivatives

2.21 with *N,N*-dimethylformamide dimethyl acetal (~10 eq.) in DMF at rt using a slightly modified literature procedure.⁴³

General Protocol for the Cyclization of Intermediate 2.21 to the 4-amino-pyridopyrimidine core (2.23 or 2.25): In a pressure vessel equipped with a magnetic stir bar, a compound of general structure **2.21** was added, with ammonium acetate (1.1 eq) and acetic acid. The mixture was heated at 100°C for 1-2 h. The resulting mixture was cooled, concentrated under vacuum, the residual acetic acid was co-evaporated with toluene and the residue was suspended in 30% EtOAc in hexanes. The precipitate was filtered, washed several times with 30% EtOAc in hexanes and dried under vacuum. The crude products **2.23** or **2.25** (usually >95% homogeneity) were used in the subsequent step without further purification.

2-Amino-6-(methylthio)-4-(trimethylsilyl)nicotinonitrile (2.14b): The synthesis of 2-(1-(trimethylsilyl)ethylidene)malononitrile (**2.12c**) was previously reported.³⁷ In a 100-mL round bottom flask, **2.12c** (2.00 g, 12.17 mmol), K₂CO₃ (1.94 g, 14.0 mmol) and dimethyl *N*-cyanodithioiminocarbonate (3.08 g, 21.1 mmol) were suspended in DMF (30 mL) and stirred for 12 h at rt. Piperidine (1.9 mL, 19.5 mmol) was then added and the mixture was stirred at 60°C for 12 h. The resulting mixture was diluted with EtOAc and water. The organic layer was collected and washed with water (3x), then brine (once), and finally dried with anhydrous MgSO₄. The solvent was removed under vacuum to obtain a black residue, which was purified by normal phase column chromatography on silica gel (solvent gradient from 0% to 20% EtOAc in hexanes with 0.1% Et₃N). The product was obtained as yellow oil (1.39 g, 48%). The desilylated product (**2.14c**) was also isolated in small amount (~10% yield).

^1H NMR (500 MHz, CDCl_3) δ 6.63 (s, 1H), 5.12 (br_s, 2H), 2.49 (s, 3H), 0.36 (s, 9H). ^{13}C NMR (126 MHz, CDCl_3) δ 163.9, 159.3, 154.3, 118.6, 116.2, 89.0, 13.0, -1.90.

HRMS [ESI⁺] calculated for $\text{C}_{10}\text{H}_{16}\text{N}_3\text{SSi}$ m/z : 238.08287; found 238.08299 [M + H⁺].⁺

2-Amino-6-(methylthio)nicotinonitrile (2.14c): The product was obtained as a light yellow powder (in >85% after the mixture of **2.14b** and **2.14c** was treated with TBAF).

^1H NMR (400 MHz, CDCl_3) δ 7.43 (d, J = 8.2 Hz, 1H), 6.58 (d, J = 8.2 Hz, 1H), 5.14 (br_s, 2H), 2.50 (s, 3H). ^{13}C NMR (125 MHz, CDCl_3) δ 165.7, 158.8, 139.8, 117.3, 111.0, 85.2, 13.2

MS [ESI⁺] m/z : 166.23 [M + H⁺].⁺

2-Amino-6-methoxynicotinonitrile (2.19, R₄ = R₅ = H, R₆ = OMe): The product was isolated as white solid (38.7 mg, 83%).

^1H NMR (300 MHz, CDCl_3): δ 7.50 (d, J = 8.5 Hz, 1H), 6.11 (d, J = 8.5 Hz, 1H), 5.13 (br_s, 2H), 3.86 (s, 3H). ^{13}C NMR (75 MHz, CDCl_3): δ 166.2, 159.7, 142.8, 117.7, 100.9, 81.7, 53.8.

MS [ESI⁺] m/z : 150.15 [M + H⁺].⁺

2-Amino-5-bromo-6-(methylthio)-4-(trimethylsilyl)nicotinonitrile (2.20a): Compound **2.14b** was isolated as yellow-orange solid (935 mg, 78%).

^1H NMR (500 MHz, CDCl_3) δ 5.16 (br_s, 2H), 2.44 (s, 3H), 0.54 (s, 9H). ^{13}C NMR (126 MHz, CDCl_3) δ 164.8, 158.3, 152.6, 118.2, 113.4, 91.1, 15.3, 1.3. HRMS [ESI⁺] calculated for $\text{C}_{10}\text{H}_{15}\text{BrN}_3\text{SSi}$ m/z : 315.99338; found 315.99258 [M + H⁺].⁺

2-Amino-5-bromo-6-(methylthio)nicotinonitrile (2.20b): Tetra-*n*-butylammonium fluoride (3.13 mL, 3.13 mmol) was added to **2.20a** (900 mg, 2.85 mmol) in THF (15.0 mL). The mixture was stirred for 12 h at rt. The solvent was removed under vacuum and the residue was re-dissolved

in EtOAc, washed with water and brine. The combined organic layers were dried over anhydrous MgSO₄, and then concentrated under vacuum. The crude product was purified by chromatography on silica gel (2% - 30% EtOAc in hexanes with 0.1% Et₃N) to give the final product as a light yellow powder (694 mg, quantitative).

¹H NMR (500 MHz, CDCl₃) δ 7.59 (s, 1H), 5.15 (br_s, 2H), 2.48 (s, 3H).

¹³C NMR (126 MHz, CDCl₃) δ 164.9, 157.3, 141.7, 116.0, 104.9, 86.5, 14.5.

MS [ESI⁺] *m/z*: 243.95 [M + H⁺].⁺

2-Amino-5-bromonicotinonitrile (2.20c, R₄ = R₆ = H): Compound **2.20c** was isolated as an off-white solid (438 mg, 88%).

¹H NMR (400 MHz, CDCl₃) δ 8.28 (d, *J* = 2.4 Hz, 1H), 7.78 (d, *J* = 2.4 Hz, 1H), 5.23 (br_s, 2H).

¹³C NMR (126 MHz, CDCl₃) δ 157.7, 153.9, 142.8, 115.2, 106.8, 92.8.

MS [ESI⁺] *m/z*: 197.96 [M + H⁺].⁺

***N'*-(3-cyano-6-(methylthio)-4-(trimethylsilyl)pyridin-2-yl)-*N,N*-dimethylformimidamide**

(2.21a, R₄ = TMS, R₅ = H, R₆ = SMe): Product was obtained as a yellow solid (552 mg, 90%).

¹H NMR (400 MHz, CDCl₃): δ 8.65 (s, 1H), 6.83 (s, 1H), 3.20 (s, 3H), 3.15 (s, 3H), 2.54 (s, 3H), 0.39 (s, 9H).

¹³C NMR (126 MHz, CDCl₃): δ 162.7, 162.1, 155.7, 154.9, 119.3, 119.1, 101.1, 41.0, 35.0, 13.1, -1.93.

MS [ESI⁺] *m/z*: 293.12 [M + H⁺].⁺

***N'*-(3-Cyano-6-(methylthio)pyridin-2-yl)-*N,N*-dimethylformimidamide (2.21b, R₄ = R₅ = H, R₆ = SMe):** The product was obtained as a yellow orange oil that solidifies upon standing at room temperature (298.1 mg, 93%).

^1H NMR (400 MHz, CDCl_3) δ 8.65 (s, 1H), 7.54 (d, $J=8.1$ Hz, 1H), 6.74 (d, $J=8.2$ Hz, 1H), 3.18 (s, 3H), 3.15 (s, 3H), 2.54 (s, 3H).

MS [ESI⁺] m/z : 221.078 [M + H⁺]⁺.

***N'*-(5-Bromo-3-cyano-6-(methylthio)pyridin-2-yl)-*N,N*-dimethylformimidamide (2.21c, R₄ = H, R₅ = Br, R₆ = SMe):** The product was obtained as a yellow-orange solid (246 mg, 72%).

^1H NMR (400 MHz, CDCl_3): δ 8.65 (s, 1H), 7.70 (s, 1H), 3.19 (s, 3H), 3.16 (s, 3H), 2.53 (s, 3H).

^{13}C NMR (126 MHz, CDCl_3): δ 162.7, 161.0, 155.8, 142.7, 116.9, 108.7, 97.7, 41.2, 35.1, 14.5.

MS [ESI⁺] m/z : 298.99 [M + H⁺]⁺.

***N'*-(3-Cyanopyridin-2-yl)-*N,N*-dimethylformimidamide (2.21d, R₄ = R₅ = R₆ = H):**

The product was isolated as a colorless oil (115 mg, 79%).

^1H NMR (400 MHz, acetone- d_6) δ 8.67 (s, 1H), 8.37 (dd, $J = 4.8, 2.0$ Hz, 1H), 7.92 (dd, $J = 7.6, 2.0$ Hz, 1H), 6.97 (dd, $J = 7.7, 4.8$ Hz, 1H), 3.23 (s, 3H), 3.14 (s, 3H).

MS [ESI⁺] m/z : 175.09 [M + H⁺]⁺.

***N'*-(5-Bromo-3-cyanopyridin-2-yl)-*N,N*-dimethylformimidamide (2.21e, R₄ = R₆ = H, R₅ = Br):** The product was isolated as a white solid (289.7 mg, 76%).

^1H NMR (400 MHz, CDCl_3): δ 8.56 (s, 1H), 8.35 (d, $J = 2.5$ Hz, 1H), 7.86 (d, $J = 2.6$ Hz, 1H), 3.18 (s, 3H), 3.16 (s, 3H).

MS [ESI⁺] m/z : 253.00 [M + H⁺]⁺.

***N'*-(3-Cyano-5-(4-methoxyphenyl)-6-(methylthio)-4-(trimethylsilyl)pyridin-2-yl)-*N,N*-dimethylformimidamide (2.21f, R₄ = TMS, R₅ = *p*-methoxyphenyl, R₆ = SMe):**

The product was isolated as a yellow solid (43.5 mg, 83%).

^1H NMR (400 MHz, CDCl_3): δ 8.70 (s, 1H), 7.09 (d, $J = 8.7$ Hz, 2H), 6.93 (d, $J = 8.7$ Hz, 2H), 3.85 (s, 3H), 3.21 (s, 3H), 3.15 (s, 3H), 2.39 (s, 3H), 0.06 (s, 9H).

MS [ESI $^+$] m/z : 399.16 [M + H $^+$] $^+$.

***N'*-(3-Cyano-5-(3-methoxyphenyl)-6-(methylthio)pyridin-2-yl)-*N,N*-dimethylformimidamide (2.21g, R $_4$ = H, R $_5$ = *m*-methoxyphenyl, R $_6$ = SMe):**

The product was isolated as a yellow solid (46.6 mg, 85%).

^1H NMR (400 MHz, CDCl_3): δ 8.73 (s, 1H), 7.48 (s, 1H), 7.38 – 7.31 (m, 1H), 7.00 - 6.90 (m, 3H), 3.84 (s, 3H), 3.21 (s, 3H), 3.18 (s, 3H), 2.49 (s, 3H)

^{13}C NMR (126 MHz, DMSO-d_6): δ 161.3, 161.3, 159.6, 156.6, 141.0, 138.2, 129.8, 128.5, 121.7, 118.2, 114.9, 114.0, 95.8, 55.5, 41.1, 34.9, 13.7.

MS [ESI $^+$] m/z : 327.22 [M + H $^+$] $^+$.

***N'*-(3-Cyano-6-(methylthio)-5-(thiophen-3-yl)pyridin-2-yl)-*N,N*-dimethylformimidamide**

(2.21h, R $_4$ = H, R $_5$ = 3-thiophenyl, R $_6$ = SMe): The product was isolated as a yellow solid (54.1 mg, 76%).

^1H NMR (400 MHz, CDCl_3): δ 8.72 (s, 1H), 7.54 (s, 1H), 7.40 (ddd, $J = 7.9, 3.9, 2.2$ Hz, 2H), 7.22 (dd, $J = 4.9, 1.4$ Hz, 1H), 3.21 (s, 3H), 3.17 (s, 3H), 2.51 (s, 3H).

^{13}C NMR (126 MHz, DMSO-d_6): δ 161.6, 161.0, 155.7, 140.5, 136.8, 128.3, 125.7, 124.3, 124.2, 118.1, 96.5, 41.1, 35.0, 13.7.

MS [ESI $^+$] m/z : 303.16 [M + H $^+$] $^+$.

***N'*-(3-Cyano-6-(methylthio)-5-phenylpyridin-2-yl)-*N,N*-dimethylformimidamide (2.21i, R $_4$ = H, R $_5$ = phenyl, R $_6$ = SMe):** The product was isolated as a light yellow solid (24.3 mg, 82%).

¹H NMR (400 MHz, CDCl₃): δ 8.73 (s, 1H), 7.47 (s, 1H), 7.46-7.36 (m, 5H), 3.21 (s, 3H), 3.18 (s, 3H), 2.49 (s, 3H).

¹³C NMR (126 MHz, CDCl₃): δ 161.6, 161.2, 155.7, 140.6, 136.8, 129.3, 129.2, 128.5, 128.2, 118.2, 96.5, 41.1, 35.0, 13.7.

MS [ESI⁺] *m/z*: 297.21 [M + H⁺]⁺.

***N'*-(3-Cyano-5-phenylpyridin-2-yl)-*N,N*-dimethylformimidamide (2.21j, R₄ = R₆ = H, R₅ = phenyl):** The product was isolated as a yellow solid (185.3 mg, 74%).

¹H NMR (400 MHz, CDCl₃): δ 8.63 (s, 1H), 8.58 (d, *J* = 2.6 Hz, 1H), 8.00 (d, *J* = 2.6 Hz, 1H), 7.54 – 7.49 (m, 2H), 7.49 – 7.43 (m, 2H), 7.41 – 7.31 (m, 1H), 3.21 (s, 3H), 3.17 (s, 3H).

MS [ESI⁺] *m/z*: 251.18 [M + H⁺]⁺.

***N'*-(3-Cyano-5-(4-isopropoxyphenyl)pyridin-2-yl)-*N,N*-dimethylformimidamide (2.21k, R₄ = R₆ = H, R₅ = 4-isopropoxyphenyl):** The product was isolated as a yellow solid (252.7 mg, 82%).

¹H NMR (400 MHz, CDCl₃) δ 8.60 (s, 1H), 8.54 (d, *J* = 2.6, 1H), 7.94 (d, *J* = 2.6, 1H), 7.42 (d, *J* = 8.6 Hz, 2H), 6.96 (d, *J* = 8.7 Hz, 2H), 4.59 (hept, *J* = 6.0 Hz, 1H), 3.20 (s, 3H), 3.16 (s, 3H), 1.37 (s, 3H), 1.35 (s, 3H).

MS [ESI⁺] *m/z*: 309.26 [M + H⁺]⁺.

***N'*-(3-Cyano-5-(thiophen-2-yl)pyridin-2-yl)-*N,N*-dimethylformimidamide (2.21l, R₄ = R₆ = H, R₅ = 2-thiophenyl):** The product was isolated as a yellow solid (51.7 mg, 51%).

¹H NMR (400 MHz, CDCl₃): δ 8.62 (s, 1H), 8.59 (d, *J* = 2.6 Hz, 1H), 7.97 (d, *J* = 2.6 Hz, 1H), 7.31 (dd, *J* = 5.1, 1.1 Hz, 1H), 7.25 – 7.23 (m, 1H), 7.10 (dd, *J* = 5.1, 3.6 Hz, 1H), 3.20 (s, 3H), 3.17 (s, 3H).

MS [ESI⁺] *m/z*: 257.08 [M + H⁺]⁺.

***N'*-(3-Cyano-5-(thiophen-3-yl)pyridin-2-yl)-*N,N*-dimethylformimidamide (2.21m, R₄ = R₆ = H, R₅ = 3-thiophenyl):** The product was isolated as a brown solid (100.5 mg, 66%).

¹H NMR (500 MHz, CDCl₃): δ 8.63 (s, 1H), 8.59 (d, *J* = 2.5 Hz, 1H), 7.98 (d, *J* = 2.5 Hz, 1H), 7.45 – 7.41 (m, 2H), 7.31 (dd, *J* = 4.8, 1.6 Hz, 1H), 3.20 (s, 3H), 3.17 (s, 3H).

MS [ESI⁺] *m/z*: 257.08 [M + H⁺]⁺.

***N'*-(3-Cyano-5-(3,5-dimethylisoxazol-4-yl)pyridin-2-yl)-*N,N*-dimethylformimidamide**

(2.21n, R₄ = R₆ = H, R₅ = 3,5-dimethylisoxazol-4-yl): The product was obtained as a yellow solid (74.5 mg, 70%).

¹H NMR (400 MHz, CDCl₃) δ 8.64 (s, 1H), 8.24 (d, *J* = 2.4 Hz, 1H), 7.67 (d, *J* = 2.5 Hz, 1H), 3.22 (s, 3H), 3.18 (s, 3H), 2.41 (s, 3H), 2.26 (s, 3H).

MS [ESI⁺] *m/z*: 270.13 [M + H⁺]⁺.

***N'*-(3-Cyano-5-(4-methoxyphenyl)pyridin-2-yl)-*N,N*-dimethylformimidamide (2.21o, R₄ = R₆ = H, R₅ = 4-methoxyphenyl):** The product was isolated as a light brown solid (110.2 mg, 66%).

¹H NMR (500 MHz, CDCl₃) δ 8.63 (s, 1H), 8.53 (d, *J* = 2.6 Hz, 1H), 7.95 (d, *J* = 2.5 Hz, 1H), 7.48 – 7.40 (m, 2H), 7.02 – 6.95 (m, 2H), 3.85 (s, 3H), 3.20 (s, 3H), 3.17 (s, 3H). MS [ESI⁺] *m/z*: 281.23 [M + H⁺]⁺.

***N'*-(3-Cyano-5-(*p*-tolyl)pyridin-2-yl)-*N,N*-dimethylformimidamide (2.21p, R₄ = R₆ = H, R₅ = *p*-tolyl):** The product was isolated as a yellow solid (45.6 mg, 87%).

¹H NMR (500 MHz, CDCl₃): δ 8.62 (s, 1H), 8.56 (d, *J* = 2.6 Hz, 1H), 7.97 (d, *J* = 2.6 Hz, 1H), 7.42 – 7.39 (m, 2H), 7.28 – 7.26 (m, 2H), 3.20 (s, 3H), 3.16 (s, 3H), 2.40 (s, 3H). MS [ESI⁺] *m/z*: 265.14 [M + H⁺]⁺.

***N'*-(3-Cyano-6-(thiophen-2-yl)pyridin-2-yl)-*N,N*-dimethylformimidamide (2.21q, R₄ = R₅ = H, R₆ = 2-thiophenyl):** Prepared following the protocol described by Knochel and co-workers.³⁸ To a dry argon-flushed 50-mL round bottom flask equipped with a septum and a magnetic stirrer bar, intermediate **2.21b** was added (100.0 mg, 0.454 mmol), Pd(OAc)₂ (2.5 mol%), and S-Phos (5.0 mol %) dissolved in THF (1.0 mL). After 10 min of stirring, the organozinc reagent was added drop-wise and the reaction mixture was stirred at RT for 1 h and then at 50°C for 16 h. The resulting reaction mixture was cooled, quenched with saturated solution of aqueous NH₄Cl and extracted with EtOAc (3 x 15 mL). The crude product was purified by chromatography on silica gel (1% - 25% EtOAc in hexanes with 0.1% triethylamine). The product was isolated as a yellow solid (49.6 mg, 43%).

¹H NMR (500 MHz, CDCl₃) δ 8.71 (s, 1H), 7.76 (d, *J* = 8.0 Hz, 1H), 7.62 (dd, *J* = 3.7, 1.1 Hz, 1H), 7.44 (dd, *J* = 5.0, 1.1 Hz, 1H), 7.22 (d, *J* = 8.0 Hz, 1H), 7.12 (dd, *J* = 5.0, 3.7 Hz, 1H), 3.20 (s, 3H), 3.19 (s, 3H).

¹³C NMR (126 MHz, CDCl₃) δ 162.9, 156.1, 153.9, 144.3, 142.2, 129.0, 128.2, 126.2, 118.0, 111.5, 99.9, 41.1, 35.0.

MS [ESI⁺] *m/z*: 257.078 [M + H⁺]⁺.

***N'*-(3-Cyano-6-(methylthio)-5-(3-nitrophenyl)-4-(trimethylsilyl)pyridin-2-yl)-*N,N*-dimethylformimidamide (2.21r, R₄ = TMS, R₅ = 3-nitrophenyl, R₆ = SMe):** Product was obtained as a yellow solid (75.5 mg, 80%).

¹H NMR (400 MHz, CDCl₃): δ 8.71 (s, 1H), 8.29 (ddd, *J* = 8.1, 2.3, 1.3 Hz, 1H), 8.11 – 8.09 (t, *J* = 1.9 Hz, 1H), (m, 1H), 7.60 (t, *J* = 7.8 Hz, 1H), 7.54 (dt, *J* = 7.6, 1.4 Hz, 1H), 3.23 (s, 3H), 3.18 (s, 3H), 2.42 (s, 3H), 0.05 (s, 9H).

MS [ESI⁺] *m/z*: 414.13 [M + H⁺]⁺.

***N'*-(3-Cyano-6-methoxypyridin-2-yl)-*N,N*-dimethylformimidamide (2.21s, R₄ = R₅ = H, R₆ =**

OMe): The product was isolated as a white solid (104 mg, 95%).

¹H NMR (300 MHz, CDCl₃): δ 8.58 (s, 1H), 7.60 (d, *J* = 8.4 Hz, 1H), 6.27 (d, *J* = 8.4 Hz, 1H), 3.89 (s, 3H), 3.15 (s, 3H), 3.13 (s, 3H).

¹³C NMR (75 MHz, CDCl₃): δ 165.0, 163.1, 155.9, 143.3, 118.6, 104.0, 93.4, 53.5, 41.0, 35.0.

MS [ESI⁺] *m/z*: 205.13 [M + H⁺]⁺.

***N*-(3-Cyano-5-(4-methoxyphenyl)-6-(methylthio)-4-(trimethylsilyl)pyridin-2-yl)formamide**

(2.22a, R₄ = TMS, R₅ = 4-methoxyphenyl, R₆ = SMe): The product was isolated as a light yellow solid (22.3 mg, 60%).

¹H NMR (500 MHz, CDCl₃): δ 9.64 (d, *J* = 9.9 Hz, 1H), 8.18 (d, *J* = 9.8 Hz, 1H), 7.11 – 7.03 (m, 2H), 6.99 – 6.94 (m, 2H), 3.87 (s, 3H), 2.38 (s, 3H), 0.08 (s, 9H).

¹³C NMR (126 MHz, CDCl₃): δ 166.1, 161.4, 160.2, 152.8, 151.5, 136.8, 131.8, 129.2, 117.1, 114.1, 93.4, 55.3, 14.6, 0.3.

HRMS [ESI⁺] calculated for C₁₈H₂₂N₃O₂SSi *m/z*: 372.11965; found 372.11850[M + H⁺]⁺.

***N*-(3-Cyano-6-(methylthio)-5-(3-nitrophenyl)-4-(trimethylsilyl)pyridin-2-yl)formamide**

(2.22b, R₄ = TMS, R₅ = 3-nitrophenyl, R₆ = SMe): The product was isolated as a yellow solid (32.5 mg, 70%).

¹H NMR (500 MHz, CDCl₃): δ 9.65 (d, *J* = 9.8 Hz, 1H), 8.34 (ddd, *J* = 8.3, 2.3, 1.0 Hz, 1H), 8.21 (d, *J* = 9.7 Hz, 1H), 8.09 (t, *J* = 1.9 Hz, 1H), 7.66 (t, *J* = 7.9 Hz, 1H), 7.57 – 7.51 (m, 1H), 2.42 (s, 3H), 0.08 (s, 9H).

^{13}C NMR (126 MHz, CDCl_3) δ 165.2, 161.2, 153.2, 152.2, 148.3, 138.8, 136.9, 134.1, 129.9, 125.9, 124.1, 116.7, 93.8, 14.6, 0.4.

HRMS [ESI $^-$] calculated for $\text{C}_{17}\text{H}_{17}\text{N}_4\text{O}_3\text{SSi}$ m/z : 385.07961; found 385.07983 [M - H $^+$] $^-$.

7-(Methylthio)pyrido[2,3-*d*]pyrimidin-4-amine (2.23a, R₅ = R₆ = H, R₇ = SMe): Product was isolated as yellow solid (26 mg, 100%)

^1H NMR (400 MHz, CD_3OD) δ 8.45 (s, 1H), 8.11 (d, J = 8.0 Hz, 1H), 7.24 (d, J = 8.0 Hz, 1H), 2.65 (s, 3H).

^{13}C NMR (125 MHz, $\text{DMSO-}d_6$) δ 167.0, 163.3, 159.3, 159.2, 132.9, 120.1, 105.9, 12.9.

MS [ESI $^+$] m/z : 193.05 [M + H $^+$] $^+$.

6-Bromo-7-(methylthio)pyrido[2,3-*d*]pyrimidin-4-amine (2.23b, R₆ = Br):

The product was isolated as a yellow solid (167.1 mg, 88%).

^1H NMR (400 MHz, $\text{DMSO-}d_6$) δ 8.82 (s, 1H), 8.46 (s, 1H), 8.03 (br_s, 2H), 2.57 (s, 3H).

^{13}C NMR (126 MHz, $\text{DMSO-}d_6$) δ 165.9, 162.7, 159.6, 157.6, 135.6, 114.6, 107.0, 14.7. MS [ESI $^+$] m/z : 270.96 [M + H $^+$] $^+$.

7-(Methylthio)-6-phenylpyrido[2,3-*d*]pyrimidin-4-amine (2.23c, R₆ = phenyl):

Product was isolated as light yellow powder (42.5 mg, 94%).

^1H NMR (400 MHz, CD_3OD) δ 8.49 (s, 1H), 8.22 (s, 1H), 7.53 – 7.43 (m, 5H), 2.62 (s, 3H).

^{13}C NMR (126 MHz, CD_3OD) δ 168.1, 163.6, 157.2, 155.9, 136.7, 135.5, 131.2, 129.1, 128.4, 128.2, 105.0, 12.7.

HRMS [ESI $^{+/-}$] calculated for $\text{C}_{14}\text{H}_{13}\text{N}_4\text{S}$ m/z : 269.08554; found 269.08445 [M + H $^+$] $^+$.

6-(3-Methoxyphenyl)-7-(methylthio)pyrido[2,3-d]pyrimidin-4-amine (2.23d, R₆ = 3-

methoxyphenyl): Product was isolated as yellow powder (30.4 mg, 86%).

¹H NMR (400 MHz, DMSO-d₆): δ 8.45 (s, 1H), 8.36 (s, 1H), 7.91 (br_s, 2H), 7.41 (t, *J* = 7.7 Hz, 1H), 7.08 – 7.00 (m, 3H), 3.79 (s, 3H), 2.51 (s, 3H).

¹³C NMR (126 MHz, DMSO-d₆): δ 165.4, 163.5, 159.6, 159.2, 158.1, 138.5, 133.8, 132.5, 130.1, 122.0, 115.4, 114.5, 105.0, 55.7, 13.8.

MS [ESI⁺] *m/z*: 299.20 [M + H⁺]⁺.

7-(Methylthio)-6-(thiophen-3-yl)pyrido[2,3-d]pyrimidin-4-amine (2.23e, R₆ = 3-thiophenyl):

Product was isolated as a yellow powder (37.4 mg, 94%).

¹H NMR (400 MHz, DMSO-d₆): δ 8.44 (s, 2H), 7.92 (br_s, 2H), 7.79 (dd, *J* = 2.9, 1.3 Hz, 1H), 7.70 (dd, *J* = 5.0, 3.0 Hz, 1H), 7.37 (dd, *J* = 5.0, 1.3 Hz, 1H), 2.54 (s, 3H).

¹³C NMR (126 MHz, DMSO-d₆): δ 165.5, 163.4, 159.2, 157.9, 137.2, 132.5, 129.2, 129.0, 127.0, 126.1, 105.8, 13.8.

MS [ESI⁺] *m/z*: 275.15 [M + H⁺]⁺.

6-(4-Isopropoxyphenyl)-7-(methylthio)pyrido[2,3-d]pyrimidin-4-amine (2.23f, R₆ = 4-

isopropoxyphenyl): The product was isolated as a yellow solid (104.2 mg, 57%).

¹H NMR (400 MHz, DMSO-d₆): δ 8.45 (s, 1H), 8.33 (s, 1H), 7.88 (br_s, 2H), 7.41 (d, *J* = 8.6 Hz, 2H), 7.03 (d, *J* = 8.7 Hz, 2H), 4.70 (hept, *J* = 6.0 Hz, 1H), 2.53 (s, 3H), 1.31 (s, 3H), 1.30 (s, 3H).

¹³C NMR (126 MHz, DMSO-d₆): δ 165.4, 163.0, 158.6, 157.6, 157.5, 133.4, 131.8, 130.7, 128.7, 115.4, 105.4, 69.2, 21.8, 13.4.

MS [ESI⁺] *m/z*: 327.12 [M + H⁺]⁺.

Pyrido[2,3-*d*]pyrimidin-4-amine (2.25a, R₅ = R₆ = R₇ = H): Product was isolated as white solids (63.0 mg, 75%).

¹H NMR (400 MHz, DMSO-*d*₆): δ 8.98 (dd, *J* = 4.4, 1.9 Hz, 1H), 8.66 (dd, *J* = 8.2, 1.9 Hz, 1H), 8.52 (s, 1H), 8.09 (br_s, 2H), 7.52 (dd, *J* = 8.2, 4.4 Hz, 1H).

¹³C NMR (126 MHz, DMSO-*d*₆): δ 163.6, 159.1, 159.0, 156.4, 133.7, 121.6, 109.5.

6-Bromopyrido[2,3-*d*]pyrimidin-4-amine (2.25b, R₅ = R₇ = H, R₆ = Br): Product was isolated as light yellow powder (210.7 mg, 95%).

¹H NMR (400 MHz, DMSO-*d*₆): δ 9.03 (d, *J* = 2.5 Hz, 1H), 8.97 (d, *J* = 2.5 Hz, 1H), 8.53 (s, 1H), 8.19 (br_s, 2H).

¹³C NMR (126 MHz, DMSO-*d*₆) δ 162.9, 159.5, 157.5, 157.0, 135.6, 115.7, 110.6; MS [ESI⁺] *m/z*: 224.97 [M + H⁺]⁺.

6-Phenylpyrido[2,3-*d*]pyrimidin-4-amine (2.25c, R₅ = R₇ = H, R₆ = phenyl):

Product was isolated as light yellow powder (160.0 mg, 97%).

¹H NMR (400 MHz, DMSO-*d*₆): δ 9.33 (d, *J* = 2.5 Hz, 1H), 8.99 (d, *J* = 2.5 Hz, 1H), 8.51 (s, 1H), 7.89 – 7.83 (m, 2H), 7.58 – 7.51 (m, 2H), 7.48 – 7.41 (m, 1H).

¹³C NMR (126 MHz, DMSO-*d*₆): δ 163.8, 159.0, 158.3, 154.8, 136.7, 133.1, 130.7, 129.7, 128.8, 127.4, 109.2.

MS [ESI⁺] *m/z*: 223.09 [M + H⁺]⁺.

6-(4-Isopropoxyphenyl)pyrido[2,3-*d*]pyrimidin-4-amine (2.25d, R₅ = R₇ = H, R₆ = 4-isopropoxyphenyl): Product was isolated as light yellow powder (160 mg, 97%).

¹H NMR (500 MHz, DMSO-d₆): δ 9.31 (d, *J* = 2.5 Hz, 1H), 8.93 (d, *J* = 2.5 Hz, 1H), 8.50 (s, 1H), 8.12 (br_s, 2H), 7.80 (d, *J* = 8.8 Hz, 2H), 7.09 (d, *J* = 8.8 Hz, 2H), 4.71 (hept, *J* = 6.0 Hz, 1H), 1.31 (s, 3H), 1.30 (s, 3H).

¹³C NMR (101 MHz, DMSO-d₆): δ 163.7, 158.6, 158.2, 157.8, 154.5, 132.9, 129.6, 128.7, 128.6, 116.7, 109.3, 69.8, 22.2.

MS [ESI⁺] *m/z*: 281.24 [M + H⁺]⁺.

Synthesis of 6-(thiophen-2-yl)pyrido[2,3-*d*]pyrimidin-4-amine (2.25e, R₅ = R₇ = H, R₆ = 2-thiophenyl): The product was isolated as a yellow solid (80.3 mg; 80%).

¹H NMR (500 MHz, DMSO-d₆): δ 9.35 (d, *J* = 2.5 Hz, 1H), 8.93 (d, *J* = 2.5 Hz, 1H), 8.54 (s, 1H), 8.30 (br_s, 2H), 7.76 (dd, *J* = 3.6, 1.1 Hz, 1H), 7.72 (dd, *J* = 5.1, 1.1 Hz, 1H), 7.25 (dd, *J* = 5.1, 3.6 Hz, 1H).

MS [ESI⁺] *m/z*: 229.05 [M + H⁺]⁺.

6-(3,5-Dimethylisoxazol-4-yl)pyrido[2,3-*d*]pyrimidin-4-amine (2.25f, R₅ = R₇ = H, R₆ = 3,5-dimethylisoxazol-4-yl): The product was isolated as a yellow solid (79.5 mg, 69%).

¹H NMR (500 MHz, DMSO-d₆) δ 9.02 (d, *J* = 2.4 Hz, 1H), 8.65 (d, *J* = 2.4 Hz, 1H), 8.56 (s, 1H), 8.19 (s, 2H), 2.32 (s, 3H), 1.91 (s, 3H).

MS [ESI⁺] *m/z*: 242.10 [M + H⁺]⁺.

6-(*p*-Tolyl)pyrido[2,3-*d*]pyrimidin-4-amine (2.25g, R₅ = R₇ = H, R₆ = *p*-tolyl): The product was isolated as a light orange solid (29.4 mg, 63%).

¹H NMR (500 MHz, DMSO-d₆): δ 9.33 (d, *J* = 2.5 Hz, 1H), 8.97 (d, *J* = 2.5 Hz, 1H), 8.52 (s, 1H), 8.17 (br_s, 2H), 7.78 (d, *J* = 8.1 Hz, 2H), 7.37 (d, *J* = 7.9 Hz, 2H), 2.38 (s, 3H),

MS [ESI⁺] *m/z*: 237.11 [M + H⁺]⁺.

6-(4-Methoxyphenyl)pyrido[2,3-d]pyrimidin-4-amine (2.25h, R₅ = R₇ = H, R₆ = 4-methoxyphenyl): The product was isolated as a yellow solid (85.6 mg, 95%).

¹H NMR (500 MHz, DMSO-d₆): δ 9.32 (d, *J* = 2.5 Hz, 1H), 8.94 (d, *J* = 2.5 Hz, 1H), 8.51 (s, 1H), 8.13 (br_s, 2H), 7.83 (d, *J* = 8.8 Hz, 2H), 7.12 (d, *J* = 8.8 Hz, 2H), 3.84 (s, 3H).

¹³C NMR (126 MHz, DMSO-d₆): δ 163.7, 160.0, 158.7, 157.9, 154.5, 132.9, 129.6, 129.0, 128.6, 115.1, 109.3, 55.8.

MS [ESI⁺] *m/z*: 253.19 [M + H⁺]⁺.

6-(Thiophen-3-yl)pyrido[2,3-d]pyrimidin-4-amine (2.25i, R₅ = R₇ = H, R₆ = 3-thiophenyl):

The product was isolated as a light brown solid (85.4 mg, quantitative).

¹H NMR (500 MHz, DMSO-d₆): δ 9.43 (d, *J* = 2.4 Hz, 1H), 9.00 (d, *J* = 2.5 Hz, 1H), 8.51 (s, 1H), 8.15 (dd, *J* = 2.9, 1.4 Hz, 1H), 8.10 (br_s, 2H), 7.78 (dd, *J* = 5.0, 2.9 Hz, 1H), 7.75 (dd, *J* = 5.0, 1.4 Hz, 1H).

MS [ESI⁺] *m/z*: 229.08 [M + H⁺]⁺.

7-(Thiophen-2-yl)pyrido[2,3-d]pyrimidin-4-amine (2.25j, R₅ = R₆ = H, R₇ = 2-thiophenyl):

The product was isolated as a light yellow solid (28.5 mg, 49%).

¹H NMR (400 MHz, DMSO-d₆): δ 8.65 (d, *J* = 8.6 Hz, 1H), 8.47 (s, 1H), 8.08 (d, *J* = 8.6 Hz, 1H), 8.05 (dd, *J* = 3.7, 1.0 Hz, 1H), 8.01 (br_s, 2H), 7.79 (dd, *J* = 5.0, 0.9 Hz, 1H), 7.23 (dd, *J* = 5.0, 3.8 Hz, 1H).

¹³C NMR (126 MHz, DMSO-d₆): δ 163.8, 160.2, 159.6, 158.0, 145.0, 135.3, 132.1, 129.7, 129.4, 118.0, 108.6.

MS [ESI⁺] *m/z*: 229.047 [M + H⁺]⁺.

6-(3-Methoxyphenyl)pyrido[2,3-d]pyrimidin-4-amine (2.25k, R₅ = R₆ = H, R₇ = 3-methoxyphenyl): The product was isolated as a yellow orange solid (28.0 mg, 50%).

¹H NMR (400 MHz, DMSO-d₆): δ 9.37 (d, *J* = 2.4 Hz, 1H), 9.00 (d, *J* = 2.5 Hz, 1H), 8.54 (s, 1H), 8.16 (br_s, 2H), 7.51 – 7.42 (m, 3H), 7.04 (dt, *J* = 7.0, 2.4 Hz, 1H), 3.88 (s, 3H).

¹³C NMR (126 MHz, DMSO-d₆): δ 163.4, 160.0, 158.5, 157.7, 154.4, 137.6, 132.5, 130.4 (2xC overlapping), 119.2, 113.9, 112.5, 108.7, 55.3.

MS [ESI⁺] *m/z*: 253.23 [M + H⁺]⁺.

7-Methoxypyrido[2,3-d]pyrimidin-4-amine (2.25l, R₅ = R₆ = H, R₇ = OMe): The product was obtained as a white solid (69.4 mg, 80%)

¹H NMR (300 MHz, DMSO-d₆): δ 8.48 (d, *J* = 8.9 Hz, 1H), 8.40 (s, 1H), 7.79 (br_s, 2H), 6.94 (d, *J* = 8.9 Hz, 1H), 3.94 (s, 3H).

¹³C NMR (75 MHz, DMSO-d₆): δ 166.7, 162.9, 159.3, 159.2, 136.2, 111.7, 104.5, 54.0.

MS [ESI⁺] *m/z*: 177.07 [M + H⁺]⁺.

General protocols for the synthesis of bisphosphonate tetraethyl esters 2.26:

The pyrido[2,3-*d*]pyrimidin-4-amine intermediate (*i.e.* **2.23** or **2.25**; 1 eq), diethyl phosphite (6 eq), and triethyl orthoformate (1.6 eq) were dissolved in dry DMF or toluene. The mixture was heated in a microwave at 150°C for 1.5 h or thermally at 100°-110°C for ~48 h. The resulting mixture was cooled to rt and concentrated under vacuum. The product was purified by column chromatography on silica gel. Any product isolated with <90% homogeneity was further purified by reversed-phase preparative HPLC using a Waters Atlantis T3 C18 5µm column: Solvent A: H₂O, 0.1% formic acid. Solvent B: CH₃CN, 0.1% formic acid. Mobile phase: gradient from 95% A and 5% B to 5% A and 95% B in 17 min acquisition time; flow rate: 1 mL/min.

Tetraethyl ((pyrido[2,3-*d*]pyrimidin-4-ylamino)methylene)bis(phosphonate) (2.26a, R₆ = R₇ = H): The product was isolated as a light yellow solid (11.4 mg, 38%).

¹H NMR (500 MHz, CD₃OD): δ 9.06 (d, *J* = 3.0 Hz, 1H), 8.87 (d, *J* = 7.4 Hz, 1H), 8.76 (s, 1H), 7.65 (dd, *J* = 8.2, 4.4 Hz, 1H), 6.08 (t, *J* = 23.5 Hz, 1H), 4.29 – 4.14 (m, 8H), 1.30 (t, *J* = 7.1 Hz, 6H), 1.25 (t, *J* = 7.1 Hz, 6H).

³¹P NMR (81 MHz, CD₃OD) δ 16.59.

¹³C NMR (126 MHz, CD₃OD) δ 160.6, 157.9, 157.5, 156.2, 132.7, 122.2, 110.1, 63.8 (t, *J* = 3.1 Hz), 15.3-15.1 (m), C-α to the phosphonate overlaps with the solvent peak.

MS [ESI⁺] *m/z*: 433.13 [M + H⁺]⁺.

Tetraethyl (7-(methylthio)pyrido[2,3-*d*]pyrimidin-4-ylamino)methylenediphosphonate (2.26b, R₆ = H, R₇ = SMe): The product was isolated as a yellow solid (37.8 mg, 30%).

¹H NMR (300 MHz, CDCl₃): δ 8.74 (s, 1H), 8.11 (d, *J* = 8.7 Hz, 1H), 7.27 (d, *J* = 8.7 Hz, 1H), 6.72 (d, *J* = 9.7 Hz, 1H), 5.86 (td, *J* = 22.0, 9.7 Hz, 1H), 3.89-4.33 (m, 8H), 2.71 (s, 3H), 1.29 (t, *J* = 7.1 Hz, 6H), 1.20 (t, *J* = 7.1 Hz, 6H).

¹³C NMR (75 MHz, CDCl₃): δ 167.3, 159.1, 159.0, 158.2, 133.0, 113.0, 104.8, 63.4-63.9 (m), 54.4, 44.8 (t, *J* = 147.2 Hz), 16.3-16.4 (m).

³¹P NMR (81 MHz, CDCl₃): δ 17.46 .

MS [ESI⁺] *m/z*: 479.18 [M+H⁺]⁺

Tetraethyl (((7-(thiophen-2-yl)pyrido[2,3-*d*]pyrimidin-4-yl)amino)methylene)bis(phosphonate) (2.26c, R₆ = H, R₇ = 2-thiophenyl): The product was isolated as a yellow solid (8.0 mg, 9%).

^1H NMR (400 MHz, CD_3OD): δ 8.78 (d, $J = 8.7$ Hz, 1H), 8.70 (s, 1H), 8.09 (d, $J = 8.7$ Hz, 1H), 8.00 (dd, $J = 3.7, 0.7$ Hz, 1H), 7.70 (dd, $J = 5.0, 0.8$ Hz, 1H), 7.22 (dd, $J = 5.0, 3.8$ Hz, 1H), 6.07 (t, $J = 23.5$ Hz, 1H), 4.29 – 4.12 (m, 8H), 1.31 (t, $J = 7.1$ Hz, 6H), 1.26 (t, $J = 7.1$ Hz, 6H).

^{13}C NMR (126 MHz, CD_3OD): δ 160.2 (t, $J = 4.3$ Hz), 158.5, 158.0, 157.7, 143.4, 132.9, 130.8, 128.4, 128.2, 113.0, 108.3, 63.9-63.7 (m), 16.2-14.7 (m); C- α to the bisphosphonate overlaps with the solvent peak, as determined by HSQC.

^{31}P NMR (81 MHz, CD_3OD): δ 16.67.

MS [ESI $^+$] m/z : 515.12 [M + H $^+$]. $^+$

Tetraethyl (((7-(methylsulfonyl)pyrido[2,3-*d*]pyrimidin-4-

yl)amino)methylene)bis(phosphonate) (2.26d, $R_6 = \text{H}$, $R_7 = \text{SO}_2\text{Me}$): Product was isolated as a yellow solid (20 mg, 54%)

^1H NMR (300 MHz, CDCl_3): δ 9.01 (d, $J = 8.5$ Hz, 1H), 8.89 (s, 1H), 8.09 (d, $J = 8.5$ Hz, 1H), 7.88 (d, $J = 9.6$ Hz, 1H), 5.93 (td, $J = 22.2, 9.6$ Hz, 1H), 4.39 – 4.00 (m, 8H), 3.48 (s, 3H), 1.35 (t, $J = 7.1$ Hz, 6H), 1.21 (t, $J = 7.1$ Hz, 6H).

^{31}P NMR (81 MHz, CDCl_3) δ 16.85.

^{13}C NMR (75 MHz, CDCl_3) : δ 163.3, 161.4, 159.6, 157.7, 136.4, 116.3, 112.0, 63.9 (t, $J = 3.1$ Hz), 45.4 (t, $J = 147.5$ Hz), 38.9, 16.4 (t, $J = 2.5$ Hz).

MS [ESI $^+$] m/z : 511.32 [M + H $^+$]. $^+$

Tetraethyl (7-methoxypyrido[2,3-*d*]pyrimidin-4-ylamino)methylenediphosphonate (2.26e,

$R_6 = \text{H}$, $R_7 = \text{OMe}$): The product was isolated as a white solid (25 mg, 16%).

^1H NMR (300 MHz, CDCl_3): δ 8.71 (s, 1H), 8.24 (d, $J = 9.0$ Hz, 1H), 6.89 (d, $J = 9.0$ Hz, 1H), 6.63 (d, $J = 9.7$ Hz, 1H), 5.87 (td, $J = 22.1, 9.7$ Hz, 1H), 4.11-4.31 (m, 8H), 4.10 (s, 3H), 1.28 (t, $J = 7.1$ Hz, 6H), 1.19 (t, $J = 7.1$ Hz, 6H).

^{13}C NMR (75 MHz, CDCl_3): δ 167.3, 159.1, 158.2, 148.11, 133, 113.0, 104.8, 63.6-63.8 (m), 54.4, 44.8 (t, $J = 147.2$ Hz), 16.3-16.4 (m).

^{31}P NMR (81 MHz, CDCl_3): δ 16.49.

MS [ESI $^+$] m/z : 463.3 [M + H $^+$]. $^+$

Tetraethyl (((6-bromopyrido[2,3-d]pyrimidin-4-yl)amino)methylene)bis(phosphonate)

(**2.26f**, $\text{R}_6 = \text{Br}$, $\text{R}_7 = \text{H}$): The product was isolated as a yellow solid (169.2 mg, 50%).

^1H NMR (500 MHz, CD_3OD): δ 9.16 (s, 1H), 9.11 (s, 1H), 8.78 (s, 1H), 6.04 (t, $J = 23.4$ Hz, 1H), 4.29 – 4.14 (m, 8H), 1.30 (t, $J = 7.1$ Hz, 6H), 1.27 (t, $J = 7.1$ Hz, 6H).

^{13}C NMR (126 MHz, CD_3OD): δ 159.9, 157.7, 157.3, 156.4, 134.6, 117.0, 111.0, 63.85 (t, $J = 3.2$ Hz), 15.3 (t, $J = 2.8$ Hz) and 15.2 (t, $J = 3.0$ Hz) (two P-O-CH $_2$ -CH $_3$); C- α to the bisphosphonate overlaps with the solvent peak.

^{31}P NMR (81 MHz, CD_3OD): δ 16.42.

MS [ESI $^+$] m/z : 511.04 [M + H $^+$]. $^+$

Tetraethyl (((6-(thiophen-2-yl)pyrido[2,3-d]pyrimidin-4-

yl)amino)methylene)bis(phosphonate) (2.26g, $\text{R}_6 = 2\text{-thiophenyl}$, $\text{R}_7 = \text{H}$): The product was isolated as a yellow solid (24.3 mg, 18%).

^1H NMR (500 MHz, CD_3OD): δ 9.37 (s, 1H), 9.10 (d, $J = 2.3$ Hz, 1H), 8.72 (s, 1H), 7.70 (dd, $J = 3.7, 1.1$ Hz, 1H), 7.59 (dd, $J = 5.1, 1.1$ Hz, 1H), 7.21 (dd, $J = 5.1, 3.7$ Hz, 1H), 6.11 (t, $J = 23.6$ Hz, 1H), 4.29 – 4.16 (m, 8H), 1.31 (t, $J = 7.1$ Hz, 6H), 1.27 (t, $J = 7.1$ Hz, 6H).

^{13}C NMR (126 MHz, CD_3OD): δ 160.6 (t, $J = 4.1$ Hz), 156.9, 156.7, 153.6, 138.8, 129.3, 128.4, 127.5, 127.0, 125.5, 110.1, 63.8 (t, $J = 3.3$ Hz), 45.2 (t, $J = 151.0$ Hz), 15.3 (t, $J = 2.8$ Hz) and 15.2 (t, $J = 3.0$ Hz) (two P-O- CH_2CH_3).

^{31}P NMR (81 MHz, CD_3OD): δ 16.7.

MS [ESI $^+$] m/z : 515.12 [M + H $^+$]. $^+$

Tetraethyl (((6-(3,5-dimethylisoxazol-4-yl)pyrido[2,3-d]pyrimidin-4-

yl)amino)methylene)bis(phosphonate) (2.26h, $R_6 = 3,5$ -dimethylisoxazol-4-yl, $R_7 = \text{H}$): The product was isolated as a yellow solid (22.0 mg, 17%).

^1H NMR (400 MHz, CD_3OD) δ 9.07 (s, 1H), 8.87 (s, 1H), 8.80 (s, 1H), 6.11 (t, $J = 23.5$ Hz, 1H), 4.29 – 4.16 (m, 8H), 2.50 (s, 3H), 2.34 (s, 3H), 1.31 (t, $J = 7.1$ Hz, 6H), 1.26 (t, $J = 7.1$ Hz, 6H).

^{31}P NMR (81 MHz, CD_3OD) δ 16.60.

MS [ESI $^+$] m/z : 528.17 [M + H $^+$]. $^+$

Tetraethyl (((6-(4-isopropoxyphenyl)pyrido[2,3-d]pyrimidin-4-

yl)amino)methylene)bis(phosphonate) (2.26i, $R_6 = 4$ -isopropoxyphenyl, $R_7 = \text{H}$): The product was isolated as a yellow oil (13.3 mg, 22%).

^1H NMR (500 MHz, CDCl_3): δ 9.34 (d, $J = 2.4$ Hz, 1H), 8.83 (s, 1H), 8.45 (br_s, -NH), 7.69 – 7.57 (m, 2H), 7.04 – 6.99 (m, 2H), 5.91 (td, $J = 21.9, 9.7$ Hz, 1H), 4.62 (hept, $J = 6.1$ Hz, 1H), 4.37 – 4.04 (m, 8H), 1.38 (s, 3H), 1.37 (s, 3H), 1.31 (t, $J = 7.1$ Hz, 6H), 1.22 (t, $J = 7.1$ Hz, 6H).

^{13}C NMR (126 MHz, CDCl_3): δ 159.6, 158.6, 157.5, 157.3, 155.6, 134.7, 128.5, 128.4, 126.9, 116.5, 109.5, 70.0, 64.0 (t, $J = 3.2$ Hz) and 63.7 (t, $J = 3.1$ Hz) (two P-O- CH_2CH_3), 45.1 (t, $J = 147.1$ Hz), 22.0, 16.4 – 16.3 (m).

^{31}P NMR (162 MHz, CDCl_3): δ 16.42.

MS [ESI⁺] *m/z*: 567.36 [M + H⁺]⁺.

Tetraethyl (((6-phenylpyrido[2,3-*d*]pyrimidin-4-yl)amino)methylene)bis(phosphonate)

(2.26j, R₆ = phenyl, R₇ = H): The product was isolated as a yellow solid (12.2 mg, 11%).

¹H NMR (500 MHz, CD₃OD): δ 9.36 (s, 1H), 9.14 (d, *J* = 2.3 Hz, 1H), 8.76 (s, 1H), 7.89-7.80 (m, 2H), 7.60-7.53 (m, 2H), 7.50-7.45 (m, 1H), 6.12 (t, *J* = 23.5 Hz, 1H), 4.30-4.15 (m, 8H), 1.31 (t, *J* = 7.1 Hz, 6H), 1.26 (t, *J* = 7.1 Hz, 6H).

¹³C NMR (126 MHz, CD₃OD): δ 160.7, 157.2, 157.0, 155.0, 136.2, 135.3, 129.6, 129.0, 128.5, 127.0, 110.0, 63.8 (t, *J* = 3.3 Hz), 15.3 (t, *J* = 2.8 Hz) and 15.2 (t, *J* = 3.0 Hz) (two P-O-CH₂CH₃); C-α to the bisphosphonate overlaps with the solvent peak.

³¹P NMR (81 MHz, CD₃OD): δ 16.68.

MS [ESI⁺] *m/z*: 509.164 [M + H⁺]⁺.

Tetraethyl (((7-(methylthio)-6-phenylpyrido[2,3-*d*]pyrimidin-4-

yl)amino)methylene)bis(phosphonate) (2.26k, R₆ = phenyl, R₇ = SMe): The product was isolated as a light yellow solid (18.5 mg, 45%).

¹H NMR (400 MHz, DMSO-*d*₆): δ 9.00 (d, *J* = 9.3 Hz, -NH), 8.88 (s, 1H), 8.64 (s, 1H), 7.58 – 7.45 (m, 5H), 5.88 (td, *J* = 23.5, 9.0 Hz, 1H), 4.13 – 3.95 (m, 8H), 2.53 (s, 3H), 1.17 (t, *J* = 7.0 Hz, 6H), 1.08 (t, *J* = 7.0 Hz, 6H).

¹³C NMR (126 MHz, DMSO-*d*₆): δ 166.1, 160.5, 158.1, 157.9, 137.0, 134.6, 132.3, 129.8, 129.1, 128.9, 106.8, 63.4 (t, *J* = 3.0 Hz) and 63.2 (t, *J* = 3.0 Hz) (two P-O-CH₂CH₃), 46.7 – 44.2 (m), 16.7 – 16.5 (m), 13.8.

³¹P NMR (203 MHz, CD₃OD): δ 16.74.

MS [ESI⁺] *m/z*: 555.35 [M + H⁺]⁺.

Tetraethyl (((7-(methylthio)-6-(thiophen-3-yl)pyrido[2,3-d]pyrimidin-4-

yl)amino)methylene)bis(phosphonate) (2.26l, R₆ = 3-thiophenyl, R₇ = SMe): Product was isolated as a yellow solid (35.0 mg, 34%).

¹H NMR (500 MHz, CD₃OD): δ 8.68 (s, 1H), 8.53 (s, 1H), 7.74 – 7.70 (m, 1H), 7.57 (ddd, *J* = 5.0, 3.0, 0.9 Hz, 1H), 7.41 – 7.37 (m, 1H), 6.06 (t, *J* = 23.5 Hz, 1H), 4.27 – 4.14 (m, 8H), 2.65 (s, 3H), 1.30 (t, *J* = 7.1 Hz, 6H) and 1.25 (t, *J* = 7.1 Hz, 6H).

¹³C NMR (126 MHz, CD₃OD) δ 168.2, 160.40 (t, *J* = 4.1 Hz), 157.2, 156.7, 136.6, 130.8, 130.0, 128.1, 125.7, 125.3, 106.1, 63.8 – 63.7 (m), 44.9 (t, *J* = 149.8 Hz), 15.3 (t, *J* = 2.8 Hz) and 15.2 (t, *J* = 3.1 Hz) (two P-O-CH₂CH₃), 12.7.

³¹P NMR (81 MHz, CD₃OD): δ 16.74.

MS [ESI⁺] *m/z*: 561.108 [M + H⁺].⁺

Tetraethyl (((6-(4-isopropoxyphenyl)-7-(methylthio)pyrido[2,3-d]pyrimidin-4-

yl)amino)methylene)bis(phosphonate) (2.26m, R₆ = 4-isopropoxyphenyl, R₇ = SMe): The product was isolated as a yellow solid (12.6 mg, 22%).

¹H NMR (400 MHz, CD₃OD): δ 8.68 (s, 1H), 8.41 (s, 1H), 7.44 (d, *J* = 8.6 Hz, 2H), 7.02 (d, *J* = 8.7 Hz, 2H), 6.06 (t, *J* = 23.5 Hz, 1H), 4.69 (hept, *J* = 6.1 Hz, 1H), 4.25 – 4.14 (m, 8H), 2.63 (s, 3H), 1.37 (s, 3H), 1.36 (s, 3H), 1.30 (t, *J* = 7.1 Hz, 6H), 1.25 (t, *J* = 7.1 Hz, 6H).

¹³C NMR (126 MHz, CD₃OD): δ 168.6, 160.4, 158.5, 157.0, 156.7, 136.7, 130.4, 129.8, 128.6, 115.3, 106.2, 69.6, 63.9 – 63.7 (m), 20.9, 15.3 (t, *J* = 2.9 Hz) and 15.2 (t, *J* = 3.0 Hz) (two P-O-CH₂CH₃), 12.7; C-α to the bisphosphonate overlaps with the solvent peak.

³¹P NMR (162 MHz, CD₃OD): δ 16.78.

MS [ESI⁺] *m/z*: 613.34 [M + H⁺].⁺

Tetraethyl (((6-bromo-7-(methylthio)pyrido[2,3-d]pyrimidin-4

yl)amino)methylene)bis(phosphonate) (2.26n, R₆ = Br, R₇ = SMe): The product was isolated as a yellow solid (55.6 mg, 30%).

¹H NMR (500 MHz, DMSO-d₆): δ 9.40 (s, 1H), 8.65 (s, 1H), 5.82 (t, *J* = 23.5 Hz, 1H), 4.12 - 3.97 (m, 8H), 2.59 (s, 3H), 1.17 (t, *J* = 7.0 Hz, 6H), 1.09 (t, *J* = 7.0 Hz, 6H).

MS [ESI⁺] *m/z*: 557.03 [M + H⁺]⁺.

General protocols for the synthesis of bisphosphonate tetraethyl esters 2.27:

The pyrido[2,3-*d*]pyrimidin-4-amine intermediate (*i.e.* **2.23** or **2.25**; 1 eq), and tetraethylethene-1,1-diylbisphosphonate(1.1-2.0 eq.), which was previously prepared according to literature procedures,⁴³ were dissolved in anhydrous THF. The mixture was stirred at RT for 16 h, and then concentrated under vacuum. The product was purified by column chromatography on silica gel. Any product isolated with <90% homogeneity was further purified by reversed-phase preparative HPLC using a Waters Atlantis T3 C18 5μm column, as described for the bisphosphonate tetra esters **26**.

Tetraethyl (2-(pyrido[2,3-d]pyrimidin-4-ylamino)ethane-1,1-diyl)bis(phosphonate) (2.27a,

R₆ = R₇ = H): Product was isolated as a pale yellow solid (28.6 mg, 47%).

¹H NMR (500 MHz, CD₃OD): δ 9.01 (d, *J* = 2.8 Hz, 1H), 8.70 (s, 1H), 8.58 (dd, *J* = 8.3, 1.7 Hz, 1H), 7.59 (dd, *J* = 8.3, 4.4 Hz, 1H), 4.31 - 4.05 (m, 10H), 3.62 - 3.49 (m, 1H), 1.30 - 1.27 (m, 12H).

¹³C NMR (126 MHz, CD₃OD) δ 160.8, 158.0, 157.4, 155.7, 132.4, 121.8, 110.1, 63.5 - 62.5 (m), 37.9 (t, *J* = 3.6 Hz), 34.5 (t, *J* = 132.7 Hz), 15.6 - 14.6 (m).

^{31}P NMR (81 MHz, CD_3OD) δ 21.28.

MS [ESI $^+$] m/z : 447.148 [M + H $^+$]. $^+$

Tetraethyl (2-(((6-phenylpyrido[2,3-d]pyrimidin-4-yl)amino)ethane-1,1-

diyl)bis(phosphonate) (2.27b, R $_6$ = phenyl, R $_7$ = H): The product was isolated as a light yellow oil (16.2 mg, 23%).

^1H NMR (500 MHz, CDCl_3): δ 9.31 (d, J = 2.3 Hz, 1H), 8.84 (s, 1H), 8.33 (d, J = 2.2 Hz, 1H), 7.80 (t, J = 4.8 Hz, -NH), 7.67 (d, J = 7.3 Hz, 2H), 7.52 (t, J = 7.6 Hz, 2H), 7.45 (t, J = 7.4 Hz, 1H), 4.45 – 4.02 (m, 10H), 2.87 (tt, J = 22.9, 6.2 Hz, 1H), 1.38 (t, J = 7.1 Hz, 6H), 1.32 (t, J = 7.1 Hz, 6H).

^{13}C NMR (126 MHz, CDCl_3): δ 160.4, 158.2, 157.4, 155.3, 136.7, 134.7, 129.4, 128.5, 128.1, 127.4, 109.6, 63.4 – 63.0 (m), 37.8 (t, J = 4.4 Hz), 36.4 (t, J = 131.9 Hz), 16.4 – 16.3 (m).

^{31}P NMR (162 MHz, CDCl_3): δ 21.11.

MS [ESI $^+$] m/z : 523.21 [M + H $^+$]. $^+$

Tetraethyl (2-(((6-(thiophen-3-yl)pyrido[2,3-d]pyrimidin-4-yl)amino)ethane-1,1-

diyl)bis(phosphonate) (2.27c, R $_6$ = 3-thiophenyl, R $_7$ = H): The product was isolated as a yellow oil (16.5 mg, 47%).

^1H NMR (500 MHz, CDCl_3): δ 9.30 (d, J = 2.4 Hz, 1H), 8.77 (s, 1H), 8.33 (d, J = 2.4 Hz, 1H), 7.86 (t, J = 4.7 Hz, -NH), 7.63 (dd, J = 2.5, 1.8 Hz, 1H), 7.49 – 7.42 (m, 2H), 4.29 – 4.13 (m, 10H), 2.89 (tt, J = 22.9, 6.3 Hz, 1H), 1.37 (t, J = 7.1 Hz, 6H), 1.30 (t, J = 7.1 Hz, 6H).

^{13}C NMR (126 MHz, CDCl_3): δ 160.3, 158.2, 157.5, 154.6, 137.7, 129.4, 127.4, 126.9, 125.9, 122.2, 109.7, 63.4 – 62.9 (m), 37.7 (t, J = 4.4 Hz), 36.3 (t, J = 132 Hz), 16.5 – 16.3 (m).

^{31}P NMR (203 MHz, CDCl_3): δ 21.15.

MS [ESI⁺] *m/z*: 529.17 [M + H⁺]⁺.

Tetraethyl (2-((6-(*p*-tolyl)pyrido[2,3-*d*]pyrimidin-4-yl)amino)ethane-1,1-

diyl)bis(phosphonate) (2.27d, R₆ = *p*-tolyl, R₇ = H): The product was isolated as a yellow solid (21.2 mg, 78%).

¹H NMR (500 MHz, CD₃OD): δ 9.30 (s, 1H), 8.78 (s, 1H), 8.72 (s, 1H), 7.68 (d, *J* = 8.1 Hz, 2H), 7.36 (d, *J* = 7.9 Hz, 2H), 4.18 (m, 10H), 3.57 (tt, *J* = 23.1, 7.1 Hz, 1H), 2.42 (s, 3H), 1.33 – 1.25 (m, 12H).

¹³C NMR (126 MHz, CD₃OD): δ 160.9, 157.8, 156.3, 154.2, 138.7, 134.8, 133.3, 129.7, 129.0, 126.7, 105.0, 63.3 – 62.8 (m), 37.9 (br), 34.5 (t, *J* = 132.7 Hz), 19.8, 15.3 – 15.2 (m)

³¹P NMR (81 MHz, CD₃OD): δ 21.29.

MS [ESI⁺] *m/z*: 537.195 [M + H⁺]⁺.

Tetraethyl (2-((6-(4-methoxyphenyl)pyrido[2,3-*d*]pyrimidin-4-yl)amino)ethane-1,1-

diyl)bis(phosphonate) (2.27e, R₆ = 4-methoxyphenyl, R₇ = H): The product was isolated as a light yellow oil (15.0 mg, 46%).

¹H NMR (500 MHz, CDCl₃): δ 9.25 (d, *J* = 2.4 Hz, 1H), 8.78 (s, 1H), 8.24 (d, *J* = 2.4 Hz, 1H), 7.75 (t, *J* = 4.9 Hz, -NH), 7.58 – 7.53 (m, 2H), 7.03 – 6.95 (m, 2H), 4.30 – 4.14 (m, 10H), 3.86 (s, 3H), 2.87 (tt, *J* = 22.9, 6.3 Hz, 1H), 1.37 (t, *J* = 7.1 Hz, 6H), 1.30 (t, *J* = 7.1 Hz, 6H).

¹³C NMR (126 MHz, CDCl₃): δ 160.3, 160.0, 158.1, 157.4, 155.0, 134.2, 129.1, 128.4, 127.1, 114.8, 109.6, 63.4 – 63.0 (m), 55.4, 37.7 (t, *J* = 4.1 Hz), 36.4 (t, *J* = 131.8 Hz), 16.4 – 16.3 (m).

³¹P NMR (162 MHz, CDCl₃) 21.16.

MS [ESI⁺] *m/z*: 553.36 [M + H⁺]⁺.

Tetraethyl (2-((6-(3-methoxyphenyl)pyrido[2,3-d]pyrimidin-4-yl)amino)ethane-1,1-

diyl)bis(phosphonate) (2.27f, R₆ = 3-methoxyphenyl, R₇ = H): The product was isolated as a yellow oil (30.0 mg, 55%).

¹H NMR (400 MHz, CDCl₃): δ 9.27 (d, *J* = 2.4 Hz, 1H), 8.81 (s, 1H), 8.31 (d, *J* = 2.4 Hz, 1H), 7.81 (t, *J* = 4.8 Hz, -NH), 7.40 (t, *J* = 8.0 Hz, 1H), 7.20 (ddd, *J* = 7.6, 1.6, 0.9 Hz, 1H), 7.16 – 7.11 (m, 1H), 6.95 (ddd, *J* = 8.3, 2.5, 0.7 Hz, 1H), 4.30 – 4.14 (m, 10H), 2.89 (tt, *J* = 22.9, 6.3 Hz, 1H), 1.37 (t, *J* = 7.1 Hz, 6H), 1.31 (t, *J* = 7.1 Hz, 6H).

¹³C NMR (101 MHz, CDCl₃): δ 160.4, 160.2, 158.4, 157.8, 155.2, 138.1, 134.4, 130.4, 128.2, 119.7, 113.7, 113.2, 109.6, 63.4 – 63.0 (m), 55.4, 37.8 (t, *J* = 4.3 Hz), 36.4 (t, *J* = 131.8 Hz), 16.4 – 16.3 (m).

³¹P NMR (162 MHz, CDCl₃): 21.15.

MS [ESI⁺] *m/z*: 553.35 [M + H⁺]⁺.

Tetraethyl (2-((6-bromo-7-(methylthio)pyrido[2,3-d]pyrimidin-4-yl)amino)ethane-1,1-

diyl)bis(phosphonate) (2.27g, R₆ = Br, R₇ = SMe): Product was isolated as a yellow oil (107.4 mg, 44%).

¹H NMR (500 MHz, CDCl₃): δ 8.72 (s, 1H), 8.14 (s, 1H), 7.65 (br_s, -NH), 4.31 – 4.12 (m, 10H), 2.86 (tt, *J* = 22.9, 6.2 Hz, 1H), 1.38 (t, *J* = 7.1 Hz, 6H), 1.32 (t, *J* = 7.1 Hz, 6H).

¹³C NMR (126 MHz, CDCl₃): δ 167.6, 159.4, 158.8, 156.9, 132.4, 116.0, 107.1, 63.4 – 63.0 (m), 37.7 (t, *J* = 4.4 Hz), 36.3 (t, *J* = 131.9 Hz), 16.5 – 16.3 (m), 15.1.

³¹P NMR (203 MHz, CDCl₃) δ 21.13.

MS [ESI⁺] *m/z*: 571.23 [M + H⁺]⁺.

Tetraethyl (2-((7-(methylthio)-6-phenylpyrido[2,3-d]pyrimidin-4-yl)amino)ethane-1,1-diyl)bis(phosphonate) (2.27h, R₆ = phenyl, R₇ = SMe): Product was isolated as a yellow oil (35.4 mg, 71%).

¹H NMR (500 MHz, CDCl₃): δ 8.74 (s, 1H), 7.70 (s, 1H), 7.48 – 7.40 (m, 5H), 7.36 (br_s, -NH), 4.26 – 4.11 (m, 10H), 2.81 (tt, *J* = 22.9, 6.2 Hz, 1H), 2.65 (s, 3H), 1.35 (t, *J* = 7.1 Hz, 6H), 1.30 (t, *J* = 7.1 Hz, 6H).

¹³C NMR (126 MHz, CDCl₃) δ 167.4, 160.3, 158.5, 157.5, 136.8, 135.2, 129.4, 128.8, 128.7, 128.6, 106.0, 63.3 – 62.9 (m), 37.6 (t, *J* = 4.4 Hz), 36.5 (t, *J* = 131.9 Hz), 16.5 – 16.2 (m), 14.1.

³¹P NMR (203 MHz, CDCl₃): δ 21.20.

MS [ESI⁺] *m/z*: 569.27 [M + H⁺]⁺.

Tetraethyl (2-(((6-(3-methoxyphenyl)-7-(methylthio)pyrido[2,3-d]pyrimidin-4-yl)amino)ethane-1,1-diyl)bis(phosphonate) (2.27i, R₆ = 3-methoxyphenyl, R₇ = SMe): The product was isolated as a yellow solid (20.0 mg, 66%).

¹H NMR (500 MHz, CD₃OD): δ 8.61 (s, 1H), 8.15 (s, 1H), 7.42 – 7.35 (m, 1H), 7.06 – 7.00 (m, 3H), 4.20 – 4.13 (m, 8H), 4.12 – 4.05 (m, 2H), 3.84 (s, 3H), 3.51 (tt, *J* = 23.1, 7.1 Hz, 1H), 2.61 (s, 3H), 1.30 – 1.26 (m, 12H).

¹³C NMR (126 MHz, CD₃OD): δ 167.2, 160.8, 159.8, 157.8, 156.6, 138.0, 135.1, 130.1, 129.3, 121.3, 114.7, 113.8, 105.9, 63.2 – 62.8 (m), 54.4, 37.7 (t, *J* = 3.6 Hz), 34.4, 15.3 – 15.1 (m).

³¹P NMR (81 MHz, CD₃OD): δ 21.37.

MS [ESI⁺] *m/z*: 599.178 [M + H⁺]⁺.

Tetraethyl (2-((6-(4-isopropoxyphenyl)-7-(methylthio)pyrido[2,3-*d*]pyrimidin-4-

yl)amino)ethane-1,1-diyl)bis(phosphonate) (2.27j, R₆ = 4-isopropoxyphenyl, R₇ = SMe): The product was isolated as a light yellow oil (36.2 mg, 66%).

¹H NMR (500 MHz, CDCl₃): δ 8.73 (s, 1H), 7.66 (s, 1H), 7.36 – 7.31 (m, 2H), 7.30 (t, *J* = 5.4 Hz, -NH), 6.97 – 6.90 (m, 2H), 4.65 – 4.57 (m, 1H), 4.26 – 4.12 (m, 10H), 2.81 (tt, *J* = 22.9, 6.2 Hz, 1H), 1.39 (s, 3H), 1.37 (s, 3H), 1.35 (t, *J* = 7.1 Hz, 6H), 1.30 (t, *J* = 7.1 Hz, 6H).

¹³C NMR (126 MHz, CDCl₃): δ 167.7, 160.2, 158.3, 158.3, 157.4, 135.0, 130.6, 128.7, 128.6, 115.7, 106.1, 69.9, 63.3 – 62.9 (m), 37.6 (t, *J* = 4.6 Hz), 36.5 (t, *J* = 131.9 Hz), 22.1, 16.5 – 16.3 (m), 14.2.

³¹P NMR (203 MHz, CDCl₃): δ 21.22.

MS [ESI⁺] *m/z*: 627.38 [M + H⁺]⁺.

Tetraethyl (2-((7-(methylthio)-6-(thiophen-3-yl)pyrido[2,3-*d*]pyrimidin-4-

yl)amino)ethane-1,1-diyl)bis(phosphonate) (2.27k, R₆ = 3-thiophenyl, R₇ = SMe): The product was obtained as a yellow oil (16.4 mg, 52%).

¹H NMR (500 MHz, CD₃OD): δ 8.61 (s, 1H), 8.24 (s, 1H), 7.68 (dd, *J* = 2.9, 1.3 Hz, 1H), 7.57 (dd, *J* = 5.0, 3.0 Hz, 1H), 7.36 (dd, *J* = 5.0, 1.3 Hz, 1H), 4.25 – 4.09 (m, 10H), 3.51 (tt, *J* = 23.2, 7.2 Hz, 1H), 2.64 (s, 3H), 1.31 – 1.26 (m, 12H).

³¹P NMR (81 MHz, CD₃OD): δ 21.30.

MS [ESI⁺] *m/z*: 575.12 [M + H⁺]⁺.

Characterization Data of Final Inhibitors:

((Pyrido[2,3-*d*]pyrimidin-4-ylamino)methylene)diphosphonic acid (2.8a): Product was isolated as a light yellow solid (3.7 mg, 50%).

^1H NMR (500 MHz, D_2O): δ 8.84 (dd, $J = 4.6, 1.8$ Hz, 1H), 8.68 (dd, $J = 8.3, 1.8$ Hz, 1H), 8.47 (s, 1H), 7.55 (dd, $J = 8.3, 4.6$ Hz, 1H), 4.68 (t, $J = 18.5$ Hz, 1H).

^{13}C NMR (126 MHz, D_2O): δ 159.9, 158.7, 156.5, 154.8, 134.1, 121.8, 111.2, 52.50 (t, $J = 124.7$ Hz).

^{31}P NMR (81 MHz, D_2O): δ 12.67.

HRMS [ESI $^-$] calculated for $\text{C}_8\text{H}_9\text{N}_4\text{O}_6\text{P}_2$ m/z : 319.00028; found: 319.00139 [M - H^+] $^-$.

7-(Methylthio)pyrido[2,3-*d*]pyrimidin-4-ylamino)methylenediphosphonic acid (2.8b):

Product was isolated as a yellow solid (21.9 mg, 96%).

^1H NMR (500 MHz, D_2O): δ 8.31 (s, 1H), 8.29 (d, $J = 8.7$ Hz, 1H), 7.30 (d, $J = 8.7$ Hz, 1H), 4.53 (t, $J = 18.8$ Hz, 1H), 2.53 (s, 3H).

^{13}C NMR (125 MHz, D_2O): δ 168.1, 159.8, 158.6, 157.3, 132.6, 119.7, 107.3, 39.7 (t, $J = 142.2$ Hz), 12.7.

^{31}P NMR (162 MHz, D_2O): δ 12.74.

HRMS [ESI $^-$] calculated for $\text{C}_9\text{H}_{11}\text{O}_6\text{N}_4\text{P}_2\text{S}$ m/z : 364.98800; found: 364.98814 [M - H^+] $^-$.

((7-(Thiophen-2-yl)pyrido[2,3-*d*]pyrimidin-4-yl)amino)methylene)diphosphonic acid

(2.8c): The product was isolated as a yellow solid (4.5 mg, 82%).

^1H NMR (400 MHz, D_2O): δ 8.66 (d, $J = 8.7$ Hz, 1H), 8.58 (s, 1H), 8.00 (d, $J = 8.7$ Hz, 1H), 7.93 (d, $J = 3.3$ Hz, 1H), 7.72 (d, $J = 4.8$ Hz, 1H), 7.29 – 7.21 (m, 1H), 5.08 (t, $J = 19.3$ Hz, 1H).

^{13}C NMR (126 MHz, D_2O): δ 160.1 (t, $J = 4.0$ Hz), 158.6, 157.5, 157.1, 142.3, 134.3, 130.9, 128.9, 128.8, 118.3, 109.0, 50.0 (t, $J = 144.1$ Hz).

^{31}P NMR (81 MHz, D_2O): δ 12.21.

HRMS [ESI $^-$] calculated for $\text{C}_{12}\text{H}_{11}\text{N}_4\text{O}_6\text{P}_2\text{S}$ m/z : 400.98800; found: 400.98798 [M - H^+] $^-$.

(((7-(Methylsulfonyl)pyrido[2,3-d]pyrimidin-4-yl)amino)methylene)diphosphonic acid

(2.8d): Product was isolated as a light yellow solid (16.3 mg, quantitative yield)

^1H NMR (500 MHz, D_2O): δ 8.91 (d, $J = 8.4$ Hz, 1H), 8.49 (s, 1H), 8.04 (d, $J = 8.4$ Hz, 1H), 4.59 (t, $J = 19.9$ Hz, 1H), 3.30 (s, 3H).

^{13}C NMR (126 MHz, D_2O): δ 163.3, 155.9, 154.7, 153.6, 132.0, 107.8, 101.8, 50.4, 48.0 (t, $J = 125.3$ Hz).

^{31}P NMR (162 MHz, D_2O): δ 12.25.

HRMS [ESI] calculated for $\text{C}_9\text{H}_{11}\text{N}_4\text{O}_8\text{P}_2\text{S}$ m/z : 396.97783; found: 396.97773 [$\text{M} - \text{H}^+$] $^-$.

(7-Methoxyprido[2,3-d]pyrimidin-4-ylamino)methylenediphosphonic acid (2.8e): Product was isolated as a white solid (31.5 mg, 75%).

^1H NMR (200 MHz, D_2O): δ 8.35 (d, $J = 9.0$ Hz, 1H), 8.28 (s, 1H), 6.86 (d, $J = 9.0$ Hz, 1H), 3.90 (s, 3H).

^{13}C NMR (126 MHz, D_2O): δ 167.0, 159.6, 158.4, 157.3, 135.7, 111.5, 105.5, 54.1 ($\text{C}\alpha$, t, $J = 124.8$ Hz, and $-\text{OCH}_3$).

^{31}P NMR (81 MHz, D_2O): δ 12.86.

HRMS [ESI] calculated for $\text{C}_9\text{H}_{11}\text{O}_7\text{N}_4\text{P}_2$ m/z : 349.01084; found: 349.01071 [$\text{M} - \text{H}^+$] $^-$.

(((6-bromopyrido[2,3-d]pyrimidin-4-yl)amino)methylene)diphosphonic acid (2.8f): The product was isolated as a light yellow solid (7.10 mg, 74%).

^1H NMR (500 MHz, D_2O): δ 8.98 (d, $J = 2.3$ Hz, 1H), 8.94 (d, $J = 2.4$ Hz, 1H), 8.54 (s, 1H); α C-H to the bisphosphonate overlaps with the solvent peak.

^{13}C NMR (126 MHz, D_2O): δ 159.6, 158.6, 156.2, 155.3, 136.0, 116.1, 111.8, 52.4 – 49.7 (m).

^{31}P NMR (81 MHz, D_2O): δ 12.61.

HRMS [ESI⁻] calculated for C₈H₈BrN₄O₆P₂ *m/z*: 396.91079; found 396.91105 [M - H⁺]⁻.

(((6-(Thiophen-2-yl)pyrido[2,3-*d*]pyrimidin-4-yl)amino)methylene)diphosphonic acid

(2.8g): Product was isolated as a yellow solid (12.1 mg, 77%).

¹H NMR (500 MHz, D₂O): δ 9.12 (d, *J* = 2.3 Hz, 1H), 8.84 (d, *J* = 2.3 Hz, 1H), 8.47 (s, 1H), 7.54 (d, *J* = 3.6 Hz, 1H), 7.48 (d, *J* = 5.1 Hz, 1H), 7.12 (dd, *J* = 5.0, 3.7 Hz, 1H), 5.05 (t, *J* = 19.6 Hz, 1H).

¹³C NMR (126 MHz, D₂O): δ 160.5, 157.2, 154.5, 152.8, 138.5, 128.7, 128.7, 127.4 (two overlapping carbons), 125.5, 110.4, 50.2 (t, *J* = 126.0 Hz).

³¹P NMR (203 MHz, D₂O): δ 12.22.

HRMS [ESI⁻] calculated for C₁₂H₁₁N₄O₆P₂S *m/z*: 400.98800; found: 400.98799 [M - H⁺]⁻.

(((6-(3,5-Dimethylisoxazol-4-yl)pyrido[2,3-*d*]pyrimidin-4-yl)amino)methylene)diphosphonic acid

(2.8h): The product was isolated as a yellow solid (7.2 mg, 46%).

¹H NMR (400 MHz, D₂O): δ 8.83 (d, *J* = 2.2 Hz, 1H), 8.70 (d, *J* = 2.2 Hz, 1H), 8.55 (s, 1H), 2.43 (s, 3H), 2.28 (s, 3H); α-CH to the bisphosphonate overlaps with the solvent peak.

¹³C NMR (126 MHz, D₂O): δ 168.1, 160.4, 160.1, 158.8, 156.1, 155.6, 134.3, 124.2, 112.9, 110.8, 50.9 (t, *J* = 121.1 Hz), 10.6, 9.6.

³¹P NMR (81 MHz, D₂O): δ 12.65.

HRMS [ESI⁻] calculated for C₁₃H₁₄N₅O₇P₂ *m/z*: 414.03739; found: 414.03731 [M - H⁺]⁻.

(((6-(4-isopropoxyphenyl)pyrido[2,3-*d*]pyrimidin-4-yl)amino)methylene)diphosphonic acid

(2.8i): Product was isolated as a yellow solid (9.2 mg, 95%).

^1H NMR (500 MHz, D_2O): δ 8.89 (d, $J = 2.2$ Hz, 1H), 8.62 (d, $J = 2.3$ Hz, 1H), 8.34 (s, 1H), 7.45 (d, $J = 8.8$ Hz, 2H), 6.85 (d, $J = 8.9$ Hz, 2H), 4.97 (t, $J = 19.3$ Hz, 1H), 4.52 (hept, $J = 6.1$ Hz, 1H), 1.18 (s, 3H), 1.17 (s, 3H).

^{13}C NMR (126 MHz, D_2O): δ 160.5, 157.2, 156.5, 153.7, 153.2, 134.1, 129.8, 128.2 (two overlapping carbons), 116.6, 110.1, 71.3, 50.2 (t, $J = 124.6$ Hz), 21.0.

^{31}P NMR (162 MHz, D_2O): δ 12.22.

HRMS [ESI $^-$] calculated for $\text{C}_{17}\text{H}_{19}\text{N}_4\text{O}_7\text{P}_2$ m/z : 453.07345; found: 453.07364 [$\text{M} - \text{H}^+$] $^-$.

(((6-Phenylpyrido[2,3-*d*]pyrimidin-4-yl)amino)methylene)diphosphonic acid (2.8j): The product was isolated as a light yellow solid (3.59 mg, 66%).

^1H NMR (500 MHz, D_2O): δ 9.22 (d, $J = 1.6$ Hz, 1H), 9.04 (d, $J = 1.5$ Hz, 1H), 8.59 (s, 1H), 7.85 (d, $J = 7.4$ Hz, 2H), 7.60 (t, $J = 7.6$ Hz, 2H), 7.51 (t, $J = 7.4$ Hz, 1H), 5.09 – 4.89 (m, 1H).

^{31}P NMR (203 MHz, D_2O): δ 12.80.

HRMS [ESI $^-$] calculated for $\text{C}_{14}\text{H}_{13}\text{N}_4\text{O}_6\text{P}_2$ m/z : 395.03158; found: 395.03182 [$\text{M} - \text{H}^+$] $^-$.

(((7-(methylthio)-6-phenylpyrido[2,3-*d*]pyrimidin-4-yl)amino)methylene)diphosphonic acid (2.8k): The product was isolated as light yellow solid (3.9 mg, 81%).

^1H NMR (500 MHz, D_2O): δ 8.34 (s, 1H), 8.21 (s, 1H), 7.47 – 7.33 (m, 5H), 2.44 (s, 3H); α -CH to the bisphosphonate overlaps with the solvent peak.

^{13}C NMR (126 MHz, D_2O): δ 166.3, 160.2, 158.2, 156.5, 136.8, 134.6, 131.9, 129.4, 128.7, 128.6, 106.9, 51.8 - 49.9 (m), 13.2.

^{31}P NMR (81 MHz, D_2O): δ 12.77.

HRMS [ESI $^-$] calculated for $\text{C}_{15}\text{H}_{15}\text{N}_4\text{O}_6\text{P}_2\text{S}$ m/z : 441.01930; found 441.02082 [$\text{M} - \text{H}^+$] $^-$.

(((7-(Methylthio)-6-(thiophen-3-yl)pyrido[2,3-*d*]pyrimidin-4-

yl)amino)methylene)diphosphonic acid (2.8l): The product was isolated as a light yellow solid (17.9 mg, 93%).

¹H NMR (400 MHz, D₂O): δ 8.33 (s, 1H), 8.29 (s, 1H), 7.58 (dd, *J* = 2.9, 1.2 Hz, 1H), 7.44 (dd, *J* = 5.0, 3.0 Hz, 1H), 7.29 (dd, *J* = 5.0, 1.2 Hz, 1H), 2.46 (s, 3H); α-CH to the bisphosphonate overlaps with the solvent peak.

¹³C NMR (126 MHz, D₂O): δ 166.6, 160.4, 158.2, 156.4, 136.7, 131.8, 129.9, 128.7, 126.5, 126.0, 106.9, 50.8 (t, *J* = 122.1 Hz), 13.4.

³¹P NMR (81 MHz, D₂O): δ 12.84.

HRMS [ESI⁻] calculated for C₁₃H₁₃N₄O₆P₂S₂ *m/z*: calculated 446.97572; found: 446.97566 [M - H⁺]⁻.

(((6-(4-Isopropoxyphenyl)-7-(methylthio)pyrido[2,3-*d*]pyrimidin-4-

yl)amino)methylene)diphosphonic acid (2.8m): The product was isolated as a yellow solid (6.8 mg, 70%).

¹H NMR (500 MHz, D₂O): δ 8.50 (s, 1H), 8.32 (s, 1H), 7.52 (d, *J* = 8.7 Hz, 2H), 7.12 (d, *J* = 8.7 Hz, 2H), 2.58 (s, 3H), 1.37 (s, 3H), 1.35 (s, 3H); α-CH to the bisphosphonates and *i*Pr-CH overlaps with the solvent peak as confirmed by HSQC.

HSQC (¹H-¹³C): δ 4.79 (¹H) correlates to δ 50.0 (¹³Cα), and δ 4.69 correlates to ¹³C δ 71.1.

¹³C NMR (101 MHz, D₂O): δ 166.8, 160.4, 158.1, 157.2, 156.4, 134.4, 131.7, 131.0, 129.8, 116.3, 106.9, 71.7, 21.1, 13.3; Cα to the bisphosphonate was observed by HSQC.

³¹P NMR (162 MHz, D₂O) δ 13.04.

HRMS [ESI⁻] calculated for C₁₈H₂₁N₄O₇P₂S *m/z*: 499.06117; found: 499.06137 [M - H⁺]⁻.

(2-(Pyrido[2,3-*d*]pyrimidin-4-ylamino)ethane-1,1-diyl)diphosphonic acid (2.9a):

The product was isolated as light yellow solid (6.8 mg, 33%).

¹H NMR (500 MHz, D₂O): δ 8.87 (dd, *J* = 4.6, 1.8 Hz, 1H), 8.49 (s, 1H), 8.44 (dd, *J* = 8.3, 1.8 Hz, 1H), 7.58 (dd, *J* = 8.3, 4.6 Hz, 1H), 3.94 – 3.87 (m, 2H), 2.26 – 2.14 (m, 1H).

¹³C NMR (126 MHz, D₂O): δ 160.0, 158.2, 156.2, 155.2, 133.8, 122.3, 110.7, 39.9 (br; Cβ), 38.8 (t, *J* = 112.7 Hz, Cα).

³¹P NMR (81 MHz, D₂O): δ 16.72.

HRMS [ESI⁻] calculated for C₉H₁₁N₄O₆P₂ *m/z*: 333.01593; found 333.01652 [M - H⁺].

(2-((6-Phenylpyrido[2,3-*d*]pyrimidin-4-yl)amino)ethane-1,1-diyl)diphosphonic acid (2.9b):

The product was isolated as a yellow solid (9.7 mg, 82%).

¹H NMR (500 MHz, D₂O): δ 8.99 (d, *J* = 1.9 Hz, 1H), 8.42 (d, *J* = 1.8 Hz, 1H), 8.40 (s, 1H), 7.55 (d, *J* = 7.5 Hz, 2H), 7.41 (t, *J* = 7.5 Hz, 2H), 7.34 (t, *J* = 7.3 Hz, 1H), 3.99 (td, *J* = 14.1, 7.2 Hz, 2H), 2.50 (tt, *J* = 20.7, 7.0 Hz, 1H).

¹³C NMR (101 MHz, D₂O): δ 160.0, 157.3, 154.7, 153.8, 135.0, 134.0, 130.1, 129.2, 128.6, 126.5, 110.1, 39.3 (br, Cβ), 39.5-37.3 (m, Cα).

³¹P NMR (162 MHz, D₂O): δ 17.02.

HRMS [ESI⁻] calculated for C₁₅H₁₅N₄O₆P₂ *m/z*: 409.04723; found: 409.04714 [M - H⁺].

(2-((6-(Thiophen-3-yl)pyrido[2,3-*d*]pyrimidin-4-yl)amino)ethane-1,1-diyl)diphosphonic acid (2.9c):

The product was isolated as a yellow solid (10.5 mg, 84%).

¹H NMR (500 MHz, D₂O): δ 8.86 (d, *J* = 2.0 Hz, 1H), 8.27 (s, 1H), 8.23 (d, *J* = 1.9 Hz, 1H), 7.66 (d, *J* = 1.5 Hz, 1H), 7.47 (dd, *J* = 5.0, 2.9 Hz, 1H), 7.34 (d, *J* = 4.8 Hz, 1H), 3.96 (td, *J* = 14.2, 7.1

Hz, 2H), 2.54 (tt, $J = 20.9, 7.1$ Hz, 1H). ^{13}C NMR (126 MHz, D_2O): δ 157.5, 154.4, 151.4, 150.8, 133.5, 126.9, 126.0, 125.5, 122.8, 120.6, 107.6, 37.1 (br, $\text{C}\beta$), 36.1 (t, $J = 114.9$ Hz, $\text{C}\alpha$).

^{31}P NMR (203 MHz, D_2O): δ 16.98.

HRMS [ESI $^-$] calculated for $\text{C}_{13}\text{H}_{13}\text{N}_4\text{O}_6\text{P}_2\text{S}$ m/z : 415.00365; found: 415.00400 [$\text{M} - \text{H}^+$] $^-$.

(2-((6-(*p*-Tolyl)pyrido[2,3-*d*]pyrimidin-4-yl)amino)ethane-1,1-diyl)diphosphonic acid (2.9d):

The product was isolated as a yellow solid (14.1 mg, 92%).

^1H NMR (500 MHz, D_2O): δ 9.06 (s, 1H), 8.49 (s, 1H), 8.45 (s, 1H), 7.49 (d, $J = 7.8$ Hz, 2H), 7.23 (d, $J = 7.8$ Hz, 2H), 4.05 (td, $J = 14.4, 6.5$ Hz, 2H), 2.62 – 2.47 (m, 1H), 2.32 (s, 3H).

^{13}C NMR (126 MHz, D_2O): δ 160.1, 157.3, 155.0, 153.7, 138.9, 134.0, 132.4, 129.9, 129.8, 126.5, 110.2, 39.5-39.2 (m, two overlapping carbons, $\text{C}\alpha$ and $\text{C}\beta$), 20.3.

^{31}P NMR (203 MHz, D_2O): δ 17.07 and 17.04 (the two phosphonates are non-equivalent).

HRMS [ESI $^-$] calculated for $\text{C}_{16}\text{H}_{17}\text{N}_4\text{O}_6\text{P}_2$ m/z : 423.06288; found: 423.06290 [$\text{M} - \text{H}^+$] $^-$.

(2-((6-(4-methoxyphenyl)pyrido[2,3-*d*]pyrimidin-4-yl)amino)ethane-1,1-diyl)diphosphonic acid (2.9e): The product was isolated as a yellow solid (10.0 mg, 86%).

^1H NMR (500 MHz, D_2O): δ 8.85 (d, $J = 2.2$ Hz, 1H), 8.35 (s, 1H), 8.11 (d, $J = 2.3$ Hz, 1H), 7.28 (d, $J = 8.7$ Hz, 2H), 6.72 (d, $J = 8.7$ Hz, 2H), 4.00 (td, $J = 14.1, 7.2$ Hz, 2H), 3.76 (s, 3H), 2.54 (tt, $J = 20.9, 7.2$ Hz, 1H).

^{13}C NMR (126 MHz, D_2O): δ 159.8, 158.7, 156.6, 154.0, 153.2, 133.2, 128.9, 127.4, 127.4, 114.1, 109.9, 55.1, 39.3 (br, $\text{C}\beta$), 38.4 (t, $J = 111.5$ Hz, $\text{C}\alpha$).

^{31}P NMR (203 MHz, D_2O): δ 17.05.

HRMS [ESI $^-$] calculated for $\text{C}_{16}\text{H}_{17}\text{N}_4\text{O}_7\text{P}_2$ m/z : 439.05780; found: 439.05809 [$\text{M} - \text{H}^+$] $^-$.

(2-((6-(3-Methoxyphenyl)pyrido[2,3-*d*]pyrimidin-4-yl)amino)ethane-1,1-diyl)diphosphonic acid (2.9f): The product was isolated as a yellow solid (6.0 mg, 80%).

¹H NMR (500 MHz, D₂O): δ 8.96 (d, *J* = 1.8 Hz, 1H), 8.44 (s, 1H), 8.39 (d, *J* = 1.4 Hz, 1H), 7.30 (t, *J* = 8.0 Hz, 1H), 7.16 (d, *J* = 7.6 Hz, 1H), 6.96 (s, 1H), 6.82 (dd, *J* = 8.2, 1.9 Hz, 1H), 4.02 (td, *J* = 14.0, 7.3 Hz, 2H), 3.82 (s, 3H), 2.54 (tt, *J* = 20.8, 7.2 Hz, 1H).

¹³C NMR (101 MHz, D₂O): δ 160.1, 159.1, 157.3, 154.8, 153.8, 136.6, 133.6, 130.5, 130.3, 119.4, 113.7, 111.8, 110.0, 55.3, 39.3 (br, Cβ), 38.40 (t, *J* = 113.9 Hz, Cα).

³¹P NMR (203 MHz, D₂O): δ 17.02.

HRMS [ESI⁻] calculated for C₁₆H₁₇N₄O₇P₂ *m/z*: 439.05780; found: 439.05776 [M - H⁺]⁻.

(2-((6-Bromo-7-(methylthio)pyrido[2,3-*d*]pyrimidin-4-yl)amino)ethane-1,1-diyl)diphosphonic acid (2.9g): The product was isolated as a white solid (5.7 mg, 62%).

¹H NMR (400 MHz, D₂O): δ 8.49 (s, 1H), 8.31 (s, 1H), 4.08-3.90 (m, 2H), 2.59 (s, 3H), 2.56-2.36 (m, 1H).

¹³C NMR (126 MHz, D₂O): δ 167.4, 159.2, 157.4, 154.7, 133.9, 115.8, 107.0, 39.3 (br, Cβ), 14.2;

C-α to the bisphosphonate was observed by HSQC

HSQC (¹H-¹³C): ¹H at δ 2.46 correlates to ¹³Cα at δ 38.5.

³¹P NMR (162 MHz, D₂O): δ 16.90.

HRMS [ESI⁻] calculated for C₁₀H₁₂BrN₄O₆P₂S *m/z*: 456.91416; found 456.91445 [M - H⁺]⁻.

(2-((7-(Methylthio)-6-phenylpyrido[2,3-*d*]pyrimidin-4-yl)amino)ethane-1,1-diyl)diphosphonic acid (2.9h): The product was isolated as a yellow solid (4.7 mg, 65%).

¹H NMR (500 MHz, D₂O) δ 8.52 (s, 1H), 8.08 (s, 1H), 7.60 – 7.52 (m, 5H), 3.98 - 3.91 (m, 2H), 2.60 (s, 3H), 2.35 - 2.24 (m, 1H).

^{13}C NMR (126 MHz, D_2O): δ 167.8, 160.2, 156.0, 153.5, 136.1, 135.5, 130.9, 129.3, 129.0, 128.7, 106.0, 39.3 ($\text{C}\beta$), 13.4; C- α to the bisphosphonates was observed by HSQC (^1H - ^{13}C): ^1H δ 2.46 correlates to ^{13}C δ 38.5.

^{31}P NMR (203 MHz, D_2O): δ 16.84.

HRMS [ESI] calculated for $\text{C}_{16}\text{H}_{17}\text{N}_4\text{O}_6\text{P}_2\text{S}$ m/z : 455.03495; found: 455.03498 [$\text{M} - \text{H}^+$].

(2-((6-(3-Methoxyphenyl)-7-(methylthio)pyrido[2,3-*d*]pyrimidin-4-yl)amino)ethane-1,1-diyl)diphosphonic acid (2.9i): The product was isolated as an off-white solid (7.9 mg, 90%).

^1H NMR (400 MHz, D_2O): δ 8.49 (s, 1H), 8.05 (s, 1H), 7.46 (t, $J = 8.1$ Hz, 1H), 7.17-7.05 (m, 3H), 3.92 (br, 2H), 3.85 (s, 3H), 2.56 (s, 3H), 2.27 (br, 1H).

^{13}C NMR (126 MHz, D_2O): δ 166.7, 160.2, 158.8, 158.0, 156.4, 138.1, 134.7, 131.4, 130.1, 122.3, 115.0, 114.7, 106.6, 55.5, 39.5-39.3 ($\text{C}\beta$), 39.4-38.0 (m, $\text{C}\alpha$), 13.3.

^{31}P NMR (203 MHz, D_2O): δ 16.49.

HRMS [ESI] calculated for $\text{C}_{17}\text{H}_{19}\text{N}_4\text{O}_7\text{P}_2\text{S}$ m/z : 485.04552; found: 485.04596 [$\text{M} - \text{H}^+$].

(2-((6-(4-Isopropoxyphenyl)-7-(methylthio)pyrido[2,3-*d*]pyrimidin-4-yl)amino)ethane-1,1-diyl)diphosphonic acid (2.9j): Product was isolated as a yellow solid (4.04 mg, 37%).

^1H NMR (500 MHz, D_2O) δ 8.49 (s, 1H), 8.03 (s, 1H), 7.52 (d, $J = 7.8$ Hz, 2H), 7.12 (d, $J = 8.1$ Hz, 2H), 3.97 – 3.90 (m, 2H), 2.58 (s, 3H), 2.33 – 2.25 (m, 1H), , 1.37 (s, 3H), 1.36 (s, 3H); *i*Pr-CH overlaps with the solvent peak; confirmed by HSQC.

HSQC (^1H - ^{13}C): δ ^1H δ 4.68 correlates to ^{13}C δ 71.7.

^{13}C NMR (126 MHz, D_2O) δ 167.1, 160.2, 157.8, 157.3, 156.2, 134.7, 131.2, 131.0, 129.6, 116.3, 106.6, 71.7, 39.3 ($\text{C}\beta$), 38.7 ($\text{C}\alpha$), 21.1, 13.4.

^{31}P NMR (203 MHz, D_2O) δ 16.94.

HRMS [ESI⁻] calculated for C₁₉H₂₃N₄O₇P₂S *m/z*: 513.07682; found 513.07668 [M - H⁺].

(2-((7-(Methylthio)-6-(thiophen-3-yl)pyrido[2,3-*d*]pyrimidin-4-yl)amino)ethane-1,1-

diyl)diphosphonic acid (2.9k): The product was isolated as a light yellow solid (4.9 mg, 41%).

¹H NMR (500 MHz, D₂O): δ 8.48 (s, 1H), 8.12 (s, 1H), 7.76 – 7.72 (m, 1H), 7.58 (dd, *J* = 4.9, 3.0 Hz, 1H), 7.43 (dd, *J* = 5.0, 1.1 Hz, 1H), 3.92 (br, 2H), 2.60 (s, 3H), 2.26 (br, 1H).

¹³C NMR (126 MHz, D₂O): δ 166.7, 160.0, 157.8, 156.0, 136.4, 131.2, 130.0, 128.5, 126.4, 126.0, 106.5, 39.4(br, Cβ), 36.9 (Cα), 13.2.

³¹P NMR (81 MHz, D₂O): δ 17.01.

HRMS [ESI⁻] calculated for C₁₄H₁₅N₄O₆P₂S₂ *m/z*: 460.99137; found: 460.99184 [M - H⁺].

Primer extension polymerase Scintillation Proximity Assay (SPA):⁴⁰

The following primer sequences were used in the HIV RT primer extension Scintillation Proximity Assay (SPA) (Bosworth and Towers 1989). Biotinylated PPT80 (5'- ATC TTG TCT TCG TTG GGA GTG AAT TAG CCC TTC CAG TCC CCC CTT TTC TTT TAA AAA GTG GCT AAG CTC TAC AGC TGC CC-3') was used as a template. The underlined nucleotides are the portion of the template that annealed to the primer. Primer DNA PPT (5'- TTA AAA GAA AAG GGG GG -3') was used in the assay.

A 10 step threefold dilution series of the compound to be tested was prepared in either reaction buffer (50 mM Tris pH 7.8, 50 mM NaCl, 6mM MgCl₂) or DMSO, depending on compound solubility, to obtain a final concentration in the experiment of between 100 μM-10 nM. The concentration of DMSO in the final reaction did not exceed 5%.

50nM of DNA PPT/Biotinylated PPT80 primer-template hybrid was pre-incubated for 5 min at 37°C in a buffer containing 50 mM Tris pH 7.8, 50 mM NaCl, 6mM MgCl₂, 4 μM dCTP, 4 μM dGTP, 4 μM dTTP, and 0.5 μM [8-3H (N)]-dATP in presence of inhibitor to be tested. Nucleotide incorporation was initiated by the addition of the HIV RT polymerase and reaction was allowed to proceed for 5 min. The reaction was quenched by the addition of one reaction volume of 0.5 M EDTA containing 1 mg/mL Streptavidin coated PVT SPA beads. The concentration of HIV RT used in the reaction was empirically determined to produce 1000 cpm in an uninhibited positive control.

The SPA beads were then allowed to settle for approximately 8 hours upon which the samples were counted using a liquid scintillation counter. The liquid scintillation count represents the total amount of incorporation of [8-3H (N)]-dATP and is related to the amount of polymerase activity. Liquid scintillation counts were converted to relative activity by dividing the activity of an inhibited experiment count by an average of at least three uninhibited positive control counts. This data was then plotted using Graph Pad Prism (Version 5.0). The IC₅₀ values were calculated by fitting at least 8 data points to a sigmoidal dose-response (variable slope) equation using Graph Pad Prism. Standard deviation for all experiments were determined on the basis of at least two independent replicates.

2.8. Associated Content

Supporting Information

NMR spectra and homogeneity data for key inhibitors **2.8m**, **2.9h**, **2.9i**, and **2.9j** are provided.

2.9. Author Information

Corresponding Author

*Phone 514-398-3638. Fax 514-398-3797. Email: youla.tsantrizos@mcgill.ca

2.10. Acknowledgements

Financial support for this work was provided by the Natural Sciences and Engineering Research Council of Canada (NSERC) and the Canadian Institute of Health Research (CIHR) to M. Götte and Y.S. Tsantrizos.

2.11. Abbreviations Used

HIV-1, human immunodeficiency virus type 1; RT reverse transcriptase; PYPY-BPs, pyrido[2,3-*d*]pyrimidine bisphosphonates; NRTIs, nucleoside reverse transcriptase inhibitors; NNRTIs, non-nucleoside reverse transcriptase inhibitors; NcRTIs, nucleotide competitive reverse transcriptase inhibitors; P_i, inorganic pyrophosphate; NTP, nucleotide triphosphate; NDP, nucleotide diphosphate; PFA, foscarnet.

2.12. References

- 1) Sofia, M.J.; Chang, W.; Furman, P.A.; Mosley, R.T.; Ross, B.S. Nucleoside, nucleotide, and non-nucleoside inhibitors of hepatitis C virus NS5B RNA-dependent RNA-polymerase. *J. Med. Chem.* **2012**, *55*, 2481-2531.
- 2) De Clercq, E. The nucleoside reverse transcriptase inhibitors, non-nucleoside reverse transcriptase inhibitors, and protease inhibitors in the treatment of HIV infections (AIDS). *Advances in Pharmacology* **2013**, *67*, 317-358.

- 3) Yin, Y.W.; Steitz, T.A. The structural mechanism of translocation and helicase activity in T7 RNA polymerase. *Cell* **2004**, *116*, 393-404.
- 4) Vaisman, A.; Ling, H.; Woodgate, R.; Yang, W. Fidelity of Dpo4: effect of metal ions, nucleotide selection and pyrophosphorolysis. *EMBO J.* **2005**, *24*, 2957-2967.
- 5) Garcia-Diaz, M.; Bebenek, K.; Krahn, J.M.; Kunkel, T.A.; Pedersen, L.C. A closed conformation for the Pol λ catalytic cycle. *Nature Struct. Mol. Biol.* **2005**, *12*, 97-98.
- 6) Garcia-Diaz, M.; Bebenek, K.; Krahn, J.M.; Pedersen, L.C.; Kunkel, T.A. Structural analysis of strand misalignment during DNA synthesis by a human DNA polymerase. *Cell* **2006**, *124*, 331-342.
- 7) Summa, V.; Petrocchi, A.; Pace, P.; Matassa, V.G.; De Francesco, R.; Altamura, S.; Tomei, L.; Koch, U.; Neuner, P. Discovery of α,γ -diketo acids as potent selective and reversible inhibitors of hepatitis C virus NS5b RNA-dependent RNA polymerase. *J. Med. Chem.* **2004**, *47*, 14-17.
- 8) Hazuda, D.J.; Felock, P.; Witmer, M.; Wolfe, A.; Stillmock, K.; Grobler, J.A.; Espeseth, A.; Gabryelski, L.; Schleif, W.; Blau, C.; Miller, M.D. Inhibitors of strand transfer that prevent integration and inhibit HIV-1 replication in cells. *Science* **2000**, *287*, 646-650.
- 9) (a) Summa, V.; Petrocchi, A.; Bonelli, F.; Crescenzi, B.; Donghi, M.; Ferrara, M.; Fiore, F.; Gardelli, C.; Paz, O.G.; Hazuda, D.J.; Jones, P.; Kinzel, O.; Laufer, R.; Monteagudo, E.; Muraglia, E.; Nizi, E.; Orvieto, F.; Pace, P.; Pescatore, G.; Scarpelli, R.; Stillmock, K.; Witmer, M.V.; Rowley, M. Discovery of raltegravir, a potent, selective orally bioavailable HIV-

integrase inhibitor for the treatment of HIV-AIDS infection. *J. Med. Chem.* **2008**, *51*, 5843-5855.

(b) Yilmaz, A.; Gisslèn, M.; Spudich, S.; Lee, E.; Jayewardene, A.; Aweeka, F.; Price, R.W. Raltegravir cerebrospinal fluid concentrations in HIV-1 infection. *PLoS ONE* **2009**, *4*, e6877.

10) De Clercq, E. Antiviral drugs in current clinical use. *J. Clin. Virol.* **2004**, *30*, 115-133.

11) Meyer, P.R.; Rutvisuttinunt, W.; Matsuura, S.E.; So, A.G.; Scott, W.A. Stable complexes formed by HIV-1 reverse transcriptase at distinct positions on the primer-template controlled by binding deoxynucleoside triphosphate or foscarnet. *J. Mol. Biol.* **2007**, *369*, 41-54.

12) Marchand, B.; Tchesnokov, E.P.; Götte, M. The pyrophosphate analogue foscarnet traps the pre-translocational state of HIV-1 reverse transcriptase in a Brownian ratchet model of polymerase translocation. *J. Biol. Chem.* **2007**, *282*, 3337-3346.

13) Shaw-Reid, C.A.; Munshi, V.; Graham, P.; Wolfe, A.; Witmer, M.; Danzeisen, R.; Olsen, D.B.; Carroll, S.S.; Embrey, M.; Wai, J.S.; Miller, M.D.; Cole, J.L.; Hazuda, D.J. Inhibition of HIV-1 ribonuclease H by a novel diketo acid, 4-[5-(benzoylamino)thien-2-yl]-2,4-dioxobutanoic acid. *J. Biol. Chem.* **2003**, *278*, 2777-2780.

14) (a) Jochmans, D.; Deval, J.; Kesteleyn, B.; Van Marck, H.; Bettens, E.; De Baere, I.; Dehertogh, P.; Ivens Van Ginderewn, T.M.; Van Schoubroeck, B.; Ehteshami, M.; Wigerinck, P.; Götte, M.; Hertogs, K. Indolopyridones inhibit human immunodeficiency virus reverse transcriptase with a novel mechanism of action. *J. Virol.* **2006**, *80*, 12283-12292.

(b) Ehteshami, M.; Scarth, B.J.; Tchesnokov, E.P.; Dash, C.; Le Grice, S.F.J.; Hallenberger, S.; Jochmans, D.; Götte, M. Mutations M184V and Y115F in HIV-1 reverse transcriptase discriminate against “nucleotide-competing reverse transcriptase inhibitors”. *J. Biol. Chem.* **2008**, *283*, 29904-29911.

15) Rajotte, D.; Tremblay, S.; Pelletier, A.; Salois P.; Bourgon, L.; Coulombe, R.; Mason, S.; Lamorte, L.; Sturino, C.F.; Bethell, R. Identification and characterization of a novel HIV-1 nucleotide-competing reverse transcriptase inhibitor series. *Antimicrob. Agents Chemother.* **2013**, *57*, 2712-2718.

16) (a) Lin, Y.-S.; Park, J.; De Schutter, J.W.; Huang, X.F.; Berghuis, A.M.; Sebag, M.; Tsantrizos, Y.S. Design and synthesis of active site inhibitors of the human farnesyl pyrophosphate synthase – apoptosis and inhibition of ERK phosphorylation in multiple myeloma cells. *J. Med. Chem.* **2012**, *55*, 3201-3215.

(b) De Schutter, J.W.; Shaw, J.; Lin, Y.-S.; Tsantrizos, Y.S. Design of potent bisphosphonate inhibitors of the human farnesyl pyrophosphate synthase *via* targeted interactions with the active site “capping” phenyls. *Bioorg. Med. Chem.* **2012**, *20*, 5583-5591.

(c) Leung, C.-Y.; Park, J.; De Schutter, J.W.; Sebag, M.; Berghuis, A.M.; Tsantrizos, Y.S. Thienopyrimidine bisphosphonates (ThPBP) inhibitors of the human farnesyl pyrophosphate synthase: optimization and characterization of the mode of inhibition. *J. Med. Chem.* **2013**, *56*, 7939-7950.

17) (a) Kavanagh, K.L.; Guo, K.; Dunford, J.E.; Wu, X.; Knapp, S.; Ebetino, F.H.; Rogers, M.J.; Russell, R.G.G.; Oppermann, U. The molecular mechanism of nitrogen-containing bisphosphonates as antiosteoporosis drugs. *Proc. Natl. Acad. Sci. USA* **2006**, *103*, 7829-7834.

(b) Rondeau, J.-M.; Bitsch, F.; Bourgier, E.; Geiser, M.; Hemmig, R.; Kroemer, M.; Lehmann, S.; Ramage, P.; Rieffel, S.; Strauss, A.; Green, J.R.; Jahnke, W. Structural basis for the exceptional *in vivo* efficacy of bisphosphonate drugs. *ChemMedChem* **2006**, *1*, 267-273.

18) Dunford, J.E. Molecular Targets of the Nitrogen Containing Bisphosphonates: The molecular pharmacology of prenyl synthase inhibition. *Curr. Pharm. Des.* **2010**, *16*, 2961-2969.

19) Andreeva, O.I.; Efimtseva, E.V.; Padyukova, N.S.; Kochetkov, S.N.; Mikhailov, S.N.; Dixon, H.B.F.; Karpeisky, M.Y. Interaction of HIV-1 reverse transcriptase and T7 RNA polymerase with phosphonate analogs of NTP and inorganic pyrophosphate. *Molecular Biology* **2001**, *35*, 717-729.

20) Song, Y.; Chan, J.M.W.; Tovian, Z.; Secrest, A.; Nagy, E.; Krysiak, K.; Bergan, K.; Parniak, M.A.; Oldfield E. Bisphosphonate inhibitors of ATP-mediated HIV-1 reverse transcriptase catalyzed excision of chain-terminating 3'-azido,3'-deoxythymidine: A QSAR investigation. *Bioorg. Med. Chem.* **2008**, *16*, 8959-8967.

21) Agapkina, J.; Yanvarev, D.; Anisenko, A.; Korolev, S.; Vepsäläinen, J.; Kochetkov, S.; Gottikh, M. Specific features of HIV-1 integrase inhibition by bisphosphonates derivatives. *Eur. J. Med. Chem.* **2014**, *73*, 73-82.

22) Yanvarev, D.V.; Korovina, A.N.; Usanov, N.N.; Kochetkov, S.N. Non-hydrolysable analogues of inorganic pyrophosphate as inhibitors of hepatitis C virus RNA-dependent RNA polymerase. *Russian J. Bioorg. Chem.* **2012**, *38*, 224-229.

23) (a) Krueger, A.C.; Madigan, D.L.; Beno, D.W.; Betebenner, D.A.; Carrick, R.; Green, B.E.; He, W.; Liu, D.; Maring, C.J.; McDaniel, K.F.; Mo, H.; Molla, A.; Motter, C.E.; Pilot-Matias, T.J.; Tufano, M.D.; Kempf, D.J. Novel hepatitis C virus replicon inhibitors: synthesis and structure-activity relationship of fused pyrimidine derivatives. *Bioorg. Med. Chem. Lett.* **2012**, *22*, 2212-2215.

(b) DeGoey, D.A.; Betebenner, D.A.; Grampovnik, D.J.; Liu, D.; Pratt, J.K.; Tufano, M.D.; He, W.; Krishnan, P.; Pilot-Matias, T.J.; Marsh, K.C.; Molla, A.; Kempf, D.J.; Maring, C.J. Discovery of pyrido[2,3-*d*]pyrimidine-base inhibitors of HCV NS5A. *Bioorg. Med. Chem. Lett.* **2013**, *23*, 3627-3630.

24) Nell, P.; Vakalopoulos, A.; Süßmeier, F.; Albrecht-Küpfer, B.; Zimmermann, K.; Keldenich, J. Fused cynopyridines and the use thereof. WO **2009**/080198 A1.

25) León, R.; Marco-Contelles, J.; García, A.G.; Villarroya, M. Synthesis, acetylcholinesterase inhibition and neuroprotective activity of new tacrine analogues. *Bioorg. Med. Chem.* **2005**, *13*, 1167-1175.

26) Chan, D.C.M.; Rosowsky, A. Synthesis of the lipophilic antifolate piritrexim via a palladium(0)-catalyzed cross-coupling reaction. *J. Org. Chem.* **2005**, *70*, 1364-1368.

27) Antonsson, T.; Bach, P.; Bylund, R.; Giordanetto, F.; Hovdal, D.; Johansson, J.; Sellén, M. Ketone pyridine analogues and their use in the treatment of cardiovascular disorders. WO **2010/005384 A1**

28) (a) Abadi, A.H.; Ibrahim, T.M.; Abouzid, K.M.; Lehmann, J.; Tinsley, H.N.; Gary, B.D.; Piazza, G.A. Design, synthesis and biological evaluation of novel pyridine derivatives as anticancer agents and phosphodiesterase 3 inhibitors. *Bioorg. Med. Chem* **2009**, *17*, 5974-5982.

(b) Abadi, A.H.; Abouel-Ella, D.A.; Lehmann, J.; Tinsley, H.N.; Gary, B.D.; Piazza, G.A.; Abdel-Fattah, M.A.O. Discovery of colon tumor cell growth inhibitory agents through a combinatorial approach. *Eur. J. Med. Chem.* **2010**, *45*, 90-97.

29) Mantri, M.; de Graaf, O.; van Veldhoven, J.; Göblyös, A.; von Frijtag Drabbe Künzel, J.K.; Mulder-Krieger, T.; Link, R.; de Vries, H.; Beukers, M.W.; Brussee, J.; Ijzerman, A.P. 2-Amino-6-furan-2-yl-4-substituted nicotinonitriles as A_{2A} adenosine receptor antagonists. *J. Med. Chem.* **2008**, *51*, 4449-4455.

30) Reddy, T.R.K.; Mutter, R.; Heal, W.; Guo, K.; Gillet, V.J.; Pratt, S.; Chen, B. Library design, synthesis, and screening: pyridine dicarbonitriles as potential prion diseases therapeutics. *J. Med. Chem.* **2006**, *49*, 607-615.

31) Murata, T.; Shimada, M.; Sakakibara, S.; Yoshina, T.; Kadono, H.; Masuda, T.; Shimazaki, M.; Shintani, T.; Fuchikami, K.; Sakai, K.; Inbe, H.; Takeshita, K.; Niki, T.; Umeda, M.; Bacon,

K.B.; Ziegelbauer, K.B.; Lowinger, T.B. Discovery of novel and selective IKK- β serine-threonine protein kinase inhibitors. Part 1. *Bioorg. Med. Chem. Lett.* **2003**, *13*, 913-918.

32) (a) Shi, F.; Tu, S.; Fang, F.; Li, T. One-pot synthesis of 2-amino-3-cyanopyridine derivatives under microwave irradiation without solvent. *ARKIVOC* **2005** (i) 137-142.

(b) Kambe, S.; Saito, K.; Sakurai, A.; Midorikawa, H. A simple method for the preparation of 2-amino-4-aryl-3-cyanopyridines by the condensation of malononitrile with aromatic aldehydes and alkyl ketones in the presence of ammonium acetate. *Synthesis* **1980**, 366-368.

33) Tu, S.; Zhou, D.; Cao, L.; Li, C.; Shao, Q. A simple three-component condensation: highly efficient microwave-assisted one-pot synthesis of polyfunctional pyridine derivatives. *J. Heterocyclic Chem.* **2009**, *46*, 54-57.

34) Tang, J.; Wang, L.; Yao, Y.; Zhang, L.; Wang, W. One-pot synthesis of 2-amino-3-cyanopyridine derivatives catalyzed by ytterbium perfluorooctanoate [Yb(PFO)₃]. *Tetrahedron Lett.* **2011**, *52*, 509-511.

35) Teague, S.J. Synthesis of heavily substituted 2-aminopyridines by displacement of a 6-methylsulfinyl group. *J. Org. Chem.* **2008**, *73*, 9765-9766.

36) Debenham, J.S.; Madsen-Duggan, C.B.; Walsh, T.F. Substituted pyrido[2,3-*d*]pyrimidine derivatives as cannabinoid-1 receptor modulators. WO **2008/121257** A1.

- 37) Leung, C.-Y.; Langille, A.M.; Mancuso, J.; Tsantrizos, Y.S. Discovery of thienopyrimidine-based inhibitors of the human farnesyl pyrophosphate synthase – Parallel synthesis of analogs via a trimethylsilyl ylidene intermediate. *Bioorg. Med. Chem.* **2013**, *21*, 2229-2240.
- 38) Metzger, A.; Melzig, L.; Despotopoulou, C.; Knochel, P., Pd-catalyzed cross-coupling of functionalized organozinc reagents with thiomethyl-substituted heterocycles. *Org. Lett.* **2009**, *11*, 4228-4231.
- 39) Graham, T.H.; Liu, W.; Shen, D.-M. A method for the reductive scission of heterocyclic thioethers. *Org. Lett.* **2011**, *13*, 6232-6235.
- 40) Bosworth, N.; Towers, P. Scintillation proximity assay. *Nature* **1989**, *341*, 167-168.
- 41) Freisz, S.; Bec, G.; Radi, M.; Wolff, P.; Crespan, E.; Angeli, L.; Dumas, P.; Maga, G.; Botta, M.; Ennifar, E. Crystal structure of HIV-1 reverse transcriptase bound to a non-nucleoside inhibitor with a novel mechanism of action. *Angew Chem. Int. Ed.* **2010**, *49*, 1805-1808.
- 42) Cañibano, V.; Rodríguez, J.F.; Santos, M; Sanz-Tejedor, A.; Carreño, M.C.; Gonzalez, G.; García-Ruano, J.L. Mild regioselective halogenation of activated pyridines with *N*-bromosuccinimide. *Synthesis* **2001**, 2175–2179.
- 43) Betebenner, D.A., DeGoey, D.A., Maring, C.J., Krueger, A.C., Iwasaki, N., Rockway, T.W., Cooper, C.S., Anderson, D.D., Donner, P.L., Green, B.E., Kempf, D.J., Liu, D., McDaniel, K.F.,

Madigan, D., Motter, C.E., Pratt, J.K., Shanley, J.P., Tufano, M.D., Wagner, R., Zhang, R., Molla, A., Mo, H., Pilot-Matias, T., Masse Sherie, VL., Carrick, R.J., He, W., Lu, L., Grampovnik, D.J. Anti-viral compounds. WO **2007/076034** A2

44) Degenhardt, C.R. and Burdsall, D.C. Synthesis of ethenylidenebis(phosphonic acid) and its tetraalkyl esters. *J. Org. Chem.* **1986**, *51*, 3488-3490.

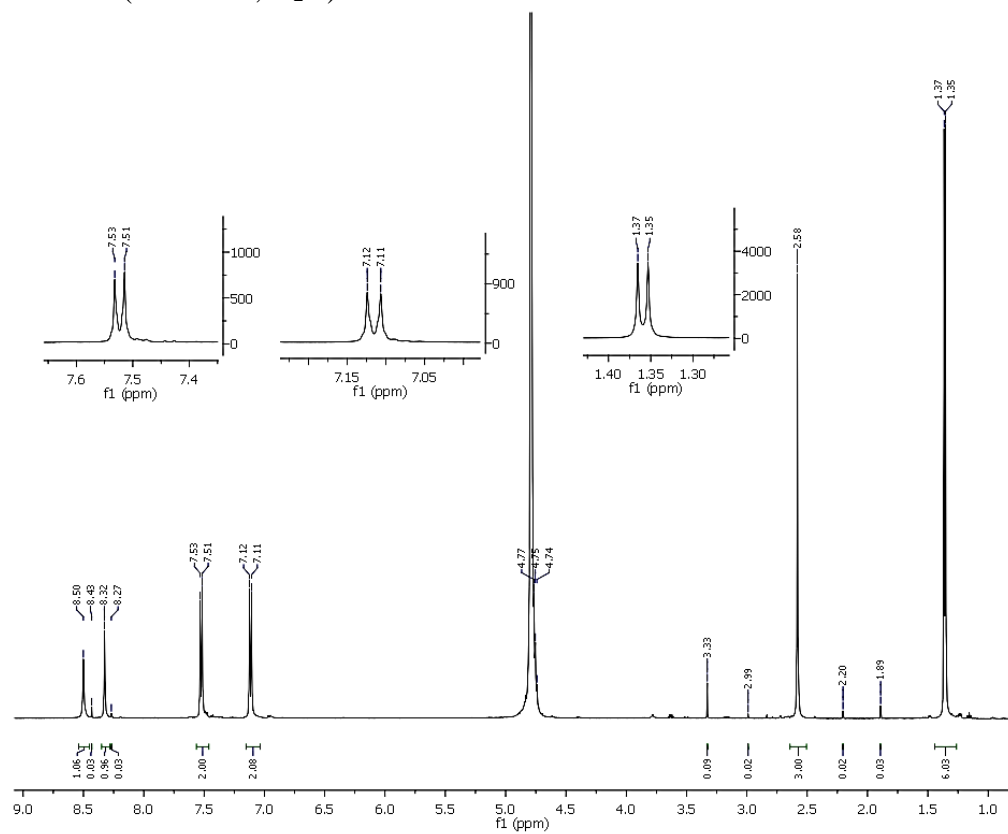
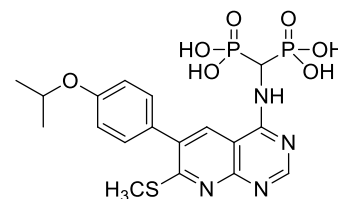
45) Menendez-Arias, L. Mechanisms of resistance to nucleoside analogue inhibitors of HIV-1 reverse transcriptase. *Virus Res.* **2008**, *134*, 147-156.

Chapter 2: Supporting Information

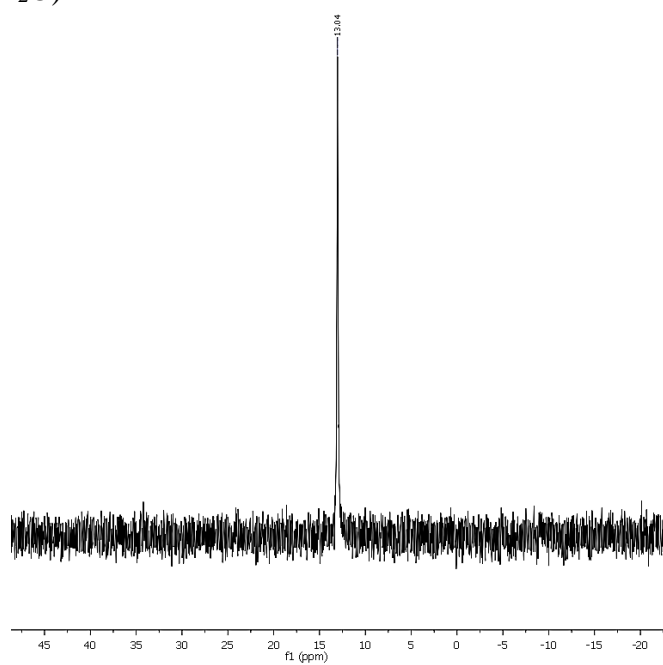
Modular Assembly of Purine-Like Bisphosphonates as Inhibitors of HIV-1
Reverse Transcriptase

Inhibitor 2.8m

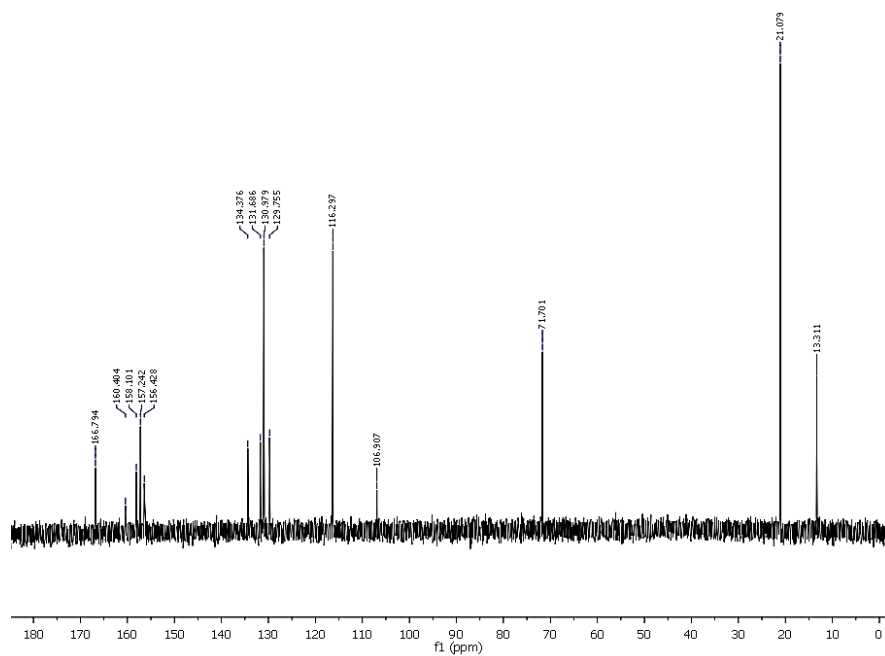
^1H NMR (500 MHz, D_2O)



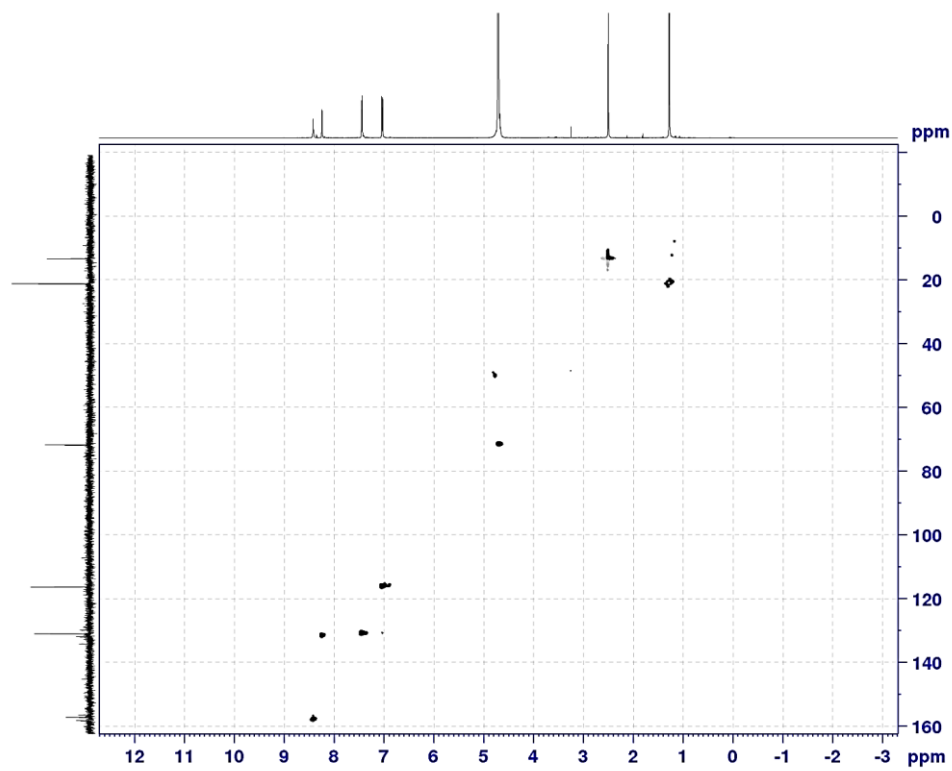
^{31}P NMR (162 MHz, D_2O)



^{13}C NMR (126 MHz, D_2O) (2.8m)

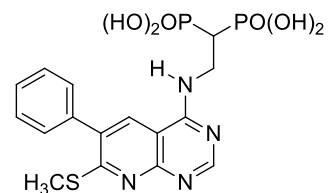
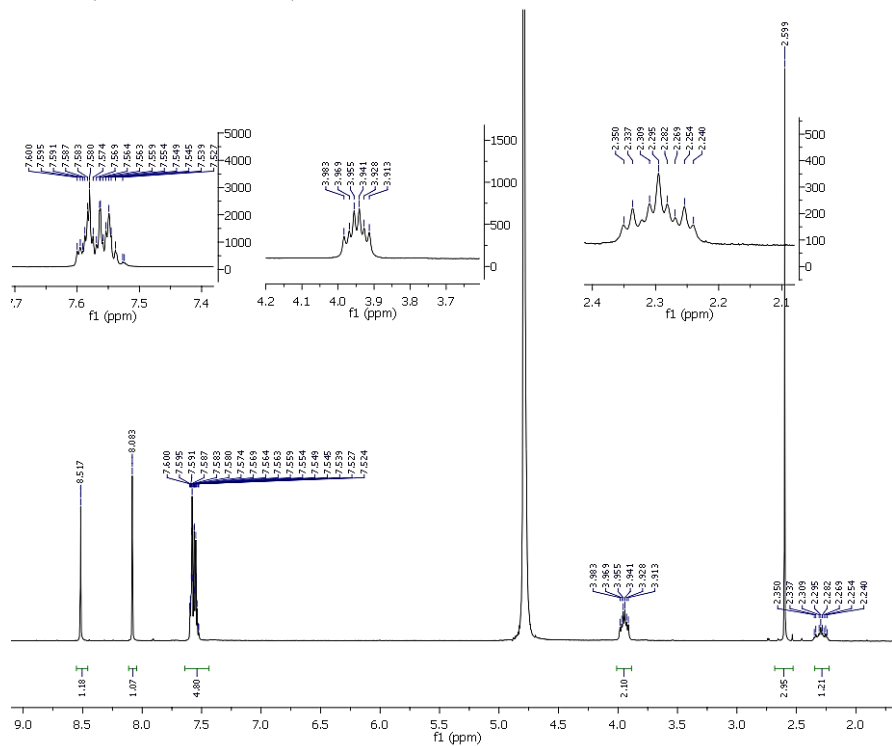


^1H - ^{13}C HSQC NMR (2.8m)

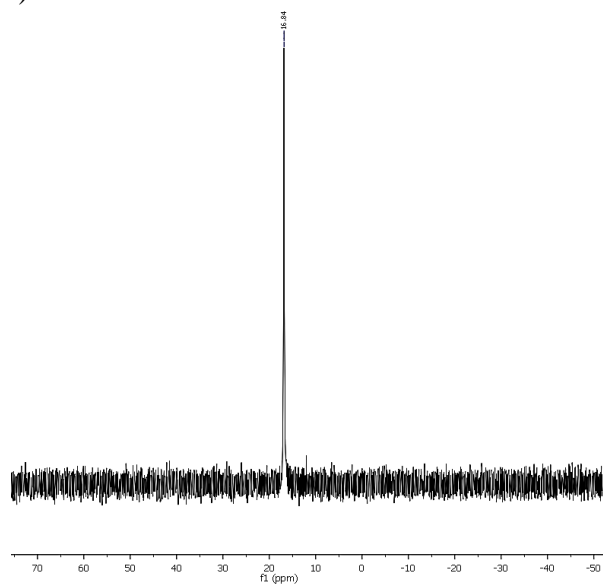


Inhibitor 2.9h

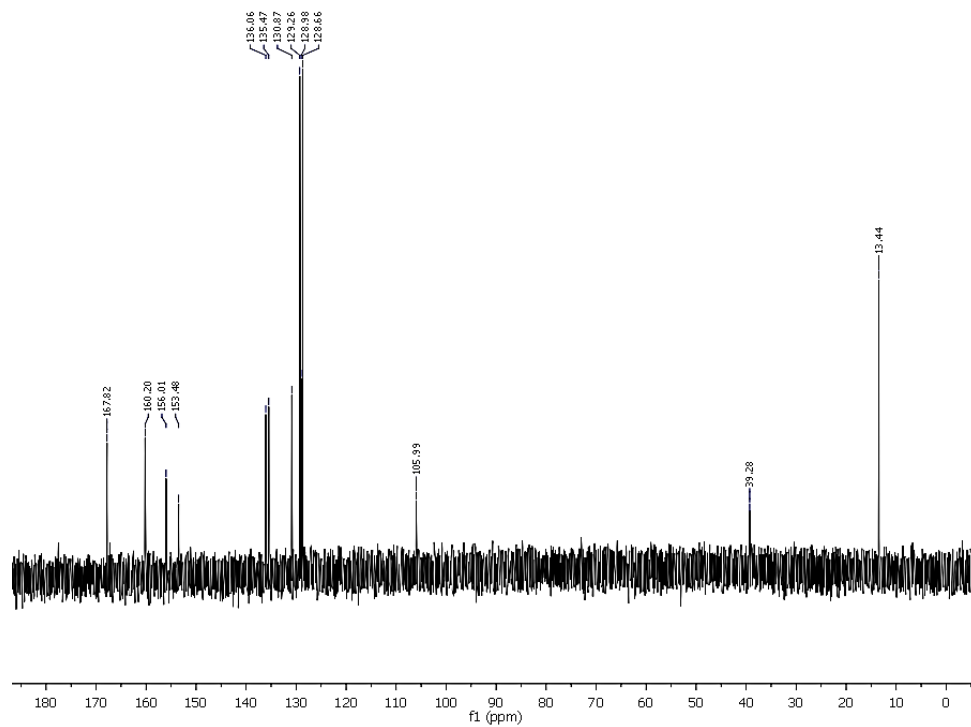
^1H NMR (500 MHz, D_2O)



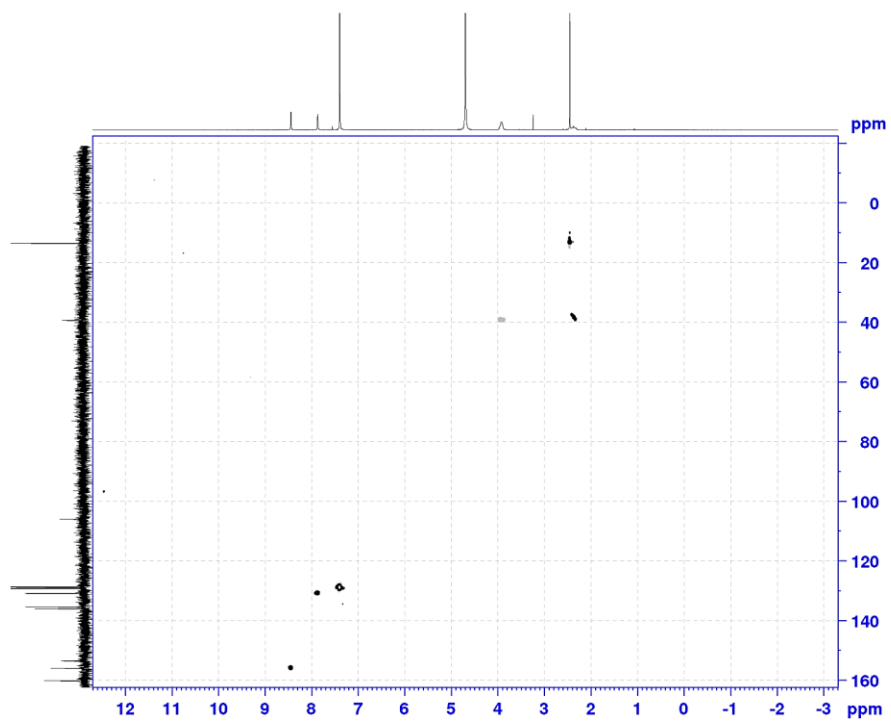
^{31}P NMR (203 MHz, D_2O)



^{13}C NMR (126 MHz, D_2O) (2.9h)

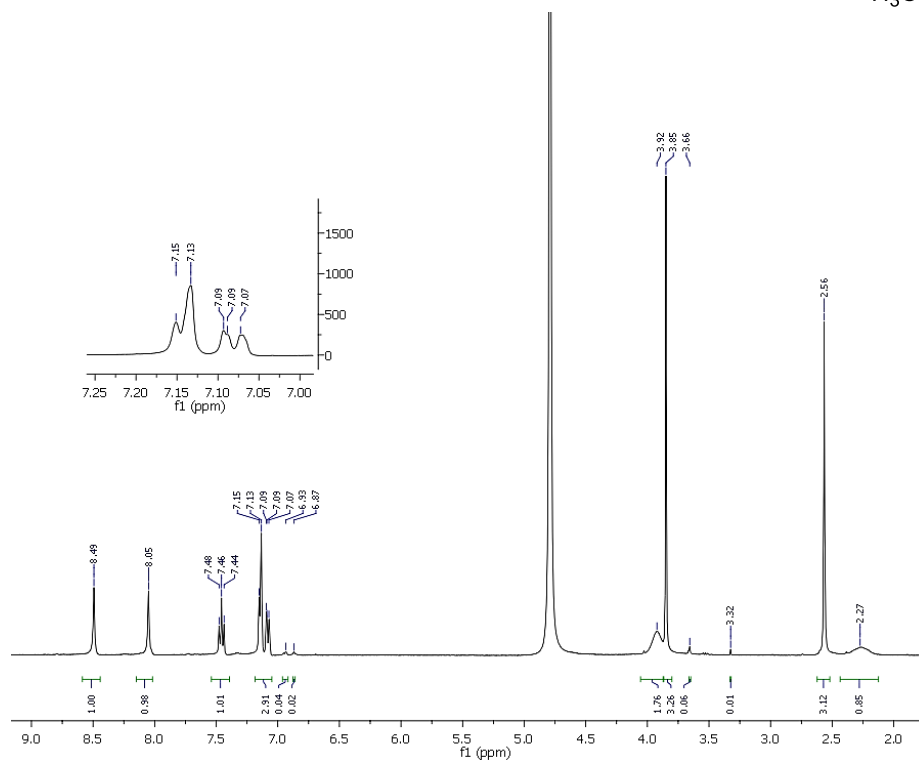
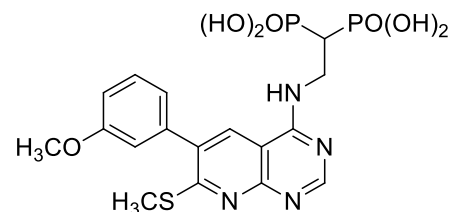


^1H - ^{13}C HSQC NMR (2.9h)

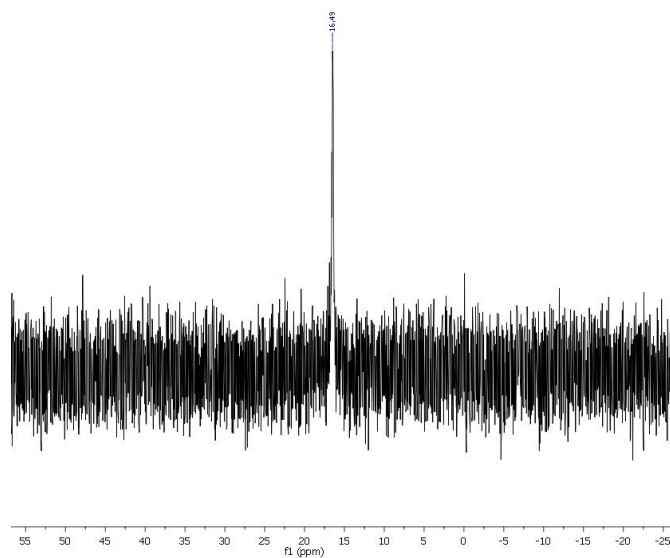


Inhibitor 2.9i

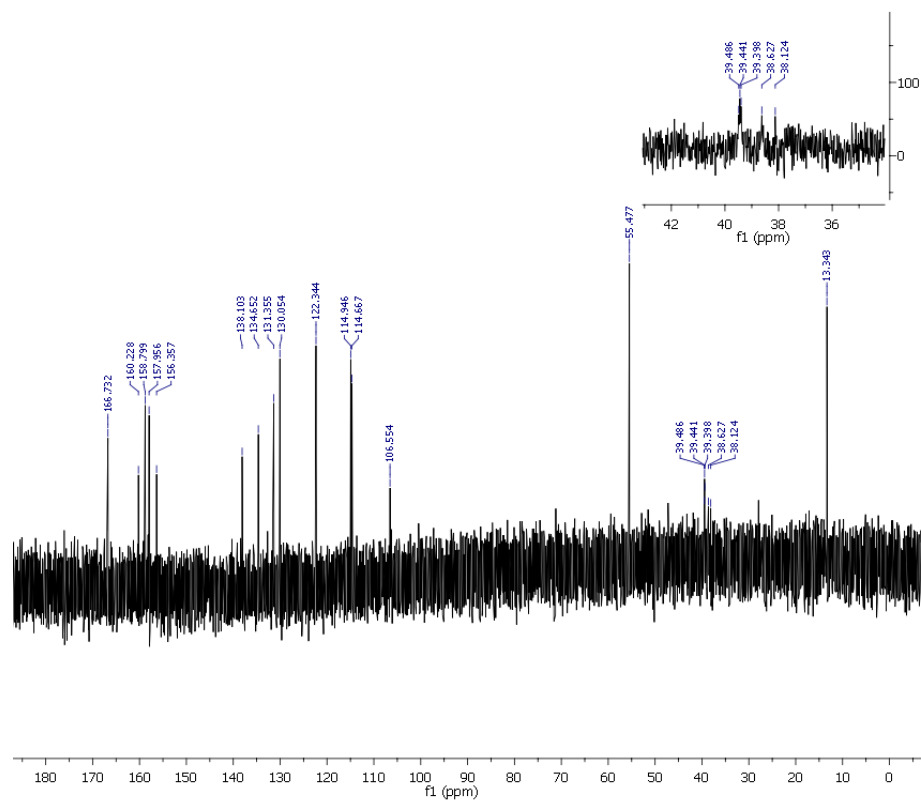
^1H NMR (400 MHz, D_2O)



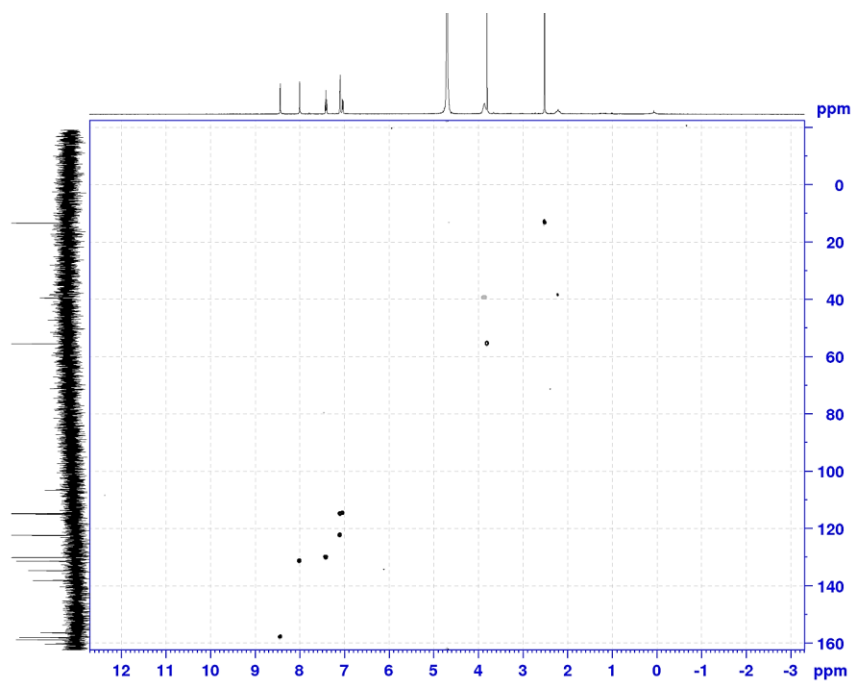
^{31}P NMR (203 MHz, D_2O)



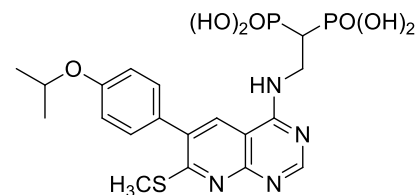
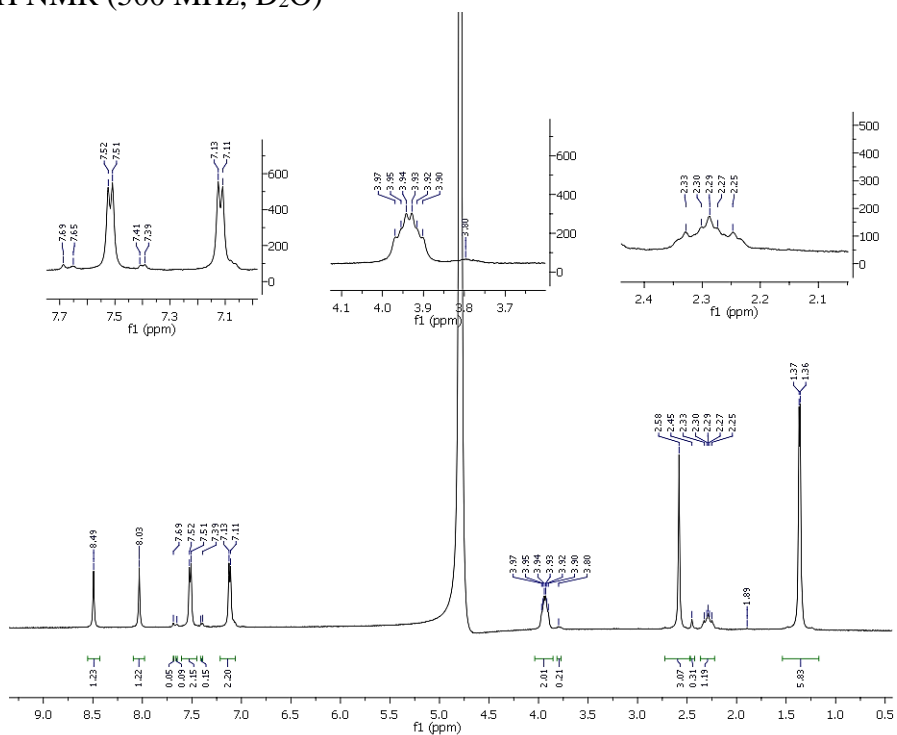
^{13}C NMR (126 MHz, D_2O) (**2.9i**)



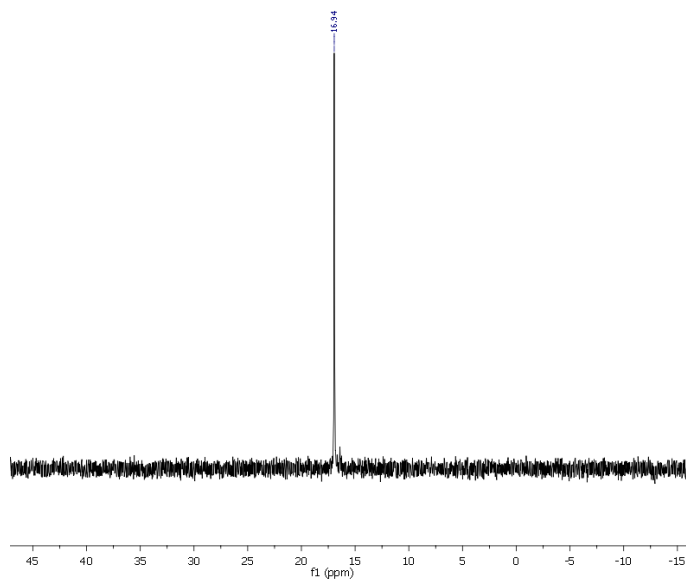
^1H - ^{13}C HSQC NMR (**2.9i**)



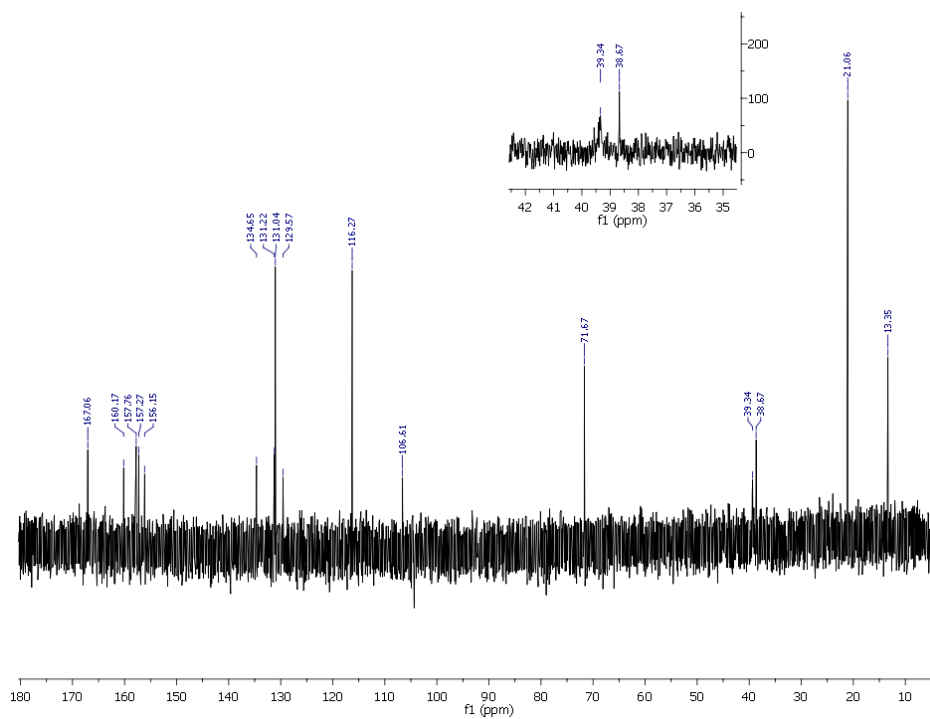
Inhibitor 2.9j
¹H NMR (500 MHz, D₂O)



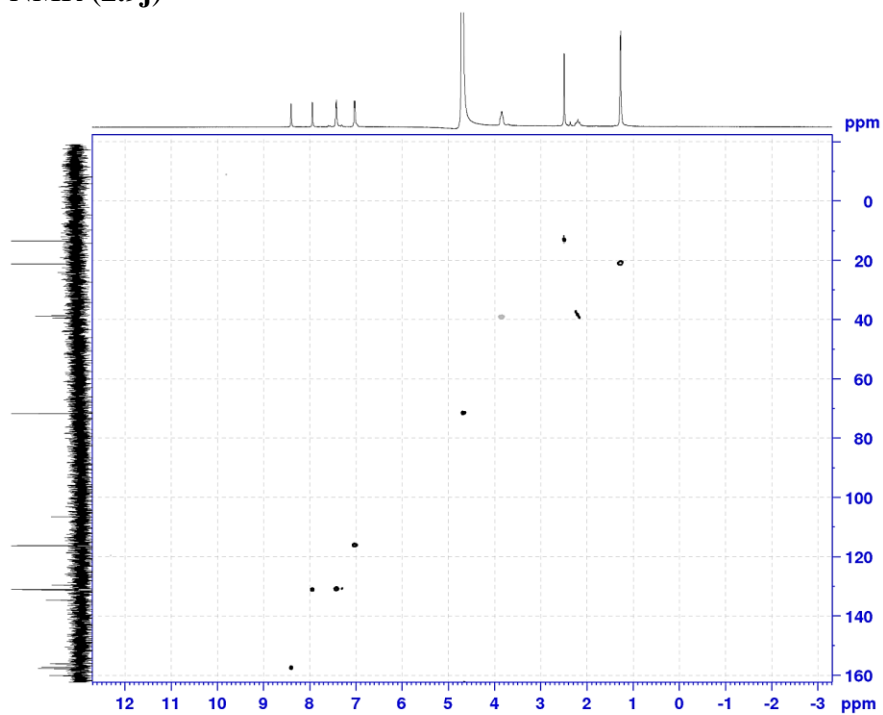
³¹P NMR (203 MHz, D₂O)



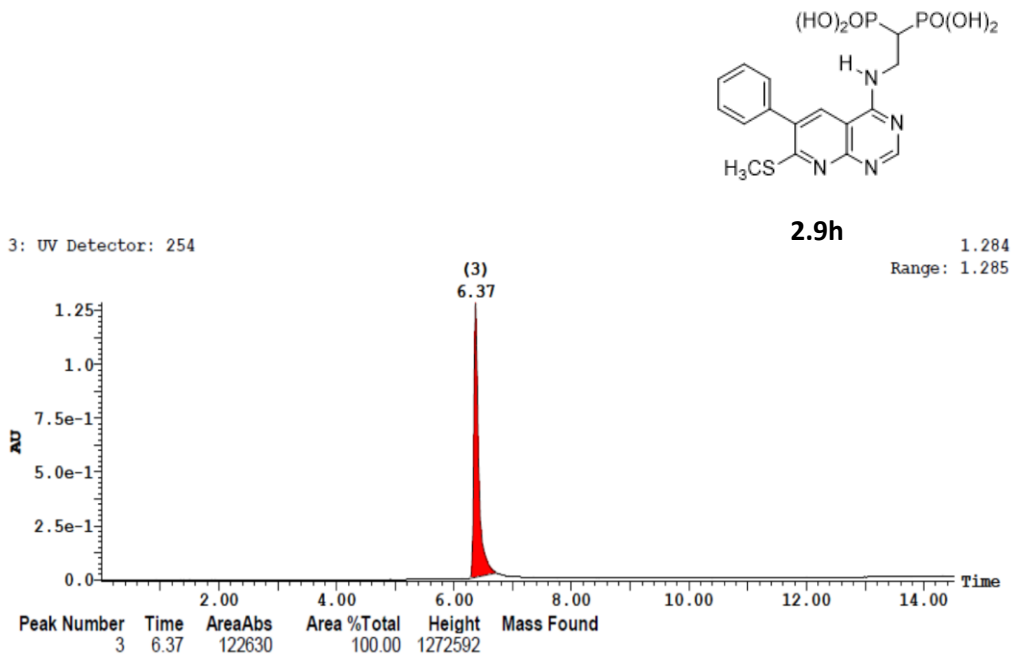
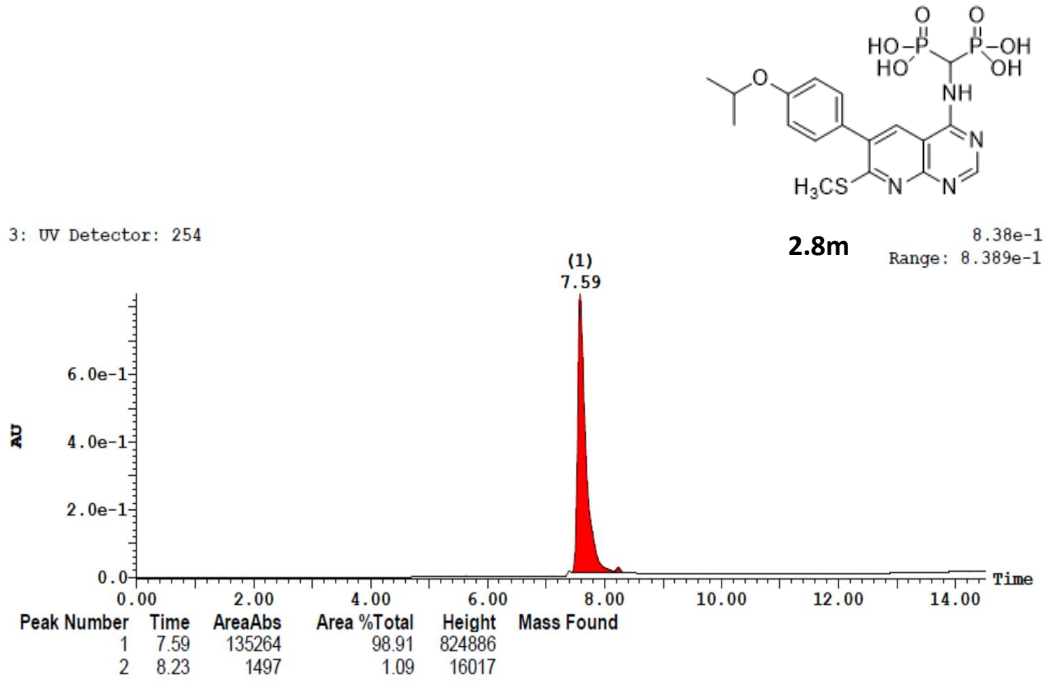
^{13}C NMR (126 MHz) (2.9j)

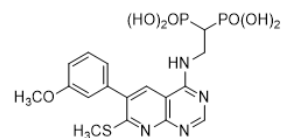


^1H - ^{13}C HSQC NMR (2.9j)



HPLC Chromatograms:

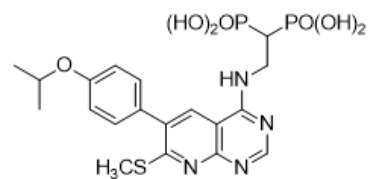
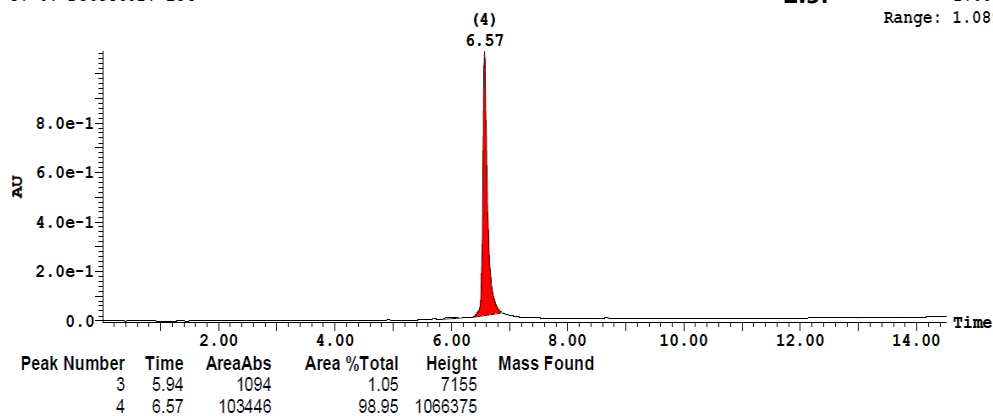




2.9i

1.088
Range: 1.089

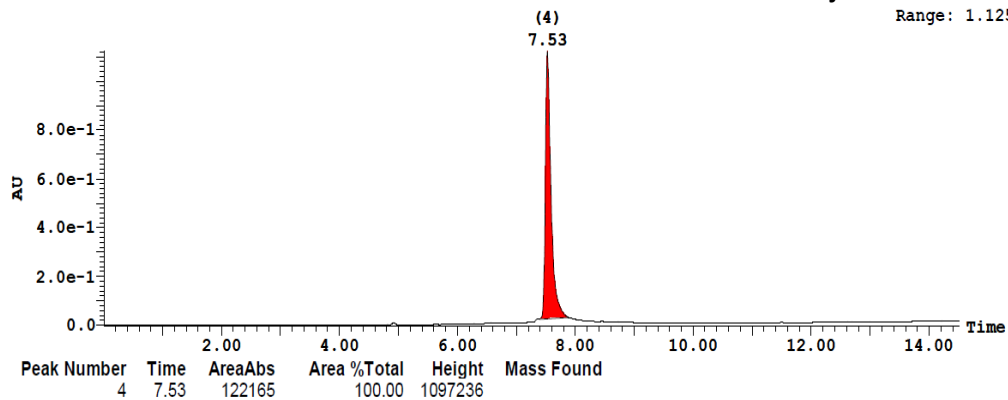
3: UV Detector: 254



2.9j

1.123
Range: 1.125

3: UV Detector: 254



CHAPTER 3: Diketo Acid Bioisosteres and Structure-Activity Relationship Studies of Mechanistically Unique Inhibitors of HIV-1 Reverse Transcriptase

3.1. Preface

This chapter covers the design, synthesis, and SAR studies of a new class of HIV-1 RT inhibitors that target RT translocation. A portion of this chapter is already drafted in a manuscript form and will be submitted for publication to *J Med. Chem.* in the very near future. As part of our collaboration, this will be a joint publication with the group of Prof. Mathias Götte (Department of Medical Microbiology and Immunology, University of Alberta). I designed and performed the synthesis of all inhibitors described in this chapter under the guidance of Prof. Youla S. Tsantrizos. Michael Menni and Dr. Jean Bernatchez conducted the biochemical evaluation of these compounds in the laboratory of Prof. Mathias Götte.

3.2. Abstract

Reverse transcriptase (RT) is responsible for replicating the HIV-1 genome and is a validated therapeutic target for the treatment of the infection. Inorganic pyrophosphate (PP_i) is the by-product formed during each catalytic cycle of nucleotide incorporation into the growing oligonucleotide chain catalyzed by RT. Interestingly, the PP_i analog foscarnet (PFA) and the hydrazone derivative, CPHM have been shown to inhibit HIV-1 RT by binding to the active site of the enzyme *via* metal-mediated interactions and freezing the catalytic cycle at the pre-translocation complex. This mechanism is unique when compared with currently known clinically validated RT inhibitors. Our present study showed that analogs of pyrimidinol carboxylic acid (a diketo acid bioisostere) can also exhibit the same mode of inhibition. Our preliminary SAR and selectivity studies compared the ability of these compounds to inhibit the HIV-1 RT polymerase versus the RNase H enzyme and identified mechanistically distinct compounds that are selective

in inhibiting RT polymerase. The drug-like properties of these compounds are far superior to PFA and CPHM; hence they are promising new leads for further optimization into novel antiviral agents for the treatment of HIV infection.

3.3. Introduction

A number of polyoxygenated compounds, such as PFA, malonic acid derivatives (e.g. CPHM), 1,3- diketo acids (DKA; **3.1**), and other literature compounds (some examples are shown in **Fig. 3.1**; **Table 3.1**) were reported to inhibit nucleic acid processing enzymes, including HIV-1 RT polymerase. Since the target selectivity was often poor in inhibiting the HIV-1 RT polymerase versus other related enzymes, the exact mechanism of inhibition was mostly undetermined. However, given that these compounds share a common structural feature (*i.e.* by having a metal-binding element), it is reasonable to assume that if they were binding to the enzyme's active site, they are coordinating with the two Mg^{2+} ions that are critical for catalytic activity.

In order to effectively probe the catalytic cycle of the HIV-1 RT polymerase, we needed to identify compounds that are (a) chemically stable, (b) selective for HIV-1 RT polymerase, and (c) selective for blocking a specific step in the catalytic cycle of the enzyme. Additionally, we were hoping to identify compounds that exhibit good “drug-like” properties that could serve as hits or leads for further medicinal chemistry investigation towards the ultimate goal of discovering new therapeutic agents for treating HIV with a novel mechanism of action. We chose to initiate our studies by exploring the target selectivity and structure-activity relationship of analogs having the metal-binding heterocyclic motif, pyrimidinol carboxylic acid **3.2** (**Fig. 3.1**).¹ As mentioned, this is a clinically validated structural motif found in the drug raltegravir.^{2,3}

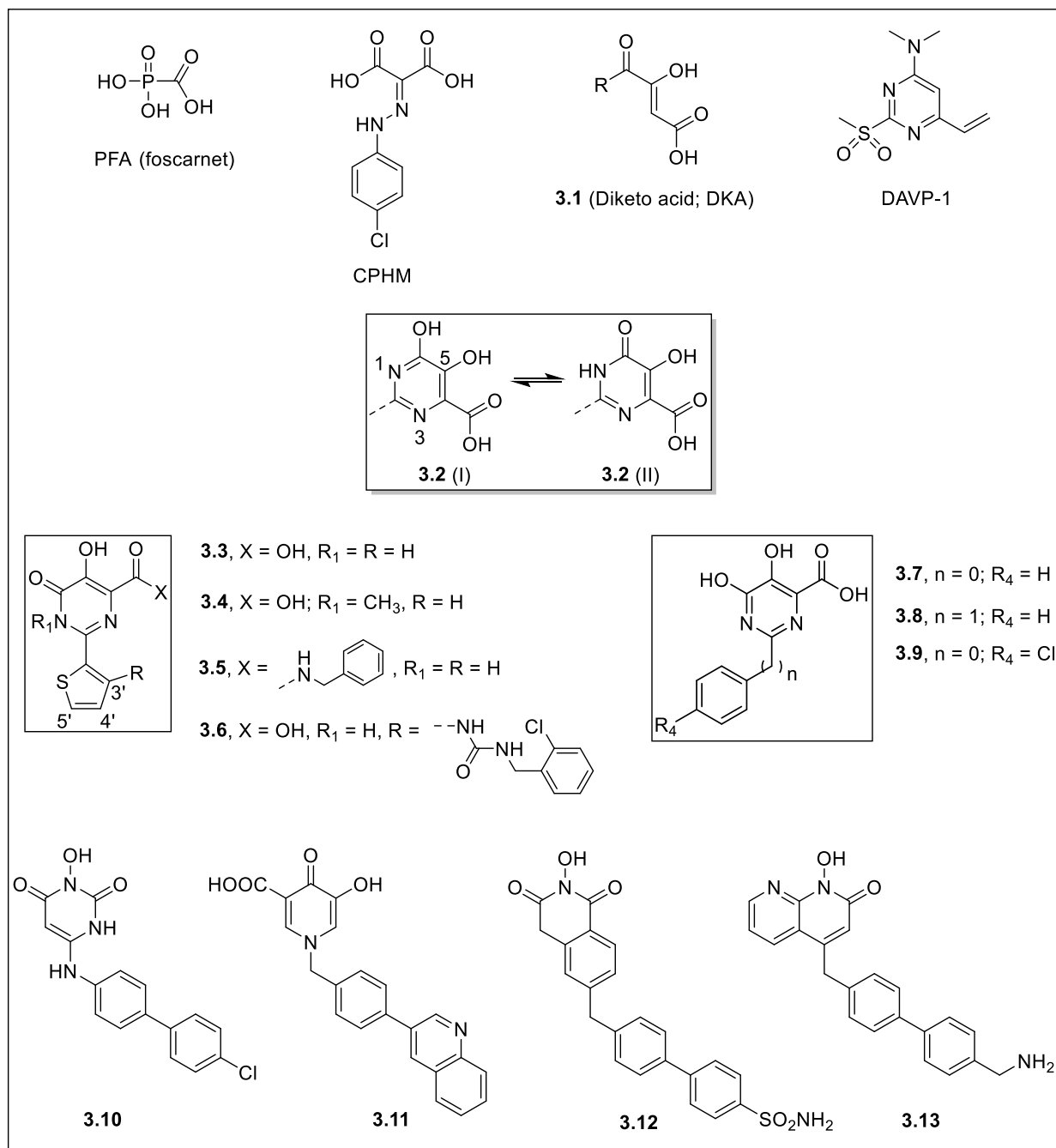


Figure 3.1. Examples of inhibitors of nucleic acid processing enzymes.

Table 3.1. Bioactivity of some literature polyoxygenated compounds shown in **Fig. 3.1**.

Code	Biological Activity (IC ₅₀ , μM)			
	HCV NS5B	HIV-1	HIV-1 RT	
	Polymerase	Integrase	Polymerase	RNase H
3.3	2.6 ^[a]	Inactive	46	<i>Nd</i> ^[b]
3.4	4.7 ^[a]	<i>Nd</i>	<i>Nd</i>	<i>Nd</i>
3.5	Inactive	0.085 ^[c]	<i>Nd</i>	<i>Nd</i>
3.6	0.15 ^[d]	<i>Nd</i>	<i>Nd</i>	<i>Nd</i>
3.7	30 ^[e]	>50 ^[e]	>100	12.9 ^[f]
3.8	<i>Nd</i>	<i>Nd</i>	<i>Nd</i>	2.5 ^[f]
3.9	29 ^[e]	>50 ^[e]	4.5 (23) ^[e]	<i>Nd</i>
3.10	<i>Nd</i>	<i>Nd</i>	0.99 ^[g]	0.47 ^[g]
3.11	<i>Nd</i>	16 ^[h]	1.1 ^[h]	0.90 ^[h]
3.12	<i>Nd</i>	3.6 ^[i]	0.50 ^[i]	0.40 ^[i]
3.13	<i>Nd</i>	24 ^[j]	13 ^[j]	0.045 ^[j]

^[a]from Stansfield *et. al.*⁴; ^[b]*Nd*=data not available or reported; ^[c]from Petrocchi *et. al.*⁵; ^[d]from Koch *et. al.*⁶; ^[e]from Summa *et. al.*¹; ^[f]from Kirschberg *et. al.*⁷; ^[g]from Tang *et. al.*⁸; ^[h]from Kankanala *et. al.*⁹; ^[i]from Vernekar *et. al.*¹⁰; ^[j]from Williams *et. al.*¹¹

The pyrimidinol carboxylic acid chemotype can exist in tautomeric forms: the dihydroxy **3.2 (I)** and pyrimidinone **3.2 (II)** (**Fig. 3.1**), which are both capable of binding to two Mg²⁺ cations. It is interesting to note that previous investigations showed that introduction of a methyl group at N-1 of compound **3.3** (**Fig. 3.1; Table 3.1**), which leads to the *N*-methyl pyrimidinone tautomer analog **3.4** did not adversely effect the potency in inhibiting the HCV NS5B RNA-dependent RNA polymerase enzyme.⁴ However, replacement of the carboxylic acid moiety with a substituted amide (e.g. analog **3.5**) led to loss in potency towards inhibiting HCV NS5B but increase in potency in inhibiting the HIV-1 integrase enzyme (HIV-1 IN).⁵ Such observations clearly demonstrate that in addition to the key metal-binding pharmacophore, substitutions around the core can modulate both the potency and selectivity of these compounds towards a specific nucleic acid processing target.

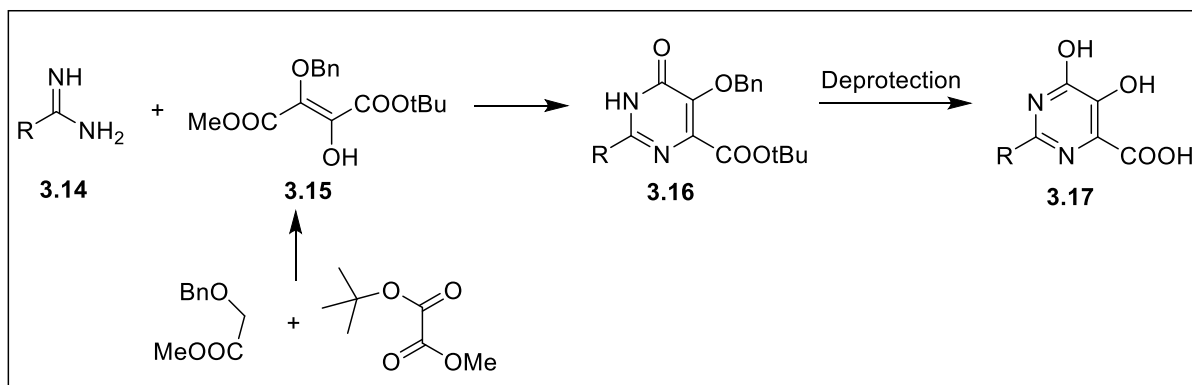
Other investigators have reported compounds that are presumed to be active site inhibitors of HIV-1 RT polymerase that are not nucleoside or nucleotide analogs. Examples include derivatives of 4-dimethylamino-6-vinylpyrimidines (e.g. DAVP-1, **Fig. 3.1**).¹² DAVP-1 was shown to be competitive with the incoming nucleotide substrate similar with other NcRTIs, such as INDOPY-1 (**Chapter 1, Fig. 1.15**). However, in contrast to INDOPY-1, which is highly specific in binding to the HIV RT P/T complex and does not bind to free RT, DAVP-1 has been shown to inhibit RT even in its unligated state.¹³ Crystallographic studies also revealed that DAVP-1 binds to a site adjacent to the polymerase active site and this alternative binding mode has been suggested to cause changes in the enzyme-bound P/T conformation that interfere with the proper incorporation of the nucleotide substrate.¹⁴ Consequently, the mode of action of DAVP-1 is more similar to an allosteric inhibitor than a true active site inhibitor. Recently, Wang and co-workers reported a series of HIV-1 RT RNase H inhibitors with varying metal binding motifs that also inhibit RT polymerase; examples include compounds **3.10**,⁸ **3.11**,⁹ and **3.12**;¹⁰ (**Fig. 3.1; Table 3.1**). In contrast, compounds containing the 1-hydroxy-1,8-naphthyridin-2(1H)-one core (**3.13**) reported by Williams *et. al.* showed significant selectivity between RT RNase H and polymerase but the *in vitro* potency of these compounds in RT polymerase was only modest.¹¹ As mentioned, while these inhibitors are likely to operate *via* metal chelation in the polymerase active site, the exact mode of inhibition was unclear.

In our present work, we prepared several derivatives of **3.2** in order to test if these compounds can prevent HIV-1 RT pre- or post-translocation and to improve the potency and selectivity for this target. We disclose herein the results of our studies that led to the identification of low micromolar inhibitors ($IC_{50} \sim 1-2 \mu M$) exhibiting the desired mechanism of action, and at the same time display some selectivity against RNase H (~16-fold). Our results may contribute to the development of

mechanistically unique non-nucleoside active site inhibitors of HIV-1 RT with therapeutic potential.

3.4 Chemistry

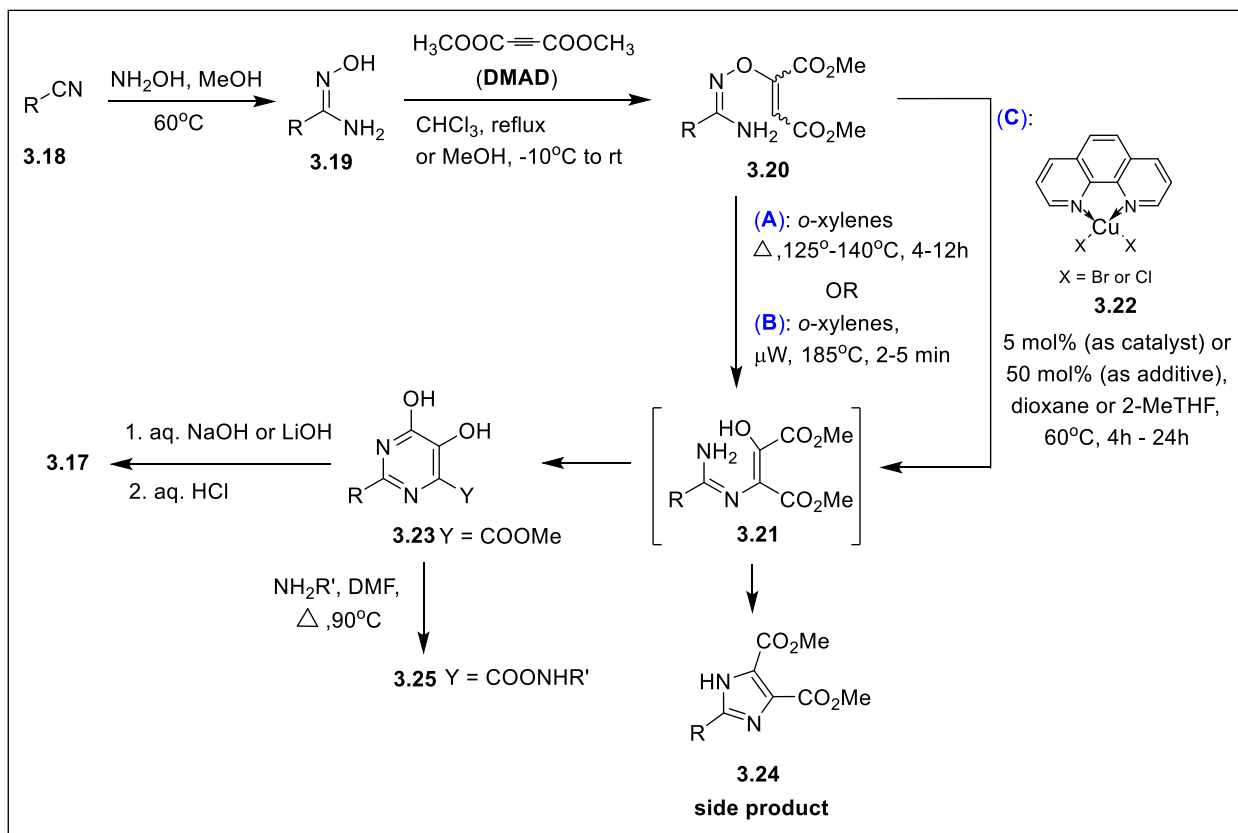
Synthesis of functionalized pyrimidinones, such as **3.16** (Scheme 3.1) and **3.23** (Scheme 3.2) can be achieved in several ways based on slightly modified protocols to those developed by scientists from Merck. Route 1 (Scheme 3.1) involves condensation of amidine **3.14** with the fumarate reagent **3.15**.¹⁵ This approach allows access of several C-2 alkyl- and aryl-substituted pyrimidinones in good to excellent yield; however, **3.15** has been reported to be unstable^{15, 16} and in addition to the extra steps in preparing the main starting materials (**3.14** and **3.15**), two different deprotection steps may be necessary for some substrates in removing the benzyl- and tert-butyl ester protecting groups of **3.16**, making the overall synthetic process longer.



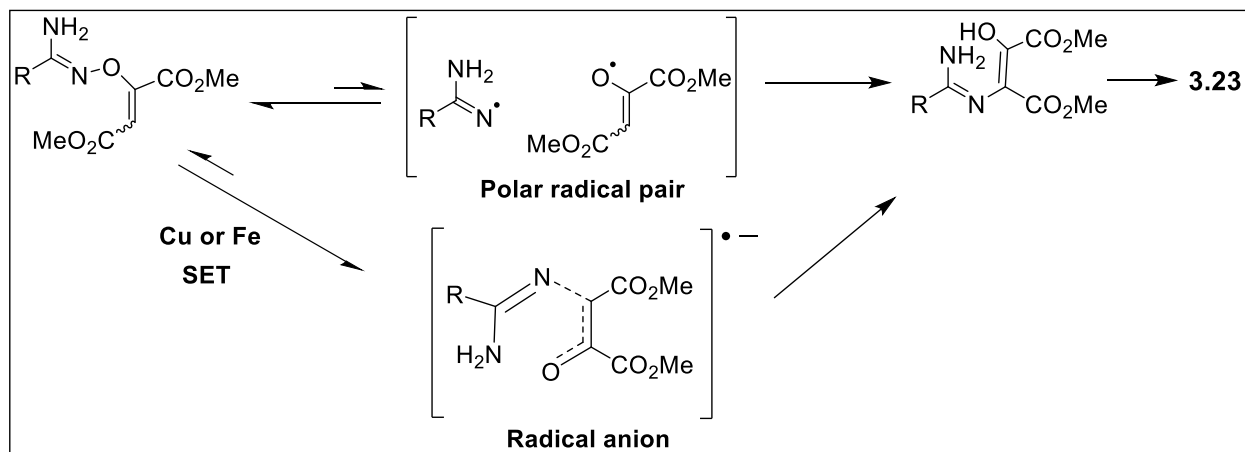
Scheme 3.1. Route 1 synthetic approach for the preparation of analogs of **3.17**.

Route 2 (Scheme 3.2) involves a Michael reaction between *N*-hydroxy amidine **3.19** and dimethylacetylene dicarboxylate (DMAD), followed by thermal dissociation/association giving the desired pyrimidinone ester **3.23** in typically 20% – 40% overall yield (Scheme 3.2A).^{3,16} The formation of the imidazole side product **3.24** and decomposition of thermally labile compounds

account for the low yields observed for this route. Microwave assisted rearrangement has been also explored leading to better but still moderate yield (~40-60%), but a shorter reaction time (**Scheme 3.2B**).¹⁷ In 2008, Merck conducted an in-depth mechanistic investigation on the formation of **3.23** and proposed that the mechanism involves a thermally induced homolytic N-O cleavage to form a radical polar pair (**Scheme 3.3**) that has a strong preference for recombination.¹⁸ In 2012, another study successfully demonstrated the use of additives and catalysts in improving this reaction.¹⁹ It was proposed that the transition state energy of the radical anion is favored over the neutral species based on the calculated free energies, *i.e.* the dissociation and recombination of the radical anion was much more facile.¹⁹ The group also reported several metal ions (mainly Cu and Fe) that improved the outcome of this reaction, presumably by reducing the energy of the transition state through a single electron transfer (SET) reduction mechanism.¹⁹ One of the best catalysts/additives identified was dibromo- or dichloro-(1,10-phenanthroline)/Cu II (**3.22**; **Scheme 3.2C**). For example, in the presence of **3.22**, the reaction temperature was reduced to 60°C and yield of ~50%-90% was typically observed. Depending on the substrate, **3.22** can be added in catalytic amount (5 mol%) or as an additive (50 mol%) to improve the yield.



Scheme 3.2. Route 2 synthetic approach for the preparation of analogs of **3.17**.

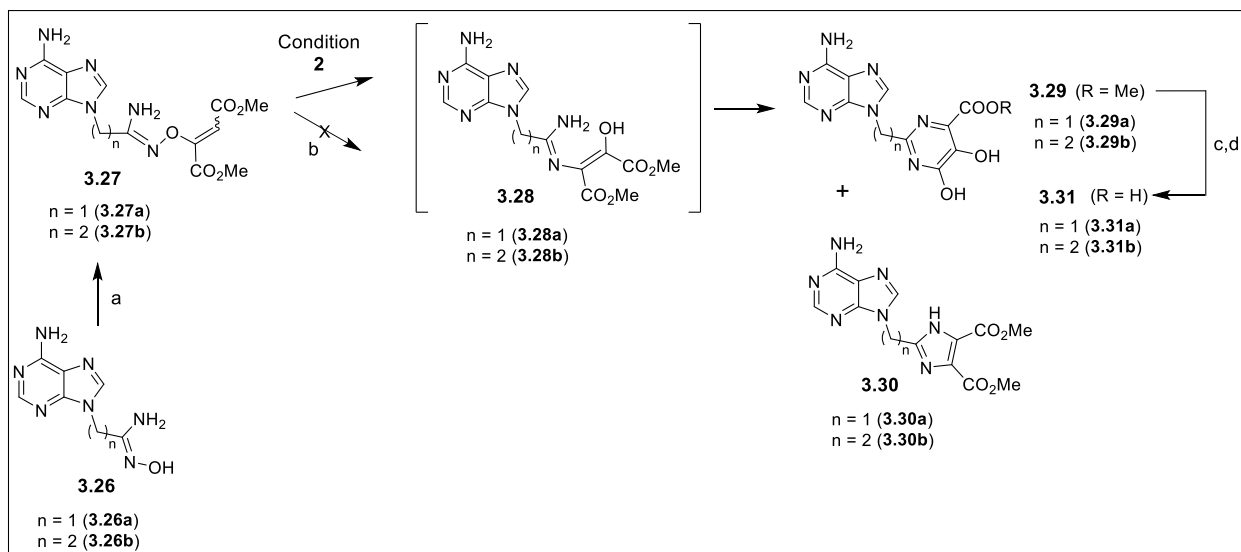


Scheme 3.3. Proposed formation of **3.23** involving a polar radical pair mechanism.

Consequently, we chose to follow route 2, and more specifically **Scheme 3.2A** for the synthesis of most of our inhibitors with slight modifications as detailed in the experimental section. Analogs of **3.23** are known to streak on silica and in using **Scheme 3.2A** or **B**, these compounds can easily be isolated and purified *via* filtration and trituration. **Scheme 3.2C** was employed for compounds containing a natural nucleobase (e.g. adenine; general structure **3.31**; **Scheme 3.4**) as our initial attempts following **Scheme 3.2A** led to mostly decomposition. The syntheses of **3.31** and of compounds with purine-like specificity domains (e.g. **3.38**; **Scheme 3.5**) are discussed below.

Synthesis of adenine-based compounds was initiated *via* preparation of the amidoxime **3.26** (**Scheme 3.4**) from the corresponding nitrile intermediate. It was observed that reaction of **3.26** with DMAD to give the Michael adduct **3.27** can be achieved in DMSO in the presence of triethylamine (**Scheme 3.4**, step a). Thermal rearrangement then amidation to **3.29** in xylenes at 130°C gave poor yield (<5%), leading mostly to decomposition. We then considered adding CuBr, an inexpensive and readily available additive that was screened by Bellomo *et. al.* and found to give reasonable yields when added in 50 mol%.¹⁹ In our preliminary studies, we set-up three reaction conditions in the synthesis of compound **3.29a** (as the test reaction) shown in **Table 3.2**. The reaction progress was monitored by LC-MS. Our results showed that the reaction was not finished in Conditions **1** (without CuBr, 130°C) after 2h and **3** (with 50 mol% CuBr, 60°C) after 1.5h, whereas full consumption of the starting materials was observed with Condition **2** (with 50 mol% CuBr, 130°C) after 30 min. A mixture of desired product **3.29a** and side product **3.30a** (**Scheme 3.4**) in ~7:3 ratio was also observed with Condition **2**. The known intermediate **3.28** and imidazole side product **3.30** of this reaction were not isolated but were assigned based on the corresponding mass observed by LC-MS. Without further optimization, Condition **2** was followed

and analogs of **3.29** (**a** and **b**) were isolated in ~30% yield. It is noteworthy that due to the high polarity of these adenine-based compounds, the purification was very challenging, accounting in part for the low isolated yield.



Scheme 3.4. Synthesis of adenine-based compounds.

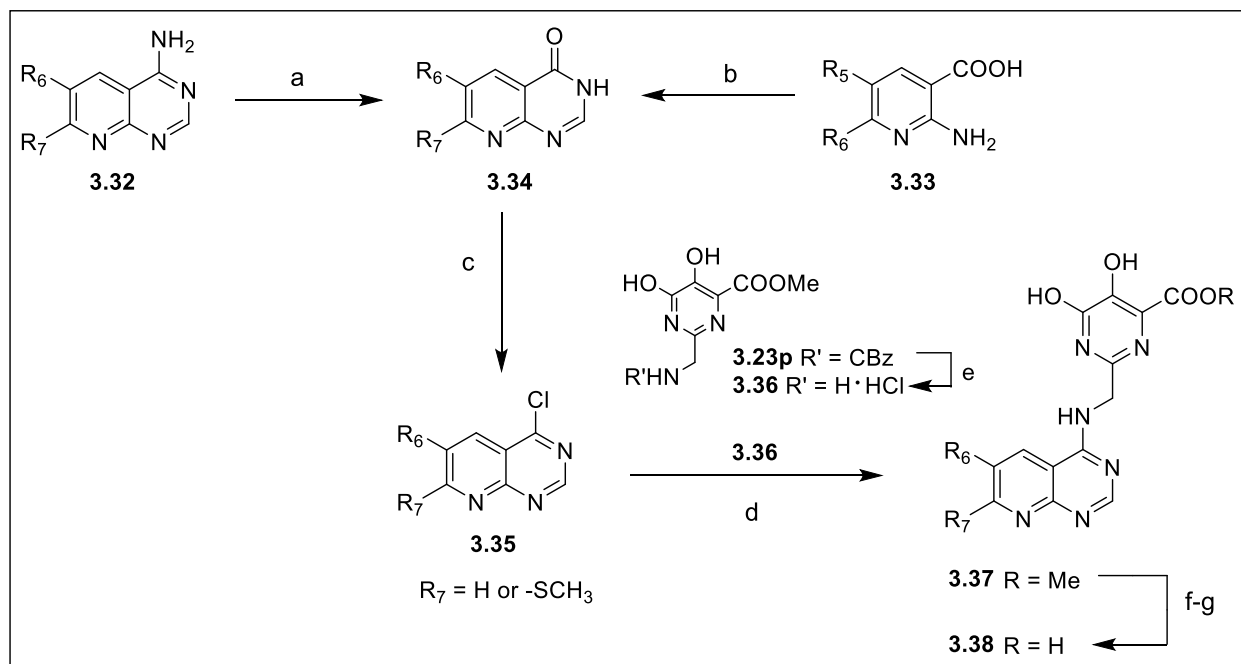
Conditions: (a) DMAD, Et₃N (~0.1-1.0 eq), DMSO, rt, 4-16 h, 50%-80%; (b) *o*-xylenes, 130°C, 6-12 h, trace (mostly decomposition); (Condition 2; Table 3.2) CuBr (50 mol %), dioxane, 130°C, 30 min, ~30%; (c) LiOH, MeOH:THF:H₂O (2:2:1), 50°-60°C, 4-12 h; (d) aq. HCl.

Table 3.2. Preliminary results on the use of CuBr as additive in the synthesis of **3.29a** from **3.27a**^[a] as depicted in **Scheme 3.4**

Condition	Temp. (°C)	Additive	Time, h	% Conversion ^[b]	
				3.29a	3.30a
1	130	none	2	22	5
2	130	CuBr, 50 mol%	0.5	70 (30) ^[c]	30
3	60	CuBr, 50 mol%	1.5	36 ^[d]	33

Note: ^[a]Test reactions were done using 0.043 mmol of **3.27a** and dioxane as solvent; ^[b]Calculated based on % area; ^[c]Number in parenthesis represents isolated yield; ^[d]**3.27a** was fully consumed but intermediate **3.28a** was still present (~32%).

We recently reported the modular synthesis of pyrido[2,3-*d*]pyrimidines (**3.32**),²⁰ a heterobicyclic scaffold that can serve as purine mimics. We identified several analogs of pyridopyrimidines with bisphosphonate anchor (PYPY-BPs, **Chapter 2** of this thesis) that can inhibit the HIV-1 RT-catalyzed DNA synthesis. In this study, we were interested in investigating the biological properties of non-bisphosphonate compounds. As a first step, we decided to replace the metal-chelating bisphosphonate moiety of PYPY-BPs with the pyrimidinol carboxylic acid bioisostere. Synthesis of these compounds was accomplished as outlined in **Scheme 3.5**. Pyrimidinone intermediate **3.34** was prepared in two ways: (a) reaction of **3.32**²⁰ with methanesulfonic acid/water under refluxing conditions, and (b) cyclization of 2-aminonicotinonitrile **3.33** with formamide. Treatment of **3.34** with POCl₃ afforded the 4-chloropyridopyrimidine intermediate **3.35**, which was subjected to an S_NAr reaction with amine **3.36**. Compound **3.36** was synthesized *via* hydrogenolysis of methyl 2-(((benzyloxy)carbonyl)amino)methyl)-5,6-dihydropyrimidine-4-carboxylate (**3.23m**), which was prepared from the CBz-protected aminoacetonitrile following **Scheme 3.2A**. In cases where the R₆ moiety was a bromide, intermediate **3.37** was subjected to Suzuki cross-coupling reactions in order to introduce a variety of aryl or heteroaryl groups at C-6. The final inhibitors were obtained upon hydrolysis of the methyl ester. Representative compounds from our mini library are shown in **Figure 3.2**.



Scheme 3.5. Synthesis of pyridopyrimidine-based compounds.

Conditions: (a) Methanesulfonic acid/ H_2O , 100°C , 1h, 60%-94%; (b) Formamide, 145°C , 20-48h, 58%-68%; (c) POCl_3 , toluene, pyridine, $115^\circ\text{-}180^\circ\text{C}$, ~2h, 30%-65%; (d) DMSO/dioxane, Et_3N , 100°C , 1h, ~50%-70%; (e) H_2 , Pd/C, 6N HCl 76%; (f) LiOH, MeOH:THF: H_2O (2:2:1), $50^\circ\text{-}60^\circ\text{C}$; (g) aq. HCl.

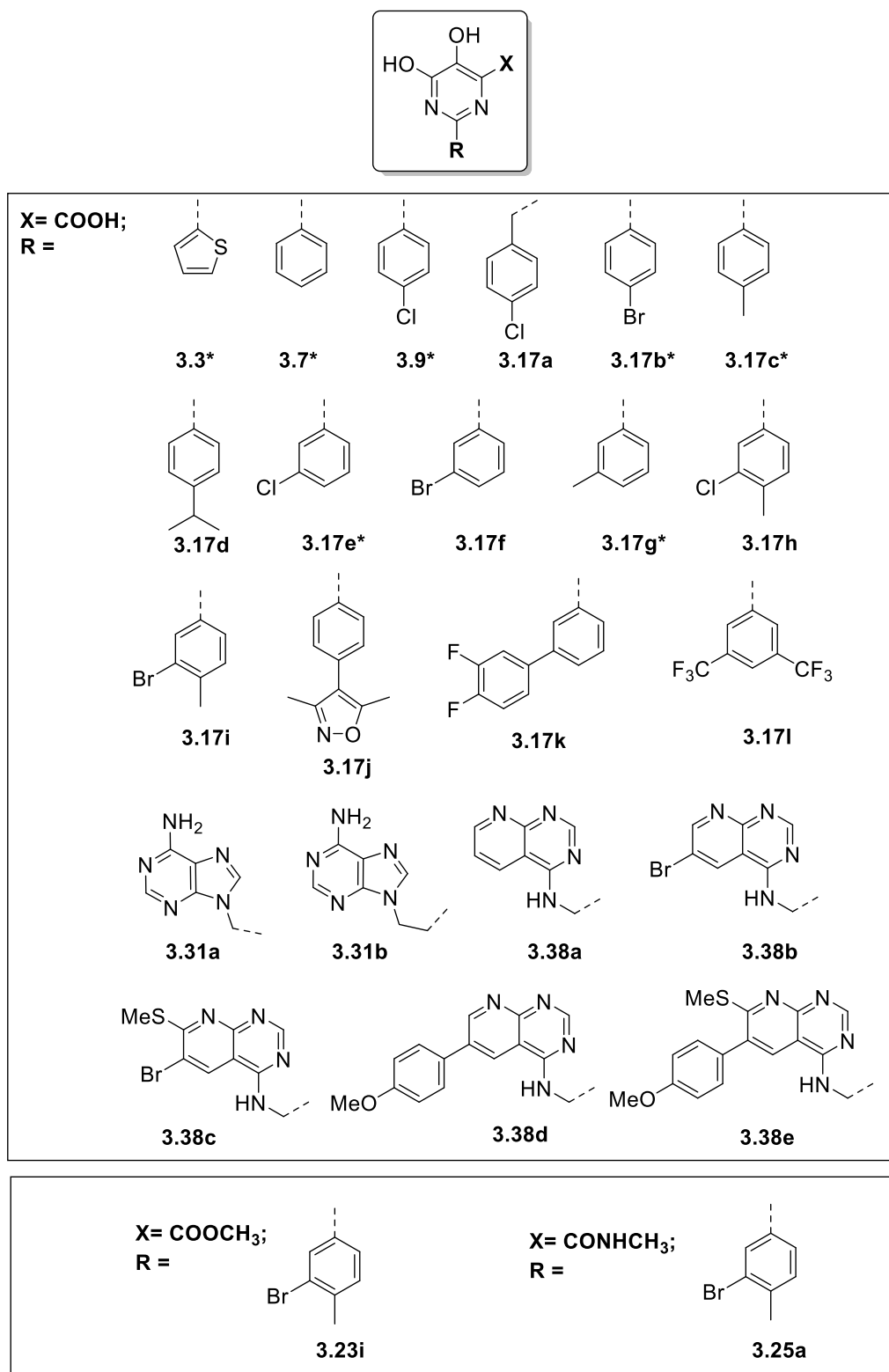


Figure 3.2. Representative examples of HIV-1 RT inhibitors from our compound library.
*Literature compounds which were also re-synthesized for the purpose of our SAR investigations.

3.5 Results and Discussion

“Translocation” is a key step that occurs during DNA polymerization catalyzed by the HIV-1 RT polymerase. This step refers primarily to the translocation of the elongated primer terminus to the so-called priming site (P-site), which frees the nucleotide binding site (N-site) for binding of the next dNTP substrate (**Fig. 3.3**). Previous studies suggest that the polymerase establishes a dynamic equilibrium between the pre- and post-translocational conformations and site-specific footprinting experiments were used to confirm the “freezing” of either one of these two translocation states by an inhibitor.^{21, 22} For instance, in our present study, PFA or CPHM and INDOPY-1 or α -CNP (**Chapter 1, Fig. 1.15**) were used in the same assay as positive (reference) controls to confirm the specific trapping of the pre-translocation and post-translocation complexes, respectively.

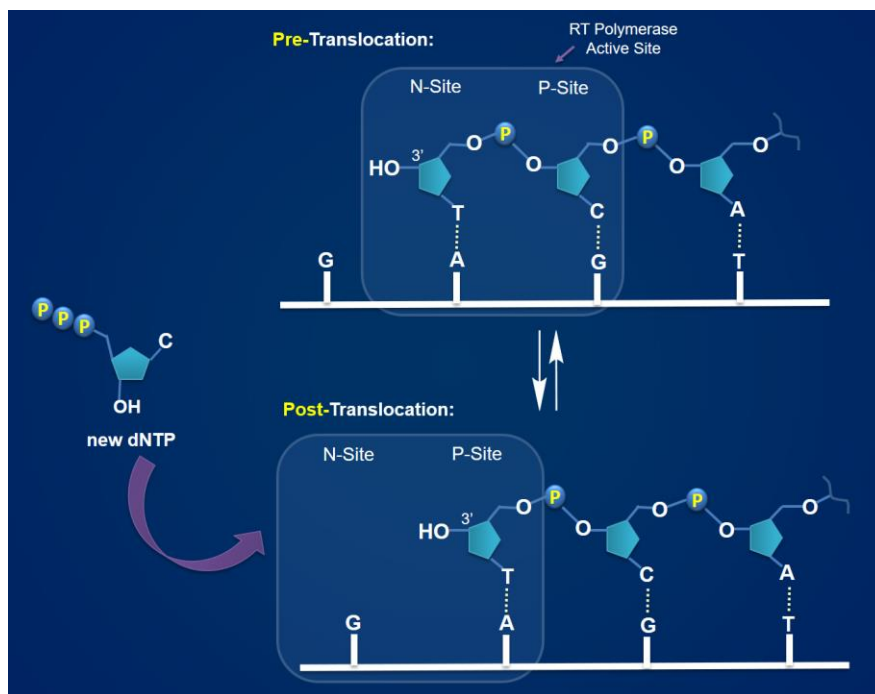


Figure 3.3. Representation of the translocation step in the DNA polymerization cycle catalyzed by HIV-1 RT polymerase.

Using two established biochemical assays: (1) DNA synthesis assay (a gel-based primer extension assay that measure the potency of inhibitors in HIV-1 RT polymerase and at the same time show actual pausing pattern associated with inhibition)^{22, 23} and (2) site-specific footprinting experiments (to evaluate specific pre- or post-translocation binding),²¹⁻²³ we explored the potential of our pyrimidinol carboxylic acids to exhibit a mechanism specific for inhibition of HIV-1 RT. We prepared several exploratory compounds varied at C-2 of the basic scaffold (**Fig. 3.2**). It is noteworthy that the structurally related analogs, compound **3.9** and CPHM, differ by about 3-fold in terms of potency (**Table 3.3**) but gave identical profiles in both the DNA synthesis inhibition assay and footprinting assay, which suggest that the mode of inhibition of these two compounds is highly related (data not shown). As mentioned earlier, analog **3.9** has been reported previously to also inhibit the HCV NS5B polymerase enzyme¹ and was included in our library as a reference compound. Mindful of these findings, we continued with our studies by exploring the structural requirements optimal for binding to the HIV- 1 RT translocation complex.

The summary of DNA synthesis inhibition data for representative compounds is shown in **Table 3.3**. The reference unsubstituted phenyl group at C-2, compound **3.7** was inactive at 100 μ M; however, analogs with a chloro, bromo, or methyl group at *para*- position of the C-2 phenyl (compounds **3.9**, **3.17b**, and **3.17c**, **Fig. 3.2**) exhibited potencies in the 3-6 μ M range. Generally, *meta* substitution was less favorable than the corresponding *para*-substitution, for example 4-, 5-, and 8-fold decrease in potency was observed between the *para*- and *meta*- substituents for the chloro (**3.9** vs **3.17e**), bromo (**3.17b** vs **3.17f**), and methyl (**3.17c** vs **3.17g**) derivatives, respectively (**Table 3.3**). Incorporation of much bigger groups either at *meta*- or *para*- positions resulted in significant loss of potency (e.g. **3.17j** and **3.17k**), suggesting a limited volume of space in the binding site of these inhibitors (at this point, we assume that these analogs are adopting the same

binding mode; however, the possibility of multiple binding modes cannot be ruled out). Introducing a longer linker (e.g. **3.9** vs **3.17a**) also resulted in a significant loss of potency. Incorporating different groups at C-2 other than a phenyl (e.g. thiophene **3.3**, adenine **3.31**, and, pyridopyrimidines **3.38**) did not offer any advantages. Di-substituted inhibitors **3.17h** and **3.17i** were the best analogs identified from this library of compounds with IC₅₀ values in the 1-2 μM range (Fig. 3.2; Table 3.3). Our results also demonstrated the importance of the carboxylic acid group for inhibitory activity as the corresponding esters and amides were found to be inactive (e.g. **3.17i** vs ester **3.23i** and amide **3.25a**).

Table 3.3. Inhibition data in HIV-1 RT polymerase and RNase H.

Compound	IC ₅₀ RT Pol (μM)	IC ₅₀ RT RNase H (μM)	Compound	IC ₅₀ RT Pol (μM)	IC ₅₀ RT RNase H (μM)
PFA	0.8 ± 0.2	>100	3.17i	1.4 ± 0.2	23.0 ± 5.1
CPHM	1.5 ± 0.2	>100	3.17j	>100	nd ^[c]
β-thujaplicinol	>50 ^[a]	0.8 ± 0.3	3.17k	>100	nd
3.3	46 ± 3.5	nd	3.17l	20 ± 0.6	nd
3.7	>100	12.9 ^[b]	3.31a	>100	nd
3.9	4.5 ± 0.5	nd	3.31b	41	nd
3.17a	97 ± 13	5.1 ± 1.6	3.38a	65.3 ± 5.8	nd
3.17b	2.8 ± 0.2	nd	3.38b	48.8 ± 5.4	nd
3.17c	6.3 ± 0.4	nd	3.38c	>100	nd
3.17d	22 ± 1.3	nd	3.38d	25 ± 16	1.5 ± 0.1
3.17e	18 ± 2.6	nd	3.38e	62	2.0 ± 1.3
3.17f	14 ± 3.6	nd	3.23i	>100	>100
3.17g	49 ± 10	nd	3.25a	>100	>100
3.17h	1.6 ± 0.2	25.0 ± 5.3			

IC₅₀ values are average of at least three determinations; ^[a]IC₅₀ value from Budahas *et. al.*²⁴;

^[b]from Kirschberg *et. al.*⁷ ^[c]nd = Not determined

It is not surprising that in addition to the polymerase catalytic activity of HIV-1 RT, the RNase H activity may also be affected by these compounds since the function of the RNase H also relies on binding to two metal ions.²⁵ We were pleased to find that our most potent inhibitors in the RT

polymerase (e.g. **3.17h** and **3.17i**) were less potent in inhibiting RNase H. For example, a selectivity difference of approximately 16-fold was observed for analog **3.17i** (IC_{50} of 1.4 μ M and 23 μ M in polymerase and RNase H, respectively; **Table 3.3**) using our own *in vitro* assays. In contrast, some of our pyridopyrimidine-based compounds (e.g. **3.38d** and **3.38e**; **Fig. 3.2**), which were weak inhibitors of the polymerase enzyme exhibited better potency in inhibiting RNase H with IC_{50} values in the low micromolar range (**Table 3.3**). The pyridopyrimidines are promising novel inhibitors of RNase H for further optimization. Furthermore, introduction of a methylene linker is favored for RNase H inhibition (e.g. **3.17a**), which is consistent with the observation by Kirschberg *et. al.*⁷ It should be noted that the natural product β -thujaplicinol (**Fig. 3.4**),²⁴ a known RNase H inhibitor, was used as the positive control compound in our RNase H inhibition assay.

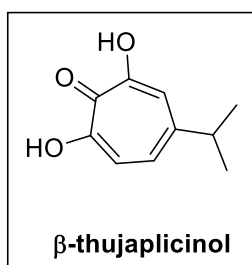


Figure 3.4. Structure of β -thujaplicinol.

Previously, mutagenesis studies on HIV-1 RT revealed that introduction of the mutation D185N in the polymerase active site abolished the activity of PFA and CPHM. Another mutation, E89K, which diminishes the stability of the pre-translocated complex²² was also able to raise resistance against both PFA and CPHM, whereas the NRTI-resistant K65R confers some level of resistance to PFA but not with CPHM. The inhibition profile of key compounds from our library using various HIV-1 RT mutants is currently in progress; preliminary results are encouraging and have shown that the inhibitory activity of compound **3.9** was also not compromised by the K65R mutation (a more extensive biological profiling is in progress).

Finally, our key compounds were investigated for their mechanism of action using the site-specific footprinting assay. Our results showed that the mode of inhibition of our most potent polymerase inhibitors, analogs **3.17h** and **3.17i** are identical to that of PFA as evidenced by the same pausing profiles in HIV-1 RT catalyzed DNA synthesis (**Fig. 3.5**) and by “freezing” of the pre-translocated state of RT as confirmed by site-specific footprinting experiments (**Fig. 3.6**). Compounds, such as **3.17h** and **3.17i** represent a new class of RT pre-translocation binders that are virtually equipotent to PFA and CPHM but have significantly better drug-like properties. These compounds are new “hits” for drug discovery of antiviral agents to treat HIV-1 infection with a novel mechanism of action. Our preliminary SAR studies suggest that these compounds are likely to bind in a constrained space of the active site in the pre-translocation complex. Based on our results and the knowledge that PFA mimics the PP_i by-product of the polymerase catalytic reaction, it is reasonable to assume that such compounds may also compete for binding in the PP_i site of the pre-translocation complex. In contrast, much larger molecules, such as α -CNP and INDOPY-1 (**Chapter 1, Fig. 1.15**) “freeze” the post-translocation complex of the enzyme, consistent with the much larger available space at the empty N-site.

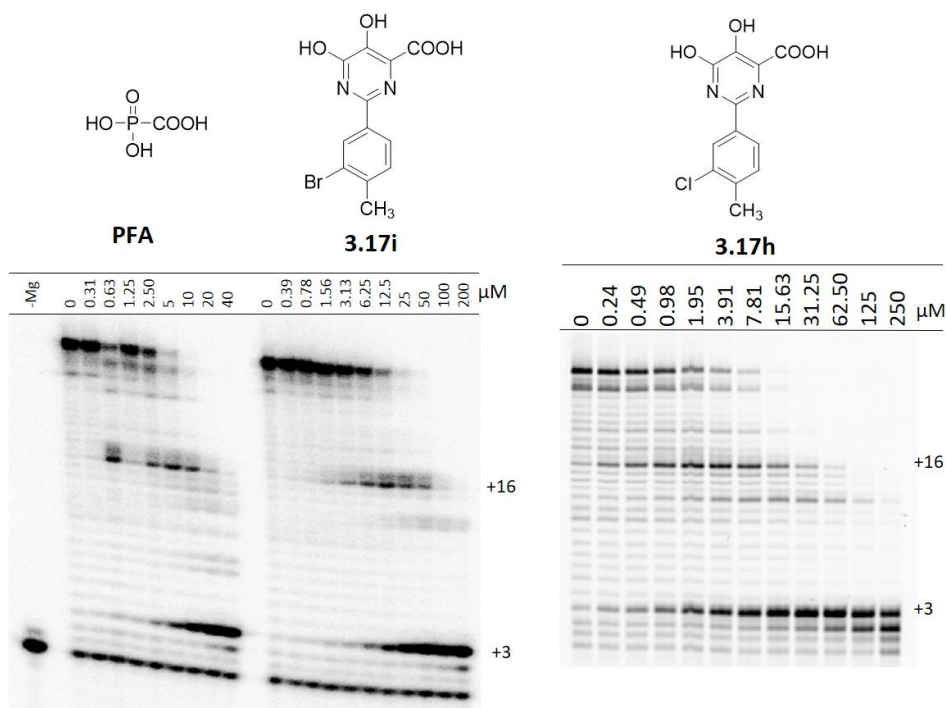


Figure 3.5. Inhibition of HIV-1 RT DNA synthesis by PFA and compounds **3.17h** and **3.17i**. All three compounds induced identical pausing patterns in DNA synthesis, which occurs predominantly at positions +3 and +16. These experiments were performed based on the previously described protocol as detailed in the experimental section.²³

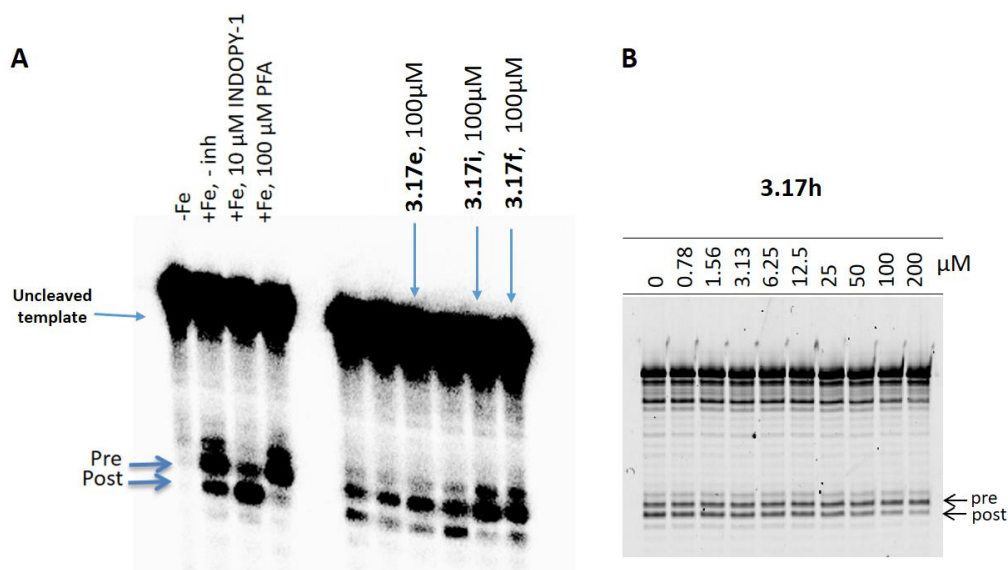


Figure 3.6. Investigation of the mechanism of action *via* site-specific footprinting assay performed using the previously described protocol.^{21, 23} (A) Cleavage fragments corresponding to pre- and

post-translocation complexes are indicated with arrows. PFA and INDOPY-1 were tested in parallel as the positive controls for confirming the freezing of the pre- and post-translocation complexes, respectively. Compounds, such as **3.17e**, **3.17f**, and **3.17i** trapped the pre-translocated complex the same way as PFA; **(B)** Dose-dependent inhibition of the pre-translocation complex of HIV-1 RT by analog **3.17h**.

3.6 Conclusions

In the absence of cure for HIV, the quest for finding better therapeutic agents to combat this infection continues. Discovery of small molecule inhibitors that function with a different mode of action and, consequently, offer an advantage against the current clinically relevant drug resistant HIV mutants may help in the development of more effective treatments against this infection. This work identified a new series of pyrimidinol carboxylic acid-based inhibitors that are likely to bind in the pyrophosphate binding site and stabilize the untranslocated state of HIV-1 RT. However, confirmation of our hypothesis with respect to binding in the PP_i site is pending crystallographic data. Our preliminary SAR studies provided some evidence on the structural requirements suitable in targeting the pre-translocation complex. RNase H selectivity assays further support that the activity of our best compounds is directed towards polymerase inhibition. Although investigations of the resistance profile of our best compounds are still on-going, the analogs tested so far appear to retain their activity in the NRTI-resistant K65R mutant. Taken together, our results provide a venue for the development of mechanistically distinct active site inhibitors of HIV-1 RT with potential therapeutic applications.

3.7 Experimental Section

Purification by normal phase flash column chromatography on silica gel was performed using a CombiFlash instrument using the indicated solvent gradient. Final inhibitors were purified by

reversed-phase preparative HPLC using a Waters Atlantis Prep T3 OBD C18 5 μ m 19 x 50 mm column; Solvent A: H₂O, 0.1% formic acid; Solvent B: CH₃CN, 0.1% formic acid; Mobile phase: gradient from 95% A and 5% B to 5% A and 95% B in 17 min acquisition time; flow rate: 1 mL/min. The homogeneity of final inhibitors was confirmed to be \geq 95% by reversed-phase HPLC using a Waters ALLIANCE® instrument (e2695 with 2489 UV detector, 3100 mass spectrometer, C18 5 μ m column): Solvent A: H₂O, 0.1% formic acid; Solvent B: CH₃CN, 0.1% formic acid; Mobile phase: linear gradient from 95% A and 5% B to 0% A and 100% B in 13 min. Key compounds were fully characterized by ¹H, ¹³C NMR, and HRMS. Chemical shifts (δ) are reported in ppm relative to the internal deuterated solvent (¹H, ¹³C), unless otherwise indicated. The high resolution MS spectra of final products were recorded using electrospray ionization (ESI+/-) and Fourier transform ion cyclotron resonance mass analyzer (FTMS).

General Synthetic Protocols:

Method A. General Protocol for the Suzuki Cross-Coupling Reaction

Aryl halide (1 eq), boronic acid (1.3 eq), Pd(PPh₃)₄ (10 mol%), and KF (2.5 eq) were placed in a microwave reactor vial and the mixture was purged with argon. The mixture was dissolved in MeOH/dioxane, 4:1 (~2.5 mL per 0.15 mmol of aryl halide) and purged again with argon. The reaction mixture was stirred thermally at 120°C for at least 2h. The reaction mixture was cooled down, filtered through celite, and concentrated to dryness under vacuum. Crude product was purified either by silica gel column chromatography using a solvent gradient of 5% to 100% EtOAc in hexanes and then from 0% to 20% MeOH in EtOAc. Typical isolated yield was 50% to quantitative.

Method B. General Protocols for the Synthesis of Pyrimidinol Carboxylic Acids **3.17** (based on previous protocols with some modifications)^{3, 16}

Method B.1. Preparation of the amidoxime (3.19)

A 1.0 M solution of hydroxylamine hydrochloride in MeOH (2.0 eq) and a 1.0 M solution of KOH in MeOH (2.0 eq) were combined at 0°C and stirred for ~30 min (slowly warming from 0°C to rt). The potassium chloride salt formed was removed by filtration. The filtrate was added to the nitrile (1.0 eq; the corresponding nitrile was either purchased from commercial source or synthesized using established methods) and the mixture was heated at 60°C for 17-24 h. MeOH was removed *in vacuo* and the residue was diluted with EtOAc, washed with brine, and the organic layer was concentrated. The product (typically obtained in quantitative yield and >90% purity) was used in the next step without further purification.

Method B.2. Preparation of the pyrimidinone ester (3.23)

The amidoxime **3.19** (1.0 eq) in CHCl₃ (1.3 mL per 1.0 mmol **3.19**) was added dropwise with dimethylacetylene dicarboxylate (DMAD; 1.1 eq) and heated at 60°C for 1-2 h. Chloroform was removed *in vacuo* and the crude residue (Michael adduct) was either purified by silica-gel column chromatography (gradient 5% to 50% EtOAc in hexanes) or used immediately in the next step. Michael adduct **3.20** was typically obtained as a mixture of E/Z isomers (isolated yield was typically ≥ 70%). Alternatively, the suspension of amidoxime **3.19** (1.0 eq) and MeOH (4.0 mL per 1.0 mmol of **3.19**) was cooled to -10°C then added dropwise with DMAD (1.1 eq). The resulting mixture was slowly warmed to rt and the stirring was continued for ~16 h; monitored by TLC. MeOH was removed *in vacuo*, and the crude Michael adduct was purified by silica-gel column chromatography as described above.

Michael adduct **3.20** was added with *o*-xylenes (2.5 mL per 1.0 mmol **3.20**) and the mixture was heated to 130°-135°C for 4-12h to complete the reaction, and then cooled. Methyl *tert*-butyl ether (MTBE) and MeOH, ratio of 9:1 (5.0 mL) was added at rt (with stirring) and the resulting slurry was cooled in the fridge or ice-bath for at least 30 min. The residue was collected *via* filtration (washed several times with MTBE:MeOH, 9:1), and then dried under vacuum. Isolated yield was typically between 20%-45%. Product was further purified by trituration, as necessary.

Method B.3. Ester hydrolysis to give final inhibitors 3.17

Pyrimidinone carboxylate ester **3.23** (1.0 eq) and LiOH (3.0-10.0 eq) in MeOH/THF/H₂O (2:2:1; ~8.0 mL per 0.1 mmol **3.23**) was stirred at 50°-60°C for 4-12 h. The mixture was concentrated *in vacuo*, and then acidified (to about pH 2 – 3) by addition of either 1N or 6N HCl. The precipitate was filtered off and dried under vacuum (typical isolated yield was ~50% to quantitative). A portion of the final product was purified by reversed-phase prep chromatography.

Method C. Preparation of Adenine-based Compounds (3.31)

Method C.1. Synthesis of adenine-containing nitriles (3.18-1 and 3.18-2)

Prepared based on a literature procedure with slight modifications.²⁶ In summary, adenine (1.0 eq) was added to a suspension of NaH (1.0 eq) in dry DMF (~4.0 mL per 1.0 mmol adenine) under Ar. The mixture was heated at 80°C for ~10 min then slowly cooled to rt. The solution of the appropriate cyanobromide (1.0 eq; bromoacetonitrile or 3-bromopropionitrile) in DMF (1.0 mL) was then added at rt and the reaction was heated at 60°C for 16 h under an Ar balloon. The mixture was then cooled to rt, concentrated under reduced pressure (DMF was removed by co-evaporation with H₂O/MeOH at 50°C). The resulting residue was collected *via* filtration (washed with H₂O

several times, dried *in vacuo*, and finally, washed with 30% EtOAc/hexanes). Product was used in the next step without further purification. Typical yield was 80% to quantitative.

Method C.2. Synthesis of analogs of 3.29

The amidoxime **3.26** was prepared using *Method B.1*. The Michael adduct **3.27** was prepared as follows: amidoxime **3.26** (1.0 eq) in DMSO (3.0 mL per 1.0 mmol **3.26**) was added with Et₃N (0.1 eq to 1.0 eq; Note: 0.1 eq was used for **3.26b** and up to 1.0 eq for **3.26a**). The resulting mixture was then added dropwise with DMAD (1.1 eq). Reaction was stirred at rt for ~4-12 h. The mixture was diluted with H₂O and then extracted with EtOAc. The organic layer was collected and the aqueous layer was further extracted with EtOAc/*n*-butanol (1:1). The organic layers were combined, washed with semi-brine then dried *in vacuo*. Crude product was purified by silica gel chromatography (gradient of 50% EtOAc in hexanes to 100% EtOAc, then to 20% MeOH in EtOAc). Michael adduct **3.27** was isolated as dark brown oil in ~50% yield (for **3.27a**, based on recovered starting material) to ~80% yield (for **3.27b**) and was used immediately in the next step.

An oven-dried vial was added with **3.27** (1.0 eq) and CuBr (50 mol %).¹⁹ Air was removed by vacuum and the vial was purged with Ar. Dry dioxane (1.0 mL per 0.1 mmol **3.27**) was added and the vial was evacuated again and purged with Ar. The mixture was sonicated for ~30 seconds and then stirred at 130°C for 30 min under Ar. The reaction mixture was cooled to rt and then diluted with 1:1 MeOH:H₂O. CuBr was removed *via* filtration. The filtrate was collected, concentrated, and the remaining H₂O was removed using a lyophilizer. Crude product (**3.29**) was purified by reversed phase chromatography; isolated yield was ~30%.

Ester hydrolysis of **3.29** to give **3.31** was performed following *Method B.3* except that the final compound was purified by trituration.

Method D. General Protocol for the Synthesis of 4-chloropyridopyrimidine **3.35**

Chlorination was done using a slightly modified procedure described by Sun *et. al.*²⁷ Pyridopyrimidinone **3.34** (1.0 eq), dry toluene (~1.0 mL per 1.0 mmol **3.34**), and pyridine (1.0 eq) were mixed in the pressure vessel. POCl₃ (5.0 eq) was added with stirring. The tube was then sealed and heated at 115°-180°C for ~2h (Note: 115°C was used for **3.34c** while 180°C for **3.34a** and **3.34b**). The reaction was cooled, concentrated *in vacuo*, diluted with EtOAc, and washed with cold NaHCO₃ solution, dried over Na₂SO₄ and concentrated *in vacuo*. The crude product was purified by silica gel chromatography (24g column, 2%-85% EtOAc in hexanes with 0.1% Et₃N) and used immediately in the next step. Typical yield was ~30%-65%.

Method E. General Protocol for the Preparation of Pyridopyrimidine-based Compounds **3.38**

Amine **3.36** (1.1 to 1.3 eq) and Et₃N (3.0 eq) were dissolved in dry DMSO (~2.0 mL per 0.15 mmol **3.36**) and stirred at rt for 5 min. The aryl chloride **3.35** (1.0 eq; dissolved in 1.0 mL dry dioxane) was then added and the mixture was heated at 100°C for 1h (under Ar balloon). The reaction was cooled to rt, concentrated *in vacuo*, added with H₂O (to crash out the product), and then filtered. Crude product **3.37** was purified by trituration. Typical isolated yield was ~50%-70%. When R₆ of **3.37** = Br, Suzuki cross-coupling to introduce several aryl groups at the said position was performed using **Method A** (Note: the product was purified by trituration, not by silica-gel chromatography).

Ester hydrolysis to give **3.38** was done using **Method B.3**. Final compounds were converted first to their corresponding monosodium salt prior to purification by reversed-phase prep chromatography.

Synthesis of Key Compounds and Intermediates

Pyrido[2,3-d]pyrimidin-4(3H)-one (**3.34a**, R₆ = R₇ = H). Prepared *via* reaction of 2-aminonicotinic acid (1.0 eq) with formamide (50.0 eq) at 145°C for 20 h.²⁸ Isolated as a beige solid (1.6g, 58%). ¹H NMR (500 MHz, DMSO-d₆) δ 12.55 (br_s, 1H), 8.95 (dd, *J* = 4.5, 2.0 Hz, 1H), 8.51 (dd, *J* = 7.9, 2.0 Hz, 1H), 8.32 (s, 1H), 7.55 (dd, *J* = 7.9, 4.6 Hz, 1H). ¹³C NMR (126 MHz, DMSO-d₆) δ 162.1, 159.1, 156.2, 149.2, 136.1, 123.0, 118.3. MS [ESI⁺] *m/z*: 148.0 [M + H⁺]⁺

6-bromopyrido[2,3-d]pyrimidin-4(3H)-one (**3.34b**, R₆ = Br, R₇ = H). Prepared in two ways: (1) reaction of 2-amino-5-bromonicotinic acid (1.0 eq) with formamide (50.0 eq) at 145°C for 20h (yield of 667 mg, 68%, beige solid) using a slightly modified protocol reported by Zhang *et.al.*²⁸; or (2) treatment of 6-bromopyrido[2,3-d]pyrimidin-4-amine²⁰ with methane sulfonic acid/H₂O²⁹ at 100°C (yield of 18.2 mg, 60%). ¹H NMR (500 MHz, DMSO-d₆) δ 12.74 (br_s, 1H), 9.05 (d, *J* = 2.6 Hz, 1H), 8.63 (d, *J* = 2.6 Hz, 1H), 8.36 (s, 1H).

6-bromo-7-(methylthio)pyrido[2,3-d]pyrimidin-4(3H)-one (**3.34c**, R₆ = Br, R₇ = SMe). Prepared by treatment of 6-bromo-7-(methylthio)pyrido[2,3-d]pyrimidin-4-amine²⁰ with methane sulfonic acid/H₂O²⁹ at 100°C. Isolated as a yellow solid. ¹H NMR (400 MHz, DMSO-d₆) δ 12.65 (br_s, 1H), 8.44 (s, 1H), 8.32 (s, 1H), 2.61 (s, 3H). ¹³C NMR (126 MHz, DMSO-d₆) δ 166.4, 160.9, 157.8, 150.0, 137.3, 116.1, 115.5, 14.9.

4-chloropyrido[2,3-d]pyrimidine (**3.35a**, R₆ = R₇ = H). Prepared *via* **Method D**. Isolated as a light yellow solid. ¹H NMR (500 MHz, CDCl₃) δ 9.33 (dd, *J* = 4.3, 1.9 Hz, 1H), 9.27 (s, 1H), 8.65 (dd, *J* = 8.3, 1.9 Hz, 1H), 7.72 (dd, *J* = 8.3, 4.3 Hz, 1H). ¹³C NMR (126 MHz, CDCl₃) δ 163.3, 158.8, 158.8, 157.1, 135.3, 124.6, 119.5. MS [ESI⁺] *m/z*: 166.0 [M + H⁺]⁺

6-bromo-4-chloropyrido[2,3-d]pyrimidine (**3.35b**, R₆ = Br, R₇ = H). Prepared *via* **Method D**. Isolated as a light yellow solid. ¹H NMR (400 MHz, CDCl₃) δ 9.32 (d, *J* = 2.5 Hz, 1H), 9.30 (s, 1H), 8.78 (d, *J* = 2.5 Hz, 1H).

6-bromo-4-chloro-7-(methylthio)pyrido[2,3-d]pyrimidine (**3.35c**, R₆ = Br, R₇ = SMe). Prepared *via* **Method D**. Isolated as a yellow solid. ¹H NMR (500 MHz, CDCl₃) δ 9.15 (s, 1H), 8.53 (s, 1H), 2.77 (s, 3H). ¹³C NMR (126 MHz, CDCl₃) δ 172.2, 161.3, 157.4, 157.1, 135.2, 120.3, 117.4, 15.6.

2-(6-amino-9H-purin-9-yl)acetonitrile (**3.18-1**, R = adeninyl). Prepared following **Method C.1** using adenine and bromoacetonitrile. Isolated as a light brown solid. ¹H NMR (500 MHz, DMSO-d₆) δ 8.22 (s, 1H), 8.21 (s, 1H), 7.40 (br_s, 2H), 5.44 (s, 2H). ¹³C NMR (126 MHz, DMSO-d₆) δ 156.6, 153.6, 149.6, 140.6, 118.8, 116.2, 31.4.

3-(6-amino-9H-purin-9-yl)propanenitrile (**3.18-2**, R = adeninyl). Prepared following **Method C.1** using adenine and 3-bromopropionitrile. Isolated as a light yellow solid. ¹H NMR (400 MHz, DMSO-d₆) δ 8.20 (s, 1H), 8.17 (s, 1H), 7.28 (br_s, 2H), 4.45 (t, *J* = 6.5 Hz, 2H), 3.17 (t, *J* = 6.5 Hz, 2H). ¹³C NMR (126 MHz, DMSO-d₆) δ 156.5, 153.1, 149.9, 141.0, 119.2, 118.8, 39.3, 18.6. MS [ESI⁺] *m/z*: 189.1 [M + H⁺]⁺

Synthesis of amine **3.36**:

CBz-protected intermediate **3.23m** was prepared from *N*-(Benzyloxycarbonyl)-2-aminoacetonitrile following the sequence of steps described for **Method B**. Amidoxime: Benzyl-(2-amino-2-(hydroxyimino)ethyl)carbamate (**3.19m**, R = CBzNHCH₂-) was isolated as a white solid. ¹H NMR (500 MHz, DMSO-d₆) δ 9.03 (s, 1H), 7.45 (t, *J* = 5.9 Hz, 1H), 7.40 – 7.26 (m, 5H), 5.29 (br_s, 2H), 5.03 (s, 2H), 3.59 (d, *J* = 6.1 Hz, 2H). ¹³C NMR (126 MHz, DMSO-d₆) δ 157.0,

150.8, 137.5, 128.8, 128.3, 128.2, 65.9, 41.2 MS [ESI⁺] m/z: 224.1 [M + H⁺]⁺ Pyrimidinone Ester:
Methyl 2-(((benzyloxy)carbonyl)amino)methyl)-5,6-dihydroxypyrimidine-4-carboxylate
(**3.23m**, R = CBzNHCH₂-) was isolated as a beige solid. ¹H NMR (400 MHz, DMSO-d₆) δ 12.73
(s, 1H), 10.32 (s, 1H), 7.65 (t, *J* = 5.8 Hz, 1H), 7.41 – 7.22 (m, 5H), 5.05 (s, 2H), 4.05 (d, *J* = 5.9
Hz, 2H), 3.81 (s, 3H). MS [ESI⁺] m/z: 334.1 [M + H⁺]⁺

Methyl 2-(aminomethyl)-5,6-dihydroxypyrimidine-4-carboxylate (**3.36**). Prepared *via*
hydrogenolysis of **3.23m**. In summary, a mixture of **3.23m** (1.0g, 3.0 mmol), 6 N HCl (0.50 mL;
3.0 mmol), and 10% Pd/C (200 mg) in MeOH (60.0 mL) was hydrogenated. Once complete, the
reaction mixture was filtered through celite, then washed with additional MeOH (~50 mL). The
combined filtrate was concentrated and dried under vacuum to afford product as its HCl salt (peach
solid; 540.0 mg, 76%). ¹H NMR (500 MHz, DMSO-d₆) δ 13.26 (br_s, 1H), 10.53 (br_s, 1H), 8.55
(br_s, 3H (-NH₂•HCl)), 3.95 (s, 2H), 3.83 (s, 3H). ¹³C NMR (126 MHz, DMSO-d₆) δ 165.9, 158.9,
146.0, 144.4, 128.8, 52.7, 39.6. -CH₂NH₂ was observed by HSQC (¹H-¹³C): ¹H δ 3.95 correlates
to ¹³C δ 39.6. MS [ESI⁺] m/z: 200.1 [M + H⁺]⁺

Final Inhibitors:

Inhibitors **3.3**, **3.7**, **3.9**, and **3.17a** to **3.17l** were synthesized following the sequence of steps
described for **Method B**. NMR data for compounds **3.3**, **3.7**, **3.9**, and **3.17** (**e**, **f**, **h**, **j**) agree with
previous reports:^{1, 6, 7, 30}

Inhibitor 3.3:

Amidoxime: *N*'-hydroxythiophene-2-carboximidamide (**3.19-1**, R = 2-thiophenyl) was isolated as
a light yellow oil and used directly in the next step.

Pyrimidinone Ester: Methyl 5,6-dihydroxy-2-(thiophen-2-yl)pyrimidine-4-carboxylate (**3.23-1**, R = 2-thiophenyl) was isolated as a peach solid. ¹H NMR (500 MHz, DMSO-d₆) δ 13.21 (br_s, 1H), 10.50 (br_s, 1H), 7.99 (d, *J* = 3.3 Hz, 1H), 7.76 (dd, *J* = 5.0, 0.9 Hz, 1H), 7.17 (dd, *J* = 5.0, 3.8 Hz, 1H), 3.84 (s, 3H). MS [ESI⁺] *m/z*: 253.1 [M + H⁺]⁺

Final Inhibitor: 5,6-dihydroxy-2-(thiophen-2-yl)pyrimidine-4-carboxylic acid (**3.3**).⁴ Isolated as cream solid. ¹H NMR (500 MHz, DMSO-d₆) δ 13.08 (br_s, 1H), 7.99 (dd, *J* = 3.8, 0.9 Hz, 1H), 7.76 (dd, *J* = 5.0, 0.9 Hz, 1H), 7.16 (dd, *J* = 5.0, 3.8 Hz, 1H). MS [ESI⁻] *m/z*: 237.0 [M - H⁺]⁻

Inhibitor 3.7:

Amidoxime: *N*'-hydroxybenzimidamide (**3.19-2**, R = phenyl) was isolated as a yellow oil. ¹H NMR (500 MHz, DMSO-d₆) δ 9.61 (s, 1H), 7.69 – 7.64 (m, 2H), 7.39 – 7.35 (m, 3H), 5.78 (br_s, 2H). MS [ESI⁺] *m/z*: 137.1 [M + H⁺]⁺

Pyrimidinone Ester: Methyl 5,6-dihydroxy-2-phenylpyrimidine-4-carboxylate (**3.23-2**, R = phenyl) was isolated as a light orange solid. ¹H NMR (400 MHz, DMSO-d₆) δ 8.02 - 7.99 (m, 2H), 7.53 – 7.47 (m, 3H), 3.85 (s, 3H). MS [ESI⁺] *m/z*: 247.1 [M + H⁺]⁺

Final Inhibitor: 5,6-dihydroxy-2-phenylpyrimidine-4-carboxylic acid (**3.7**).^{1, 7} Isolated as a light peach solid. ¹H NMR (400 MHz, DMSO-d₆) δ 8.04 (d, *J* = 8.0, 2H), 7.56 – 7.45 (m, 3H). MS [ESI⁻] *m/z*: 231.1 [M - H⁺]⁻

Inhibitor 3.9:

Amidoxime: 4-chloro-*N*'-hydroxybenzimidamide (**3.19-3**, R = 4-chlorophenyl) was isolated as a white solid. ¹H NMR (500 MHz, DMSO-d₆) δ 9.72 (s, 1H), 7.70 – 7.66 (m, 2H), 7.45 – 7.41 (m, 2H), 5.86 (br_s, 2H). MS [ESI⁺] *m/z*: 171.3 [M + H⁺]⁺

Pyrimidinone Ester: Methyl 2-(4-chlorophenyl)-5,6-dihydroxypyrimidine-4-carboxylate (**3.23-3**, R = 4-chlorophenyl) was isolated as orange solid. ^1H NMR (500 MHz, DMSO- d_6) δ 8.03 (d, J = 8.7 Hz, 2H), 7.57 (d, J = 8.8 Hz, 2H), 3.85 (s, 3H). MS [ESI $^+$] m/z : 281.1 [M + H $^+$] $^+$

Final Inhibitor: 2-(4-chlorophenyl)-5,6-dihydroxypyrimidine-4-carboxylic acid (**3.9**).¹ Isolated as off-white solid. ^1H NMR (500 MHz, DMSO- d_6) δ 8.07 (d, J = 8.7 Hz, 1H), 7.56 (d, J = 8.7 Hz, 1H). ^{13}C NMR (126 MHz, DMSO- d_6) δ 169.0, 159.3, 148.3, 144.4, 135.4, 131.1, 129.0, 128.6, 128.2. HRMS [ESI $^-$] calculated for C $_{11}$ H $_6$ ClN $_2$ O $_4$ m/z , 265.00216; found 265.00220 [M - H $^+$] $^-$

Inhibitor 3.17a:

Amidoxime: 2-(4-chlorophenyl)- N' -hydroxyacetimidamide (**3.19a**, R = 4-chlorobenzyl) was isolated as off-white solid. ^1H NMR (500 MHz, DMSO- d_6) δ 8.90 (s, 1H), 7.35 – 7.31 (m, 2H), 7.30 – 7.26 (m, 2H), 5.42 (s, 2H), 3.25 (s, 2H). MS [ESI $^+$] m/z : 185.5 [M + H $^+$] $^+$

Pyrimidinone Ester: Methyl 2-(4-chlorobenzyl)-5,6-dihydroxypyrimidine-4-carboxylate (**3.23a**, R = 4-chlorobenzyl) was isolated as a light brown solid. ^1H NMR (500 MHz, DMSO- d_6) δ 12.92 (s, 1H), 10.24 (s, 1H), 7.38 (d, J = 8.5 Hz, 2H), 7.30 (d, J = 8.5 Hz, 2H), 3.81 (s, 2H), 3.79 (s, 3H). MS [ESI $^+$] m/z : 295.0 [M + H $^+$] $^+$

Final Inhibitor: 2-(4-chlorobenzyl)-5,6-dihydroxypyrimidine-4-carboxylic acid (**3.17a**). Isolated as a white solid. ^1H NMR (500 MHz, DMSO- d_6) δ 7.40 (d, J = 8.5 Hz, 2H), 7.35 (d, J = 8.5 Hz, 2H), 3.92 (s, 2H). ^{13}C NMR (101 MHz, DMSO- d_6) δ 168.0, 159.5, 151.1, 149.5, 135.1, 132.3, 131.1, 129.0, 124.2, 37.8. HRMS [ESI $^-$] calculated for C $_{12}$ H $_8$ ClN $_2$ O $_4$ m/z , 279.01781; found 279.01776 [M - H $^+$] $^-$

Inhibitor 3.17b:

Amidoxime: 4-bromo-*N'*-hydroxybenzimidamide (**3.19b**, R = 4-bromophenyl) was isolated as off-white solid. ¹H NMR (500 MHz, DMSO-d₆) δ 9.72 (s, 1H), 7.64 – 7.59 (m, 2H), 7.59 – 7.55 (m, 2H), 5.85 (br_s, 2H). MS [ESI⁺] m/z: 215.3 [M + H⁺]⁺

Pyrimidinone Ester: Methyl 2-(4-bromophenyl)-5,6-dihydroxypyrimidine-4-carboxylate (**3.23b**, 4-bromophenyl) was isolated as a light orange solid. ¹H NMR (400 MHz, DMSO-d₆) δ 7.95 (d, *J* = 8.7 Hz, 2H), 7.71 (d, *J* = 8.7 Hz, 2H), 3.85 (s, 3H). MS [ESI⁺] m/z: 325.0 [M + H⁺]⁺

Final Inhibitor: 2-(4-bromophenyl)-5,6-dihydroxypyrimidine-4-carboxylic acid (**3.17b**).³⁰ Isolated as off-white solid. ¹H NMR (400 MHz, DMSO-d₆) δ 8.00 (d, *J* = 8.7 Hz, 1H), 7.71 (d, *J* = 8.7 Hz, 1H). ¹³C NMR (101 MHz, DMSO-d₆) δ 169.1, 159.5, 149.1, 144.0, 131.5, 131.5, 129.1, 128.3, 124.2. HRMS [ESI⁻] calculated for C₁₁H₆BrN₂O₄ m/z, 308.95164; found 308.95184 [M - H⁺]⁻

Inhibitor 3.17c:

Amidoxime: *N'*-hydroxy-4-methylbenzimidamide (**3.19c**, R = *p*-tolyl) was isolated as a white solid. ¹H NMR (500 MHz, DMSO-d₆) δ 9.51 (s, 1H), 7.56 (d, *J* = 8.2 Hz, 2H), 7.17 (d, *J* = 7.9 Hz, 2H), 5.72 (br_s, 2H), 2.31 (s, 3H). MS [ESI⁺] m/z: 151.1 [M + H⁺]⁺

Pyrimidinone Ester: Methyl 5,6-dihydroxy-2-(*p*-tolyl)pyrimidine-4-carboxylate (**3.23c**, R = *p*-tolyl) was isolated as a light orange solid. ¹H NMR (500 MHz, DMSO-d₆) δ 7.91 (d, *J* = 8.3 Hz, 2H), 7.30 (d, *J* = 8.0 Hz, 2H), 3.85 (s, 3H), 2.36 (s, 3H). MS [ESI⁺] m/z: 261.1 [M + H⁺]⁺

Final Inhibitor: 5,6-dihydroxy-2-(*p*-tolyl)pyrimidine-4-carboxylic acid (**3.17c**).³⁰ Isolated as off-white solid. ¹H NMR (400 MHz, DMSO-d₆) δ 7.95 (d, *J* = 8.3 Hz, 2H), 7.30 (d, *J* = 8.0 Hz, 2H), 2.36 (s, 3H). ¹³C NMR (101 MHz, DMSO-d₆) δ 169.2, 159.4, 148.2, 145.4, 140.5, 129.4, 129.0,

128.2, 127.1, 20.9. HRMS [ESI⁻] calculated for C₁₂H₉N₂O₄ *m/z*, 245.05678; found 245.05642 [M - H⁺]⁻

Inhibitor 3.17d:

Amidoxime: *N*'-hydroxy-4-isopropylbenzimidamide (**3.19d**, R = 4-isopropylphenyl) was isolated as a yellow oil that solidified upon standing at rt. ¹H NMR (500 MHz, DMSO-d₆) δ 9.53 (s, 1H), 7.59 (d, *J* = 8.4 Hz, 2H), 7.24 (d, *J* = 8.2 Hz, 2H), 5.73 (br_s, 2H), 2.94 – 2.85 (m, 1H), 1.21 (d, *J* = 6.9 Hz, 6H). MS [ESI⁺] *m/z*: 179.1 [M + H⁺]⁺

Pyrimidinone Ester: Methyl 5,6-dihydroxy-2-(4-isopropylphenyl)pyrimidine-4-carboxylate (**3.23d**, R = 4-isopropylphenyl) was isolated as a light peach solid. ¹H NMR (500 MHz, DMSO-d₆) δ 13.02 (br_s, 1H), 10.44 (br_s, 1H), 7.93 (d, *J* = 8.4 Hz, 2H), 7.37 (d, *J* = 8.3 Hz, 2H), 3.85 (s, 3H), 3.00 – 2.90 (m, 1H), 1.22 (d, *J* = 6.9 Hz, 6H). ¹³C NMR (126 MHz, DMSO-d₆) δ 166.0, 159.5, 151.4, 146.1, 145.0, 129.7, 129.1, 127.2, 126.5, 52.2, 33.3, 23.6. MS [ESI⁺] *m/z*: 289.1 [M + H⁺]⁺

Final Inhibitor: 5,6-dihydroxy-2-(4-isopropylphenyl)pyrimidine-4-carboxylic acid (**3.17d**). Isolated as light peach solid. ¹H NMR (400 MHz, DMSO) δ 7.96 (d, *J* = 8.3 Hz, 2H), 7.35 (d, *J* = 8.3 Hz, 2H), 2.94 (hept, *J* = 6.8 Hz, 1H), 1.22 (d, *J* = 6.9 Hz, 6H). ¹³C NMR (101 MHz, DMSO-d₆) δ 169.2, 159.4, 151.2, 148.3, 145.3, 129.8, 128.3, 127.2, 126.4, 33.3, 23.6. HRMS [ESI⁻] calculated for C₁₄H₁₃N₂O₄ *m/z*, 273.08808; found 273.08809 [M - H⁺]⁻

Inhibitor 3.17e:

Amidoxime: 3-chloro-*N*'-hydroxybenzimidamide (**3.19e**, R = 3-chlorophenyl) was isolated as off-white solid. ¹H NMR (500 MHz, DMSO-d₆) δ 9.78 (s, 1H), 7.70 (t, *J* = 1.7 Hz, 1H), 7.65 - 7.63 (m, 1H), 7.44 - 7.38 (m, 2H), 5.89 (br_s, 2H). MS [ESI⁺] *m/z*: 171.3 [M + H⁺]⁺

Pyrimidinone Ester: Methyl 2-(3-chlorophenyl)-5,6-dihydroxypyrimidine-4-carboxylate (**3.23e**, R = 3-chlorophenyl) was isolated as a light orange solid. ¹H NMR (500 MHz, DMSO-d₆) δ 13.10 (br_s, 1H), 10.63 (br_s, 1H), 8.06 (t, *J* = 1.8 Hz, 1H), 8.00 – 7.95 (m, 1H), 7.60 - 7.58 (m, 1H), 7.53 (t, *J* = 7.9 Hz, 1H), 3.86 (s, 3H). MS [ESI⁺] *m/z*: 281.1 [M + H⁺]⁺

Final Inhibitor: 2-(3-chlorophenyl)-5,6-dihydroxypyrimidine-4-carboxylic acid (**3.17e**).³⁰ Isolated as off-white solid. ¹H NMR (500 MHz, DMSO-d₆) δ 8.14 (t, *J* = 1.7 Hz, 1H), 8.02 (d, *J* = 7.8 Hz, 1H), 7.57 (ddd, *J* = 7.9, 1.8, 0.9 Hz, 1H), 7.52 (t, *J* = 7.9 Hz, 1H). ¹³C NMR (126 MHz, DMSO-d₆) δ 169.0, 159.2, 148.5, 144.0, 134.2, 133.4, 130.4, 130.3, 128.1, 127.0, 125.7. HRMS [ESI⁻] calculated for C₁₁H₆ClN₂O₄ *m/z*, 265.00216; found 265.00224 [M - H⁺]⁻

Inhibitor 3.17f:

Amidoxime: 3-bromo-*N*'-hydroxybenzimidamide (**3.19f**, R = 3-bromophenyl) was isolated as a white solid. ¹H NMR (500 MHz, DMSO-d₆) δ 9.78 (s, 1H), 7.84 (t, *J* = 1.8 Hz, 1H), 7.70 – 7.67 (m, 1H), 7.57 - 7.55 (m, 1H), 7.34 (t, *J* = 7.9 Hz, 1H), 5.89 (br_s, 2H). MS [ESI⁺] *m/z*: 215.3 [M + H⁺]⁺

Pyrimidinone Ester: Methyl 2-(3-bromophenyl)-5,6-dihydroxypyrimidine-4-carboxylate (**3.23f**, R = 3-bromophenyl). Isolated as a light orange solid. ¹H NMR (500 MHz, DMSO-d₆) δ 8.20 (t, *J* = 1.7 Hz, 1H), 8.01 (d, *J* = 8.0 Hz, 1H), 7.72 (dd, *J* = 8.0, 1.1 Hz, 1H), 7.47 (t, *J* = 7.9 Hz, 1H), 3.86 (s, 3H). MS [ESI⁺] *m/z*: 325.0 [M + H⁺]⁺

Final Inhibitor: 2-(3-bromophenyl)-5,6-dihydroxypyrimidine-4-carboxylic acid (**3.17f**). Isolated as off-white solid. ¹H NMR (500 MHz, DMSO-d₆) δ 8.28 (t, *J* = 1.7 Hz, 1H), 8.05 (d, *J* = 8.0 Hz, 1H), 7.70 (dd, *J* = 8.0, 1.1 Hz, 1H), 7.45 (t, *J* = 7.9 Hz, 1H). ¹³C NMR (126 MHz, DMSO-d₆) δ

169.0, 159.3, 148.8, 143.7, 134.4, 133.1, 130.6, 129.8, 128.1, 126.0, 121.8. HRMS [ESI⁻] calculated for C₁₁H₆BrN₂O₄ *m/z*, 308.95164; found 308.95182 [M - H⁺]⁻

Inhibitor 3.17g:

Amidoxime: *N*-hydroxy-3-methylbenzimidamide (**3.19g**, R = *m*-tolyl) was isolated as a yellow oil. ¹H NMR (500 MHz, DMSO-*d*₆) δ 9.55 (s, 1H), 7.49 (s, 1H), 7.45 (d, *J* = 7.7 Hz, 1H), 7.25 (t, *J* = 7.6 Hz, 1H), 7.18 (d, *J* = 7.5 Hz, 1H), 5.73 (s, 2H), 2.32 (s, 3H). MS [ESI⁺] *m/z*: 151.1 [M + H⁺]⁺

Pyrimidinone Ester: Methyl 5,6-dihydroxy-2-(*m*-tolyl)pyrimidine-4-carboxylate (**3.23g**, R = *m*-tolyl) was isolated as a light orange solid. ¹H NMR (400 MHz, DMSO-*d*₆) δ 13.00 (s, 1H), 10.50 (s, 1H), 7.84 (s, 1H), 7.79 (d, *J* = 7.6 Hz, 1H), 7.38 (t, *J* = 7.6 Hz, 1H), 7.33 (d, *J* = 7.6 Hz, 1H), 3.85 (s, 3H), 2.37 (s, 3H). ¹³C NMR (126 MHz, DMSO-*d*₆) δ 166.0, 159.5, 146.2, 145.2, 137.8, 132.0, 131.4, 129.0, 128.5, 127.6, 124.3, 52.3, 20.9. MS [ESI⁺] *m/z*: 261.1 [M + H⁺]⁺

Final Inhibitor: 5,6-dihydroxy-2-(*m*-tolyl)pyrimidine-4-carboxylic acid (**3.17g**).³⁰ Isolated as off-white solid. ¹H NMR (500 MHz, DMSO-*d*₆) δ 7.88 (s, 1H), 7.82 (d, *J* = 7.7 Hz, 1H), 7.37 (t, *J* = 7.6 Hz, 1H), 7.32 (d, *J* = 7.5 Hz, 1H), 2.37 (s, 3H). ¹³C NMR (126 MHz, DMSO-*d*₆) δ 169.1, 159.2, 147.9, 145.7, 137.8, 132.0, 131.3, 128.4, 128.2, 127.8, 124.3, 20.9. HRMS [ESI⁻] calculated for C₁₂H₉N₂O₄ *m/z*, 245.05678; found 245.05644 [M - H⁺]⁻

Inhibitor 3.17h:

Amidoxime: 3-chloro-*N*'-hydroxy-4-methylbenzimidamide (**3.19h**, R = 3-chloro-4-methylphenyl) was isolated as a white solid. ¹H NMR (400 MHz, DMSO-*d*₆) δ 9.68 (s, 1H), 7.67 (d, *J* = 1.6 Hz, 1H), 7.53 (dd, *J* = 8.0, 1.7 Hz, 1H), 7.33 (d, *J* = 8.0 Hz, 1H), 5.84 (br_s, 2H), 2.31 (s, 3H). MS [ESI⁺] *m/z*: 185.0 [M + H⁺]⁺

Pyrimidinone Ester: Methyl 2-(3-chloro-4-methylphenyl)-5,6-dihydroxypyrimidine-4-carboxylate (**3.23h**, R = 3-chloro-4-methylphenyl) was isolated as a light orange solid. ¹H NMR (500 MHz, DMSO-d₆) δ 8.06 (s, 1H), 7.89 (d, *J* = 9.1 Hz, 1H), 7.47 (d, *J* = 8.1 Hz, 1H), 3.86 (s, 3H), 2.38 (s, 3H). ¹³C NMR (126 MHz, DMSO-d₆) δ 165.8, 159.5, 145.6, 144.6, 138.3, 133.6, 131.5, 131.4, 128.8, 127.2, 125.6, 52.3, 19.5. MS [ESI⁺] *m/z*: 295.0 [M + H⁺]⁺

Final Inhibitor: 2-(3-chloro-4-methylphenyl)-5,6-dihydroxypyrimidine-4-carboxylic acid (**3.17h**). Isolated as white solid. ¹H NMR (400 MHz, DMSO-d₆) δ 8.13 (d, *J* = 1.6 Hz, 1H), 7.93 (dd, *J* = 8.0, 1.7 Hz, 1H), 7.46 (d, *J* = 8.1 Hz, 1H), 2.38 (s, 3H). ¹³C NMR (101 MHz, DMSO-d₆) δ 169.1, 159.6, 149.7, 143.1, 137.8, 133.5, 131.9, 131.2, 128.1, 127.2, 125.5, 19.5. HRMS [ESI⁻] calculated for C₁₂H₈ClN₂O₄ *m/z*, 279.01781; found 279.01786 [M - H⁺]⁻

Inhibitor 3.17i:

Amidoxime: 3-bromo-*N'*-hydroxy-4-methylbenzimidamide (**3.19i**, R = 3-bromo-4-methylphenyl) was isolated as a white solid. ¹H NMR (400 MHz, DMSO-d₆) δ 9.69 (s, 1H), 7.84 (d, *J* = 1.7 Hz, 1H), 7.57 (dd, *J* = 7.9, 1.7 Hz, 1H), 7.33 (d, *J* = 8.0 Hz, 1H), 5.86 (br_s, 2H), 2.32 (s, 3H). MS [ESI⁺] *m/z*: 228.99 [M + H⁺]⁺

Pyrimidinone Ester: Methyl 2-(3-bromo-4-methylphenyl)-5,6-dihydroxypyrimidine-4-carboxylate (**3.23i**, R = 3-bromo-4-methylphenyl) was isolated as light orange solid. ¹H NMR (500 MHz, DMSO-d₆) δ 8.23 (d, *J* = 1.7 Hz, 1H), 7.93 (dd, *J* = 8.0, 1.8 Hz, 1H), 7.47 (d, *J* = 8.1 Hz, 1H), 3.86 (s, 3H), 2.39 (s, 3H). ¹³C NMR (126 MHz, DMSO-d₆) δ 165.8, 159.5, 145.5, 144.5, 140.1, 131.6, 131.1, 130.4, 128.8, 126.2, 124.3, 52.3, 22.3. HRMS [ESI⁻] calculated for C₁₃H₁₀BrN₂O₄ *m/z*, 336.9829; found 336.9834 [M - H⁺]⁻

Final Inhibitor: 2-(3-bromo-4-methylphenyl)-5,6-dihydroxypyrimidine-4-carboxylic acid (**3.17i**). Isolated as white solid. ^1H NMR (400 MHz, DMSO- d_6) δ 8.31 (d, $J = 1.7$ Hz, 1H), 7.97 (dd, $J = 8.0, 1.8$ Hz, 1H), 7.46 (d, $J = 8.2$ Hz, 1H), 2.39 (s, 3H). ^{13}C NMR (101 MHz, DMSO- d_6) δ 169.0, 159.3, 148.5, 143.8, 139.9, 131.7, 131.1, 130.5, 128.1, 126.2, 124.3, 22.3. HRMS [ESI $^+$] calculated for $\text{C}_{12}\text{H}_{10}\text{BrN}_2\text{O}_4$ m/z , 324.9818 found 324.9820 [$\text{M} + \text{H}^+$] $^+$

Inhibitor 3.17j:

The nitrile, 4-(3,5-dimethylisoxazol-4-yl)benzotrile (**3.18j**, R = 4-(3,5-dimethylisoxazol-4-yl)phenyl)³¹ was prepared *via* Suzuki cross-coupling between (3,5-dimethylisoxazol-4-yl)boronic acid and 4-bromobenzotrile based on the method as previously described.³² The corresponding amidoxime, 4-(3,5-dimethylisoxazol-4-yl)-*N'*-hydroxybenzimidamide (**3.19j**, R = 4-(3,5-dimethylisoxazol-4-yl)phenyl) was then made (isolated as a white solid) and used directly in the next step.

Pyrimidinone Ester: Methyl 2-(4-(3,5-dimethylisoxazol-4-yl)phenyl)-5,6-dihydroxypyrimidine-4-carboxylate (**3.23j**, R = 4-(3,5-dimethylisoxazol-4-yl)phenyl) was isolated as orange solid. ^1H NMR (400 MHz, DMSO- d_6) δ 8.11 (d, $J = 8.3$ Hz, 2H), 7.53 (d, $J = 8.3$ Hz, 2H), 3.86 (s, 3H), 2.44 (s, 3H), 2.26 (s, 3H).

Final Inhibitor: 2-(4-(3,5-dimethylisoxazol-4-yl)phenyl)-5,6-dihydroxypyrimidine-4-carboxylic acid (**3.17j**). Isolated as a white solid. ^1H NMR (400 MHz, DMSO- d_6) δ 8.13 (d, $J = 8.3$ Hz, 2H), 7.51 (d, $J = 8.3$ Hz, 2H), 2.44 (s, 3H), 2.26 (s, 3H). HRMS [ESI $^-$] calculated for $\text{C}_{16}\text{H}_{12}\text{N}_3\text{O}_5$ m/z , 326.0782; found 326.0783 [$\text{M} - \text{H}^+$] $^-$

Inhibitor 3.17k:

The nitrile, 3',4'-difluoro-[1,1'-biphenyl]-3-carbonitrile (**3.18k**, R = 3',4'-difluoro-[1,1'-biphenyl]-3-yl) was prepared from 3-bromobenzonitrile and 3,4-difluorophenyl boronic acid as Suzuki cross-coupling partners based on the previously described method.³² ¹H NMR (400 MHz, CDCl₃) δ 7.80 (s, 1H), 7.75 (d, *J* = 7.9 Hz, 1H), 7.66 (d, *J* = 7.7 Hz, 1H), 7.56 (t, *J* = 7.8 Hz, 1H), 7.41 – 7.32 (m, 1H), 7.29 - 7.27 (m, 2H). MS [ESI⁺] *m/z*: 216.1 [M + H⁺]⁺ The corresponding amidoxime, 3',4'-difluoro-*N'*-hydroxy-[1,1'-biphenyl]-3-carboximidamide (**3.19k**, R = 3',4'-difluoro-[1,1'-biphenyl]-3-yl) was then made (isolated as off-white solid) and used directly in the next step.

Pyrimidinone Ester: Methyl 2-(3',4'-difluoro-[1,1'-biphenyl]-3-yl)-5,6-dihydroxypyrimidine-4-carboxylate (**3.23k**, R = 3',4'-difluoro-[1,1'-biphenyl]-3-yl) was isolated as a peach solid. ¹H NMR (400 MHz, DMSO-*d*₆) δ 8.29 (s, 1H), 8.04 (d, *J* = 8.0 Hz, 1H), 7.96 - 7.94 (m, 1H), 7.86 (d, *J* = 7.6 Hz, 1H), 7.69 - 7.67 (m, 1H), 7.63 – 7.57 (m, 2H), 3.86 (s, 3H). MS [ESI⁺] *m/z*: 359.1 [M + H⁺]⁺

Final Inhibitor: 2-(3',4'-difluoro-[1,1'-biphenyl]-3-yl)-5,6-dihydroxypyrimidine-4-carboxylic acid (**3.17k**). Isolated as a white solid. ¹H NMR (500 MHz, DMSO-*d*₆) δ 8.31 (s, 1H), 8.09 (d, *J* = 7.9 Hz, 1H), 7.97 - 7.92 (m, 1H), 7.83 (d, *J* = 8.0 Hz, 1H), 7.70 - 7.68 (m, 1H), 7.61 – 7.56 (m, 2H). HRMS [ESI⁻] calculated for C₁₇H₉F₂N₂O₄ *m/z*, 343.0536; found 343.0531 [M - H⁺]⁻

Inhibitor 3.17l:

Amidoxime: *N'*-hydroxy-3,5-bis(trifluoromethyl)benzimidamide (**3.19l**, R = 3,5-bis(trifluoromethyl)phenyl) was isolated as off-white solid. ¹H NMR (500 MHz, DMSO-*d*₆) δ 10.10 (s, 1H), 8.32 (s, 2H), 6.22 (br_s, 2H). MS [ESI⁺] *m/z*: 273.0 [M + H⁺]⁺

Pyrimidinone Ester: Methyl 2-(3,5-bis(trifluoromethyl)phenyl)-5,6-dihydroxypyrimidine-4-carboxylate (**3.23I**, R = 3,5-bis(trifluoromethyl)phenyl) was isolated as a light yellow solid. ¹H NMR (400 MHz, DMSO-d₆) δ 8.66 (s, 2H), 8.27 (s, 1H), 3.86 (s, 3H). MS [ESI⁺] m/z: 383.0 [M + H⁺]⁺

Final Inhibitor: 2-(3,5-bis(trifluoromethyl)phenyl)-5,6-dihydroxypyrimidine-4-carboxylic acid (**3.17I**). Isolated as a white solid. ¹H NMR (500 MHz, DMSO-d₆) δ 8.77 (s, 2H), 8.26 (s, 1H). ¹³C NMR (101 MHz, DMSO-d₆) δ 169.2, 159.8, 150.0, 143.0, 135.3, 131.1 (q, *J* = 33.2 Hz), 128.2 (br), 124.1 (br), 123.7 (q, *J* = 273.0 Hz). HRMS [ESI] calculated for C₁₃H₅F₆N₂O₄ m/z, 367.0159; found 367.0143 [M - H⁺]⁻

Inhibitors **3.31a** and **3.31b** were synthesized following the sequence of steps described for **Method C**.

Inhibitor 3.31a:

Amidoxime: 2-(6-amino-9H-purin-9-yl)-*N'*-hydroxyacetimidamide (**3.26a**, n = 1; R = adeninyl). Isolated as a yellowish solid. ¹H NMR (400 MHz, DMSO-d₆) δ 9.26 (s, -OH), 8.15 (s, 1H), 8.11 (s, 1H), 7.21 (br_s, -NH₂), 5.68 (s, -NH₂), 4.75 (s, 2H). ¹³C NMR (126 MHz, DMSO-d₆) δ 156.4, 152.9, 150.2, 148.9, 141.7, 118.9, 43.2. MS [ESI⁺] m/z: 208.15 [M + H⁺]⁺

Michael Adduct: Dimethyl 2-(((1-amino-2-(6-amino-9H-purin-9-yl)ethylidene)amino)oxy)but-2-enedioate (**3.27a**, n = 1; R = adeninyl). Isolated as a dark brown oil. ¹H NMR (400 MHz, DMSO-d₆) δ 8.14 (s, 1H), 8.12 (s, 1H), 7.24 (br_s, 2H), 6.91 (br_s, 2H), 5.41 (s, 1H), 4.91 (s, 2H), 3.70 (s, 3H), 3.56 (s, 3H). MS [ESI⁺] m/z: 350.1 [M + H⁺]⁺

Pyrimidinone Ester: Methyl 2-(((6-amino-9H-purin-9-yl)methyl)-5,6-dihydroxypyrimidine-4-carboxylate (**3.29a**, n = 1; R = adeninyl). Isolated as brown solid. ¹H NMR (400 MHz, DMSO-d₆)

δ 8.16 (s, 1H), 8.12 (s, 1H), 7.24 (br_s, 2H), 5.23 (s, 2H), 3.74 (s, 3H). MS [ESI⁺] m/z: 318.0 [M + H⁺]⁺

Final Inhibitor: 2-((6-amino-9H-purin-9-yl)methyl)-5,6-dihydroxypyrimidine-4-carboxylic acid (**3.31a**, n = 1). Isolated as a peach solid. ¹H NMR (400 MHz, D₂O added with 1.5-2.0 eq NaOH) δ 8.24 (s, 1H), 8.22 (s, 1H), 5.25 (s, 2H). ¹³C NMR (101 MHz, D₂O added with 1.5-2.0 eq NaOH) δ 173.8, 168.9, 155.4, 152.9, 152.4, 149.1, 146.0, 142.9, 133.6, 118.3, 48.9. HRMS [ESI⁻] calculated for C₁₁H₈N₇O₄ m/z, 302.06433; found 302.06431 [M - H⁺]⁻

Inhibitor 3.31b:

Amidoxime: 3-(6-amino-9H-purin-9-yl)-N'-hydroxypropanimidamide (**3.26b**, n = 2; R = adeninyl). Isolated as a white solid. ¹H NMR (500 MHz, DMSO-d₆) δ 8.91 (s, -OH), 8.14 (s, 1H), 8.01 (s, 1H), 7.16 (br_s, -NH₂), 5.51 (s, -NH₂), 4.33 (t, J = 7.1 Hz, 2H), 2.54 (t, J = 7.1 Hz, 2H). ¹³C NMR (126 MHz, DMSO-d₆) δ 156.4, 152.8, 150.2, 149.9, 141.3, 119.2, 40.4, 31.6. HSQC (¹H-¹³C): ¹H δ 4.33 correlates to ¹³C δ 40.4. MS [ESI⁺] m/z: 222.10 [M + H⁺]⁺

Michael Adduct: Dimethyl 2-(((1-amino-3-(6-amino-9H-purin-9-yl)propylidene)amino)oxy)but-2-enedioate (**3.27b**, n = 2; R = adeninyl). Isolated as a dark brown oil. ¹H NMR (500 MHz, DMSO-d₆) δ 8.14 (s, 1H), 8.04 (s, 1H), 7.16 (br_s, 2H), 6.68 (br_s, 2H), 5.50 (s, 1H), 4.37 (t, J = 7.0 Hz, 2H), 3.74 (s, 3H), 3.58 (s, 3H), 2.70 (t, J = 7.0 Hz, 2H). MS [ESI⁺] m/z: 364.1 [M + H⁺]⁺

Pyrimidinone Ester: Methyl 2-(2-(6-amino-9H-purin-9-yl)ethyl)-5,6-dihydroxypyrimidine-4-carboxylate (**3.29b**, n = 2; R = adeninyl). Isolated as a brown solid. ¹H NMR (400 MHz, DMSO-d₆) δ 8.13 (s, 1H), 8.12 (s, 1H), 7.15 (br_s, 2H), 4.48 (t, J = 6.7 Hz, 2H), 3.78 (s, 3H), 2.98 (t, J = 6.7 Hz, 2H). MS [ESI⁺] m/z: 332.1 [M + H⁺]⁺

Final Inhibitor: 2-(2-(6-amino-9H-purin-9-yl)ethyl)-5,6-dihydroxypyrimidine-4-carboxylic acid (**3.31b**, n = 2). Isolated as a beige solid. ¹H NMR (500 MHz, DMSO-d₆ with ~2% ND₄OD) δ 8.21 (s, 1H), 8.13 (s, 1H), 7.14 (br_s, 2H), 4.48 (br, 2H), 2.92 (br, 2H). HRMS [ESI⁻] calculated for C₁₂H₁₀N₇O₄ m/z, 316.07998; found 316.08006 [M - H⁺]⁻

Inhibitors **3.38a** to **3.38e** were synthesized following the sequence of steps described for **Method E**.

Inhibitor 3.38a:

Pyrimidinone Ester: Methyl 5,6-dihydroxy-2-((pyrido[2,3-d]pyrimidin-4-ylamino)methyl)pyrimidine-4-carboxylate (**3.37a**, R₆ = R₇ = H). Isolated as a reddish brown solid. ¹H NMR (400 MHz, DMSO-d₆) δ 12.87 (br_s, 1H), 10.26 (br_s, 1H), 9.09 (br, -NH), 9.02 (d, J = 4.2 Hz, 1H), 8.73 (d, J = 7.4 Hz, 1H), 8.60 (s, 1H), 7.60 (dd, J = 8.1, 4.3 Hz, 1H), 4.57 (d, J = 4.7 Hz, 2H), 3.76 (s, 3H). MS [ESI⁺] m/z: 329.1 [M + H⁺]⁺

Final Inhibitor: 5,6-dihydroxy-2-((pyrido[2,3-d]pyrimidin-4-ylamino)methyl)pyrimidine-4-carboxylic acid (**3.38a**, R₆ = R₇ = H). Isolated as a peach solid. ¹H NMR (500 MHz, DMSO-d₆ with ~2% ND₄OD) δ 8.99 (dd, J = 4.3, 1.8 Hz, 1H), 8.76 (dd, J = 8.2, 1.6 Hz, 1H), 8.59 (s, 1H), 7.56 (dd, J = 8.2, 4.4 Hz, 1H), 4.53 (s, 2H). ¹³C NMR (101 MHz, DMSO-d₆ with ~2% ND₄OD) δ 169.0, 162.2, 160.8, 158.1, 158.1, 155.8, 151.6, 144.5, 133.0, 127.6, 121.5, 109.9, 43.0. HRMS [ESI⁻] calculated for C₁₃H₉N₆O₄ m/z, 313.06908; found 313.06909 [M - H⁺]⁻

Inhibitor 3.38b:

Pyrimidinone Ester: Methyl 2-(((6-bromopyrido[2,3-d]pyrimidin-4-yl)amino)methyl)-5,6-dihydroxypyrimidine-4-carboxylate (**3.37b**, R₆ = Br, R₇ = H). Isolated as a brown solid. ¹H NMR

(500 MHz, DMSO- d_6) δ 9.17 (br, -NH), 9.10 (d, $J = 2.2$ Hz, 1H), 9.07 (br, 1H), 8.64 (s, 1H), 4.58 (d, $J = 5.1$ Hz, 2H), 3.78 (s, 3H). MS [ESI⁺] m/z : 407.0 [M + H⁺]⁺

Final Inhibitor: 2-(((6-bromopyrido[2,3-d]pyrimidin-4-yl)amino)methyl)-5,6-

dihydroxypyrimidine-4-carboxylic acid (**3.38b**, R₆ = Br, R₇ = H). Isolated as a yellow solid. ¹H NMR (500 MHz, DMSO- d_6 with ~2% ND₄OD) δ 9.13 (d, $J = 2.3$ Hz, 1H), 9.10 (d, $J = 2.3$ Hz, 1H), 8.70 (s, 1H), 4.65 (s, 2H). ¹³C NMR (126 MHz, DMSO- d_6 with ~2% ND₄OD) δ 171.0, 164.4, 160.3, 158.8, 156.6, 156.5, 149.6, 148.4, 135.7, 130.7, 115.9, 111.2, 44.7. HRMS [ESI⁻] calculated for C₁₃H₈BrN₆O₄ m/z , 390.9796; found 390.9801 [M - H⁺]⁻

Inhibitor 3.38c:

Pyrimidinone Ester: Methyl 2-(((6-bromo-7-(methylthio)pyrido[2,3-d]pyrimidin-4-yl)amino)methyl)-5,6-dihydroxypyrimidine-4-carboxylate (**3.37c**, R₆ = Br, R₇ = SMe). Isolated as a brown solid. ¹H NMR (400 MHz, DMSO- d_6) δ 9.02 (br, -NH), 8.91 (s, 1H), 8.56 (s, 1H), 4.53 (br, 2H), 3.76 (s, 3H), 2.61 (s, 3H). MS [ESI⁺] m/z : 453.0 [M + H⁺]⁺

Final Inhibitor: 2-(((6-bromo-7-(methylthio)pyrido[2,3-d]pyrimidin-4-yl)amino)methyl)-5,6-dihydroxypyrimidine-4-carboxylic acid (**3.38c**, R₆ = Br, R₇ = SMe). Isolated as a light peach solid. ¹H NMR (500 MHz, DMSO- d_6 with ~2% ND₄OD) δ 8.94 (s, 1H), 8.64 (s, 1H), 4.62 (s, 2H), 2.63 (s, 3H). ¹³C NMR (126 MHz, DMSO- d_6 with ~2% ND₄OD) δ 171.4, 166.9, 165.4, 159.9, 158.8, 156.7, 149.7, 149.0, 135.3, 131.1, 114.6, 107.5, 45.0, 14.5. HRMS [ESI⁻] calculated for C₁₄H₁₀BrN₆O₄S m/z , 436.9673; found 436.9668 [M - H⁺]⁻

Inhibitor 3.38d:

Pyrimidinone Ester: Methyl 5,6-dihydroxy-2-(((6-(4-methoxyphenyl)pyrido[2,3-d]pyrimidin-4-yl)amino)methyl)pyrimidine-4-carboxylate (**3.37d**, R₆ = *p*-methoxyphenyl, R₇ = H). Prepared *via*

Suzuki cross-coupling between **3.37b** and 4-methoxyphenyl boronic acid following **Method A**. Isolated as a brown solid. ¹H NMR (400 MHz, DMSO-d₆) δ 9.36 (s, 1H), 9.14 (br_s, -NH), 9.00 (s, 1H), 8.58 (s, 1H), 7.85 (d, *J* = 8.2 Hz, 2H), 7.14 (d, *J* = 8.5 Hz, 2H), 4.60 (d, *J* = 4.2 Hz, 2H), 3.84 (s, 3H), 3.77 (s, 3H). MS [ESI⁺] *m/z*: 435.1 [M + H⁺]⁺

Final Inhibitor: 5,6-dihydroxy-2-(((6-(4-methoxyphenyl)pyrido[2,3-d]pyrimidin-4-yl)amino)methyl)pyrimidine-4-carboxylic acid (**3.38d**, R₆ = *p*-methoxyphenyl, R₇ = H). Isolated as a light yellow solid. ¹H NMR (500 MHz, DMSO-d₆ with ~2% ND₄OD) δ 9.31 (d, *J* = 2.5 Hz, 1H), 9.00 (d, *J* = 2.3 Hz, 1H), 8.55 (s, 1H), 7.83 (d, *J* = 8.6 Hz, 2H), 7.11 (d, *J* = 8.6 Hz, 2H), 4.56 (s, 2H), 3.83 (s, 3H). ¹³C NMR (101 MHz, DMSO-d₆ with ~2% ND₄OD) δ 169.6, 162.5, 160.9, 159.7, 157.6, 156.8, 153.8, 151.2, 145.7, 132.6, 129.0, 128.6, 128.5, 128.4, 114.8, 109.7, 55.5, 43.5. HRMS [ESI⁻] calculated for C₂₀H₁₅N₆O₅ *m/z*, 419.1109; found 419.1115 [M - H⁺]⁻

Inhibitor 3.38e:

Pyrimidinone Ester: Methyl 5,6-dihydroxy-2-(((6-(4-methoxyphenyl)-7-(methylthio)pyrido[2,3-d]pyrimidin-4-yl)amino)methyl)pyrimidine-4-carboxylate (**3.37e**, R₆ = *p*-methoxyphenyl, R₇ = SMe). Prepared *via* Suzuki cross-coupling between **3.37c** and 4-methoxyphenyl boronic acid following **Method A**. Isolated as a brown solid. ¹H NMR (500 MHz, DMSO-d₆) δ 8.70 (br_s, -NH), 8.53 (s, 1H), 8.39 (s, 1H), 7.46 (d, *J* = 8.6 Hz, 2H), 7.07 (d, *J* = 8.6 Hz, 2H), 4.37 (d, *J* = 4.7 Hz, 2H), 3.82 (s, 3H), 3.60 (s, 3H), 2.54 (s, 3H). MS [ESI⁺] *m/z*: 481.1 [M + H⁺]⁺

Final Inhibitor: 5,6-dihydroxy-2-(((6-(4-methoxyphenyl)-7-(methylthio)pyrido[2,3-d]pyrimidin-4-yl)amino)methyl)pyrimidine-4-carboxylic acid (**3.38e**). Isolated as a light brown solid. ¹H NMR (500 MHz, DMSO-d₆ with ~2% ND₄OD) δ 8.72 (s, 1H), 8.49 (s, 1H), 7.47 (d, *J* = 8.5 Hz, 2H),

7.10 (d, $J = 8.6$ Hz, 2H), 4.65 (s, 2H), 3.84 (s, 3H), 2.58 (s, 3H). HRMS [ESI⁻] calculated for C₂₁H₁₇N₆O₅S m/z , 465.0987; found 465.0984 [M - H⁻]

Inhibitor 3.25a:

2-(3-bromo-4-methylphenyl)-5,6-dihydroxy-*N*-methylpyrimidine-4-carboxamide (**3.25a**).

Prepared based on previously described protocols^{2, 33} using **3.23i** and methylamine (33 wt % in EtOH) as starting materials. Isolated as off-white solid (~80% yield). ¹H NMR (500 MHz, DMSO-d₆) δ 12.89 (br_s, 1H), 12.84 (br_s, 1H), 9.08 (br_s, 1H), 8.51 (d, $J = 1.6$ Hz, 1H), 8.16 (d, $J = 6.9$ Hz, 1H), 7.48 (d, $J = 8.2$ Hz, 1H), 2.87 (d, $J = 4.9$ Hz, 3H), 2.41 (s, 3H). ¹³C NMR (101 MHz, DMSO-d₆) δ 168.9, 158.4, 148.0, 144.4, 140.3, 131.2, 130.9, 130.7, 126.9, 126.5, 124.5, 25.8, 22.4. HRMS [ESI⁺] calculated for C₁₃H₁₃BrN₃O₃ m/z , 338.0135 found 338.0140 [M + H⁺]⁺

Enzymes and Nucleic Acids: Heterodimeric, HIV-1 RT (p66/p51) was expressed and purified as described previously.³⁴ All nucleic acids were synthesized through IDT DNA Technologies. The following sequences were used:

PPT18: 5'-TTAAAAGAAAAGGGGGGA-3'

PPT24: 5'-CCACTTTTTTAAAAGAAAAGGGGGG-3'

PPT57: 5'-CGTTGGGAGTGAATTAGCCCTTCCAGTCCCCCCTTTTCTTTTAAAAA-GTGGCTAAGA-3'

PBS-22dpol: 5'-CTAGCAGTGGCGCCCGAACAGG-3'

PBS-14r8d: 5'-cuguucggcgccaCTGCTAGA-3'

5'-radiolabeling was performed with [γ -³²P]ATP (PerkinElmer Life Sciences) and T4 polynucleotide kinase (Fermentas). Reactions occurred for 1 h at 37 °C. Labeled RNA was

subjected to phenol-chloroform emulsification and purified further with P-30 size exclusion columns (Bio-Rad). 5' fluorescent labeling was applied to terminal amino-modified sequences. Briefly, amino modified sequences (roughly 20 nmol) were exposed to 5x excess Cy5 dye in 80 mM sodium bicarbonate and allowed to vortex vigorously overnight. Labeled sequences were separated on a 12% denaturing acrylamide gel, extracted and then purified through ethanol precipitation.

DNA synthesis: A 3-fold molar excess of PPT57 DNA template was heat-annealed to 50 nM 5'-Cy5-labeled PPT24 primer. Substrate was then incubated with 200 nM of RT in a buffer containing 50 mM Tris-HCl pH 7.8, 50 mM NaCl and 6 mM MgCl₂. Inhibitors were titrated up to 250 μM (permitting only a maximum 5% final DMSO concentration where applicable) and were added to the samples which were then pre-incubated at 37°C for 10 min before starting the reaction. The reaction was initiated with 0.5 μM of each of dATP, dTTP, dGTP, and dCTP and allowed to proceed for 5 min. The reaction was stopped with 100% formamide loading dye containing traces of bromophenol blue. As a negative control, a lane lacking dNTP was used. Samples were loaded on a 12% denaturing polyacrylamide gel and resolved by phosphorimaging (AmershamBiosciences). Inhibitory pausing sites were quantified through QuantityOne software. Percent inhibition was calculated as total inhibitory product divided by full-length product plus inhibitory products multiplied by 100. The product fractions were normalized and plotted against inhibitor concentration using GraphPad Prism software; the normalized data was fitted to a log[Inhibitor] versus response curve with variable slope to extract IC₅₀ values for the inhibition of RT enzyme.

Site-specific footprinting: Chemical footprinting with Fe²⁺ was done using 50 nM 5'-Cy5-labeled DNA template (PPT57) annealed to 150 nM of the primer (PPT18). The hybrid was incubated

with 750 nM HIV-1 RT in a buffer containing 120 mM sodium cacodylate (pH 7), 20 mM NaCl, and 6 mM MgCl₂ in a final volume of 20 μL. Increasing concentrations of compound were added to the samples. Control lanes using the small molecule inhibitor PFA (PRE-translocation trapping) was included, in addition to samples without RT and without Fe²⁺ treatment. Pre-incubation of complexes at 37°C for 10 min was performed prior to the treatment with Fe²⁺. Treatment with Fe²⁺ was allowed to proceed using the same method as previously described.²¹

Secondary RNase H Cleavages of HIV-1 RT: A 3-fold molar excess PBS-22dpol was heat annealed to 50 nM of 5'-radiolabeled PBS-14r8d. 250 nM HIV-1 RT was incubated in a buffer of 50 mM Tris-HCl (pH 7.8), 50 mM NaCl, 0.2 mM EDTA, 6 mM MgCl₂. Inhibitors were titrated up to 250 μM (permitting only a maximum 5% final DMSO concentration, where applicable) and were added to the samples which were then pre-incubated at 37°C for 10 min before starting the reaction. The reaction was initiated by the addition of 50 nM preformed DNA-RNA/DNA hybrid and allowed to proceed for 5 min. As positive and negative controls, β-thujaplicinol, a known RNase H inhibitor, and a lane lacking MgCl₂, respectively, were used. Bands were quantified by QuantityOne software (Bio-Rad) and results were graphed using GraphPad Prism. Briefly, % inhibition was calculated by dividing primary cleavage over total cleavage and multiplying by 100, thus, IC₅₀ values are reported as values inhibiting secondary cleavage.

3.8. Associated Content

Supporting Information

NMR spectra and homogeneity data for key inhibitors **3.17h**, **3.17i**, and **3.38d** are provided.

3.9. Author Information

Corresponding Author

*Phone 514-398-3638. Fax 514-398-3797. Email: youla.tsantrizos@mcgill.ca

3.10. Acknowledgments

Financial support for this work was provided by the Natural Sciences and Engineering Research Council of Canada (NSERC) and the Canadian Institute of Health Research (CIHR) to M. Götte and Y.S. Tsantrizos.

3.11 References

1. Summa, V.; Petrocchi, A.; Matassa, V. G.; Taliani, M.; Laufer, R.; De Francesco, R.; Altamura, S.; Pace, P. HCV NS5b RNA-dependent RNA polymerase inhibitors: From α,γ -diketoacids to 4,5-dihydropyrimidine- or 3-methyl-5- hydroxypyrimidinonecarboxylic acids. Design and synthesis. *J. Med. Chem.* **2004**, 47, 5336-5339.
2. Summa, V.; Petrocchi, A.; Matassa, V. G.; Gardelli, C.; Muraglia, E.; Rowley, M.; Paz, O. G.; Laufer, R.; Monteagudo, E.; Pace, P. 4,5-dihydropyrimidine carboxamides and N-alkyl-5-hydroxypyrimidinone carboxamides are potent, selective HIV integrase inhibitors with good pharmacokinetic profiles in preclinical species. *J. Med. Chem.* **2006**, 49, 6646-6649.
3. Summa, V.; Petrocchi, A.; Bonelli, F.; Crescenzi, B.; Donghi, M.; Ferrara, M.; Fiore, F.; Gardelli, C.; Gonzalez Paz, O.; Hazuda, D. J.; Jones, P.; Kinzel, O.; Laufer, R.; Monteagudo, E.; Muraglia, E.; Nizi, E.; Orvieto, F.; Pace, P.; Pescatore, G.; Scarpelli, R.; Stillmock, K.; Witmer, M. V.; Rowley, M. Discovery of raltegravir, a potent, selective orally bioavailable HIV-integrase inhibitor for the treatment of HIV-AIDS infection. *J. Med. Chem.* **2008**, 51, 5843-5855.
4. Stansfield, I.; Avolio, S.; Colarusso, S.; Gennari, N.; Narjes, F.; Pacini, B.; Ponzi, S.; Harper, S. Active site inhibitors of HCV NS5B polymerase. The development and pharmacophore of 2-thienyl-5,6-dihydropyrimidine-4-carboxylic acid. *Bioorg. Med. Chem. Lett.* **2004**, 14, 5085-5088.

5. Petrocchi, A.; Koch, U.; Matassa, V. G.; Pacini, B.; Stillmock, K. A.; Summa, V. From dihydroxypyrimidine carboxylic acids to carboxamide HIV-1 integrase inhibitors: SAR around the amide moiety. *Bioorg. Med. Chem. Lett.* **2007**, *17*, 350-353.
6. Koch, U.; Attenni, B.; Malancona, S.; Colarusso, S.; Conte, I.; Di Filippo, M.; Harper, S.; Pacini, B.; Giomini, C.; Thomas, S.; Incitti, I.; Tomei, L.; De Francesco, R.; Altamura, S.; Matassa, V. G.; Narjes, F. 2-(2-Thienyl)-5,6-dihydroxy-4-carboxypyrimidines as inhibitors of the hepatitis C virus NS5B polymerase: Discovery, SAR, modeling, and mutagenesis. *J. Med. Chem.* **2006**, *49*, 1693-1705.
7. Kirschberg, T. A.; Balakrishnan, M.; Squires, N. H.; Barnes, T.; Brendza, K. M.; Chen, X.; Eisenberg, E. J.; Jin, W.; Kutty, N.; Leavitt, S.; Liclican, A.; Liu, Q.; Liu, X.; Mak, J.; Perry, J. K.; Wang, M.; Watkins, W. J.; Lansdon, E. B. RNase H active site inhibitors of human immunodeficiency virus type 1 reverse transcriptase: Design, biochemical activity, and structural information. *J. Med. Chem.* **2009**, *52*, 5781-5784.
8. Tang, J.; Liu, F.; Nagy, E.; Miller, L.; Kirby, K. A.; Wilson, D. J.; Wu, B.; Sarafianos, S. G.; Parniak, M. A.; Wang, Z. 3-Hydroxypyrimidine-2,4-diones as selective active site inhibitors of HIV reverse transcriptase-associated RNase H: Design, synthesis, and biochemical evaluations. *J. Med. Chem.* **2016**, *59*, 2648-2659.
9. Kankanala, J.; Kirby, K. A.; Liu, F.; Miller, L.; Nagy, E.; Wilson, D. J.; Parniak, M. A.; Sarafianos, S. G.; Wang, Z. Design, synthesis, and biological evaluations of hydroxypyridonecarboxylic acids as inhibitors of HIV reverse transcriptase associated RNase H. *J. Med. Chem.* **2016**, *59*, 5051-5062.
10. Vernekar, S. K. V.; Liu, Z.; Nagy, E.; Miller, L.; Kirby, K. A.; Wilson, D. J.; Kankanala, J.; Sarafianos, S. G.; Parniak, M. A.; Wang, Z. Design, synthesis, biochemical, and antiviral evaluations of C6 benzyl and C6 biarylmethyl substituted 2-hydroxyisoquinoline-1,3-diones: Dual inhibition against HIV reverse transcriptase-associated RNase H and polymerase with antiviral activities. *J. Med. Chem.* **2015**, *58*, 651-664.
11. Williams, P. D.; Staas, D. D.; Venkatraman, S.; Loughran, H. M.; Ruzek, R. D.; Booth, T. M.; Lyle, T. A.; Wai, J. S.; Vacca, J. P.; Feuston, B. P.; Ecto, L. T.; Flynn, J. A.; DiStefano, D. J.; Hazuda, D. J.; Bahnck, C. M.; Himmelberger, A. L.; Dornadula, G.; Hrin, R. C.; Stillmock, K. A.; Witmer, M. V.; Miller, M. D.; Grobler, J. A. Potent and selective HIV-1

- ribonuclease H inhibitors based on a 1-hydroxy-1,8-naphthyridin-2(1H)-one scaffold. *Bioorg. Med. Chem. Lett.* **2010**, *20*, 6754-6757.
12. Maga, G.; Radi, M.; Zanolli, S.; Manetti, F.; Cancio, R.; Hübscher, U.; Spadari, S.; Falciani, C.; Terrazas, M.; Vilarrasa, J.; Botta, M. Discovery of non-nucleoside inhibitors of HIV-1 reverse transcriptase competing with the nucleotide substrate. *Angew. Chem. Int. Ed.* **2007**, *46*, 1810-1813.
 13. Radi, M.; Falciani, C.; Contemori, L.; Petricci, E.; Maga, G.; Samuele, A.; Zanolli, S.; Terrazas, M.; Castria, M.; Togninelli, A.; Esté, J. A.; Clotet-Codina, I.; Armand-Ugón, M.; Botta, M. A multidisciplinary approach for the identification of novel HIV-1 non-nucleoside reverse transcriptase inhibitors: S-DABOCs and DAVPs. *ChemMedChem* **2008**, *3*, 573-593.
 14. Freisz, S.; Bec, G.; Radi, M.; Wolff, P.; Crespan, E.; Angeli, L.; Dumas, P.; Maga, G.; Botta, M.; Ennifar, E. Crystal structure of HIV-1 reverse transcriptase bound to a non-nucleoside inhibitor with a novel mechanism of action. *Angew. Chem. Int. Ed.* **2010**, *49*, 1805-1808.
 15. Dreher, S. D.; Ikemoto, N.; Gresham, V.; Liu, J.; Dormer, P. G.; Balsells, J.; Mathre, D.; Novak, T. J.; Armstrong Iii, J. D. Highly selective synthesis of 2-substituted-5-hydroxy-6-oxo-1,6-dihydropyrimidine-4-carboxylic acid derivatives using a novel protected dihydroxyfumarate. *Tetrahedron Lett.* **2004**, *45*, 6023-6025.
 16. Humphrey, G. R.; Pye, P. J.; Zhong, Y.-L.; Angelaud, R.; Askin, D.; Belyk, K. M.; Maligres, P. E.; Mancheno, D. E.; Miller, R. A.; Reamer, R. A.; Weissman, S. A. Development of a second-generation, highly efficient manufacturing route for the HIV integrase inhibitor raltegravir potassium. *Org. Process Res. Dev.* **2011**, *15*, 73-83.
 17. Zhong, Y.-L.; Zhou, H.; Gauthier Jr, D. R.; Askin, D. Efficient synthesis of functionalized pyrimidones via microwave-accelerated rearrangement reaction. *Tetrahedron Lett.* **2006**, *47*, 1315-1317.
 18. Pye, P. J.; Zhong, Y.-L.; Jones, G. O.; Reamer, R. A.; Houk, K. N.; Askin, D. A polar radical pair pathway to assemble the pyrimidinone core of the HIV integrase inhibitor raltegravir potassium. *Angew. Chem. Int. Ed.* **2008**, *47*, 4134-4136.

19. Bellomo, A.; Celebi-Olcum, N.; Bu, X.; Rivera, N.; Ruck, R. T.; Welch, C. J.; Houk, K. N.; Dreher, S. D. Rapid catalyst identification for the synthesis of the pyrimidinone core of HIV integrase inhibitors. *Angew. Chem. Int. Ed.* **2012**, *51*, 6912-6915.
20. Lacbay, C. M.; Mancuso, J.; Lin, Y.-S.; Bennett, N.; Götte, M.; Tsantrizos, Y. S. Modular assembly of purine-like bisphosphonates as inhibitors of HIV-1 reverse transcriptase. *J. Med. Chem.* **2014**, *57*, 7435-7449.
21. Marchand, B.; Götte, M. Site-specific footprinting reveals differences in the translocation status of HIV-1 reverse transcriptase: Implications for polymerase translocation and drug resistance. *J. Biol. Chem.* **2003**, *278*, 35362-35372.
22. Marchand, B.; Tchesnokov, E. P.; Götte, M. The pyrophosphate analogue foscarnet traps the pre-translocational state of HIV-1 reverse transcriptase in a brownian ratchet model of polymerase translocation. *J. Biol. Chem.* **2007**, *282*, 3337-3346.
23. Bernatchez, J. A.; Paul, R.; Tchesnokov, E. P.; Ngure, M.; Beilhartz, G. L.; Berghuis, A. M.; Lavoie, R.; Li, L.; Auger, A.; Melnyk, R. A.; Grobler, J. A.; Miller, M. D.; Hazuda, D. J.; Hecht, S. M.; Götte, M. Derivatives of mesoxalic acid block translocation of HIV-1 reverse transcriptase. *J. Biol. Chem.* **2015**, *290*, 1474-1484.
24. Budihas, S. R.; Gorshkova, I.; Gaidamakov, S.; Wamiru, A.; Bona, M. K.; Parniak, M. A.; Crouch, R. J.; McMahon, J. B.; Beutler, J. A.; Le Grice, S. F. J. Selective inhibition of HIV-1 reverse transcriptase-associated ribonuclease H activity by hydroxylated tropolones. *Nucleic Acids Res.* **2005**, *33*, 1249-1256.
25. Klumpp, K.; Hang, J. Q.; Rajendran, S.; Yang, Y.; Derosier, A.; Wong Kai In, P.; Overton, H.; Parkes, K. E. B.; Cammack, N.; Martin, J. A. Two-metal ion mechanism of RNA cleavage by HIV RNase H and mechanism-based design of selective HIV RNase H inhibitors. *Nucleic Acids Res.* **2003**, *31*, 6852-6859.
26. Hakimelahi, G. H.; Ly, T. W.; Moosavi-Movahedi, A. A.; Jain, M. L.; Zakerinia, M.; Davari, H.; Mei, H.-C.; Sambaiah, T.; Moshfegh, A. A.; Hakimelahi, S. Design, synthesis, and biological evaluation of novel nucleoside and nucleotide analogues as agents against DNA viruses and/or retroviruses. *J. Med. Chem.* **2001**, *44*, 3710-3720.
27. Sun, Z.; Wang, H.; Wen, K.; Li, Y.; Fan, E. Solvent-free or low-solvent large-scale preparation of chloropyrimidine and analogues. *J. Org. Chem.* **2011**, *76*, 4149-4153.

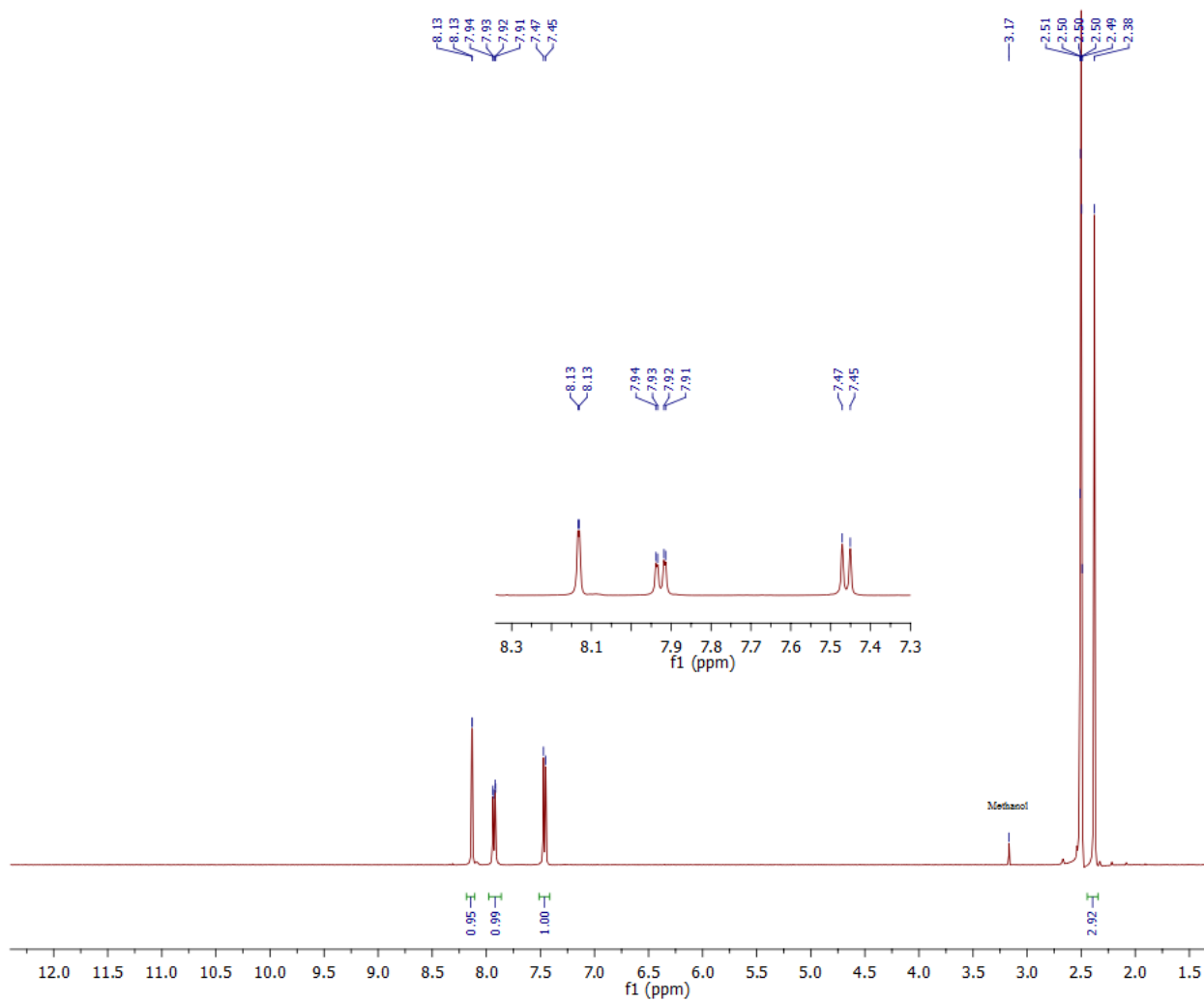
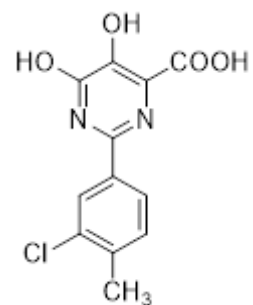
28. Zhang, D.; Ai, J.; Liang, Z.; Li, C.; Peng, X.; Ji, Y.; Jiang, H.; Geng, M.; Luo, C.; Liu, H. Discovery of novel 2-aminopyridine-3-carboxamides as c-Met kinase inhibitors. *Bioorg. Med. Chem.* **2012**, *20*, 5169-5180.
29. Debenham, J. S.; Madsen-Duggan, C. B.; Walsh, T. F. Substituted pyrido[2,3-d]pyrimidine derivatives as cannabinoid-1 receptor modulators. WO **2008/121257** A1.
30. Gardelli, C.; Giuliano, C.; Harper, S.; Koch, U.; Narjes, F.; Ontoria, O. J. M.; Poma, M.; Ponzi, S.; Stansfield, I.; Summa, V. Dihydroxypyrimidine carboxylic acids as viral polymerase inhibitors. WO 02/06246 A1.
31. Molander, G. A.; Canturk, B.; Kennedy, L. E. Scope of the Suzuki–Miyaura cross-coupling reactions of potassium heteroaryltrifluoroborates. *J. Org. Chem.* **2009**, *74*, 973-980.
32. De Schutter, J. W.; Shaw, J.; Lin, Y.-S.; Tsantrizos, Y. S. Design of potent bisphosphonate inhibitors of the human farnesyl pyrophosphate synthase via targeted interactions with the active site ‘capping’ phenyls. *Bioorg. Med. Chem.* **2012**, *20*, 5583-5591.
33. Agrawal, A.; DeSoto, J.; Fullagar, J. L.; Maddali, K.; Rostami, S.; Richman, D. D.; Pommier, Y.; Cohen, S. M. Probing chelation motifs in HIV integrase inhibitors. *Proc. Natl. Acad. Sci.* **2012**, *109*, 2251-2256.
34. Le Grice, S. F. J.; GrÜNinger-Leitch, F. Rapid purification of homodimer and heterodimer HIV-1 reverse transcriptase by metal chelate affinity chromatography. *Eur. J. Biochem.* **1990**, *187*, 307-314.

Chapter 3: Supporting Information

Diketo Acid Bioisosteres and Structure-Activity Relationship Studies of Mechanistically Unique Inhibitors of HIV-1 Reverse Transcriptase

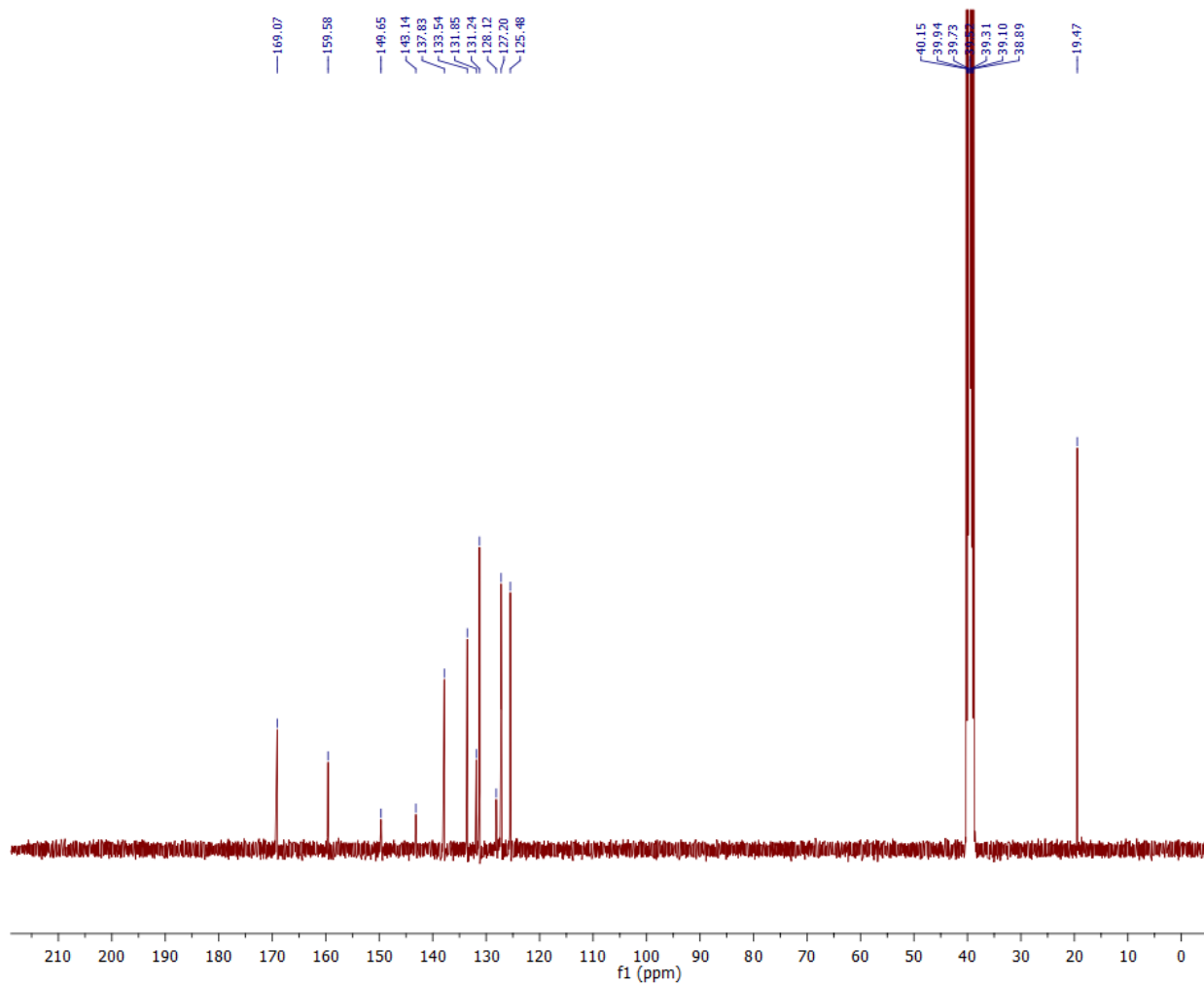
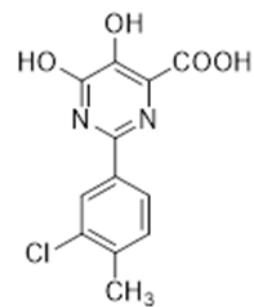
Inhibitor 3.17h:

¹H NMR (400 MHz, DMSO-d₆)



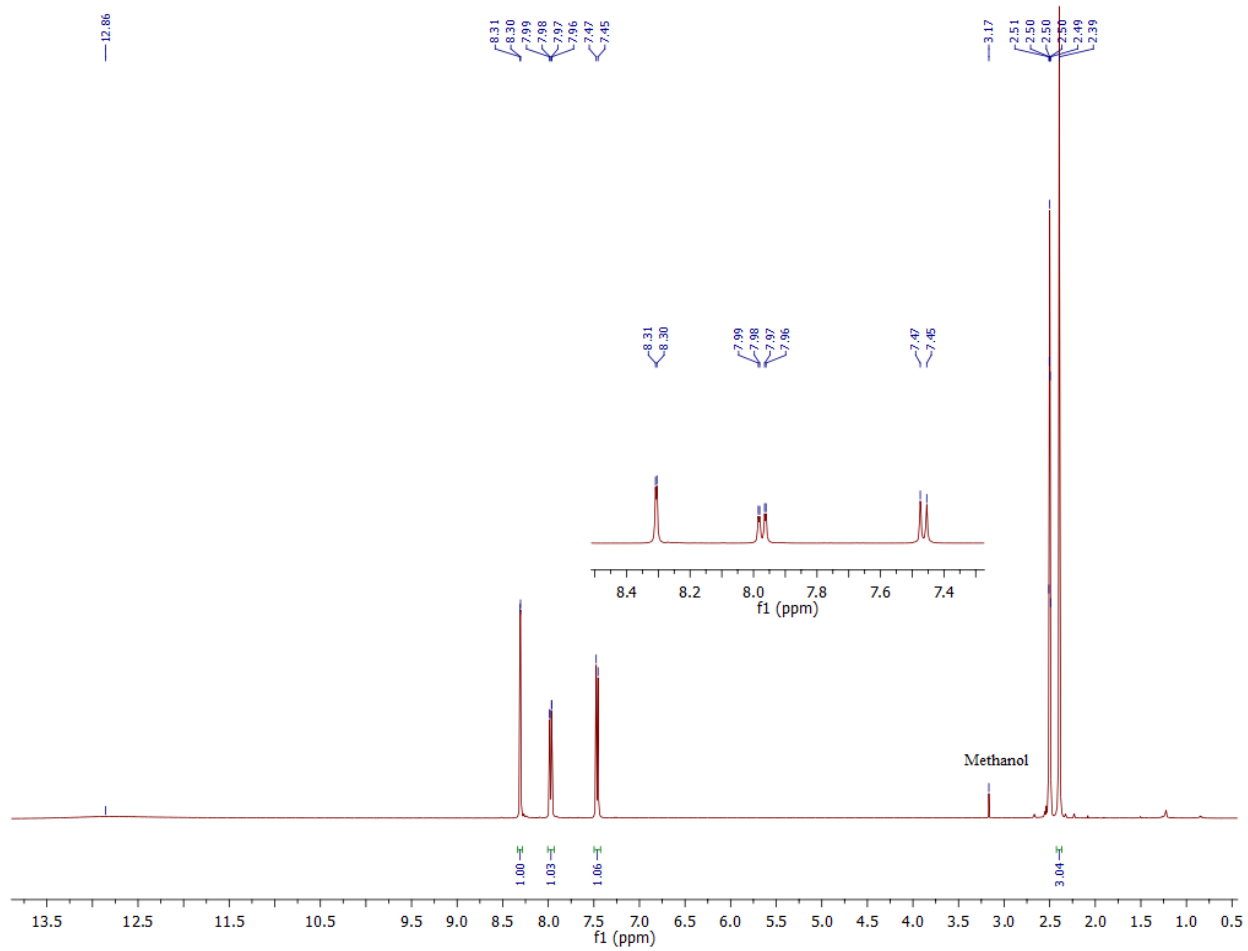
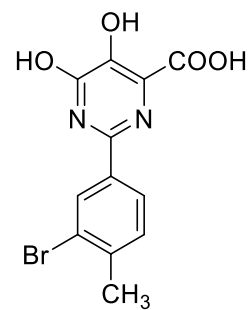
Inhibitor 3.17h:

^{13}C NMR (101 MHz, DMSO-d₆)



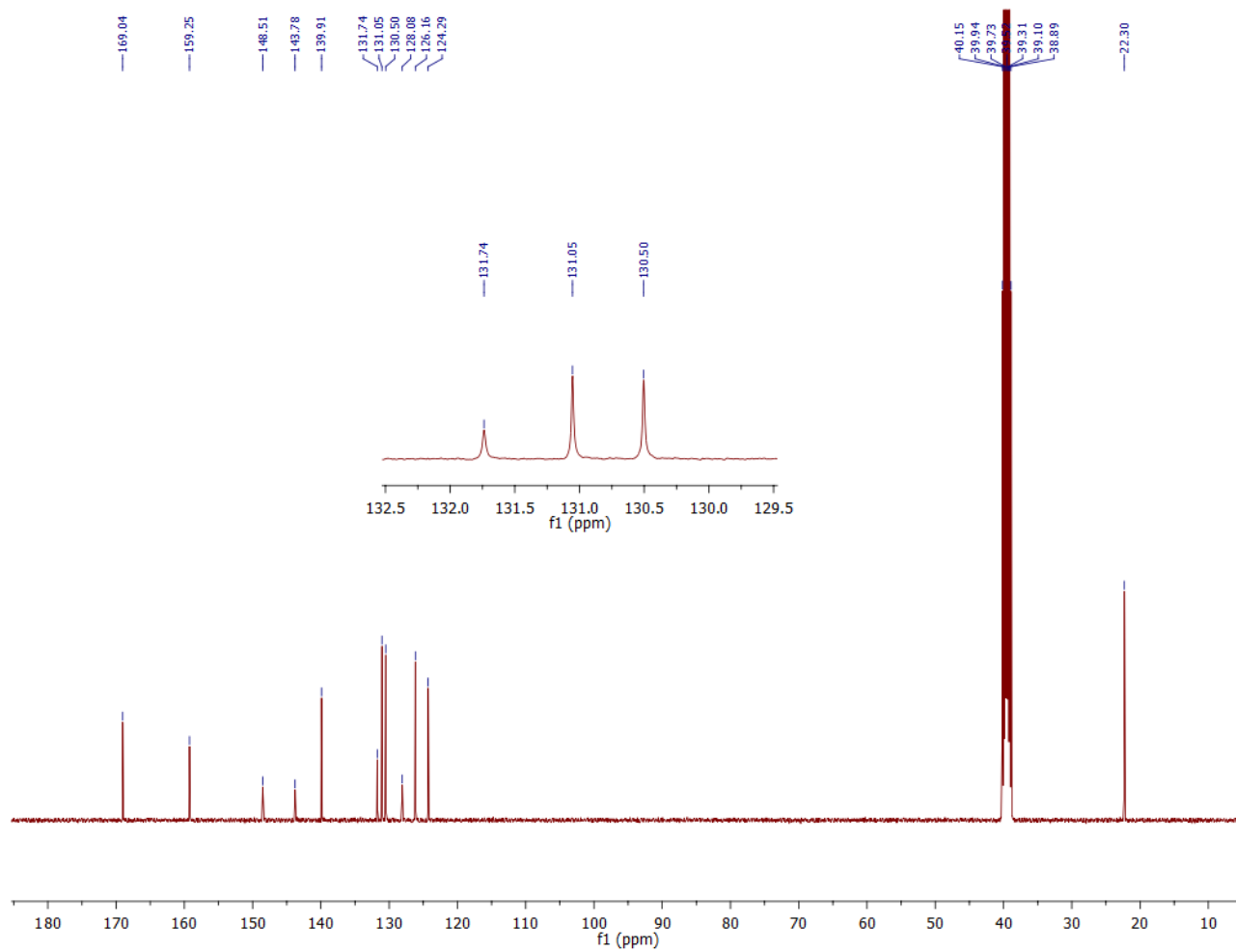
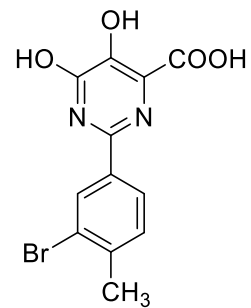
Inhibitor 3.17i:

¹H NMR (400 MHz, DMSO-d₆)



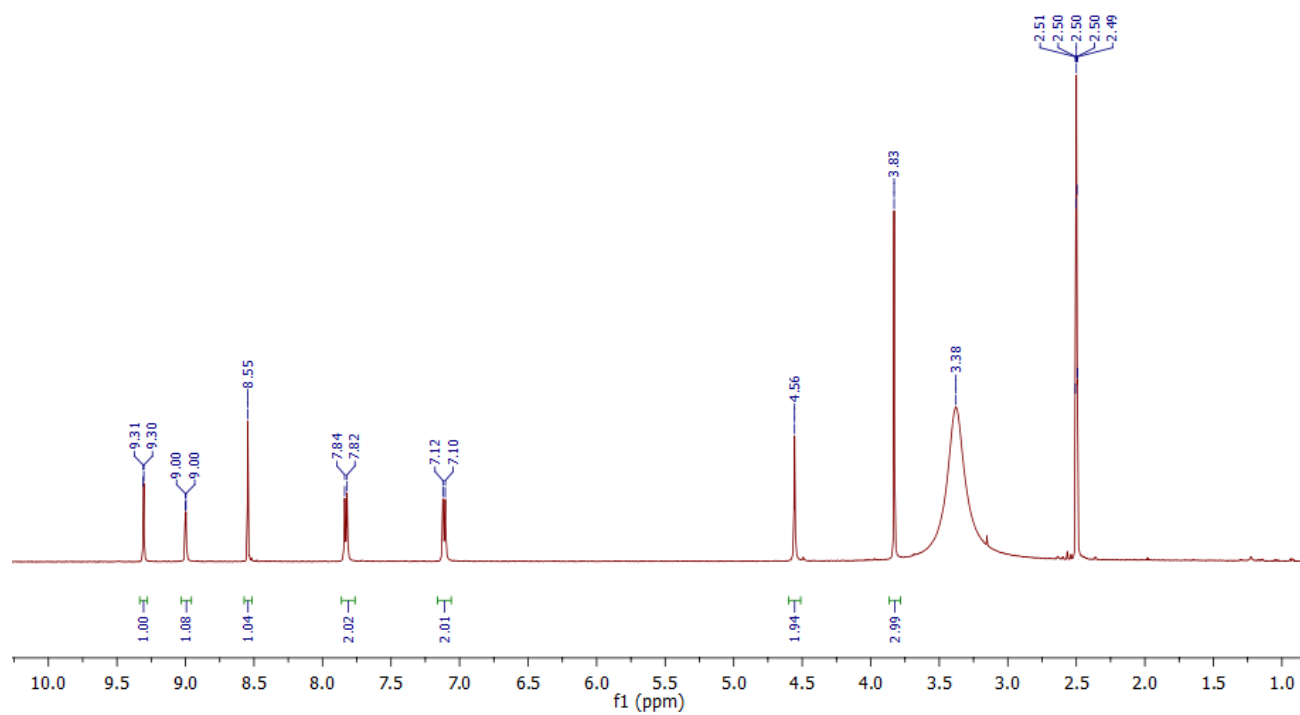
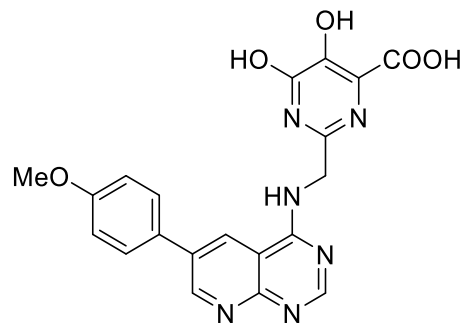
Inhibitor 3.17i:

^{13}C NMR (101 MHz, DMSO-d₆)



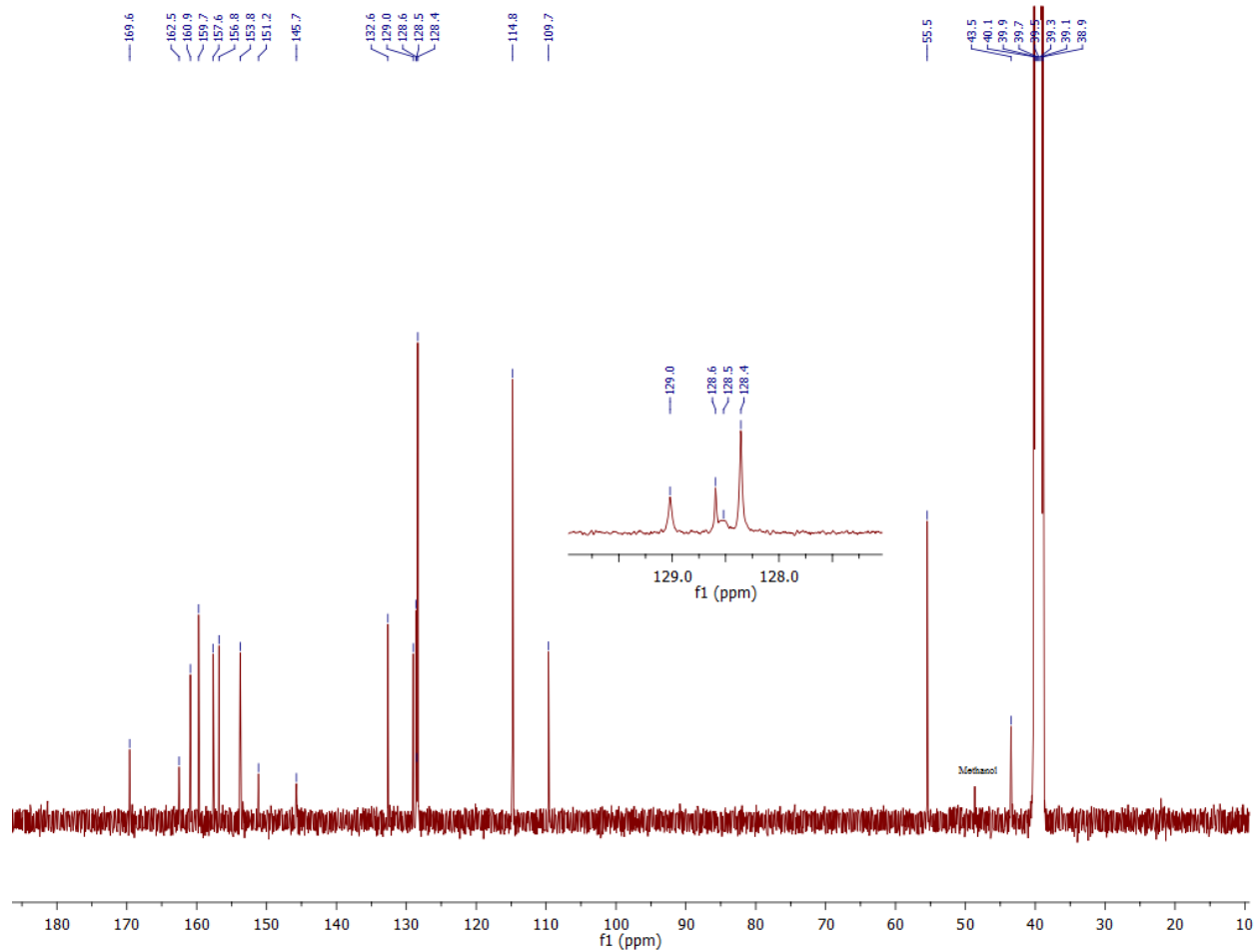
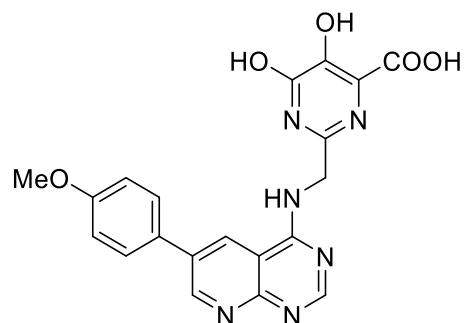
Inhibitor 3.38d:

^1H NMR (500 MHz, DMSO- d_6 with ~2% ND_4OD)



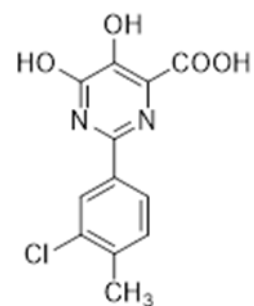
Inhibitor 3.38d:

^{13}C NMR (101 MHz, DMSO-d₆ with ~2% ND₄OD)

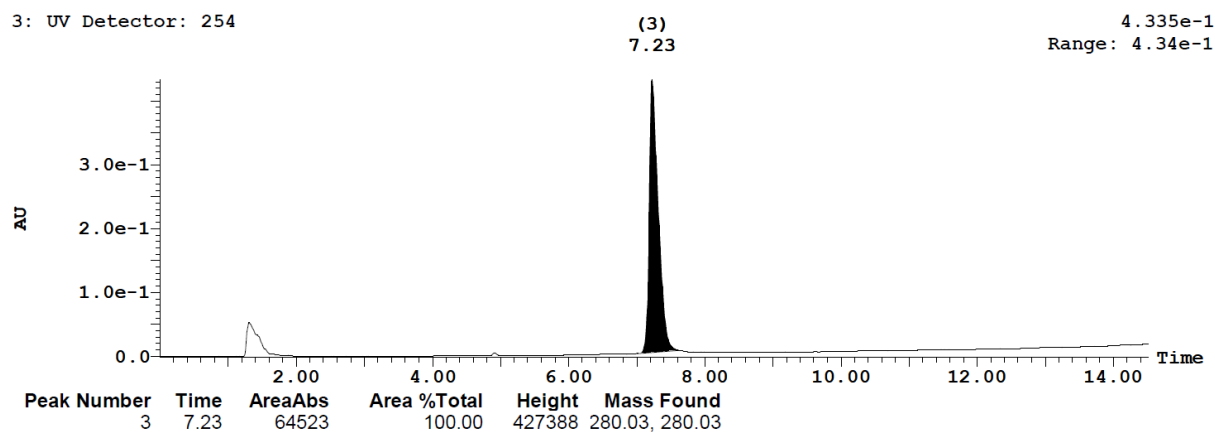


HPLC Chromatograms

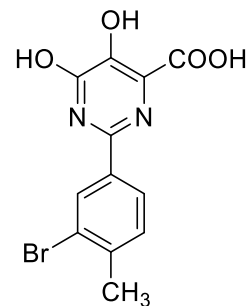
Inhibitor 3.17h:



3: UV Detector: 254



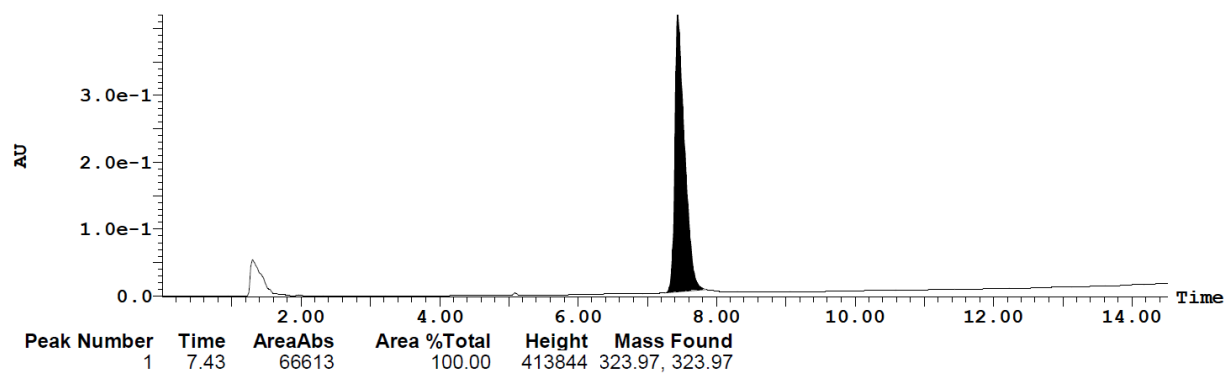
Inhibitor 3.17i:



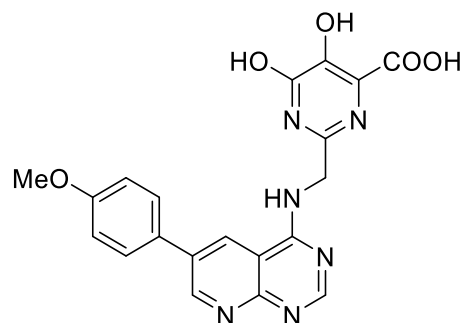
3: UV Detector: 254

(1)
7.43

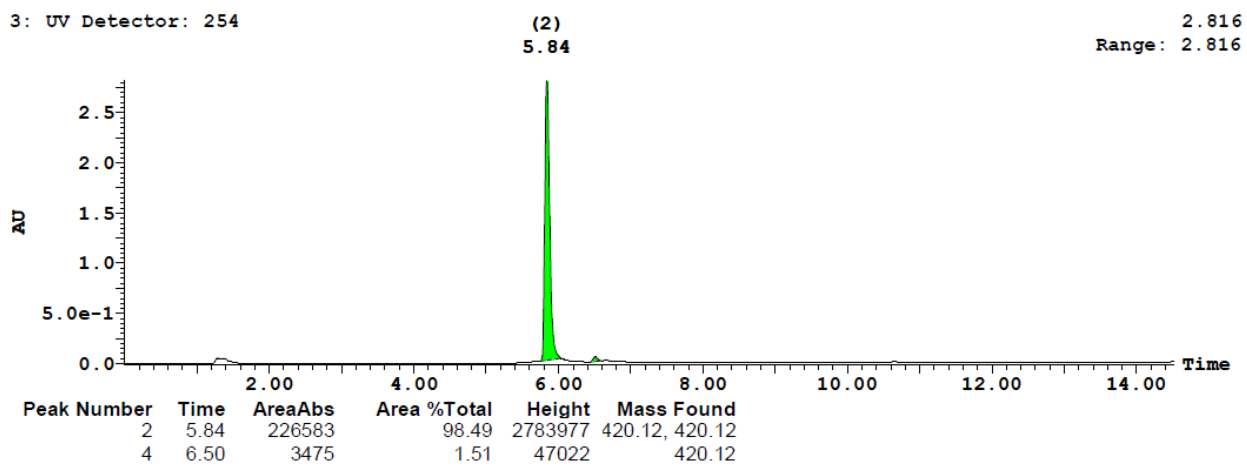
4.201e-1
Range: 4.204e-1



Inhibitor 3.38d:



3: UV Detector: 254



CHAPTER 4: The Mevalonate Pathway and the Human Geranylgeranyl Pyrophosphate Synthase (hGGPPS)

4.1. Preface

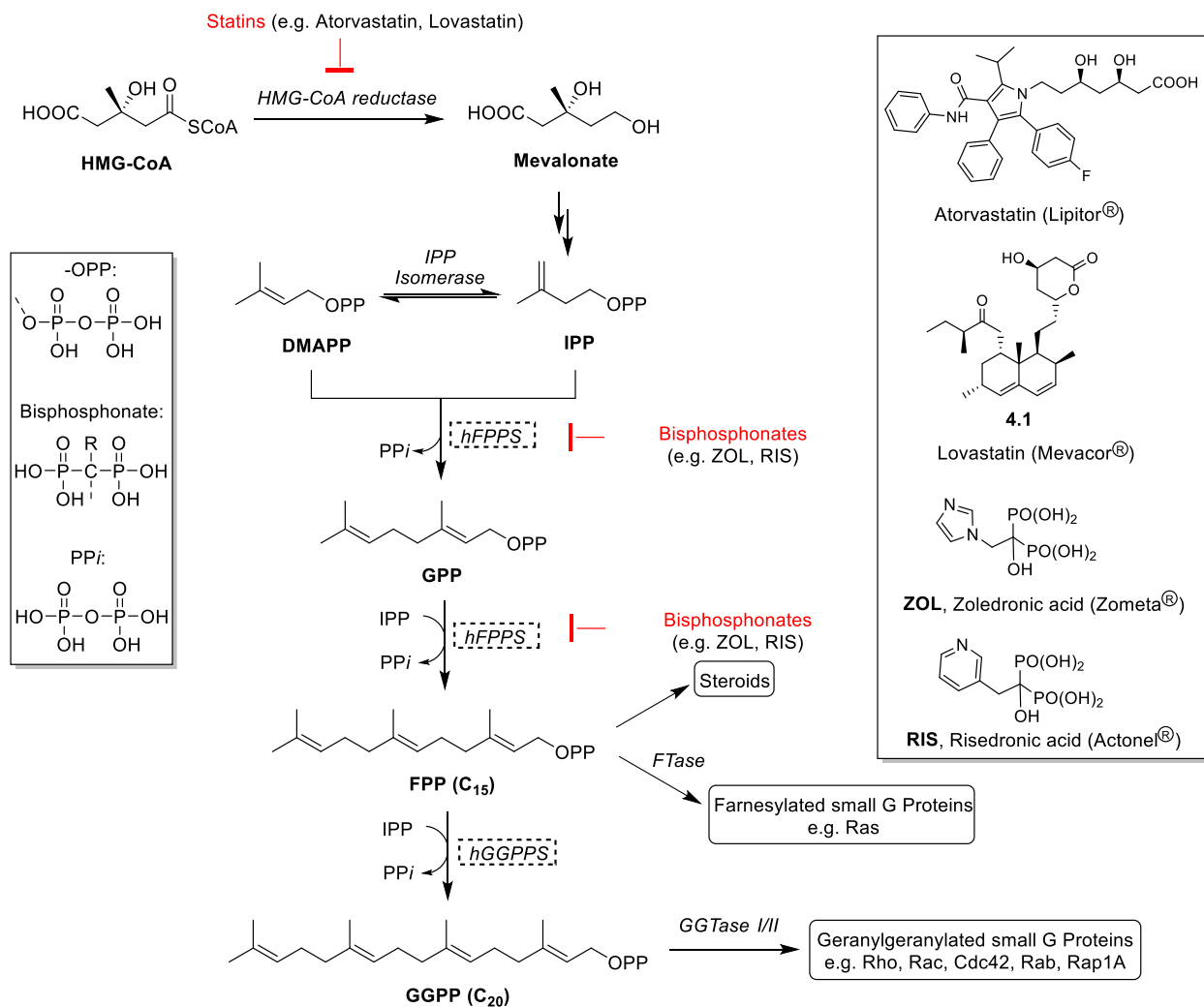
This chapter provides an overview of the mevalonate pathway and the role of its key regulatory enzymes in disease pathologies. Focus is given to hGGPPS, another phosphate-binding enzyme that is currently gaining recognition as a promising therapeutic target.

4.2. Regulatory Enzymes of the Mevalonate Pathway as Drug Targets

The mammalian mevalonate pathway is responsible for the biosynthesis of all isoprenoid metabolites that serve as precursors in the synthesis of other important biomolecules including cholesterol and other steroids.¹⁻³ Several enzymes that regulate isoprenoid biosynthesis are valuable targets for drug discovery. HMG-CoA reductase, the enzyme that catalyzes the first and rate-determining step of the pathway (*i.e.* the conversion of 3-hydroxy-3-methylglutaryl coenzyme A to mevalonate) is targeted by the cholesterol-lowering drugs, statins (e.g. atorvastatin, Lipitor®; lovastatin, Mevacor®) (**Scheme 4.1**).⁴ Mevalonate is then converted to the five-carbon metabolite isopentenyl pyrophosphate (IPP) upon phosphorylation and decarboxylation. IPP can isomerize to dimethylallyl pyrophosphate (DMAPP) and these two five-carbon units serve as the main building blocks for the biosynthesis of all downstream isoprenoids. The next step in the mevalonate pathway is occupied by the human farnesyl pyrophosphate synthase (hFPPS), which catalyzes the sequential condensations of two IPP units and one DMAPP unit to generate the 15-carbon isoprenoid farnesyl pyrophosphate (FPP). The human FPPS is inhibited by a class of drugs known as the nitrogen-containing bisphosphonates (*N*-BPs). Currently, the most potent clinically useful *N*-BP drugs are zoledronic acid (ZOL; Zometa®) and risedronic acid (RIS; Actonel®), which are used to treat bone-related malignancies.^{5, 6} Downstream elongation of FPP to a 20-carbon

geranylgeranyl pyrophosphate (GGPP) is then catalyzed by a functionally-related enzyme, the human geranylgeranyl pyrophosphate synthase (hGGPPS).^{7, 8} Both FPP and GGPP are essential for the post-translational prenylation of small guanosine triphosphate binding proteins (small GTPases), a required modification that is vital for the biological function of these signaling proteins. This modification refers to the covalent attachment of the hydrocarbon portion of FPP or GGPP to a cysteine residue at (or near) the C terminus of the protein, a process which is catalyzed by prenyltransferases. There are three known prenyltransferases: the farnesyl transferase (FTase) and two geranylgeranyl transferases (GGTase I and GGTase II, the latter is also known as Rab GGTase). Prenylation of proteins serves to increase the membrane affinity of the modified protein and mediates protein-protein interactions.^{9, 10} Farnesylated proteins include members of the Ras superfamily (H-Ras, K-Ras, N-Ras) whereas geranylgeranylated proteins include the Rho family of GTPases (Rho A/C, Rac-1, Cdc42), Rab, Ral A/B, and Rap1A.^{11, 12} These prenylated small GTPases can act as “molecular switches” that when triggered by incoming signals can activate other proteins and results in the transcription of genes involved in cell growth, differentiation, and survival. Mutated Ras, for example can cause unintended and overactive cell signaling that can ultimately lead to cancer. Depending on the type of cancer, about 8% to 93% of human cancers harbour activating oncogenic mutations in the Ras genes (K-Ras as the most frequently observed isoform) with particularly high incidence in pancreatic cancer (~90% K-Ras mutations).⁹

The number of patients taking statins and/or *N*-BPs is rising and modulation of isoprenoid biosynthesis continues to gain recognition as an important biochemical pathway for drug discovery. In addition to HMG-CoA reductase and hFPPS, the next downstream enzyme, hGGPPS is being pursued as a novel therapeutic target that can potentially offer new options in treating human diseases (**Scheme 4.1**).



Scheme 4.1. Representation of the mevalonate pathway and examples of drugs that intervene some key enzymes.

4.3. Isoprenoids and Alzheimer's Disease

Alzheimer's Disease (AD) is a chronic brain disorder characterized by progressive memory loss and behavioral changes. It accounts for 60%-70% of cases of dementia among the elderly that affected nearly 47.5 million people worldwide in 2015.¹³ The main pathological hallmarks of AD and AD-associated cognitive dysfunction are the progressive accumulation of ribbon-like intracellular neurofibrillary tangles (NFTs) composed of hyperphosphorylated tau (P-Tau) protein

and of the extracellular aggregated amyloid- β -peptide (A β) plaques derived from the proteolysis of amyloid precursor protein (APP).¹⁴⁻¹⁶

The role of the mevalonate pathway in the progression of AD has been the subject of numerous investigations. Experimental evidence suggests that cellular cholesterol levels can influence APP processing leading to A β production,¹⁷ which fueled the evaluation of statins for the treatment of AD. Sparks *et. al.* reported that rabbits fed with a cholesterol-rich diet have increased Alzheimer-like A β accumulation.¹⁸ Similar observations were reported by Refolo and colleagues in a transgenic mouse on a hypercholesterolemic diet.¹⁹ Although not a universal finding, studies on middle-aged patients taking statins for hypercholesterolemia showed that these patients confer some level of neuroprotection against late-life development of AD.^{14, 20, 21} Additionally, statins have been shown to modulate the levels of P-Tau in human brains, indicating the involvement of an alternate and/or multiple mechanisms.²² At this point, whether statin therapy could offer clinical benefit to AD patients remains controversial and in the absence of a validated AD animal model, it is difficult to prove or disprove the association between statins and the Alzheimer's disease.

Several lines of evidence, including the studies of our collaborators (*i.e.* the group of Prof. Judes Poirier; Professor of Medicine and Psychiatry, McGill University and Associate Director, Centre for the Studies on the Prevention of Alzheimer's Disease, Douglas Mental Health University Institute) have shown that high levels of isoprenoids are present in the human AD brain (confirmed at autopsy) and the activities of some prenylated GTPases (e.g. Rac, Cdc42, and Rab6) are associated with AD neuropathology. For example, Eckert *et. al.* reported that FPP and GGPP levels are elevated in the brain tissue of AD patients by 36% and 56%, respectively compared to age-matched control samples.²³ In both AD patients and control, GGPP levels were relatively higher

than FPP levels, which is consistent with previous findings in mouse brain and normal human brain.^{24, 25} Measurement of cholesterol levels in the same AD subjects showed no significant changes, indicating that the non-sterol isoprenoids, FPP and GGPP are specifically altered in AD brain. Moreover, the activity of prenylated Rac GTPase was found to be crucial in the β -amyloid signaling cascade that generate oxidative stress in the AD brain^{26, 27} and prenylated small GTPases have been also proposed to be involved in tauopathy-associated neurodegeneration *via* the cascade: FPP \rightarrow GGPP \rightarrow Cdc42 \rightarrow GSK-3 β \rightarrow P-Tau.^{1, 28, 29} Lastly, our own recent studies have also demonstrated a genetic link between hFPPS, as well as hGGPPS (unpublished data) and P-Tau levels in the human brain and inhibitors of hFPPS were found to modulate tau phosphorylation in human immortalized neurons.³⁰ Overall, these results strongly suggest that further studies toward the discovery of potent and selective inhibitors of isoprenoid biosynthesis are warranted; such compounds may provide chemical tools for probing the role of FPP and GGPP in the progression of neurodegenerative disorders, such as Alzheimer's.

4.4. Isoprenylation and Multiple Myeloma

In general, we are exploring the hypothesis that downregulation of intracellular levels of isoprenoids can lead to an effective treatment of many types of cancers. However, we are currently focusing mainly on Multiple Myeloma (MM), which is an incurable blood plasma cell malignancy that develops in the B lymphocytes of the bone marrow. MM is the second most prevalent blood cancer after non-Hodgkin's lymphoma that accounts for approximately 1.7% of all cancers.^{31, 32} Chemotherapy is initially effective in most patients but multi-drug resistance eventually develops, underscoring the importance of novel therapeutic options in treating this disease. The median life survival of patients upon diagnosis used to be only 3-5 years but recent advances may increase this number by few more years.

Clinical investigations have provided some evidence that *N*-BPs, such as ZOL (**Scheme 4.1; Fig. 4.3**) improve the survival of MM patients *via* mechanisms that are both related, as well as independent of the skeletal benefits.^{33,34} ZOL is also being used to treat metastatic bone disease, which is highly prevalent in patients with advanced forms of cancer, including MM.^{35,36} Guenther *et. al.* reported that the direct antimyeloma activity of ZOL was due to the inhibition of protein prenylation, as evidenced by the detection of non-prenylated form of Rap1A.³⁷ In the study by Holstein and Hohl, inhibitors of the isoprenoid pathway that disrupt Rab GTPase geranylgeranylation either through depletion of GGPP levels or inhibition of GGTase II also resulted in subsequent apoptosis in MM cells.³⁸ Recent studies of Pandya *et. al.* employing genome-wide RNAi analysis also provided evidence that the enzymes of mevalonate pathway are implicated in oncogenesis.³⁹ For instance, the study showed that knockdown of GGPPS gene in cancer cell lines can potentiate the statin-induced tumor cell apoptosis.³⁹ Additionally, mutant p53, which can actively contribute to tumorigenesis has been also suggested to be dependent on the mevalonate pathway.⁴⁰ Addition of isoprenoid metabolites (e.g. GGPP) to cells depleted with mutant p53 can restore the malignant state of the cancer cells.⁴⁰ Lastly, whole genome sequencing of 38 MM patient tumors revealed that 50% of the patients harboured either K-Ras or N-Ras coding mutations⁴¹ and small molecules, particularly, inhibitors of isoprenoid biosynthesis, that can downregulate the activity of these mutated Ras oncogenes may find application as novel antimyeloma therapeutic agents.

4.5. Targeting the Prenyltransferases: Farnesyl and Geranylgeranyl Transferases

As mentioned, the prenyltransferases (FTase, GGTase I and GGTase II) catalyze the transfer of the C₁₅ FPP or C₂₀ GGPP isoprenoid to a cysteine residue at (or near) the target protein's C-

terminal. Due to their role in protein prenylation, significant effort (in the past) has been invested in discovering small molecule inhibitors of prenyltransferases as potential cancer therapeutics. Four FTase inhibitors, including Tipifarnib and Lonafarnib (**Fig. 4.1**) have advanced into clinical trials but failed to produce the expected clinical outcome. These discouraging results were attributed in part to a redundancy mechanism that allows prenylation to be mediated by GGTase I when FTase is inhibited.^{42, 43} Subsequent studies targeted GGTase I as the next frontline in blocking protein prenylation. These efforts led to the identification of several inhibitors that exhibit cellular effects including inhibition of Rho signaling, G cell cycle arrest and apoptosis induction.⁴⁴ One such compound, GGTI-2418, also known as PTX-100 (**Fig. 4.1**) entered phase 1 clinical trial in 2009.^{9,10} Clinical development of GGTI-2418 was also discontinued at one point, but is expected to be reactivated at the end of 2016 in a Phase 1b/2 clinical trial for the treatment of metastatic breast cancer and multiple myeloma.⁴⁵ On the other hand, identification of GGTase II inhibitors proceeded more slowly than the other prenyltransferases as development of selective inhibitors is more challenging, partly because of its high promiscuity.^{12, 46} To date, no GGTase II inhibitor has reached clinical evaluation but progress has been made starting from the discovery of phosphonocarboxylate analogs, such as (+)-3-IPEHPC that exhibit a mixed-type inhibition,⁴⁷ to the development of more potent and selective peptidomimetic inhibitor, compound **4.2** (**Fig. 4.1**).⁴⁸

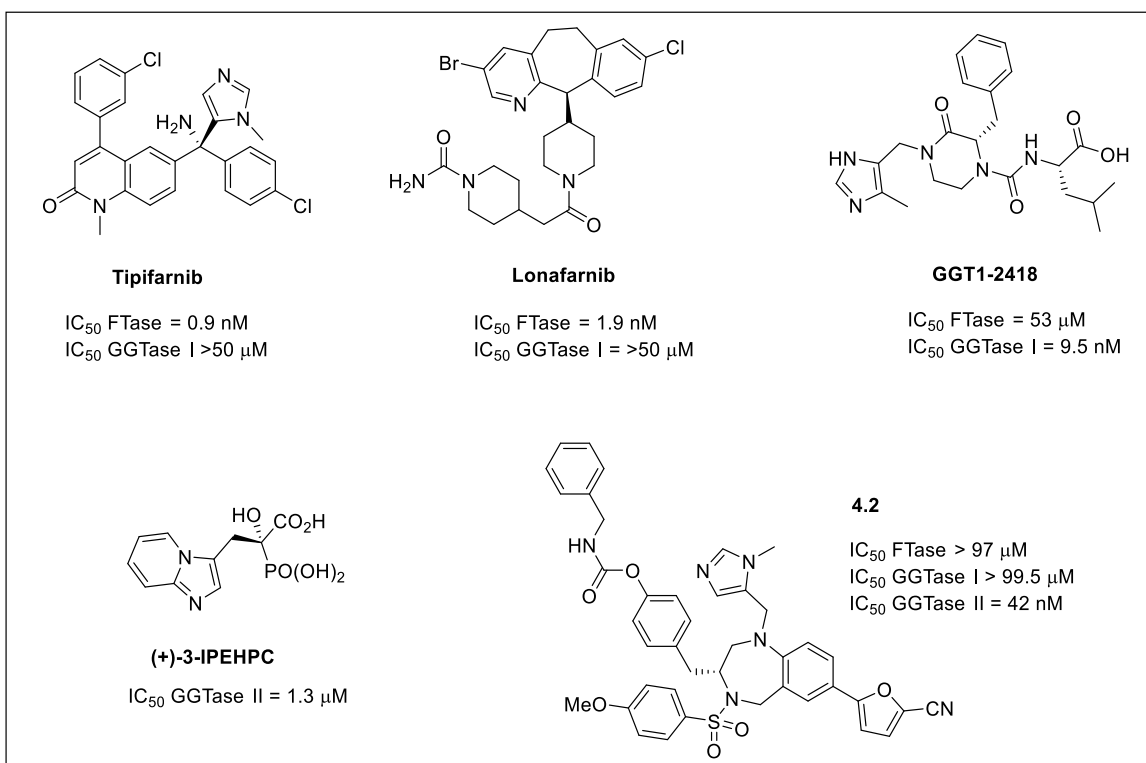


Figure 4.1. Representative inhibitors of prenyl transferases.

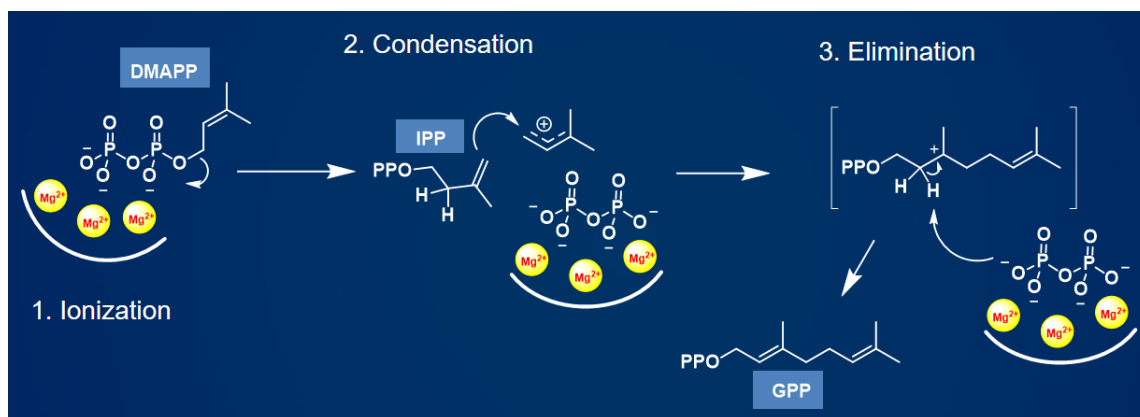
4.6. Targeting the Prenylsynthases: Farnesyl and Geranylgeranylpyrophosphate Synthases

To avoid the proposed isoprenylation redundancy mechanism observed for prenyltransferases, an alternative strategy to mediate protein prenylation is to downregulate the biosynthesis of the C₁₅ FPP and/or the C₂₀ GGPP isoprenoids by selective inhibition of the activity of the corresponding enzymes: hFPPS and hGGPPS, respectively, that catalyze their biosynthesis.

4.6.1. The human FPPS

The human FPPS is an 80-kDa homodimer that catalyzes the biosynthesis of FPP following a metal-mediated three-step ionization-condensation-elimination mechanism, initially proposed by Hosfield *et. al.*⁴⁹ (**Scheme 4.2**). Its active site is composed of two distinct sub-pockets that correspond to the IPP and DMAPP/GPP (or allylic) binding sites. The IPP binding sub-pocket is

characterized by positively-charged Arg and Lys residues that interact directly with the pyrophosphate group, whereas the allylic site is composed of highly conserved aspartate-rich domains that bind the pyrophosphate moiety of DMAPP/GPP *via* coordination with three Mg²⁺ ions.⁶ Several potent and selective active site inhibitors of hFPPS have been reported to date, including the clinically validated *N*-BPs, such as RIS and ZOL that are being used to treat bone-related diseases, including osteoporosis. The *N*-BP drugs inhibit hFPPS and disrupt the bone-destroying activity of the osteoclasts as a result of the prevention of the prenylation of GTPase signaling proteins.⁶ Numerous crystal structures have been published by our group and many others revealing the interactions between the bisphosphonate inhibitor and the hFPPS enzyme.^{6,61} For example, the crystal structure of hFPPS in complex with RIS revealed that the inhibitor binds to the allylic sub-pocket with the bisphosphonate moiety acting as a pyrophosphate mimic and chelates the Mg²⁺ triad in the active site (**Fig. 4.2**). In addition, the pyridine side chain of RIS is protonated and forms a bifurcated H-bond interaction with the hydroxyl group of Thr 201 and the carbonyl group of Lys 200, presumed to be mimicking the allylic carbocation transition state of the enzymatic reaction.⁶ These are critical interactions that account for the high potency of *N*-BPs; for instance, the phenyl analog of RIS (**4.3**; **Fig. 4.3**) was reported to be less potent by about 280-fold.⁵⁰



Scheme 4.2. Proposed mechanism for hFPPS catalysis.

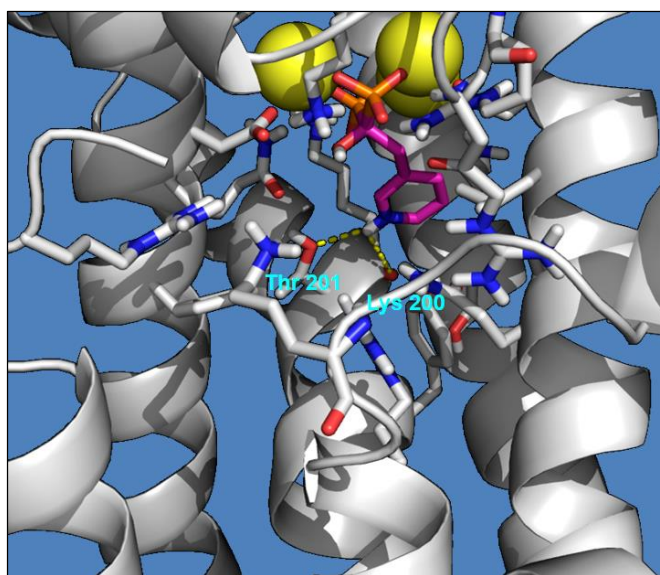


Figure 4.2. Crystal structure of hFPPS in complex with RIS (PDB: 1YV5). Mg^{2+} ions are shown as yellow spheres; H-bonding interactions are represented by yellow dashed lines.

Beyond their anti-resorptive properties, pre-clinical and clinical studies have provided some evidence that *N*-BPs have direct anti-cancer effects.^{37,51-53,54} The antitumor properties have been linked to multiple mechanisms related to the regulation of the mevalonate pathway. However, the high polarity and strong affinity of *N*-BPs for bone limit their clinical value for use in non-skeletal diseases.

Several strategies have been explored to improve the biopharmaceutical properties of *N*-BPs. Introduction of a pro-drug to mask the negative charges of the bisphosphonate moiety has been explored using pivaloyloxymethyl (POM) ester of alendronate and pamidronate⁵⁵ and of the compound **4.4** (**Fig. 4.3**) by Zhang *et. al.*⁵⁶ In comparison to its parent free BP acid, **4.4** was shown to have better antiproliferation effect (~20-fold improvement) against three different tumor cell-lines, which imply that the hydrolysis of POM to the active parent acid was facilitated by the esterases in the tested cell lines. However, these *in vitro* cell-based assays are not representative of the potential value of such prodrugs in *in vivo* studies, where the prodrug will encounter many esterases in biological fluids (e.g. blood). Notably, none of the bisphosphonate prodrug approaches have led to a clinical candidate to date.

Replacement of the bisphosphonate moiety with an effective bioisostere has been extremely challenging in the case of hFPPS. Attempts to substitute one of the phosphonates with a carboxylic acid moiety, e.g. phosphonocarboxylate analog of RIS (3-PEHPC; **Fig. 4.3**) resulted in a totally inactive compound against hFPPS, but showed some activity against GGTase II.⁵⁷ Formulation *via* liposome encapsulation of ZOL has been described recently but concerns regarding the fraction of the liposomal drug that is internalized and the impact of liposome composition in the observed activity prevented any further developments in using this approach.^{58, 59}

The conformational plasticity of hFPPS permits binding of larger and more lipophilic *N*-BPs, thus improving the cell membrane permeability of such bisphosphonate compounds. Several examples of *N*-BPs with expanded side chains, such as **4.5**⁶⁰ and **4.6**⁶¹ have been shown to have similar or slightly improved cell-based activity in MM tumor cell lines in comparison with ZOL despite a difference of about 10-fold in intrinsic potency. Furthermore, examples of BPs (or deoxy-BPs)

with reduced bone affinity have been achieved by removing the “bone hook” α -OH or by replacing the hydroxyl with a halogen substituent.⁵⁷ Finally, allosteric hFPPS inhibitors have been discovered by Novartis through fragment-based screening^{62, 63} and by our research group *via* multistage biochemical and structural screening.³⁰ In contrast to the highly charged active site pocket, targeting the allosteric site can provide non-bisphosphonate compounds ideal for pharmacological applications in soft tissues. Several hFPPS allosteric inhibitors, such as **4.7**,⁶² **4.8**,⁶³ and **4.9**³⁰ (**Fig. 4.3**) have been reported, but further optimization studies have to be undertaken as none of these inhibitors have shown significant cell-based potency.

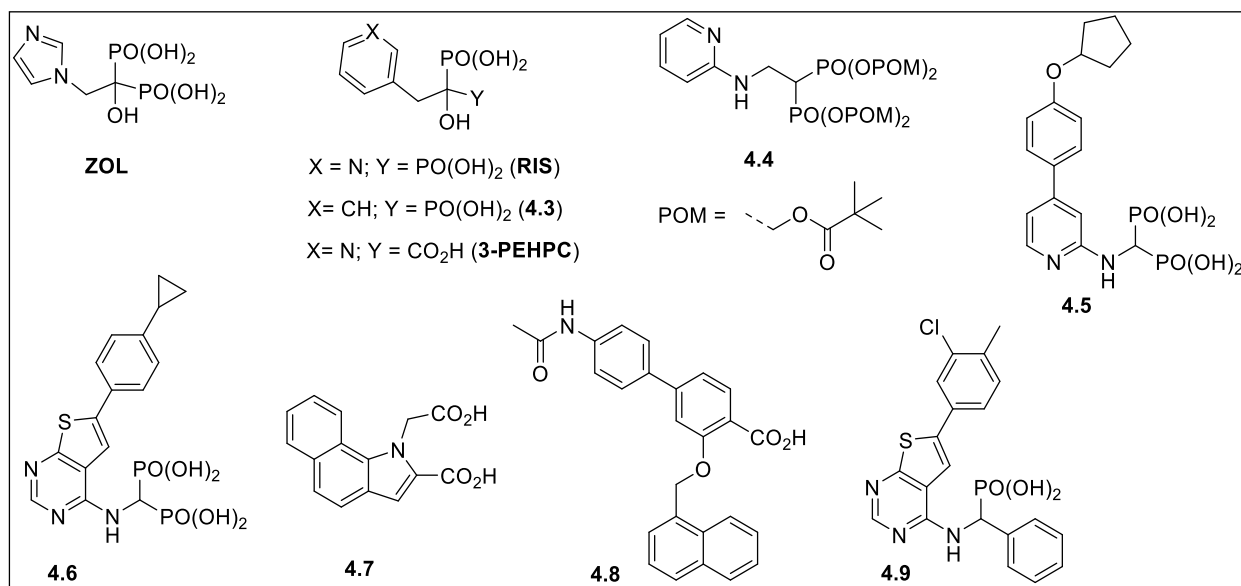


Figure 4.3. Examples of active site and allosteric inhibitors of hFPPS.

4.6.2. The human GGPPS

Our group and others have been actively pursuing inhibitors of isoprenoid biosynthesis but the majority of these studies have focused heavily on hFPPS inhibition. The current knowledge on the structure and inhibition of the functionally-related enzyme, hGGPPS, is very limited. It is believed that more GTPases, particularly those strongly implicated in a spectrum of human diseases are modified exclusively *via* geranylgeranylation. Since hGGPPS catalysis also occurs more downstream in the pathway, its selective modulation will allow the rest of the pathway to function properly. Therefore, development of potent and selective hGGPPS inhibitors are our current interest and the remaining portions of this thesis will focus in targeting this enzyme.

The human GGPPS is responsible for the production of the C₂₀ GGPP isoprenoid that is essential for the post-translational modification of several members of the Ras and Rho family of proteins. Currently, there is only one crystal structure of the human GGPPS (2.7 Å resolution) available, which revealed that the enzyme is composed primarily of α -helices where three dimers associate to form a homohexamer reminiscent of a three-blade propeller (**Fig. 4.4a**). This hexameric organization was observed in both mammalian and insect GGPPS whereas fungal, bacterial, archaeal, and plant GGPPS, resemble the structure of the human FPPS and exist as dimers. The structure also shows the presence of two Mg²⁺ ions bound with the unintended “GGPP” ligand (derived from bacterial expression that co-purified with the enzyme) in what was referred as “inhibitory site.”⁷ While obtaining a good resolution crystal was deemed challenging for the mammalian GGPPS (probably due to its large hexameric nature), Oldfield and co-workers, successfully crystallized several inhibitors in complex with GGPPS from *Saccharomyces cerevisiae*.⁶⁴⁻⁶⁶ The yeast enzyme shares ~43% sequence identity to human enzyme and crystallizes in its dimeric form. Analysis of protein-ligand interactions with several bisphosphonates showed

a broad spectrum of binding patterns. In the case of compound **4.11** (**Fig. 4.5**), the observed binding mode was found to be similar with the “GGPP” ligand⁷ described for the human enzyme. The digeranyl “V-shaped” compound, **4.13** also binds two Mg²⁺ ions through its bisphosphonate head with one of the geranyl side chains extending to the FPP substrate binding pocket while the other chain occupies the GGPP product site.⁶⁶ In addition to the observed multiple binding modes, the Mg²⁺ ions are either not seen or the number varies from one to three ions.⁶⁶

The amino acid residues involved in protein-protein interactions that form the hexameric structure were also described by Kavanagh *et. al.* (**Fig. 4.4b**).⁷ These protein inter-dimer contacts are located outside the active site pocket and were found to be conserved in mammalian and insect GGPPS. With the goal of obtaining the dimeric form of the human GGPPS that may be more useful for structural studies, our group has successfully introduced mutations that disrupt the protein-protein inter-dimer contacts without affecting the enzymatic activity. One such mutation that gave a catalytically active dimer mutant was Y246D designed based on the observed H-bond interactions between Tyr 246 and Gln 21 (**Fig. 4.4b**). The Y246D mutant, along with the wild-type enzyme as reference, is currently being used in our studies (unpublished results). For example, we determined the IC₅₀ values of the literature compounds **4.14** and **4.15** (**Fig. 4.5**) using both the wild-type and Y246D mutant GGPPS and we found that the IC₅₀ values were within the 2- to 3-fold variability of the assay.

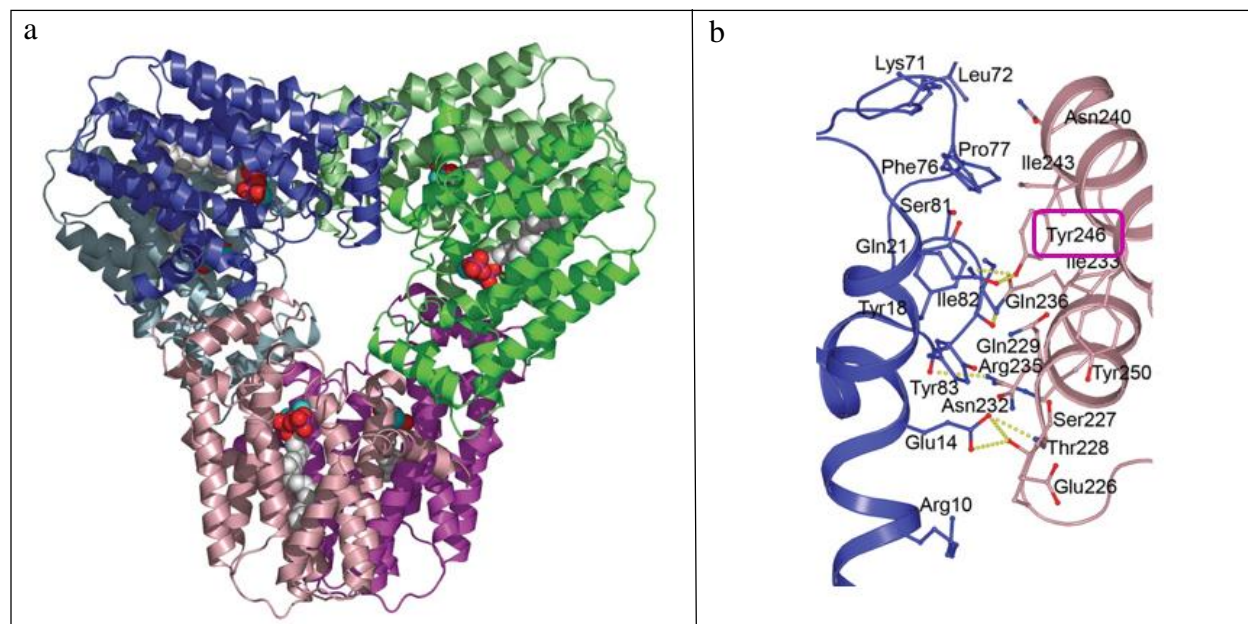


Figure 4.4. (a) Crystal structure of human GGPPS (PDB: 2Q80) revealing a homo-hexameric organization; (b) Inter dimer contact between two α -helices. H-bonding interactions are depicted by yellow dashed lines. Image was adapted from Kavanagh *et. al.*⁷

4.6.3. Inhibitors of hGGPPS

Only few potent and selective inhibitors of hGGPPS are presently known and all of these exploratory compounds are bisphosphonates. The clinically validated inhibitors of hFPPS, such as ZOL and RIS are ineffective in inhibiting hGGPPS, most likely due to their small side chains that provide minimum interactions with the larger active site cavity of hGGPPS.

In 2007, Oldfield and co-workers reported a series of bulkier BPs, such as **4.10** and **4.12** (**Fig. 4.5**) that are selective to hGGPPS but the IC_{50} values of these compounds were only about 3-4 μM .⁶⁴ Initial attempts to replace one of the phosphonate groups of **4.9** with a sulfonic acid (e.g. compound **4.11**)⁶⁶ resulted in a complete loss of activity suggesting the importance of the bisphosphonate anchor in the activity of this particular compound. The same group reported dual hFPPS/hGGPPS inhibitors with better *in vivo* activity than the clinical *N*-BPs, which can be attributed to the

enhanced cell membrane permeability and possible prevention of cross-prenylation (since both FPP and GPP levels are depleted). For example, alkyl-containing pyridinium bisphosphonate **4.13** was >100-fold more potent than ZOL in tumor cell growth inhibition.⁶⁵ Wiemer and colleagues, on the other hand, incorporated terpenoid side chains in their design of bisphosphonate inhibitors as in the case of digeranyl methylene bisphosphonate **4.14**, which was selective in hGGPPS over hFPPS and was active against human-derived K562 leukemia cells^{67, 68} and of compound **4.15**, which is the most potent hGGPPS inhibitor known to date (in terms of *in vitro* potency) with anti-myeloma properties.⁶⁹ Non-bisphosphonate inhibitors of hGGPPS are virtually unknown; Chen *et al.* reported the sulfonic acid-based compound **4.16** to inhibit hGGPPS;⁷⁰ however, in addition to the very weak potency *in vitro* ($IC_{50} = 31 \mu\text{M}$), the structure of compound **4.16** is definitely not “drug-like” due to the presence of reactive and labile groups (e.g. hydrazone). Inhibitors of hGGPPS modified with a POM prodrug have been also reported,⁷¹ the most recent example is compound **4.17**.⁷² In our preliminary search of hGGPPS inhibitors, thieno[2,3-*d*]pyrimidine-based compounds substituted at C-2 and C-6 positions (**5.28a** and **5.28v**, respectively)⁷³ were found to inhibit hGGPPS; however, fine-tuning is necessary as these compounds also showed some activity against hFPPS.

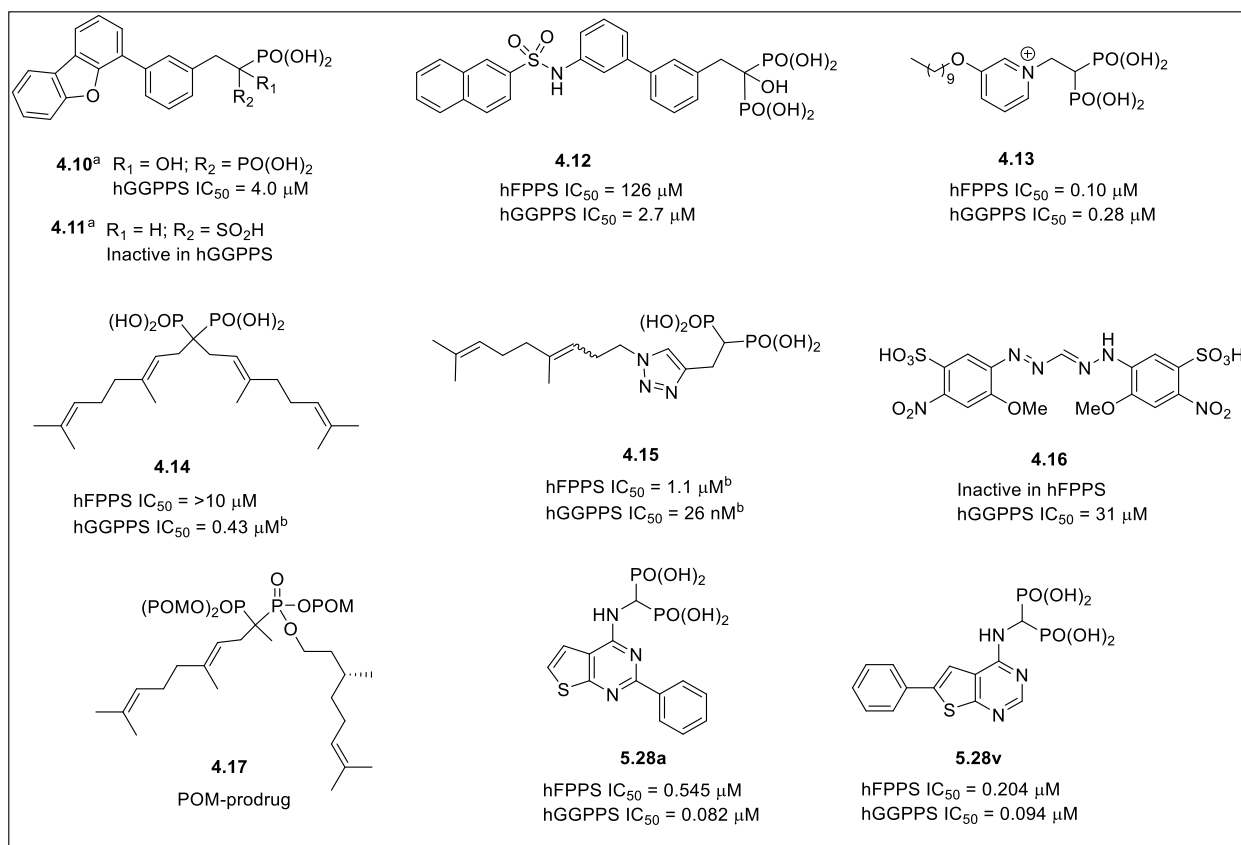


Figure 4.5. Examples of hGGPPS inhibitors. (^aActivity in hFPPS not available or reported; ^b IC_{50} values obtained from our own *in vitro* assay using the wild-type enzymes.

4.7. Research Goals (Part 2)

Recent investigations strongly implicate GGPP-mediated biochemical pathways in modulating a range of disease pathologies. Control of the intracellular levels of this isoprenoid *via* selective inhibition of the hGGPPS will be very useful in elucidating disease mechanisms and to the validation of this enzyme as a pharmacological target. Therefore, our current goals are to identify and develop selective hGGPPS inhibitors for this purpose. The synthesis, SAR, and biological evaluation of our novel hGGPPS inhibitors are presented in **Chapter 5**.

4.8. References

1. Park, J.; Matralis, A.; Berghuis, A. M.; Tsantrizos, Y. S. Human isoprenoid synthase enzymes as therapeutic targets. *Front. Chem.* **2014**, *2*, 1-21.
2. Holstein, S. A. Chapter 12 - The isoprenoid biosynthetic pathway and statins. In *The Enzymes*, Christine A. Hrycyna, M. O. B.; Fuyuhiko, T., Eds. Academic Press: 2011; Vol. 30, pp 279-299.
3. Oldfield, E. Targeting isoprenoid biosynthesis for drug discovery: Bench to bedside. *Acc. Chem. Res.* **2010**, *43*, 1216-1226.
4. Tobert, J. A. Lovastatin and beyond: the history of the HMG-CoA reductase inhibitors. *Nat. Rev. Drug Discov.* **2003**, *2*, 517-526.
5. Roelofs, A. J.; Thompson, K.; Gordon, S.; Rogers, M. J. Molecular mechanisms of action of bisphosphonates: Current status. *Clin. Cancer Res.* **2006**, *12*, 6222s-6230s.
6. Kavanagh, K. L.; Guo, K.; Dunford, J. E.; Wu, X.; Knapp, S.; Ebetino, F. H.; Rogers, M. J.; Russell, R. G. G.; Oppermann, U. The molecular mechanism of nitrogen-containing bisphosphonates as antiosteoporosis drugs. *Proc. Natl. Acad. Sci.* **2006**, *103*, 7829-7834.
7. Kavanagh, K. L.; Dunford, J. E.; Bunkoczi, G.; Russell, R. G. G.; Oppermann, U. The crystal structure of human geranylgeranyl pyrophosphate synthase reveals a novel hexameric arrangement and inhibitory product binding. *J. Biol. Chem.* **2006**, *281*, 22004-22012.
8. Wiemer, A. J.; Wiemer, D. F.; Hohl, R. J. Geranylgeranyl diphosphate synthase: An emerging therapeutic target. *Clin. Pharmacol. Ther.* **2011**, *90*, 804-812.
9. Berndt, N.; Hamilton, A. D.; Sebt, S. M. Targeting protein prenylation for cancer therapy. *Nat. Rev. Cancer* **2011**, *11*, 775-791.
10. Palsuledesai, C. C.; Distefano, M. D. Protein prenylation: Enzymes, therapeutics, and biotechnology applications. *ACS Chem. Biol.* **2015**, *10*, 51-62.
11. Philips, M. R.; Cox, A. D. Geranylgeranyltransferase I as a target for anti-cancer drugs. *J. Clin. Invest.* *117*, 1223-1225.
12. Ochocki, J. D.; Distefano, M. D. Prenyltransferase inhibitors: treating human ailments from cancer to parasitic infections. *Med. Chem. Commun.* **2013**, *4*, 476-492.
13. World Health Organization. Dementia Fact Sheet. www.who.int/mediacentre/factsheets. April 2016.

14. Silva, T.; Teixeira, J.; Remião, F.; Borges, F. Alzheimer's disease, cholesterol, and statins: The junctions of important metabolic pathways. *Angew. Chem. Int. Ed.* **2013**, *52*, 1110-1121.
15. Di Paolo, G.; Kim, T.-W. Linking lipids to Alzheimer's disease: cholesterol and beyond. *Nat. Rev. Neurosci.* **2011**, *12*, 284-296.
16. Goedert, M.; Spillantini, M. G. A century of alzheimer's disease. *Science* **2006**, *314*, 777-781.
17. Cole, S. L.; Vassar, R. Isoprenoids and alzheimer's disease: A complex relationship. *Neurobiol. Dis.* **2006**, *22*, 209-222.
18. Sparks, D. L.; Scheff, S. W.; Hunsaker Iii, J. C.; Liu, H.; Landers, T.; Gross, D. R. Induction of alzheimer-like β -amyloid immunoreactivity in the brains of rabbits with dietary cholesterol. *Exp. Neurol.* **1994**, *126*, 88-94.
19. Refolo, L. M.; Pappolla, M. A.; Malester, B.; LaFrancois, J.; Bryant-Thomas, T.; Wang, R.; Tint, G. S.; Sambamurti, K.; Duff, K. Hypercholesterolemia accelerates the alzheimer's amyloid pathology in a transgenic mouse model. *Neurobiol. Dis.* **2000**, *7*, 321-331.
20. Jick, H.; Zornberg, G. L.; Jick, S. S.; Seshadri, S.; Drachman, D. A. Statins and the risk of dementia. *Lancet* **2000**, *356*, 1627-1631.
21. Wolozin, B.; Wang, S. W.; Li, N.-C.; Lee, A.; Lee, T. A.; Kazis, L. E. Simvastatin is associated with a reduced incidence of dementia and Parkinson's disease. *BMC Med.* **2007**, *5*, 1-11.
22. Riekse, R. G.; Li, G.; Petrie, E. C.; Leverenz, J. B.; Vavrek, D.; Vuletic, S.; Albers, J. J.; Montine, T. J.; Lee, V. M.-Y.; Lee, M. Effect of statins on Alzheimer's disease biomarkers in cerebrospinal fluid. *J. Alzheimers Dis.* **2006**, *10*, 399-406.
23. Eckert, G. P.; Hooff, G. P.; Strandjord, D. M.; Igbavboa, U.; Volmer, D. A.; Müller, W. E.; Wood, W. G. Regulation of the brain isoprenoids farnesyl- and geranylgeranylpyrophosphate is altered in male Alzheimer patients. *Neurobiol. Dis.* **2009**, *35*, 251-257.
24. Hooff, G. P.; Volmer, D. A.; Wood, W. G.; Müller, W. E.; Eckert, G. P. Isoprenoid quantitation in human brain tissue: a validated HPLC-fluorescence detection method for endogenous farnesyl- (FPP) and geranylgeranylpyrophosphate (GGPP). *Anal. Bioanal. Chem.* **2008**, *392*, 673-680.

25. Tong, H.; Wiemer, A. J.; Neighbors, J. D.; Hohl, R. J. Quantitative determination of farnesyl and geranylgeranyl diphosphate levels in mammalian tissue. *Anal. Biochem.* **2008**, *378*, 138-143.
26. Lee, M.; You, H.-J.; Cho, S.-H.; Woo, C.-H.; Yoo, M.-H.; Joe, E.-H.; Kim, J.-H. Implication of the small GTPase Rac1 in the generation of reactive oxygen species in response to β -amyloid in C6 astrogloma cells. *Biochem. J.* **2002**, *366*, 937-943.
27. Gao, S.; Yu, R.; Zhou, X. The role of geranylgeranyltransferase I-mediated protein prenylation in the brain. *Mol. Neurobiol.* **2015**, 1-13.
28. Ohm, T. G.; Treiber-Held, S.; Distl, R.; Glöckner, F.; Schönheit, B.; Tamanai, M.; Meske, V. Cholesterol and tau protein - Findings in Alzheimer's and Niemann Pick C's disease. *Pharmacopsychiatry* **2003**, *36*, 120-126.
29. Sayas, C. L.; Moreno-Flores, M. T.; Avila, J.; Wandosell, F. The neurite retraction induced by lysophosphatidic acid increases Alzheimer's disease-like tau phosphorylation. *J. Biol. Chem.* **1999**, *274*, 37046-37052.
30. De Schutter, J. W.; Park, J.; Leung, C. Y.; Gormley, P.; Lin, Y.-S.; Hu, Z.; Berghuis, A. M.; Poirier, J.; Tsantrizos, Y. S. Multistage screening reveals chameleon ligands of the human farnesyl pyrophosphate synthase: Implications to drug discovery for neurodegenerative diseases. *J. Med. Chem.* **2014**, *57*, 5764-5776.
31. Raab, M. S.; Podar, K.; Breitkreutz, I.; Richardson, P. G.; Anderson, K. C. Multiple myeloma. *Lancet* **2009**, *374*, 324-339.
32. National Cancer Institute SEER Stat Fact Sheets: Myeloma. seer.cancer.gov/statfacts/html/mulmy.html. June 2016
33. Morgan, G. J.; Davies, F. E.; Gregory, W. M.; Cocks, K.; Bell, S. E.; Szubert, A. J.; Navarro-Coy, N.; Drayson, M. T.; Owen, R. G.; Feyler, S.; Ashcroft, A. J.; Ross, F.; Byrne, J.; Roddie, H.; Rudin, C.; Cook, G.; Jackson, G. H.; Child, J. A. First-line treatment with zoledronic acid as compared with clodronic acid in multiple myeloma (MRC Myeloma IX): a randomised controlled trial. *Lancet* **2010**, *376*, 1989-1999.
34. Morgan, G. J.; Davies, F. E.; Gregory, W. M.; Szubert, A. J.; Bell, S. E.; Drayson, M. T.; Owen, R. G.; Ashcroft, A. J.; Jackson, G. H.; Child, J. A. Effects of induction and maintenance plus long-term bisphosphonates on bone disease in patients with multiple myeloma: the Medical Research Council Myeloma IX trial. *Blood* **2012**, *119*, 5374-5383.

35. Coleman, R. The use of bisphosphonates in cancer treatment. *Ann. N. Y. Acad. Sci.* **2011**, 1218, 3-14.
36. Terpos, E.; Berenson, J.; Raje, N.; Roodman, G. D. Management of bone disease in multiple myeloma. *Expert Rev. Hematol.* **2014**, 7, 113-125.
37. Guenther, A.; Gordon, S.; Tiemann, M.; Burger, R.; Bakker, F.; Green, J. R.; Baum, W.; Roelofs, A. J.; Rogers, M. J.; Gramatzki, M. The bisphosphonate zoledronic acid has antimyeloma activity in vivo by inhibition of protein prenylation. *Int. J. Cancer* **2010**, 126, 239-246.
38. Holstein, S. A.; Hohl, R. J. Isoprenoid biosynthetic pathway inhibition disrupts monoclonal protein secretion and induces the unfolded protein response pathway in multiple myeloma cells. *Leuk. Res.* **2011**, 35, 551-559.
39. Pandyra, A. A.; Mullen, P. J.; Goard, C. A.; Ericson, E.; Sharma, P.; Kalkat, M.; Yu, R.; Pong, J. T.; Brown, K. R.; Hart, T.; Gebbia, M.; Lang, K. S.; Giaever, G.; Nislow, C.; Moffat, J.; Penn, L. Z. Genome-wide RNAi analysis reveals that simultaneous inhibition of specific mevalonate pathway genes potentiates tumor cell death. *Oncotarget* **2015**, 6, 26909-26921.
40. Freed-Pastor, William A.; Mizuno, H.; Zhao, X.; Langerød, A.; Moon, S.-H.; Rodriguez-Barrueco, R.; Barsotti, A.; Chicas, A.; Li, W.; Polotskaia, A.; Bissell, Mina J.; Osborne, Timothy F.; Tian, B.; Lowe, Scott W.; Silva, Jose M.; Børresen-Dale, A.-L.; Levine, Arnold J.; Bargonetti, J.; Prives, C. Mutant p53 disrupts mammary tissue architecture via the mevalonate pathway. *Cell* **2012**, 148, 244-258.
41. Chapman, M. A.; Lawrence, M. S.; Keats, J. J.; Cibulskis, K.; Sougnez, C.; Schinzel, A. C.; Harview, C. L.; Brunet, J.-P.; Ahmann, G. J.; Adli, M.; Anderson, K. C.; Ardlie, K. G.; Auclair, D.; Baker, A.; Bergsagel, P. L.; Bernstein, B. E.; Drier, Y.; Fonseca, R.; Gabriel, S. B.; Hofmeister, C. C.; Jagannath, S.; Jakubowiak, A. J.; Krishnan, A.; Levy, J.; Liefeld, T.; Lonial, S.; Mahan, S.; Mfuko, B.; Monti, S.; Perkins, L. M.; Onofrio, R.; Pugh, T. J.; Rajkumar, S. V.; Ramos, A. H.; Siegel, D. S.; Sivachenko, A.; Stewart, A. K.; Trudel, S.; Vij, R.; Voet, D.; Winckler, W.; Zimmerman, T.; Carpten, J.; Trent, J.; Hahn, W. C.; Garraway, L. A.; Meyerson, M.; Lander, E. S.; Getz, G.; Golub, T. R. Initial genome sequencing and analysis of multiple myeloma. *Nature* **2011**, 471, 467-472.

42. Whyte, D. B.; Kirschmeier, P.; Hockenberry, T. N.; Nunez-Oliva, I.; James, L.; Catino, J. J.; Bishop, W. R.; Pai, J.-K. K- and N-Ras are geranylgeranylated in cells treated with farnesyl protein transferase inhibitors. *J. Biol. Chem.* **1997**, 272, 14459-14464.
43. Konstantinopoulos, P. A.; Karamouzis, M. V.; Papavassiliou, A. G. Post-translational modifications and regulation of the RAS superfamily of GTPases as anticancer targets. *Nat. Rev. Drug Discov.* **2007**, 6, 541-555.
44. Gelb, M. H.; Brunsveld, L.; Hrycyna, C. A.; Michaelis, S.; Tamanoi, F.; Van Voorhis, W. C.; Waldmann, H. Therapeutic intervention based on protein prenylation and associated modifications. *Nat. Chem. Biol.* **2006**, 2, 518-528.
45. PTX-100 (GGTI-2418). prescienttherapeutics.com. April 2016.
46. Guo, Z.; Wu, Y. W.; Das, D.; Delon, C.; Cramer, J.; Yu, S.; Thuns, S.; Lupilova, N.; Waldmann, H.; Brunsveld, L.; Goody, R. S.; Alexandrov, K.; Blankenfeldt, W. Structures of RabGGTase–substrate/product complexes provide insights into the evolution of protein prenylation. *EMBO J.* **2008**, 27, 2444-2456.
47. Baron, R. A.; Tavaré, R.; Figueiredo, A. C.; Błażewska, K. M.; Kashemirov, B. A.; McKenna, C. E.; Ebetino, F. H.; Taylor, A.; Rogers, M. J.; Coxon, F. P.; Seabra, M. C. Phosphonocarboxylates inhibit the second geranylgeranyl addition by Rab geranylgeranyl transferase. *J. Biol. Chem.* **2009**, 284, 6861-6868.
48. Bon, R. S.; Guo, Z.; Stigter, E. A.; Wetzel, S.; Menninger, S.; Wolf, A.; Choidas, A.; Alexandrov, K.; Blankenfeldt, W.; Goody, R. S.; Waldmann, H. Structure-guided development of selective RabGGTase inhibitors. *Angew. Chem. Int. Ed.* **2011**, 50, 4957-4961.
49. Hosfield, D. J.; Zhang, Y.; Dougan, D. R.; Broun, A.; Tari, L. W.; Swanson, R. V.; Finn, J. Structural basis for bisphosphonate-mediated inhibition of isoprenoid biosynthesis. *J. Biol. Chem.* **2004**, 279, 8526-8529.
50. Dunford, J. E.; Kwaasi, A. A.; Rogers, M. J.; Barnett, B. L.; Ebetino, F. H.; Russell, R. G. G.; Oppermann, U.; Kavanagh, K. L. Structure–activity relationships among the nitrogen containing bisphosphonates in clinical use and other analogues: Time-dependent inhibition of human farnesyl pyrophosphate synthase. *J. Med. Chem.* **2008**, 51, 2187-2195.
51. Senaratne, S. G.; Pirianov, G.; Mansi, J. L.; Arnett, T. R.; Colston, K. W. Bisphosphonates induce apoptosis in human breast cancer cell lines. *Br. J. Cancer* **2000**, 82, 1459-1468.

52. Jagdev, S. P.; Coleman, R. E.; Shipman, C. M.; Rostami-H, A.; Croucher, P. I. The bisphosphonate, zoledronic acid, induces apoptosis of breast cancer cells: evidence for synergy with paclitaxel. *Br. J. Cancer* **2001**, 84, 1126-1134.
53. Goffinet, M.; Thoulouzan, M.; Pradines, A.; Lajoie-Mazenc, I.; Weinbaum, C.; Faye, J.; Séronie-Vivien, S. Zoledronic acid treatment impairs protein geranyl-geranylation for biological effects in prostatic cells. *BMC Cancer* **2006**, 6, 1-10.
54. Tassone, P.; Forciniti, S.; Galea, E.; Morrone, G.; Turco, M. C.; Martinelli, V.; Tagliaferri, P.; Venuta, S. Growth inhibition and synergistic induction of apoptosis by zoledronate and dexamethasone in human myeloma cell lines. *Leukemia* **2000**, 14, 841.
55. Saari, W. S.; Anderson, P. S. Acyloxymethyl esters of bisphosphonic acids as bone resorption inhibitors. 5227506, 1993.
56. Zhang, Y.; Leon, A.; Song, Y.; Studer, D.; Haase, C.; Koscielski, L. A.; Oldfield, E. Activity of nitrogen-containing and non-nitrogen-containing bisphosphonates on tumor cell lines. *J. Med. Chem.* **2006**, 49, 5804-5814.
57. Marma, M. S.; Xia, Z.; Stewart, C.; Coxon, F.; Dunford, J. E.; Baron, R.; Kashemirov, B. A.; Ebetino, F. H.; Triffitt, J. T.; Russell, R. G. G.; McKenna, C. E. Synthesis and biological evaluation of α -halogenated bisphosphonate and phosphonocarboxylate analogues of risedronate. *J. Med. Chem.* **2007**, 50, 5967-5975.
58. Shmeeda, H.; Amitay, Y.; Gorin, J.; Tzemach, D.; Mak, L.; Ogorka, J.; Kumar, S.; Zhang, J. A.; Gabizon, A. Delivery of zoledronic acid encapsulated in folate-targeted liposome results in potent in vitro cytotoxic activity on tumor cells. *J. Control. Release* **2010**, 146, 76-83.
59. Caraglia, M.; Luongo, L.; Salzano, G.; Zappavigna, S.; Marra, M.; Guida, F.; Lusa, S.; Giordano, C.; De Novellis, V.; Rossi, F.; Abbruzzese Saccardi, A.; De Rosa, G.; Maione, S. Stealth liposomes encapsulating zoledronic acid: A new opportunity to treat neuropathic pain. *Mol. Pharm.* **2013**, 10, 1111-1118.
60. Lin, Y.-S.; Park, J.; De Schutter, J. W.; Huang, X. F.; Berghuis, A. M.; Sebag, M.; Tsantrizos, Y. S. Design and synthesis of active site inhibitors of the human farnesyl pyrophosphate synthase: Apoptosis and inhibition of ERK phosphorylation in multiple myeloma cells. *J. Med. Chem.* **2012**, 55, 3201-3215.

61. Leung, C. Y.; Park, J.; De Schutter, J. W.; Sebag, M.; Berghuis, A. M.; Tsantrizos, Y. S. Thienopyrimidine bisphosphonate (ThPBP) inhibitors of the human farnesyl pyrophosphate synthase: Optimization and characterization of the mode of inhibition. *J. Med. Chem.* **2013**, *56*, 7939-7950.
62. Jahnke, W.; Rondeau, J.-M.; Cotesta, S.; Marzinzik, A.; Pellé, X.; Geiser, M.; Strauss, A.; Götte, M.; Bitsch, F.; Hemmig, R.; Henry, C.; Lehmann, S.; Glickman, J. F.; Roddy, T. P.; Stout, S. J.; Green, J. R. Allosteric non-bisphosphonate FPPS inhibitors identified by fragment-based discovery. *Nat. Chem. Biol.* **2010**, *6*, 660-666.
63. Marzinzik, A. L.; Amstutz, R.; Bold, G.; Bourgier, E.; Cotesta, S.; Glickman, J. F.; Götte, M.; Henry, C.; Lehmann, S.; Hartweg, J. C. D.; Ofner, S.; Pellé, X.; Roddy, T. P.; Rondeau, J.-M.; Stauffer, F.; Stout, S. J.; Widmer, A.; Zimmermann, J.; Zoller, T.; Jahnke, W. Discovery of novel allosteric non-bisphosphonate inhibitors of farnesyl pyrophosphate synthase by integrated lead finding. *ChemMedChem* **2015**, *10*, 1884-1891.
64. Guo, R.-T.; Cao, R.; Liang, P.-H.; Ko, T.-P.; Chang, T.-H.; Hudock, M. P.; Jeng, W.-Y.; Chen, C. K.-M.; Zhang, Y.; Song, Y.; Kuo, C.-J.; Yin, F.; Oldfield, E.; Wang, A. H.-J. Bisphosphonates target multiple sites in both cis- and trans-prenyltransferases. *Proc. Natl. Acad. Sci.* **2007**, *104*, 10022-10027.
65. Zhang, Y.; Cao, R.; Yin, F.; Hudock, M. P.; Guo, R.-T.; Krysiak, K.; Mukherjee, S.; Gao, Y.-G.; Robinson, H.; Song, Y.; No, J. H.; Bergan, K.; Leon, A.; Cass, L.; Goddard, A.; Chang, T.-K.; Lin, F.-Y.; Beek, E. V.; Papapoulos, S.; Wang, A. H. J.; Kubo, T.; Ochi, M.; Mukkamala, D.; Oldfield, E. Lipophilic bisphosphonates as dual farnesyl/geranylgeranyl diphosphate synthase inhibitors: An X-ray and NMR investigation. *J. Am. Chem. Soc.* **2009**, *131*, 5153-5162.
66. Chen, C. K. M.; Hudock, M. P.; Zhang, Y.; Guo, R.-T.; Cao, R.; No, J. H.; Liang, P.-H.; Ko, T.-P.; Chang, T.-H.; Chang, S.-c.; Song, Y.; Axelson, J.; Kumar, A.; Wang, A. H. J.; Oldfield, E. Inhibition of geranylgeranyl diphosphate synthase by bisphosphonates: A crystallographic and computational investigation. *J. Med. Chem.* **2008**, *51*, 5594-5607.
67. Shull, L. W.; Wiemer, A. J.; Hohl, R. J.; Wiemer, D. F. Synthesis and biological activity of isoprenoid bisphosphonates. *Bioorg. Med. Chem.* **2006**, *14*, 4130-4136.

68. Wiemer, A. J.; Tong, H.; Swanson, K. M.; Hohl, R. J. Digeranyl bisphosphonate inhibits geranylgeranyl pyrophosphate synthase. *Biochem. Biophys. Res. Commun.* **2007**, 353, 921-925.
69. Wills, V. S.; Allen, C.; Holstein, S. A.; Wiemer, D. F. Potent triazole bisphosphonate inhibitor of geranylgeranyl diphosphate synthase. *ACS Med. Chem. Lett.* **2015**, 6, 1195-1198.
70. Chen, S.-H.; Lin, S.-W.; Lin, S.-R.; Liang, P.-H.; Yang, J.-M. Moiety-linkage map reveals selective nonbisphosphonate inhibitors of human geranylgeranyl diphosphate synthase. *J. Chem. Inf. Model.* **2013**, 53, 2299-2311.
71. Wiemer, A. J.; Yu, J. S.; Shull, L. W.; Barney, R. J.; Wasko, B. M.; Lamb, K. M.; Hohl, R. J.; Wiemer, D. F. Pivaloyloxymethyl-modified isoprenoid bisphosphonates display enhanced inhibition of cellular geranylgeranylation. *Bioorg. Med. Chem.* **2008**, 16, 3652-3660.
72. Foust, B. J.; Allen, C.; Holstein, S. A.; Wiemer, D. F. A new motif for inhibitors of geranylgeranyl diphosphate synthase. *Bioorg. Med. Chem.* **2016**, 24, 3734-3741.
73. Leung, C.-Y.; Langille, A. M.; Mancuso, J.; Tsantrizos, Y. S. Discovery of thienopyrimidine-based inhibitors of the human farnesyl pyrophosphate synthase—Parallel synthesis of analogs via a trimethylsilyl ylidene intermediate. *Bioorg. Med. Chem.* **2013**, 21, 2229-2240.

CHAPTER 5: Potent and Selective Thieno[2,3-*d*]pyrimidine-Based Inhibitors of the Human Geranylgeranyl Pyrophosphate Synthase (hGGPPS): Implications for Drug Discovery

5.1. Preface

This chapter describes our multidisciplinary studies toward the discovery of high affinity and selective inhibitors of hGGPPS. Parts of this chapter will be submitted for publication in two separate manuscripts, one in collaboration with the groups of Prof. Albert Berghuis (Department of Biochemistry, McGill University) and Dr. Michael Sebag (Division of Haematology, McGill University Health Center) and another one in collaboration with the group of Dr. Judes Poirier (Douglas Mental Health University Institute). I performed the synthesis of the majority of the inhibitors shown in **Fig. 5.5** (as well as the literature control compound **4.15**;⁵⁰ **Fig. 4.5**; **Chapter 4**) except for the following, which were made by former graduate students of our group: Viviane Ta (inhibitors: **5.28c**, **5.28d**, **5.28n**, and **5.28x**) and Benita Kapuku (inhibitors: **5.28b**, **5.28f**, and **5.28g**). I also conducted part of the *in vitro* hFPPS and hGGPPS bioassays with the help of Linda Do, our research assistant. Recombinant hFPPS and hGGPPS enzymes were expressed and purified by other members of the group: Viviane Ta, Eleni Ladopoulou, and Xue Bin in collaboration with Dr. Jaek Park and Prof. Albert Berghuis. The cell-based antiproliferation assay in multiple myeloma, Western blot analysis to detect non-geranylgeranylated Rap1A, and flow cytometry to detect cell apoptosis were performed by Xian Fang Huang and Dr. Daniel D. Waller in the laboratory of Dr. Michael Sebag. Lastly, measurement of phosphorylated tau levels in immortalized human neuroblastoma cells was carried out by Dr. Sandra Pelleieux in the laboratory of Dr. Judes Poirier.

5.2. Abstract

The human geranylgeranyl pyrophosphate synthase (hGGPPS) controls the intracellular levels of the C₂₀ isoprenoid GGPP that is used in the post-translational prenylation of signaling proteins essential for various cellular functions. Bisphosphonates (BPs) are known to inhibit hFPPS and hGGPPS; however, selective inhibition of hGGPPS with potent BPs is limited to substrate-like compounds, such as **4.14** and **4.15** (**Fig. 4.5; Chapter 4**). It is noteworthy that these compounds (**4.14** and **4.15**) are expected to suffer from low chemical and metabolic stability and their structures are not considered to be “drug-like.” In contrast, the thienopyrimidine scaffold is a privileged motif in drug discovery and consequently, we chose to investigate the ability of such bisphosphonates to inhibit hGGPPS. Our studies identified potent and selective thieno[2,3-*d*]pyrimidine bisphosphonates (ThP-BPs) that possess anti-myeloma activity and downregulate the intracellular P-Tau accumulation in human immortalized neurons. Overall, our ThP-BPs provided valuable chemical probes for exploring the role of hGGPPS in multiple myeloma and neurodegeneration. As part of our drug discovery programs, our preliminary SAR also provided lead compounds for further optimization.

5.3. Introduction

The development of effective chemical probes or small-molecule “tools” for the study of protein functions and other biological processes is integral for answering mechanistic and phenotypic questions about a biological target that can lead in the successful delivery of novel therapeutics.¹ When complemented with other tools in molecular genetics and chemical biology, the use of such probes can be quite effective in validating new pharmacological targets.² Moreover, design of high quality probes is of vital importance even at the early stage of the drug discovery process as the data generated have to be meaningful, *i.e.* do not lead to misinterpretation or incorrect conclusions,

as in the case of a number of “frequent hitters” or promiscuous and reactive compounds, referred as pan assay interference compounds (PAINS) that have caused significant wasted time, money and resources (examples are shown in **Fig. 5.1**).^{3, 4} Designing small-molecule probes tailored in generating a structurally diverse library of compounds that simultaneously incorporate drug-like physicochemical features and follow general guidelines, such as the Lipinski’s “rule of five” (Ro5) can be beneficial in generating high-quality compounds with optimal biological activity and ADME (adsorption, distribution, metabolism, and excretion). Generally, the Ro5 states that an orally active drug adheres to the following criteria without violating more than two of them: (a) molecular weight of less than 500 Da; (b) octanol-water partition coefficient (logP) of less than 5; (c) no more than 5 hydrogen bond donors; and (d) no more than 10 hydrogen bond acceptors.^{5, 6} While the Ro5 and other similar guidelines⁷⁻¹¹ do not holistically represent all approved drugs in the market, they are nonetheless useful in filtering out potential problematic compounds that typically result from high throughput screening (HTS) campaigns.

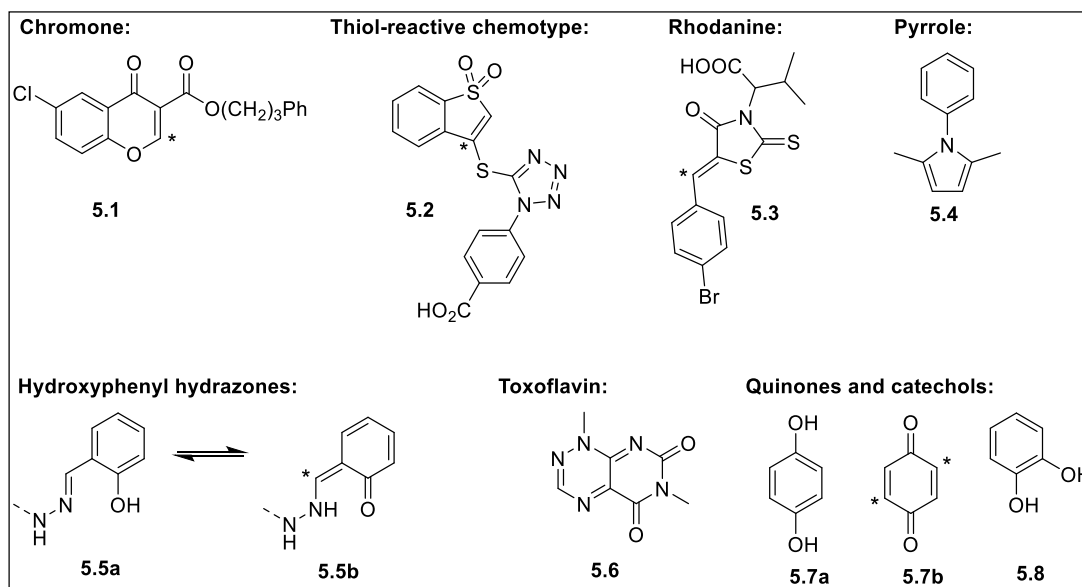


Figure 5.1. Examples of PAINS.^{3,4,12} Compounds that can act as Michael acceptors are susceptible to react with biologically relevant nucleophiles (e.g. **5.1-5.3**, **5.5b** and **5.7b**; the asterick indicates

the site of attack); the instability of **5.4** is suspected to give degradation products leading to false positives; toxoflavin (**5.6**) can convert O₂ to H₂O₂ through its reduction-oxidation (redox) capability; H₂O₂ can activate or inactivate proteins; quinones and catechols (**5.7** to **5.8**) are also known to be redox-active and covalent modifiers.

The thienopyrimidine scaffold, which can exist in three isomeric forms (**Fig. 5.2**)¹³ has been shown to exhibit a wide range of biological activities. The favorable biopharmaceutical profile and ability to serve as mimics of adenine nucleobase¹⁴ are the main reasons why this core is typically incorporated in the design of bioactive compounds. Of particular interest are the thieno[2,3-*d*]pyrimidines, which played a key role in the development of several compounds with antifungal¹⁵ and antimicrobial properties,¹⁶ antiviral activities,¹⁴ immunosuppressive activity (e.g. **5.9**; **Fig. 5.2**),¹⁷ anti-cancer activities (e.g. phosphoinositide 3-kinase α inhibitor **5.10**¹⁸ and protein kinase R (PKR)-like endoplasmic reticulum kinase (PERK) inhibitor **5.11**¹⁹), as antagonists of the adenosine A_{2A} receptor (for Parkinson's disease; e.g. **5.12**),^{20, 21} and as modulators of γ -secretase (for Alzheimer's disease; e.g. **5.13**).²² Additionally, our group also recently reported new structural classes of active site and allosteric inhibitors of the human farnesyl pyrophosphate synthase (hFPPS) bearing this scaffold that have potential applications in the treatment of bone and non-bone related diseases associated with hFPPS activity (**4.6** and **4.9**, **Fig. 4.3**; **Chapter 4**).^{23, 24}

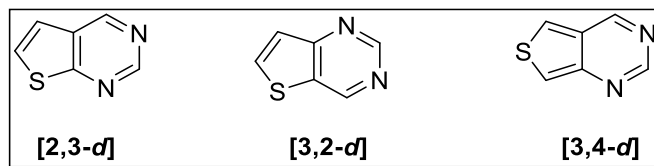


Figure 5.2. Thienopyrimidines structural isomers.

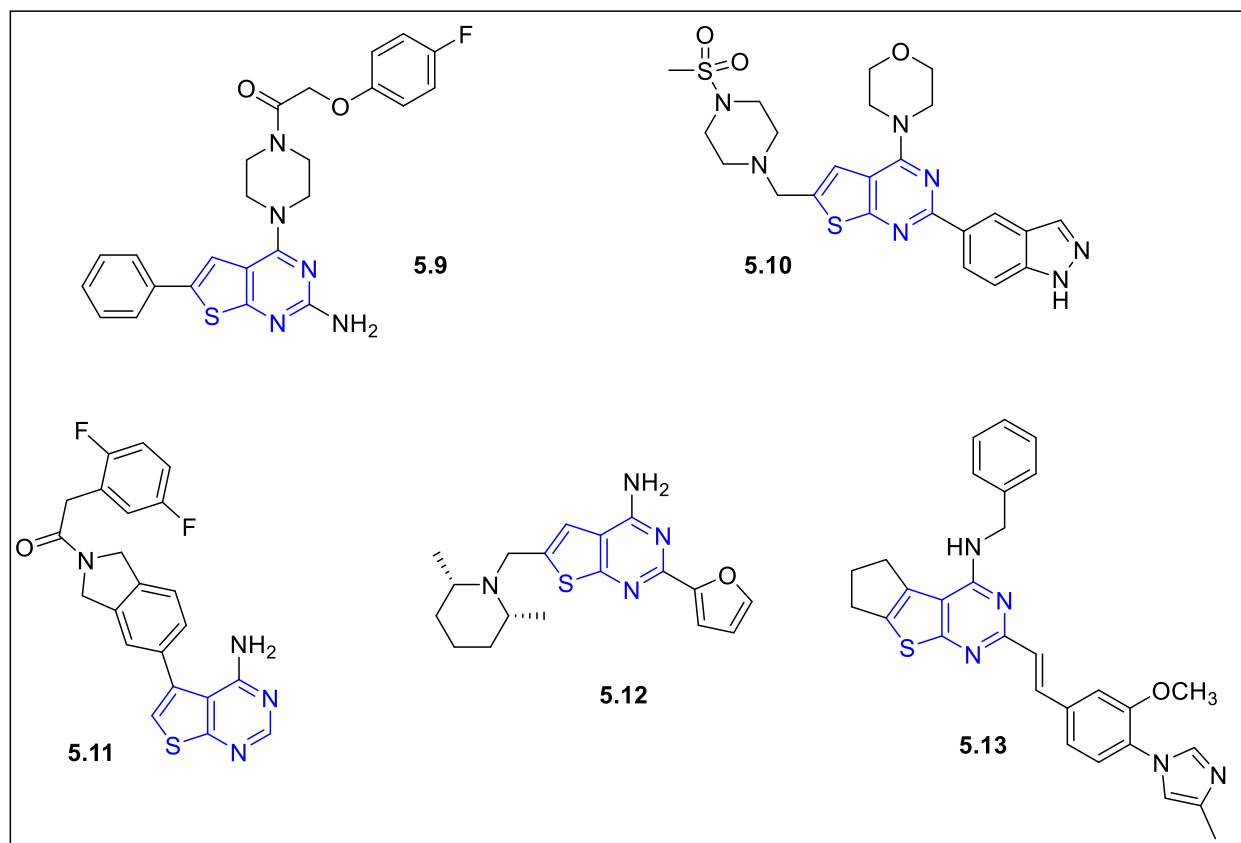
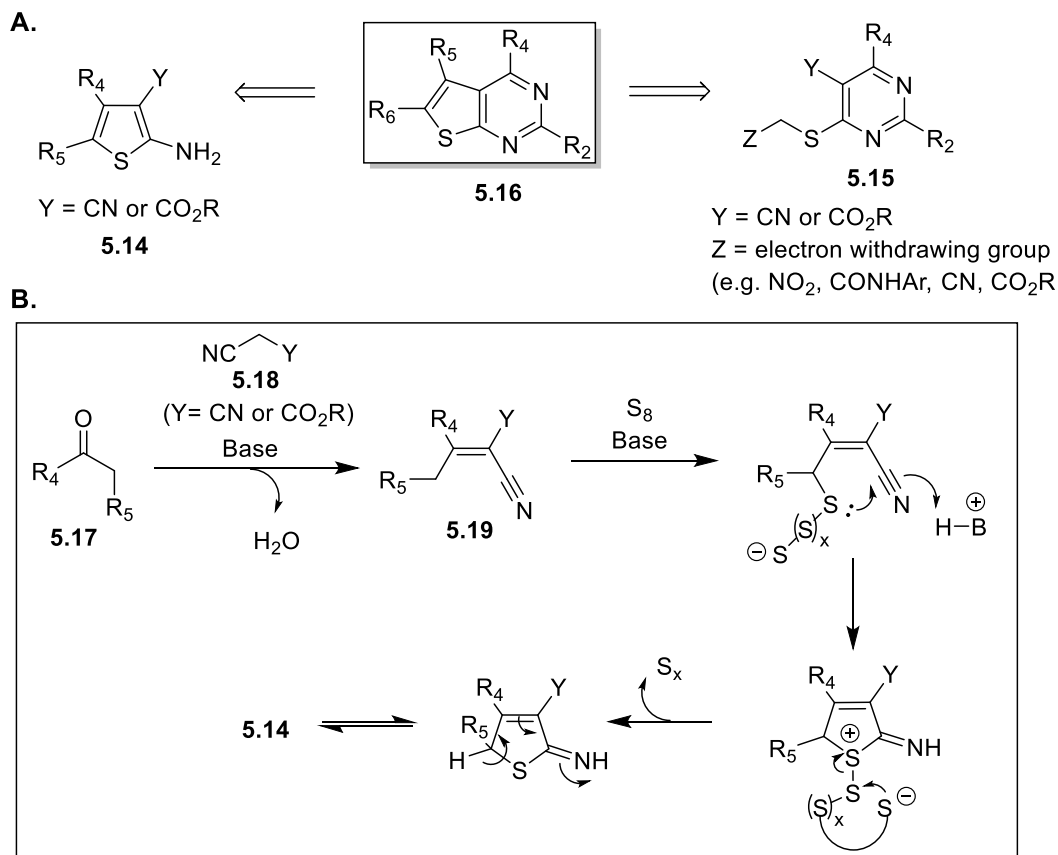


Figure 5.3. Examples of bioactive thieno[2,3-*d*]pyrimidines.

Synthesis of substituted thieno[2,3-*d*]pyrimidines **5.16** can be achieved from both pyrimidine-**5.15**^{25, 26} or thiophene- **5.14** precursors (**Scheme 5.1A**).^{27, 28} The 2-aminothiophenes **5.14**, which is readily accessible *via* the Gewald reaction²⁹⁻³¹ provides a convenient approach to build analogs of **5.16**. The classical Gewald synthesis is a multicomponent reaction involving a carbonyl compound (aldehyde or ketone; **5.17**, **Scheme 5.1B**) that undergoes Knoevenagel condensation with an activated nitrile **5.18**, e.g. malononitrile (Y= CN) or α -cyanoester (Y= CO₂R) to give the ylidene intermediate **5.19**. This is followed by the addition of elemental sulfur in the presence of a base affording the desired thiophene core. Thiophene **5.14** can then be assembled to thienopyrimidine compounds in various ways depending on the position of the substitution.

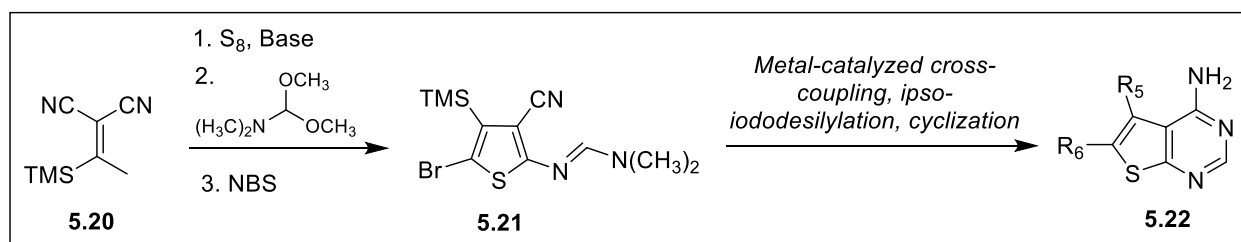


Scheme 5.1. (A) Synthetic approaches for **5.16**; (B) Gewald reaction mechanism leading to 2-aminothiophene-precursor (**5.14**) of thieno[2,3-*d*]pyrimidines.

With our current goal of investigating analogs of C-2 and/or C-6 substituted thieno[2,3-*d*]pyrimidine bisphosphonates (ThP-BPs) in modulating hGGPPS, a synthetic approach to access such compounds was developed. We disclose herein the results of our studies leading to the identification of hGGPPS inhibitors with nanomolar *in vitro* potency (~50-100 nM) and good selectivity versus hFPPS (~10 to 60-fold difference). Several analogs also disrupt cellular protein geranylgeranylation, exhibit antiproliferation activities in three different multiple myeloma tumor cell lines, and block P-Tau accumulation in human immortalized neuroblastoma cells. These compounds can serve as pharmacological tools in the study and development of potential therapeutics for hGGPPS-associated diseases.

5.4. Chemistry

We previously reported thienopyrimidine-based bisphosphonates as active site inhibitors of hFPPS.^{23, 24} These results suggested that whereas substitution at C-6 provided inhibitors that are more potent in hFPPS than hGGPPS, substitution at C-2 of the thienopyrimidine scaffold could potentially provide inhibitors that are more potent and selective in inhibiting hGGPPS. We also examined a small number of analogs substituted at the C-5 position of the thienopyrimidine core but found that these compounds were poor inhibitors of both hFPPS and hGGPPS; hence, the preparation of more C-5 substituted analogs was deprioritized. Additionally, we reported the use of trimethylsilyl ylidene **5.20** for the synthesis of the highly substituted thiophene analog **5.21** that served as the precursor to the parallel synthesis of structurally diverse C-5 and C-6 substituted thienopyrimidines **5.22** (**Scheme 5.2**).³² However, in our present study, the preparation of analogs that are substituted at C-2 of the thienopyrimidine core required development of an alternative synthetic route. This is achieved by the following the devised routes depicted in **Schemes 5.3** and **5.4**.



Scheme 5.2. Synthesis of C-5 and/or C-6 substituted thienopyrimidines *via* a modified Gewald approach starting from the ylidene **5.20** as the precursor for the construction of the thiophene core.

The commercially available dimer form of mercaptoacetaldehyde, 1,4-dithiane-2,5-diol (**5.23**) and propionaldehyde (**5.24**) were used as the starting materials for the synthesis of 2-amino-3-cyanothiophene **5.25** *via* the standard Gewald approach (**Scheme 5.3**). The thiophene core **5.25**

was then elaborated to substituted thieno[2,3-*d*]pyrimidines **5.26** in several ways. Cyclization with formamide provides the naked scaffold (**5.26c**). Installation of different moieties at C-2 can be achieved in two ways: *via* microwave irradiation of various aryl and heteroaryl nitriles with **5.25** in the presence of a base (analogs of **5.26b**) or through the use of the thioether intermediate **5.26a**, which upon introduction of the bisphosphonate tetraesters (e.g. **5.27a**; R₂ = SMe) is suitable for the Liebeskind–Srogl cross-coupling reaction with various boronic acids (**Scheme 5.3**, step h). The Liebeskind–Srogl reaction is a carbon-sulfur (C-S) activation strategy that requires the use of Cu(I) carboxylate (CuTC). As depicted in **Fig. 5.4**, CuTC serves the role of polarizing the Pd-S bond *via* Cu(I) coordination to sulfur while simultaneously activating the boronic acid through coordination of the carboxylate moiety to boron.^{33,34} Other copper (I) sources, such as copper(I) halide or CuCN did not give any coupling product,³⁵ highlighting the unique role of CuTC in this reaction. Intermediate **5.29a** (where X= NO₂; **Scheme 5.4**), for example was prepared using this C-S activation method in good yield (~80%). Compounds with expanded side chains were synthesized through the incorporation of an amide linker (e.g. **5.28h** and **5.28i**). The nitro group of **5.29a** was first reduced to the amine using tin (II) chloride and the aniline product **5.30** was then coupled with an acyl chloride or a carboxylic acid using standard peptide chemistry (**Scheme 5.4**). Some analogs were also prepared *via* Pd-catalyzed cross-coupling reactions with the aryl halide **5.29b** to give biaryl derivatives, such as analog **5.28n** (**Fig. 5.5**). To further probe the effects of disubstitution at C-2 and C-6, the C-6 position was also capped with a methyl (e.g. **5.28y**) or a phenyl (e.g. **5.28x**) in order to explore the possible volume of space around C-6 in the enzyme-bound conformation of these compounds. Representative key compounds from our mini library are summarized in **Figure 5.5**.

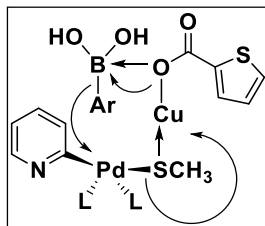
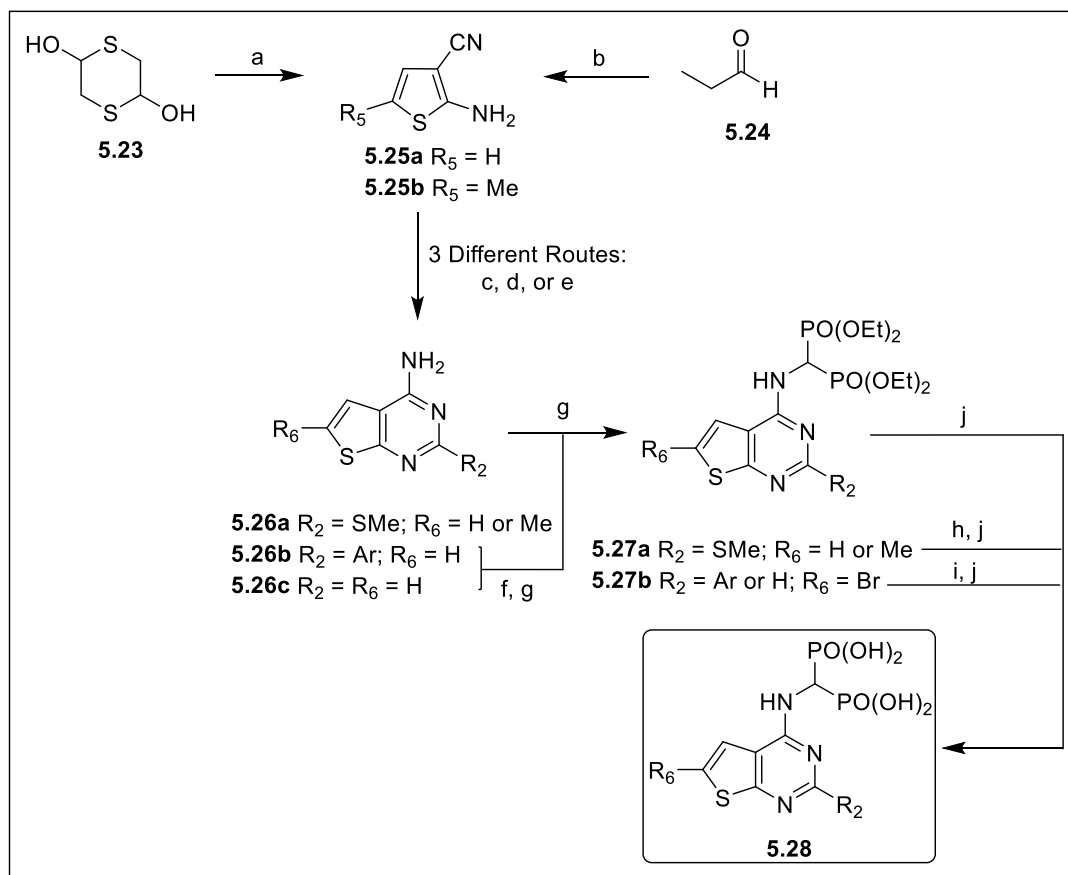


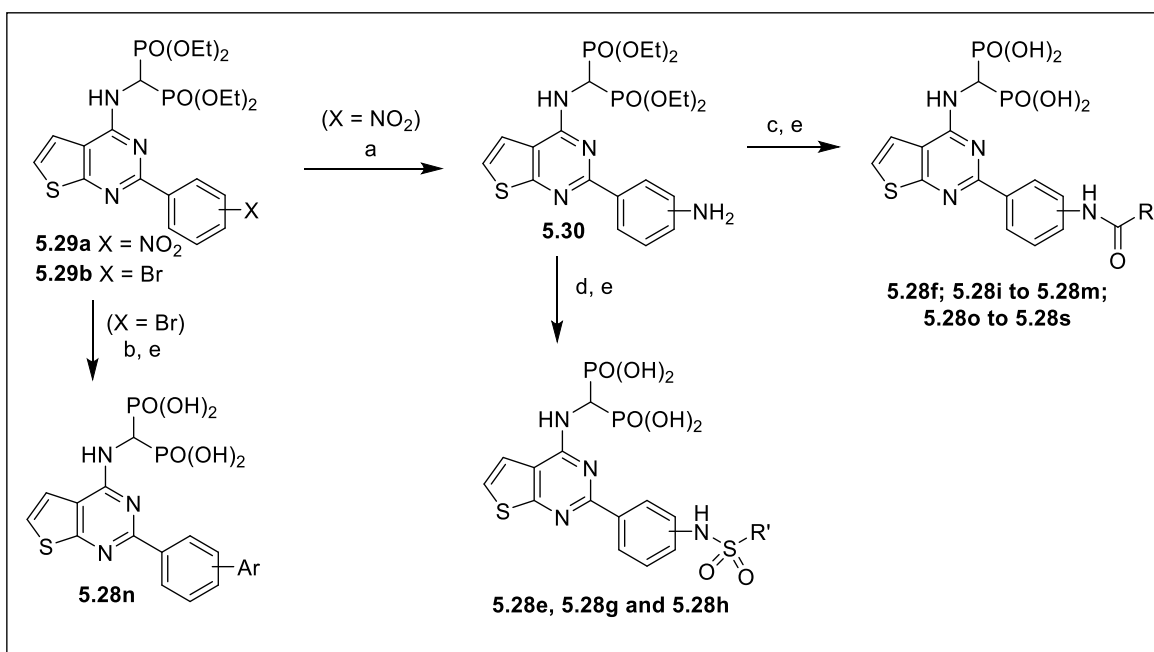
Figure 5.4. Proposed mechanism on the role of CuTC in the Liebeskind–Srogl cross-coupling of heteroaromatic thioether with boronic acid under base-free condition.



Scheme 5.3. General synthesis of C-2 and/or C-6 substituted ThP-BP.

Reaction conditions: (a) malononitrile, Et_3N , MeOH/DMF, $50^\circ C$, 70%; (b) malononitrile, sulfur, Et_3N , DMF, $0^\circ C$ to rt, 60%; (c) for the preparation of analogs of **5.26a**: methyl thiocyanate, HCl, $70^\circ C$, 60%-80%; (d) for the preparation of analogs of **5.26b**: aromatic nitrile, $t\text{-BuOK}$, $i\text{PrOH}$, μW , $80^\circ C$, ~27%-64%; (e) for the preparation of **5.26c**: formamide, $145^\circ C$, 56%; (f) NBS, DMF, rt; (g) diethyl phosphite, triethyl orthoformate, dry toluene, $115^\circ\text{-}130^\circ C$, 40%-80%; (h) aryl boronic acid,

CuTC, Pd(dppf)Cl₂•CH₂Cl₂, dry dioxane, 50°C, ~80%; (i) aryl boronic acid, KF, Pd(PPh₃)₄, MeOH, μ W, 120°C, ~50%-80%; (j) TMSBr/MeOH, rt, ~70% to quantitative.



Scheme 5.4. Synthesis of expanded ThP-BP analogs.

Reaction conditions: (a) SnCl₂•2H₂O, EtOH, 80°C, >80%; (b) aryl boronic acid, KF, Pd(PPh₃)₄, MeOH, μ W, 120°C, 82%; (c) acyl chloride, Et₃N, dry DCM, 0°C, to rt or a carboxylic acid, DIPEA, HBTU, dry DMF, rt, 75% to quant.; (d) sulfonyl chloride, pyridine, dry DCM, 0°C, to rt, 70% to quant.; (e) TMSBr/MeOH, rt, ~70% to quantitative.

5.5. Results and Discussion

The initial biological screening of our ThP-BP analogs was carried out using our routine hGGPPS inhibition assay at a fixed concentration of 100 nM, in parallel with the literature compound **4.15** (Chapter 4) as the positive control. The summary of results is shown in **Figure 5.6**. Selectivity against hFPPS and a full-dose IC₅₀ curves were only determined for the most promising inhibitors (**Table 5.1**). Consistent with our previous observations,³² substitution at C-2 or C-6 with a simple

phenyl group (**5.28a** and **5.28v**, respectively; **Fig. 5.6**) led to compounds that inhibited both hFPPS and hGGPPS. A C-5 phenyl substituted analog (compound **5.31**; **Fig. 5.5**; synthesized as previously reported),³² on the other hand was inactive in inhibiting both hFPPS and hGGPPS. Replacement of the C-2 phenyl with heterocyclic groups suggested that the more lipophilic moieties (e.g. phenyl **5.28a** and thiophene **5.28b** vs pyridine **5.28d**) have better hGGPPS activity, in general (**Fig. 5.6**). Interestingly, although the larger substituents at C-2 did not significantly improve the potency for hGGPPS, they however improved the selectivity in inhibiting hGGPPS over hFPPS (e.g. **5.28a** vs **5.28i**; **Fig. 5.6**). On the other hand, incorporation of the same amide substituent at the C-6 position was found detrimental in the inhibitory activity to both enzymes (e.g. **5.28v** vs **5.28w**). This observation suggests that the difference in target selectivity is not a simple binding orientation effect of the thienopyrimidine core and consequently, further optimization should be possible with more in-depth SAR studies. Our preliminary results for thienopyrimidine-based hGGPPS inhibitors with an amide (e.g. **5.28i**, **5.28t**) or a sulfonamide (e.g. **5.28g**) linker in the side chain resulted in compounds with very similar inhibitory activities and potency in the low nanomolar range (**Fig. 5.6**; **Table 5.1**). We are currently pursuing crystallographic studies to characterize the hGGPPS/inhibitor complex that we hope will guide our future SAR studies. In summary, starting from our original “hits” **5.28a** and **5.28v** with low selectivity in inhibiting hGGPPS over hFPPS (~7- and 2-fold, respectively), we were able to improve the selectivity to 31- and 57-fold, in the case of compounds **5.28i** and **5.28t**, respectively (**Table 5.1**). Our key compounds also displayed cell-based activity in submicromolar concentrations as will be discussed in the succeeding sections.

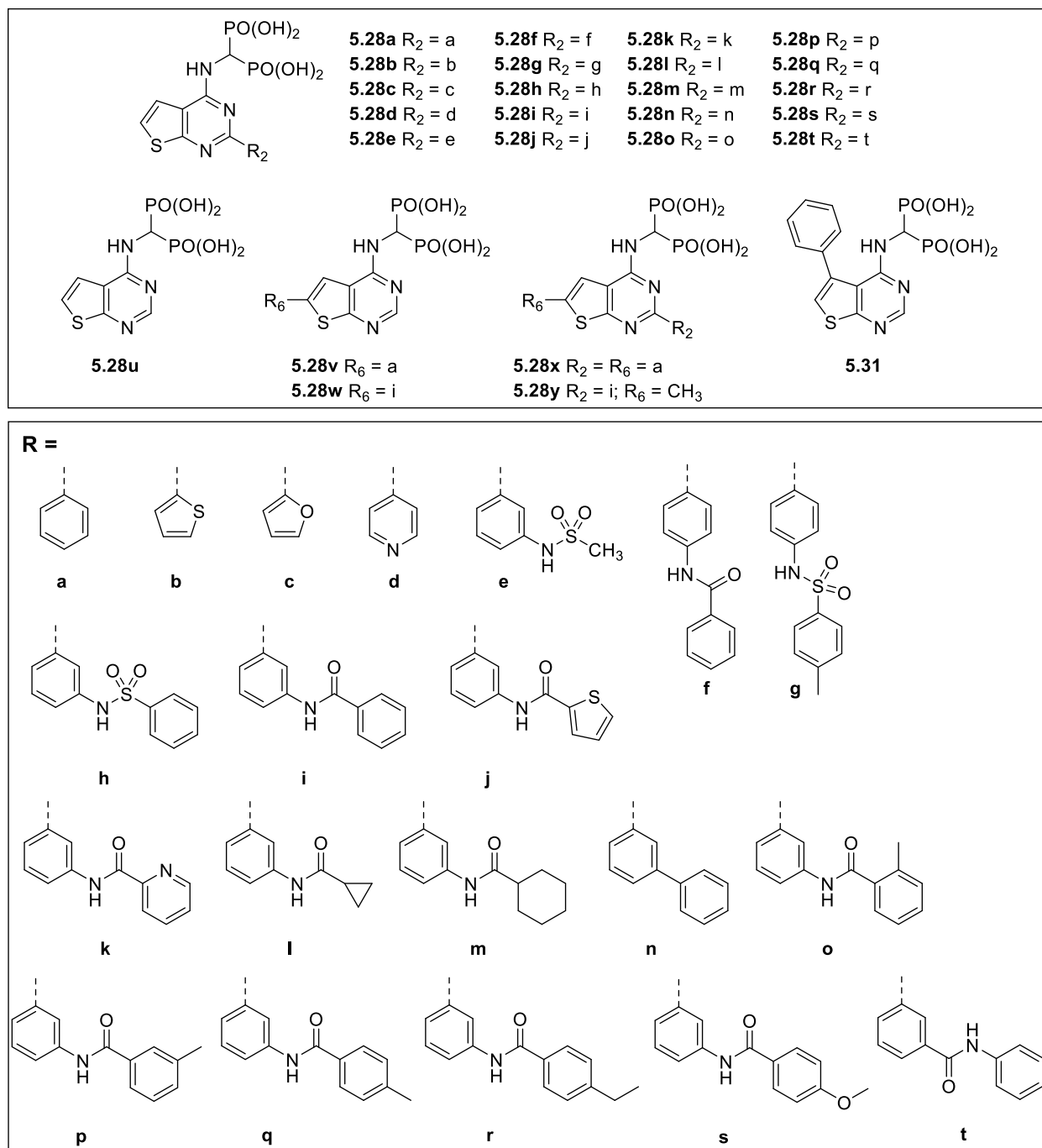


Figure 5.5. Representative examples from compound library.

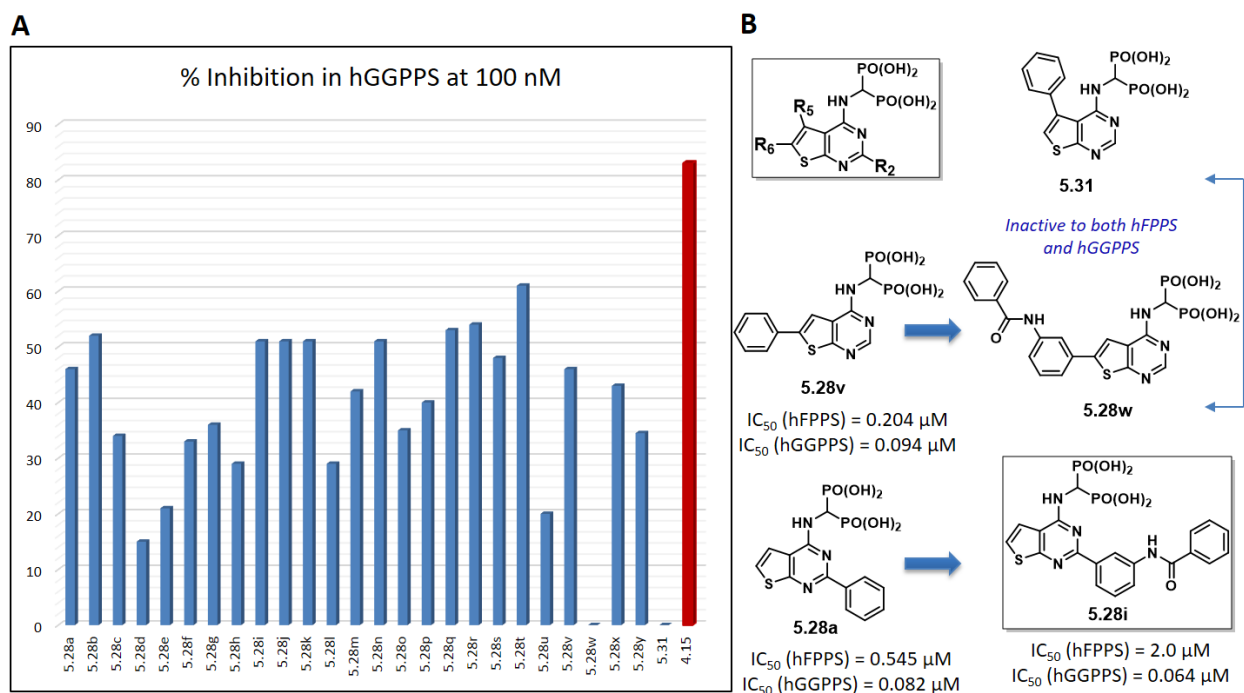


Figure 5.6. (A) *In vitro* wild-type hGGPPS inhibition data of ThP-BPs screened at a fixed concentration of 100 nM, average values of three determinations, standard deviation of $\leq 10\%$; the known hGGPPS inhibitor, **4.15** was used as the positive control; (B) Highlights of the SAR as discussed in the text.

Several lines of evidence have indicated that the observed biological effects of clinical *N*-BPs (e.g. ZOL and RIS, **Fig.4.3, Chapter 4**), particularly, the direct antitumor effect was through disruption of protein geranylgeranylation (as opposed to farnesylation).³⁶⁻⁴⁰ Therefore, inhibitors of hGGPPS may provide a more straightforward approach in the development of potential therapeutics for use in non-bone related diseases. For these reasons, we conducted a preliminary evaluation of our key hGGPPS inhibitors against a panel of multiple myeloma (MM) cell lines representing the genetic diversity of this disease, and their ability to prevent the build-up of phosphorylated tau (P-Tau) proteins in immortalized human neuroblastoma cells.

Antiproliferation and Cytotoxic Effects in Multiple Myeloma Cell Lines

The results of antiproliferation and cytotoxic effects in human-derived MM cell lines are summarized in **Table 5.1**. Cell viability was determined through 3-(4,5-dimethylthiazol-2-yl)-2,5-diphenyltetrazolium bromide (MTT) assay and the median effective concentration for 50% inhibition (EC_{50}) were calculated for each test compounds. The MTT colorimetric assay measures the conversion of yellow MTT tetrazolium salt into purple-colored MTT formazan (**Fig. 5.7**), which only occurs in metabolically active cells; hence a decrease in this conversion indicates loss of cell viability.⁴¹ Additionally, actively proliferating cells increase their metabolic activity and exposure to pharmacological or toxic substance results in diminished activity.

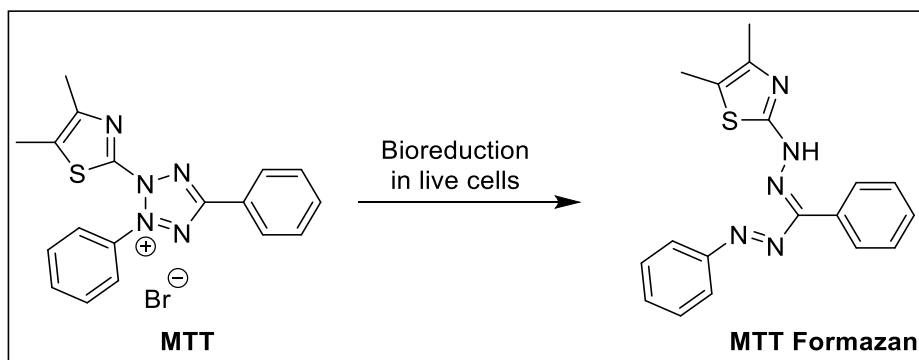


Figure 5.7. MTT reduction to formazan.

Our potent and selective hGGPS inhibitors, including the control compound **4.15** consistently showed better EC_{50} values across the three different MM cell lines as compared to the clinical *N*-BPs. For example, >90-fold improvement was observed for compounds **5.28q** and **5.28t** (EC_{50} = 0.12 μ M and 0.11 μ M, respectively; **Table 5.1**) versus ZOL and RIS (EC_{50} = 11.0 μ M and 13.0 μ M, respectively) when administered to RPMI-8226 cell line. In order to gain insights on the mechanism of cytotoxic effects in MM cells and target engagement by our inhibitors, we conducted further studies as discussed in the following sections.

Table 5.1. Activity of selected compounds in MM tumor cell lines.

Compound	hFPPS IC ₅₀ (μ M)	hGGPPS IC ₅₀ (μ M) ^[a]	Selectivity Index, <i>S.I.</i> ^[b]	MM cells EC ₅₀ , μ M ^[c]		
				JJN3	RPMI- 8226	KMS28 PE
ZOL	0.004 ^[d]	>50	$< 0.08 \times 10^{-3}$	5.0	11.0	6.4
RIS	0.005	~ 350 ^[e]	$\sim 0.01 \times 10^{-3}$	10.0	13.0	10.6
4.15	1.1	0.026	42	0.05	0.01	0.006
5.28i	2.0	0.064	31	0.50	0.10	0.55
5.28q	2.4	0.10	24	0.60	0.12	0.62
5.28s	1.0	0.086	12	1.30	0.38	1.4
5.28t	3.0	0.053	57	0.34	0.11	0.70

^[a]IC₅₀ values were determined using the wild-type hGGPPS enzyme; ^[b]*S.I.* = ratio of hFPPS IC₅₀ and hGGPPS IC₅₀; ^[c]Average of $n \geq 8$ determinations, R² values in the range of 0.94 - 0.99; ^[d]from Kavanagh *et. al.*⁴²; ^[e]from Szabo *et. al.*⁴³

Flow Cytometry to Study Cell Apoptosis

Apoptosis or programmed cell death is characterized by specific morphological features, including cell shrinkage, changes in plasma membrane asymmetry, chromatin condensation, DNA fragmentation, and cell blebbing.^{44, 45} Loss of membrane phospholipid asymmetry is one of the earliest features of apoptosis that results in the exposure of phosphatidylserine (PS) at the surface of the cell.⁴⁶ Annexin V is a Ca²⁺-dependent phospholipid-binding protein that has high affinity for PS. A fluorochrome-labeled Annexin V can be used for the analysis of cells undergoing apoptosis through detection of exposed PS using flow cytometry.⁴⁶ Flow cytometry measures the optical and fluorescence characteristics of single cells (or any other particle, including nuclei) when they pass through a light source (e.g. laser beam).⁴⁷ Light scattering at different angles can distinguish differences in structural and morphological properties of the cell. Additionally, light emitted from fluorophore-labeled antibodies correlates to the amount of fluorescent probe bound to the cell surface or cellular component.^{47, 48}

We examined the mechanism of cytotoxicity by evaluating the ability of our hGGPPS inhibitors to induce apoptosis using flow cytometry. RPMI-8226 human-derived myeloma cells were treated with inhibitor **5.28q** at increasing concentrations (**Fig. 5.9**). Velcade (a proteasome inhibitor and an approved drug for MM; **Fig. 5.8**) and compound **4.15** were also tested in parallel as positive controls. The presence of viable RPMI-8226 cells was determined using a CD138 antibody conjugated with a V450 dye. CD138, also known as syndecan-1, is a transmembrane protein strongly expressed on MM cell lines.⁴⁹ Cell apoptosis, on the other hand, was determined using Annexin V labeled with allophycocyanin (APC) fluorophore. A CD138 positive result indicates presence of viable MM cells, whereas an Annexin V positive result signifies presence of apoptotic cells.

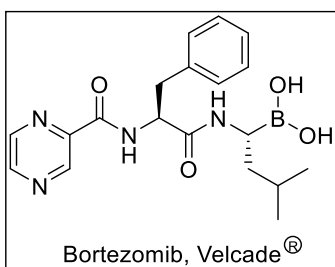
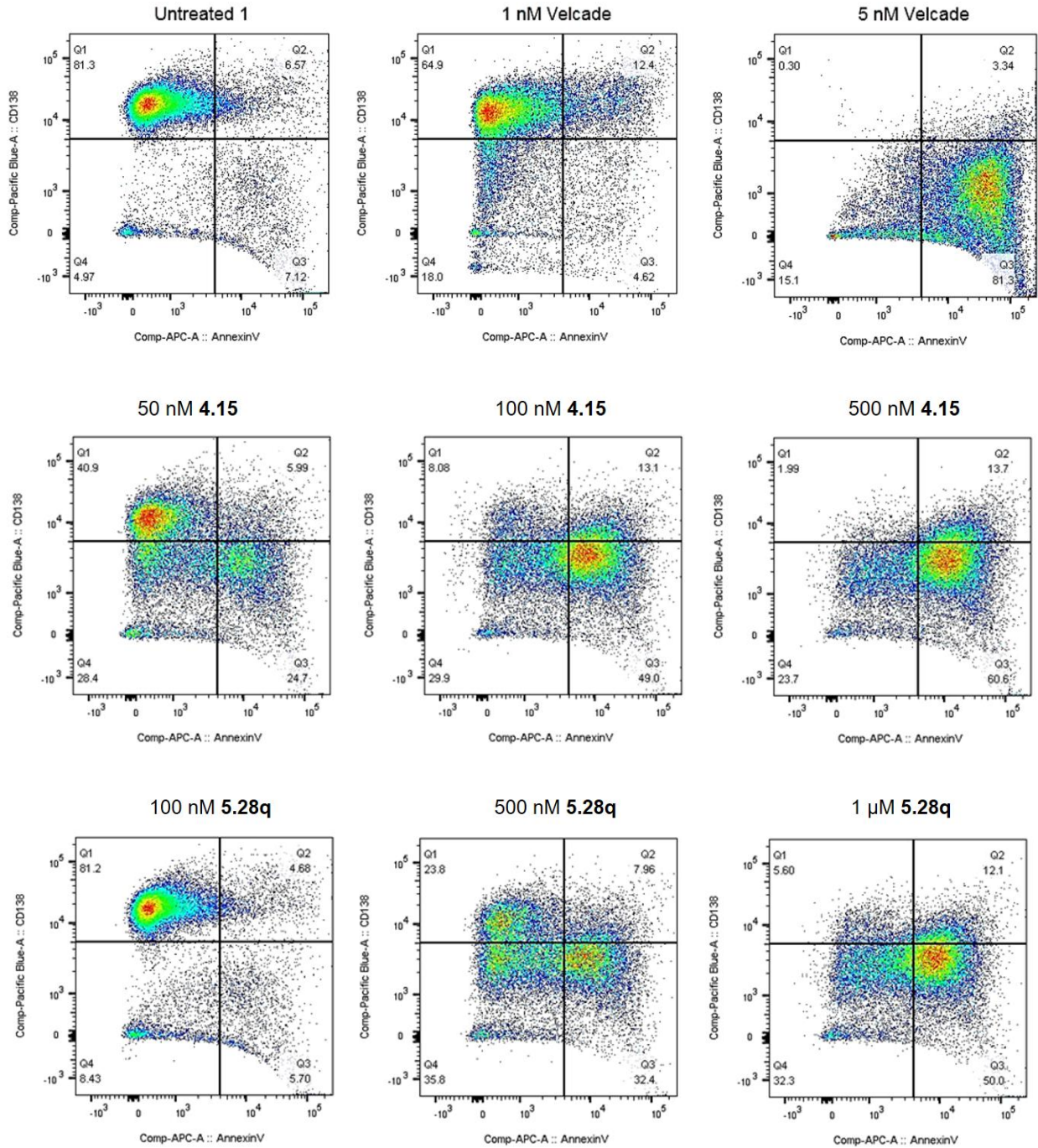


Figure 5.8. Chemical structure of velcade.

The flow cytometry results for detection of cell apoptosis are shown in **Figure 5.9**. In the case of the untreated cells, a CD138 positive quadrant 1 (Q1) shows that ~81% of RPMI-8226 cells were viable; however, treatment with increasing concentration of velcade, a shift from Q1 (CD138 positive) to Q3 (Annexin V positive) occurred and all the RPMI-8226 cells have undergone apoptosis at 5 nM concentration of velcade. Similarly, a dose-dependent increase in apoptotic fraction was observed with compound, **4.15** (e.g. ~60.6% at 500 nM, Q3; **Fig. 5.9**), as well as our hGGPPS inhibitor, **5.28q** (~50% at 1 μ M, Q3). These results provided evidence that the

cytotoxicity and antiproliferation activity of our hGGPS inhibitors in MM cells is associated with their ability to induce cell death or apoptosis.



Legend:

Q1- CD138 positive, Annexin V negative; viable RPMI-8226 cells
 Q2- CD138 positive, Annexin V positive; cells undergoing apoptosis

Q3- CD138 negative, Annexin V positive; apoptotic RPMI-8226 cells that have lost CD138 surface expression

Q4- CD138 negative, Annexin V negative; RPMI-8226 cells that have lost CD138 surface expression

Figure 5.9. Cell viability analysis using CD138 as the marker and detection of Annexin V positive apoptotic MM RPMI-8226 cells via flow cytometry: (first row) untreated cells and cells treated with velcade (1 nM and 5 nM); (second row) cells treated with **4.15** (50, 100 and 500 nM); and (third row) cells treated with **5.28q** (100, 500 and 1000 nM). Shift from Q1 to Q3 indicates cell apoptosis.

Western Blot Analysis to Investigate Protein Geranylgeranylation

To further elucidate the mechanism of action, we investigated the ability of **5.28q** to prevent cellular protein geranylgeranylation as determined by immunoblot analysis using a Rap1A antibody that only binds to the non-geranylgeranylated form of this protein.⁵⁰ As shown in **Figure 5.10**, geranylgeranylation of Rap1A was prevented *via* treatment with a high concentration of ZOL (100 μ M; lane 2). Note that ZOL is an hFPPS inhibitor that can also downregulate GGPP levels indirectly as a consequence of FPP depletion. On the other hand, control compound **4.15** disrupted Rap1A prenylation at much lower concentration (0.20 μ M; **Fig. 5.10**, lane 5). Inhibitor **5.28q**, which is ~4-fold less potent than **4.15** in inhibiting hGGPPS also prevented Rap1A prenylation at a concentration of 5.0 μ M (lane 8). Overall, these data demonstrated that the antiproliferation effects in MM cell lines correlate with the potency of the compounds in inhibiting hGGPPS and in preventing cellular protein geranylgeranylation.

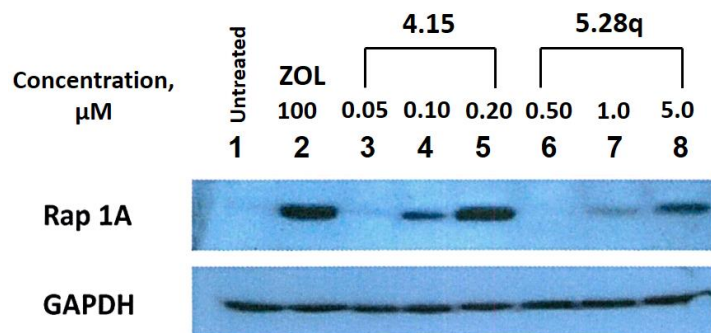


Figure 5.10. Western blot analysis to detect non-geranylgeranylated Rap1A. RPMI-8226 MM cells were incubated for 48 h with or without inhibitor **5.28q**. **ZOL** and **4.15** were used as the positive controls. The Rap1A antibody detects only unmodified protein. Glyceraldehyde 3-phosphate dehydrogenase (GAPDH) was used as a loading control.

Rescue of Cell Apoptosis via Add-Back Experiments

Since inhibition of any intracellular event or cell death cannot be attributed to a specific biological target without some evidence of target engagement by the inhibitor, we also conducted a “cell rescue” experiment in the presence of our inhibitors using flow cytometry. MM cells were treated with the hGGPPS inhibitor **5.28q** or the proteasome inhibitor, velcade in the presence and absence of geranylgeraniol (GGOH), which is metabolized to GGPP in the cells.^{51, 52} As shown in **Figure 5.11**, cell rescue was observed for inhibitor **5.28q** in the presence of GGOH (**Fig. 5.11A**) but not for velcade (since it operates *via* a different mechanism of action; **Fig. 5.11B**). These results strongly suggest that the antimyeloma effects are directly related to the intracellular inhibition of the hGGPPS enzyme by effective target engagement by our inhibitors.

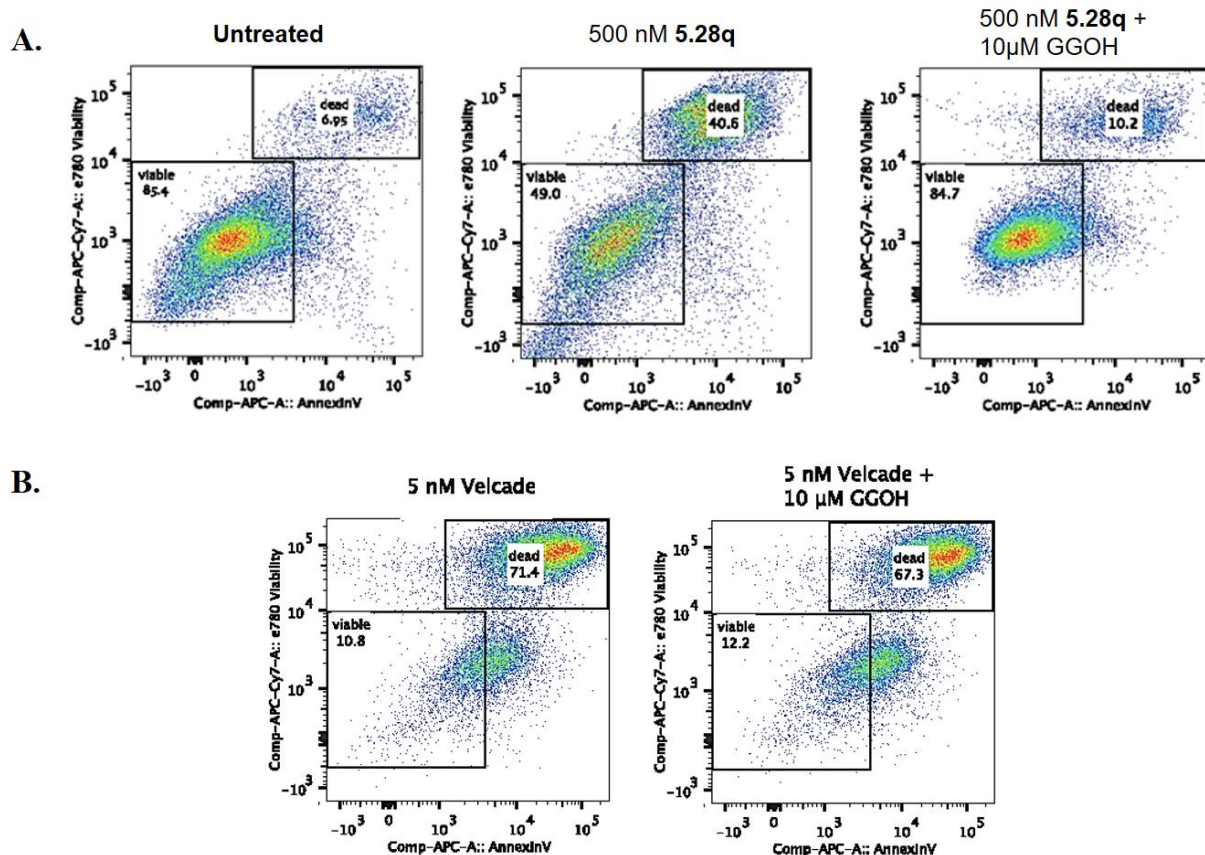


Figure 5.11. Add-back experiments using GGOH. **(A)** Untreated RPMI-8226 MM cells and those treated with **5.28q** alone and with GGOH. Treatment with 500 nM **5.28q** induced ~40.5% cell apoptosis; however, addition of 10 μM GGOH resulted in the recovery of viable cells. **(B)** Addition of GGOH in velcade-treated cells did not result in the rescue of viable cells.

Modulation of P-Tau Levels in Immortalized Human Neuroblastoma Cells

We previously reported inhibitors of hFPPS that can reduce the accumulation of P-Tau.²⁴ Considering that geranylgeranylation is more directly involved in the activation of the small GTPase Cdc42, and consequently, modulation of P-Tau, we also conducted preliminary profiling of our hGGPPS inhibitors for their ability to downregulate the intracellular concentrations of P-Tau in immortalized human neuroblastoma SH-SY5Y cells. Treatment of these cells with analog **5.28s** for a period of 12 h showed a dose-dependent decrease in the accumulation of P-Tau without detectable toxicity (**Table 5.2**). It is noteworthy that although a significant decrease in % P-

Tau/Tau levels ($\geq 50\%$) for ZOL and RIS was also observed, these compounds displayed significant toxicity in the standard LDH assay ($\sim 60\%$ higher LDH activity) compared to the untreated control at concentration of 100 nM.²⁴ Consequently, the effects of ZOL and RIS on P-Tau cannot be properly evaluated. Total-tau (T-Tau) and P-Tau levels were measured using the established enzyme-linked immunosorbent assay (ELISA) that employs Tau monoclonal antibodies that recognize different Tau and P-Tau epitopes^{24, 53} and the toxicity to neurons was estimated by the lactate dehydrogenase (LDH) assay.²⁴ The LDH assay measures the LDH released into the media from damaged cells as a biomarker for cellular toxicity and cytolysis. A more extensive biological evaluation of our compounds is currently in progress.

Table 5.2. Modulation of P-Tau levels in immortalized human neurons.

Compound	% P-Tau/Tau Reduction^[a]	% LDH^[b]
ZOL 0.10 μM	50%	+60
RIS 0.10 μM	67%	+60
5.28s 0.10 μM	43%	6
5.28s 0.50 μM	73%	-6
5.28s 1.00 μM	67%	-12

^[a]Based on the change in P-Tau/T-tau ratio in human SH-SY5Y neurons relative to the untreated cells; ^[b] % activity of LDH; assays run in triplicate and a standard deviation of $\leq 10\%$ was observed.

5.6. Conclusions and Outlook

A novel series of C-2 and C-6 substituted ThP-BPs was synthesized with our goal of identifying potent and selective inhibitors of hGGPPS. Several analogs with nanomolar *in vitro* potency were discovered and our SAR studies also showed that by increasing the size and lipophilicity of the C-2 side chain of the thieno[2,3-*d*]pyrimidine core can fine-tune the activity towards selective hGGPPS inhibition. Preliminary assessment of biological activity showed that several ThP-BP

analogs induce apoptosis in human multiple myeloma tumour cell lines in submicromolar concentrations and downregulate the intended target in the cell, as evidenced by the disruption of Rap1A geranylgeranylation and rescue experiments using GGOH. Additionally, compounds that can downregulate intracellular P-Tau levels in neurons were also identified, which warrants further investigation of the promising role of hGGPPS as the target for tauopathy-associated neurodegeneration, such as Alzheimer's. On-going structural studies in our group may also help advance the current knowledge of hGGPPS/inhibitor interactions and support further SAR studies with the goal of optimizing this class of compounds into novel therapeutics for human diseases associated with protein geranylgeranylation.

5.7. Experimental Section

Chemicals and solvents were purchased from commercial suppliers and used without further purification. Normal phase column chromatography on silica gel was performed using a CombiFlash instrument using the solvent gradient, as indicated. Reverse phase preparative HPLC was carried out using a Waters Atlantis Prep T3 OBD C18 5 μ m 19 x 50 mm column; Solvent A: H₂O, 0.1% formic acid; Solvent B: CH₃CN, 0.1% formic acid; Mobile phase: gradient from 95% A and 5% B to 5% A and 95% B in 17 min acquisition time; flow rate: 1 mL/min. The homogeneity of final inhibitors was confirmed to be $\geq 95\%$ by reversed-phase HPLC using a Waters ALLIANCE® instrument (e2695 with 2489 UV detector, 3100 mass spectrometer, C18 5 μ m column): Solvent A: H₂O, 0.1% formic acid; Solvent B: CH₃CN, 0.1% formic acid; Mobile phase: linear gradient from 95% A and 5% B to 0% A and 100% B in 13 min. Key compounds were fully characterized by ¹H, ¹³C, ³¹P NMR and HRMS. Chemical shifts (δ) are reported in ppm relative to the internal deuterated solvent. The NMR spectra of all final bisphosphonate inhibitors were acquired in D₂O (either after conversion to their corresponding tri-sodium salt or by addition of

~2% ND₄OD). In some cases, the C α to the bisphosphonate was broad and overlapped with the solvent peak, as confirmed by HSQC. The high resolution MS spectra of final products were recorded using electrospray ionization (ESI^{+/−}) and Fourier transform ion cyclotron resonance mass analyzer (FTMS).

Library Synthesis

General Synthetic Protocols:

Syntheses of **5.25a**,⁵⁴ **5.25b**,⁵⁵ and **5.26a**⁵⁶ were accomplished based on literature procedures. Analogs of **5.26b** were prepared *via* reaction of **5.25** with appropriate aryl nitriles in the presence of *t*-BuOK as described by Chen *et. al.* with slight modifications.⁵⁷ Bromination of **5.26** was achieved using NBS based on the method of Shook *et. al.*²¹ Suzuki cross-coupling reactions, and installation/deprotection of bisphosphonate esters were performed using the previously reported general protocols.²³ Preparation and characterization of inhibitors **5.28u**, **5.28a**, **5.28v**, and **5.31** have been described in our previous studies.^{23, 32}

Method A. General protocol for the Liebeskind–Srogl cross-coupling reaction between thiomethyl ether-containing analogs of **5.27a** and aryl boronic acids

The procedure was based on previously described protocols with slight modifications.^{33,56} Thiomethyl ether intermediate **5.27a** (1.0 eq), aryl boronic acid (2.5 eq), CuTC (3.0 eq) and Pd(dppf)Cl₂•CH₂Cl₂ (0.10 eq) were charged into an oven-dried round bottom flask. The flask was evacuated and purged with Ar, followed by addition of dry dioxane (5.5 mL per 1.0 mmol **5.27a**). The flask was sealed and heated at 50°C for 4-5h (under Ar balloon). The reaction mixture was cooled to rt, diluted with EtOAc, and filtered through celite. The filtrate was collected and washed with 10% aqueous NH₄OH (thrice), followed by brine. The combined organic extracts were dried over Na₂SO₄ and concentrated *in vacuo*. Crude product was purified by silica gel column

chromatography with a gradient from 25% EtOAc in hexanes to 100% EtOAc and then to 20% MeOH in EtOAc. Product typically elutes between 10%-20% MeOH in EtOAc. Typical isolated yield was ~80%.

Method B. General protocol for the synthesis of **5.30**

A pressure vessel was charged with the nitro-containing intermediate **5.29a** (1.0 eq) and EtOH (10.0 mL per 1 mmol **5.29a**). SnCl₂•2H₂O (5.0 eq) was then added and the mixture was stirred at 80°C for 2-3 h. The reaction mixture was then cooled to rt and then slowly poured into sat. NaHCO₃ solution (~10.0 mL per 1 mmol **5.29a**). It was then extracted with EtOAc (thrice), brine (once), dried over MgSO₄, filtered, and concentrated *in vacuo*. Product was generally obtained in >80% yield and was used in the next step without further purification.

Method C. General procedure for the amide bond formation

Method C.1. Reaction using acyl chlorides as coupling partner

To a stirring solution of the amine intermediate **5.30** (1.0 eq) in dry DCM (6.5 mL per 1 mmol **5.30**) at 0°C was added dry Et₃N (3.0 eq). The acid chloride (1.2 eq) was then added dropwise under Ar balloon. The solution was stirred and allowed to warm to rt (reaction progress was monitored by TLC). Once complete (typically, after ~1h), the reaction was poured into sat. NaHCO₃ solution and extracted with EtOAc (twice), washed with brine, dried over Na₂SO₄ and concentrated under vacuum. Crude product was purified by silica gel column chromatography with a gradient from 25% EtOAc in hexanes to 100% EtOAc and then to 20% MeOH in EtOAc. Product typically elutes between 10%-20% MeOH in EtOAc. Isolated yield was typically 75% to quantitative.

Method C.2. Reaction using carboxylic acids as coupling partner

To the mixture of the amine intermediate **5.30** (1.0 eq) and carboxylic acid (1.1 eq) in dry DMF (2.0 mL per 0.1 mmol **5.30**) was added DIPEA (2.0 eq) followed by HBTU (1.1 eq) under Ar balloon. The solution was stirred at rt for 1-2h. The reaction was then added with brine (10 mL) and was extracted with EtOAc (20.0 mL; twice). The organic phase was washed with sat. NH₄Cl solution (10 mL), brine, dried over Na₂SO₄ and concentrated *in vacuo*. Crude product was purified by silica-gel column chromatography as described for **Method C.1**. Isolated yield was 70% to quantitative.

Method C.3. Reaction using sulfonyl chlorides as coupling partner

The sulfonamides were prepared using amine **5.30** and various sulfonyl chlorides as starting materials following the protocol of Wydysh *et al.*⁵⁸ with slight modifications. Isolated yield was 70% to quantitative.

2-aminothiophene carbonitrile **5.25**:

2-aminothiophene-3-carbonitrile (**5.25a**).⁵⁴ Isolated as a light brown solid. ¹H NMR (500 MHz, CDCl₃) δ 6.73 (d, *J* = 5.7 Hz, 1H), 6.35 (d, *J* = 5.7 Hz, 1H), 4.74 (br_s, 2H).

2-amino-5-methylthiophene-3-carbonitrile (**5.25b**).⁵⁵ Isolated as a yellow solid. ¹H NMR (500 MHz, CDCl₃) δ 6.33 (d, *J* = 1.2 Hz, 1H), 4.65 (br_s, 2H), 2.26 (d, *J* = 1.2 Hz, 3H). ¹³C NMR (126 MHz, CDCl₃) δ 161.1, 124.8, 122.2, 115.8, 87.4, 15.0. MS [ESI⁺] *m/z*: 139.1 [M + H⁺]⁺

Thieno[2,3-*d*]pyrimidines **5.26**:

2-(methylthio)thieno[2,3-*d*]pyrimidin-4-amine (**5.26a-1**; R₂ = SMe; R₅ = R₆ = H).⁵⁶ Isolated as a light brown solid. ¹H NMR (500 MHz, DMSO-*d*₆) δ 7.55 (br_s, 2H), 7.47 (d, *J* = 5.9 Hz, 1H),

7.36 (d, $J = 5.9$ Hz, 1H), 2.46 (s, 3H). ^{13}C NMR (126 MHz, DMSO- d_6) δ 167.5, 166.5, 158.3, 120.7, 120.2, 113.4, 13.8. MS [ESI $^+$] m/z : 198.0 [M + H $^+$] $^+$

6-methyl-2-(methylthio)thieno[2,3-d]pyrimidin-4-amine (**5.26a-2**; $R_2 = \text{SMe}$; $R_5 = \text{H}$; $R_6 = \text{Me}$).⁵⁶ Isolated as yellowish brown solid. ^1H NMR (400 MHz, DMSO- d_6) δ 7.40 (br_s, 2H), 7.13 (d, $J = 1.3$ Hz, 1H), 2.46 (d, $J = 1.2$ Hz, 3H), 2.44 (s, 3H). ^{13}C NMR (126 MHz, DMSO- d_6) δ 166.4, 165.1, 156.9, 133.2, 117.0, 113.2, 15.8, 13.3. MS [ESI $^+$] m/z : 212.0 [M + H $^+$] $^+$

Thieno[2,3-d]pyrimidin-4-amine (**5.26c**; $R_2 = R_5 = R_6 = \text{H}$). Isolated as a yellow solid. ^1H NMR (400 MHz, DMSO- d_6) δ 8.26 (s, 1H), 7.57 (d, $J = 6.0$ Hz, 1H), 7.53 (d, $J = 6.0$ Hz, 1H), 7.49 (br_s, 2H). MS [ESI $^+$] m/z : 152.0 [M + H $^+$] $^+$

2-(thiophen-2-yl)thieno[2,3-d]pyrimidin-4-amine (**5.26b-1**; $R_2 = 2\text{-thiophenyl}$; $R_5 = R_6 = \text{H}$). Isolated as dark-colored solid. ^1H NMR (500 MHz, CDCl_3) δ 7.98 (d, $J = 2.7$ Hz, 1H), 7.43 (dd, $J = 5.0, 1.2$ Hz, 1H), 7.27 (d, $J = 6.0$ Hz, 1H), 7.14 (d, $J = 6.0$ Hz, 1H), 7.13 (dd, $J = 5.0, 3.7$ Hz, 1H), 5.29 (br_s, 2H).

2-(furan-2-yl)thieno[2,3-d]pyrimidin-4-amine (**5.26b-2**; $R_2 = 2\text{-furan-2-yl}$; $R_5 = R_6 = \text{H}$). Isolated as a pale orange solid. ^1H NMR (500 MHz, CDCl_3) δ 7.65 (dd, $J = 1.7, 0.8$ Hz, 1H), 7.39 (d, $J = 3.2$ Hz, 1H), 7.35 (d, $J = 6.0$ Hz, 1H), 7.26 (d, $J = 6.0$ Hz, 1H), 6.59 (dd, $J = 3.4, 1.7$ Hz, 1H), 5.84 (br_s, 2H).

2-(pyridin-4-yl)thieno[2,3-d]pyrimidin-4-amine (**5.26b-3**; $R_2 = 4\text{-pyridinyl}$; $R_5 = R_6 = \text{H}$). ^1H NMR (500 MHz, DMSO- d_6) δ 8.71 (dd, $J = 4.5, 1.6$ Hz, 2H), 8.23 (dd, $J = 4.5, 1.6$ Hz, 2H), 7.75 (br_s, 2H), 7.66 – 7.63 (m, 2H). ^{13}C NMR (126 MHz, DMSO- d_6) δ 167.2, 158.7, 157.2, 150.1, 145.2, 123.8, 121.7, 119.9, 115.3.

2-(3-bromophenyl)thieno[2,3-d]pyrimidin-4-amine (**5.26b-4**; R₂ = 3-bromophenyl; R₅ = R₆ = H).
¹H NMR (500 MHz, DMSO-d₆) δ 8.53 (t, *J* = 1.8 Hz, 1H), 8.37 – 8.34 (m, 1H), 7.68 (br_s, 2H),
7.67 - 7.65 (m, 1H), 7.61 (d, *J* = 5.9 Hz, 1H), 7.58 (d, *J* = 5.9 Hz, 1H), 7.45 (t, *J* = 7.9 Hz, 1H).
¹³C NMR (126 MHz, DMSO-d₆) δ 167.7, 159.0, 158.0, 140.7, 133.0, 131.1, 130.7, 126.9, 123.5,
122.2, 120.3, 115.1.

Bisphosphonate tetraesters 5.27:

Tetraethyl (((2-(methylthio)thieno[2,3-d]pyrimidin-4-yl)amino)methylene)bis(phosphonate)
(**5.27a-1**; R₂ = SMe; R₅ = R₆ = H). Product was obtained as a brown solid. ¹H NMR (500 MHz,
DMSO-d₆) δ 8.70 (d, *J* = 9.7 Hz, -NH), 7.97 (d, *J* = 6.0 Hz, 1H), 7.45 (d, *J* = 6.0 Hz, 1H), 5.70
(td, *J* = 23.6, 9.7 Hz, 1H), 4.14 – 4.02 (m, 8H), 2.50 (s, 3H), 1.22 – 1.12 (m, 12H). ³¹P NMR (203
MHz, DMSO-d₆) δ 16.77 (s). ¹³C NMR (126 MHz, DMSO-d₆) δ 167.3, 165.4, 155.12 (t, *J* = 4.1
Hz), 121.1, 120.1, 113.6, 62.9 - 62.7 (m), 44.4 (t, *J* = 147.3 Hz), 16.2 - 16.1 (m), 13.5. MS [ESI⁺]
m/z: 484.1 [M + H⁺]⁺

Tetraethyl (((6-methyl-2-(methylthio)thieno[2,3-d]pyrimidin-4-
yl)amino)methylene)bis(phosphonate) (**5.27a-2**; R₂ = SMe; R₅ = H; R₆ = Me). Isolated as a
yellowish brown solid. ¹H NMR (400 MHz, acetone-d₆) δ 7.48 (s, 1H), 5.78 (td, *J* = 23.0, 9.8
Hz, 1H), 4.24 – 4.10 (m, 8H), 2.53 (s, 3H), 2.52 (d, *J* = 1.1 Hz, 3H), 1.29 – 1.16 (m, 12H). ³¹P
NMR (162 MHz, acetone-d₆) δ 16.53 (s). ¹³C NMR (126 MHz, acetone-d₆) δ 168.4, 166.1,
155.4 (t, *J* = 3.9 Hz), 135.8, 117.4, 115.2, 64.0 -63.9 (m), 45.6 (t, *J* = 147.2 Hz), 16.7 - 16.6 (m),
16.1, 14.1. MS [ESI⁺] m/z: 498.1 [M + H⁺]⁺

Tetraethyl (((6-bromo-2-phenylthieno[2,3-d]pyrimidin-4-yl)amino)methylene)bis(phosphonate)
(**5.27b-1**; R₂ = phenyl; R₅ = H; R₆ = Br). Isolated as a light yellow solid. ¹H NMR (400 MHz,
CDCl₃) δ 8.45 - 8.40 (m, 2H), 7.50 – 7.44 (m, 3H), 7.42 (s, 1H), 6.07 – 5.84 (m, 2H; -NH and α-

CH to the bisphosphonate), 4.30 – 4.10 (m, 8H), 1.30 - 1.20 (m, 12H). ³¹P NMR (162 MHz, CDCl₃) δ 16.66 (s).

Bisphosphonate tetraesters 5.29:

Tetraethyl (((2-(3-nitrophenyl)thieno[2,3-d]pyrimidin-4-yl)amino)methylene)bis(phosphonate) (**5.29a-1**; X = *m*-Nitro). Prepared *via* **Method A** using thiomethyl ether intermediate **5.27a-1** and 3-nitrophenylboronic acid as coupling partners. Product was isolated as light brown solid. ¹H NMR (500 MHz, DMSO-d₆) δ 9.12 (t, *J* = 1.9 Hz, 1H), 8.85 (d, *J* = 9.6 Hz, -NH), 8.80 (d, *J* = 7.9 Hz, 1H), 8.35 (ddd, *J* = 8.2, 2.4, 0.9 Hz, 1H), 8.14 (d, *J* = 6.0 Hz, 1H), 7.84 (t, *J* = 8.0 Hz, 1H), 7.72 (d, *J* = 6.0 Hz, 1H), 5.99 (td, *J* = 23.5, 9.6 Hz, 1H), 4.19 – 4.07 (m, 8H), 1.22 – 1.11 (m, 12H). ³¹P NMR (203 MHz, DMSO-d₆) δ 16.9. ¹³C NMR (126 MHz, DMSO-d₆) δ 167.8, 156.5 (t, *J* = 4.0 Hz), 156.4, 148.7, 139.6, 134.1, 130.8, 125.3, 124.9, 122.4, 120.8, 116.4, 63.4 - 63.2 (m), 45.0 (t, *J* = 147.2 Hz), 16.7 - 16.6 (m). MS [ESI⁺] *m/z*: 559.1 [M + H⁺]⁺

Tetraethyl (((2-(4-nitrophenyl)thieno[2,3-d]pyrimidin-4-yl)amino)methylene)bis(phosphonate) (**5.29a-2**; X = *p*-Nitro). Prepared *via* **Method A** using thiomethyl ether intermediate **5.27a-1** and 4-nitrophenylboronic acid as coupling partners. Product was isolated as a tan solid. ¹H NMR (400 MHz, DMSO-d₆) δ 8.82 (d, *J* = 9.7 Hz, -NH), 8.63 (d, *J* = 9.0 Hz, 2H), 8.40 (d, *J* = 9.0 Hz, 2H), 8.15 (d, *J* = 6.0 Hz, 1H), 7.75 (d, *J* = 6.0 Hz, 1H), 5.97 (td, *J* = 23.5, 9.5 Hz, 1H), 4.20 – 4.05 (m, 8H), 1.20 – 1.10 (m, 12H). ³¹P NMR (162 MHz, DMSO-d₆) δ 16.92.

Tetraethyl (((2-(3-bromophenyl)thieno[2,3-d]pyrimidin-4-yl)amino)methylene)bis(phosphonate) (**5.29b-1**; X = *m*-Br). Isolated as a light yellow solid. ¹H NMR (400 MHz, CDCl₃) δ 8.61 (t, *J* = 1.7 Hz, 1H), 8.42 – 8.38 (m, 1H), 7.60 – 7.57 (m, 1H), 7.39 – 7.30 (m, 3H), 5.95 – 5.79 (m, 2H; -NH and α-CH to the bisphosphonate), 4.33 – 4.13 (m, 8H), 1.29 – 1.22 (m, 12H). ¹³C NMR (100

MHz, CDCl₃) δ 168.1, 157.9, 155.4, 139.8, 133.2, 131.1, 129.9, 126.7, 124.3, 122.7, 117.1, 115.4, 63.8 – 63.6 (m), 44.7 (t, *J* = 147.3 Hz), 16.4 – 16.3 (m). ³¹P NMR (162 MHz, CDCl₃) δ 16.7.

Bisphosphonate esters 5.30:

Tetraethyl (((2-(3-aminophenyl)thieno[2,3-d]pyrimidin-4-yl)amino)methylene)bis(phosphonate) (**5.30a**). Prepared *via* **Method B** using **5.29a-1** as the starting material. Product was isolated as a yellow solid. ¹H NMR (500 MHz, DMSO-d₆) δ 8.52 (d, *J* = 9.7 Hz, 1H), 8.06 (d, *J* = 6.0 Hz, 1H), 7.64 – 7.62 (m, 1H), 7.58 (d, *J* = 6.0 Hz, 1H), 7.53 (d, *J* = 7.7 Hz, 1H), 7.14 (t, *J* = 7.8 Hz, 1H), 6.67 (dd, *J* = 7.9, 1.5 Hz, 1H), 6.01 (td, *J* = 23.5, 9.7 Hz, 1H), 5.22 (s, 2H), 4.15 – 4.05 (m, 8H), 1.18 - 1.10 (m, 12H). ³¹P NMR (203 MHz, DMSO-d₆) δ 17.18 (s). MS [ESI⁺] *m/z*: 529.1 [M + H⁺]⁺

Tetraethyl (((2-(4-aminophenyl)thieno[2,3-d]pyrimidin-4-yl)amino)methylene)bis(phosphonate) (**5.30b**). Prepared *via* **Method B** using **5.29a-2** as the starting material. Product was isolated as a yellow solid. ¹H NMR (400 MHz, DMSO-d₆) δ 8.40 (d, *J* = 9.7 Hz, -NH), 8.07 (d, *J* = 8.7 Hz, 2H), 7.99 (d, *J* = 6.0 Hz, 1H), 7.45 (d, *J* = 6.0 Hz, 1H), 6.63 (d, *J* = 8.7 Hz, 2H), 6.01 (td, *J* = 23.6, 9.6 Hz, 1H), 5.59 (br_s, -NH₂), 4.16 – 4.02 (m, 8H), 1.19 – 1.10 (m, 12H). ³¹P NMR (162 MHz, DMSO-d₆) δ 17.32.

Final Inhibitors 5.28:

Inhibitor 5.28b:

Corresponding bisphosphonate ester: Tetraethyl (((2-(thiophen-2-yl)thieno[2,3-d]pyrimidin-4-yl)amino)methylene)bis(phosphonate). ¹H NMR (500 MHz, CDCl₃) δ 8.15 (br, 1H), 7.47 (d, *J* = 4.7 Hz, 2H), 7.33 (br, 1H), 7.17 – 7.14 (m, 1H), 6.16 (br_s, -NH), 5.90 – 5.79 (m, α-CH to the bisphosphonate), 4.32 – 4.10 (m, 8H), 1.30 – 1.22 (m, 12H).

Final Inhibitor: (((2-(thiophen-2-yl)thieno[2,3-d]pyrimidin-4-

yl)amino)methylene)bis(phosphonic acid) (**5.28b**). ^1H NMR (500 MHz, D_2O) δ 8.04 (d, $J = 2.6$ Hz, 1H), 7.66 (d, $J = 4.9$ Hz, 1H), 7.59 (d, $J = 5.9$ Hz, 1H), 7.44 (d, $J = 5.9$ Hz, 1H), 7.27 (t, $J = 4.2$ Hz, 1H), 4.96 (t, $J = 18.7$ Hz, 1H). ^{13}C NMR (126 MHz, D_2O) δ 164.9, 156.7, 156.6, 142.5, 129.8, 128.8, 128.6, 122.4, 119.2, 115.7, 50.2 (br). ^{31}P NMR (203 MHz, D_2O) δ 13.63.

Inhibitor 5.28c:

Corresponding bisphosphonate ester: Tetraethyl (((2-(furan-2-yl)thieno[2,3-d]pyrimidin-4-

yl)amino)methylene)bis(phosphonate). Product was isolated as a white solid. ^1H NMR (500 MHz, CDCl_3) δ 7.60 (m, 1H), 7.32-7.29 (m, 2H), 7.24 (d, $J = 3.2$ Hz, 1H), 6.54 (dd, $J = 3.3, 1.7$ Hz, 1H), 5.93-5.79 (m, 2H; -NH and α -CH to the bisphosphonate), 4.30-4.20 (m, 8H), 1.29 – 1.24 (m, 12H). ^{13}C NMR (125 MHz, CDCl_3) δ 167.8, 155.3 (t, $J = 3.6$ Hz), 152.4, 152.3, 144.7, 123.8, 117.2, 115.0, 112.8, 112.0, 63.9 – 63.6 (m), 44.3 (t, $J = 146.7$ Hz), 16.4 – 16.3 (m). ^{31}P NMR (203 MHz, CDCl_3) δ 16.68.

Final Inhibitor: (((2-(furan-2-yl)thieno[2,3-d]pyrimidin-4-yl)amino)methylene)bis(phosphonic acid) (**5.28c**). Isolated as a light brown solid. ^1H NMR (500 MHz, D_2O): δ 7.71 (s, 1H), 7.45 (d, $J = 5.9$ Hz, 1H), 7.40 (d, $J = 5.9$ Hz, 1H), 7.35 (d, $J = 3.2$ Hz, 1H), 6.63 (br, 1H), 5.22 (t, $J = 20.3$ Hz, 1H). ^{31}P NMR (203 MHz, D_2O): δ 12.9. ^{13}C NMR (125 MHz, D_2O): δ 163.4, 156.5, 151.4, 150.1, 145.6, 123.5, 118.8, 115.6, 114.0, 112.5, 48.8 (t, $J = 130.5$ Hz). MS (ESI⁺) m/z : 392.1 [M + H⁺]⁺

Inhibitor 5.28d:

Corresponding bisphosphonate ester: Tetraethyl (((2-(pyridin-4-yl)thieno[2,3-d]pyrimidin-4-

yl)amino)methylene)bis(phosphonate). Product was isolated as a yellow solid. ^1H NMR (500

MHz, CDCl₃) δ 8.80 (br, 2H), 8.33 (br, 2H), 7.41 (br, 2H), 6.17 – 6.15 (m, 1H), 5.89 (td, *J* = 21.9, 9.8 Hz, 1H), 4.26 – 4.18 (m, 8H), 1.28 – 1.20 (m, 12H). ³¹P NMR (203 MHz, CDCl₃) δ 16.7. ¹³C NMR (125 MHz, CDCl₃) δ 168.1, 157.1, 155.6, 150.1, 145.3, 125.1, 122.2, 117.5, 116.1, 63.8 – 63.6 (m), 44.8 (t, *J* = 147.6 Hz), 16.5 – 16.3 (m).

Final Inhibitor: (((2-(pyridin-4-yl)thieno[2,3-d]pyrimidin-4-yl)amino)methylene)bis(phosphonic acid) (**5.28d**). Isolated as a yellow solid. ¹H NMR (400 MHz, D₂O): δ 8.60 (br, 2H), 8.24 (br, 2H), 7.58 (d, *J* = 6.0 Hz, 1H), 7.52 (d, *J* = 5.9 Hz, 1H), 5.26 (t, *J* = 19.4 Hz, 1H). ³¹P NMR (162 MHz, D₂O): δ 13.7. ¹³C NMR (100 MHz, D₂O): δ 165.4, 157.4, 156.9, 148.5, 146.5, 124.4, 122.8, 118.8, 116.5, 48.8 (t, *J* = 124.0 Hz). MS (ESI+) *m/z*: 403.1 [M + H]⁺.

Inhibitor 5.28e:

Corresponding bisphosphonate ester: Tetraethyl (((2-(3-(methylsulfonamido)phenyl)thieno[2,3-d]pyrimidin-4-yl)amino)methylene)bis(phosphonate). Prepared using **Method C.3**. Isolated as a cream solid. ¹H NMR (400 MHz, DMSO-d₆) δ 9.93 (s, 1H), 8.65 (d, *J* = 9.7 Hz, 1H), 8.29 (t, *J* = 1.8 Hz, 1H), 8.14 (d, *J* = 7.9 Hz, 1H), 8.11 (d, *J* = 6.0 Hz, 1H), 7.65 (d, *J* = 6.0 Hz, 1H), 7.49 (t, *J* = 7.9 Hz, 1H), 7.36 (ddd, *J* = 8.0, 2.2, 0.9 Hz, 1H), 6.01 (td, *J* = 23.5, 9.7 Hz, 1H), 4.23 – 4.02 (m, 8H), 3.02 (s, 3H), 1.19 – 1.10 (m, 12H). ³¹P NMR (162 MHz, DMSO-d₆) δ 17.00 (s).

Final Inhibitor: (((2-(3-(methylsulfonamido)phenyl)thieno[2,3-d]pyrimidin-4-yl)amino)methylene)bis(phosphonic acid) (**5.28e**). Isolated as a yellow solid. ¹H NMR (400 MHz, D₂O) δ 8.19 (d, *J* = 7.9 Hz, 1H), 8.16 (s, 1H), 7.63 – 7.59 (m, 2H), 7.52 – 7.50 (m, 2H), 5.19 (t, *J* = 18.7 Hz, 1H), 3.18 (s, 3H). ³¹P NMR (203 MHz, D₂O) δ 13.83 (s). ¹³C NMR (101 MHz, D₂O) δ 165.7, 159.6, 157.0, 139.2, 137.4, 130.1, 125.3, 123.5, 123.3, 121.5, 118.9, 115.8, 38.4. C-α to the bisphosphonate was observed by HSQC. HSQC (¹H-¹³C): ¹H at δ 5.19 correlates

to ^{13}C - α at δ 48.8. HRMS [ESI $^+$] calculated for $\text{C}_{14}\text{H}_{14}\text{N}_4\text{Na}_3\text{O}_8\text{P}_2\text{S}_2$ m/z , 560.9416; found 560.9422 [M + 3 Na] $^+$

Inhibitor 5.28f:

Corresponding bisphosphonate ester: Tetraethyl (((2-(4-benzamidophenyl)thieno[2,3-*d*]pyrimidin-4-yl)amino)methylene)bis(phosphonate). ^1H NMR (400 MHz, DMSO- d_6) δ 10.46 (s, -NH), 8.60 (d, J = 9.6 Hz, -NH), 8.37 (d, J = 8.7 Hz, 2H), 8.07 (d, J = 6.0 Hz, 1H), 7.99 (d, J = 7.1 Hz, 2H), 7.95 (d, J = 8.8 Hz, 2H), 7.63 – 7.52 (m, 4H), 6.02 (td, J = 23.5, 9.5 Hz, 1H), 4.20 – 4.05 (m, 8H), 1.20 – 1.10 (m, 12H). ^{31}P NMR (162 MHz, DMSO- d_6) δ 17.16.

Final Inhibitor: (((2-(4-benzamidophenyl)thieno[2,3-*d*]pyrimidin-4-yl)amino)methylene)bis(phosphonic acid) (**5.28f**). ^1H NMR (400 MHz, D_2O) δ 8.43 (d, J = 8.7 Hz, 2H), 7.98 (d, J = 7.3 Hz, 2H), 7.80 (d, J = 8.6 Hz, 2H), 7.73 (t, J = 7.4 Hz, 1H), 7.66 – 7.60 (m, 3H), 7.49 (d, J = 6.0 Hz, 1H), 5.05 (t, J = 19.0 Hz, 1H). ^{31}P NMR (162 MHz, D_2O) δ 13.67 (s). HRMS [ESI $^+$] calculated for $\text{C}_{20}\text{H}_{16}\text{N}_4\text{Na}_3\text{O}_7\text{P}_2\text{S}$ m/z , 586.9903; found 586.9906 [M + 3 Na] $^+$

Inhibitor 5.28g:

Corresponding bisphosphonate ester: Tetraethyl (((2-(4-((4-methylphenyl)sulfonamido)phenyl)thieno[2,3-*d*]pyrimidin-4-yl)amino)methylene)bis(phosphonate). ^1H NMR (500 MHz, DMSO- d_6) δ 10.52 (s, -NH), 8.58 (d, J = 9.7 Hz, -NH), 8.21 (d, J = 8.7 Hz, 2H), 8.04 (d, J = 6.0 Hz, 1H), 7.71 (d, J = 8.3 Hz, 2H), 7.58 (d, J = 6.0 Hz, 1H), 7.35 (d, J = 8.1 Hz, 2H), 7.23 (d, J = 8.8 Hz, 2H), 5.93 (td, J = 23.4, 9.2 Hz, 1H), 4.15 – 4.00 (m, 8H), 2.32 (s, 3H), 1.16 - 1.07 (m, 12H). ^{31}P NMR (203 MHz, DMSO- d_6) δ 17.12 (s).

Final Inhibitor: (((2-(4-((4-methylphenyl)sulfonamido)phenyl)thieno[2,3-d]pyrimidin-4-yl)amino)methylene)bis(phosphonic acid) (**5.28g**). Isolated as off-white solid. ^1H NMR (400 MHz, D_2O) δ 8.12 (d, $J = 8.7$ Hz, 2H), 7.79 (d, $J = 8.3$ Hz, 2H), 7.58 (d, $J = 5.9$ Hz, 1H), 7.42 - 7.39 (m, 3H), 7.06 (d, $J = 8.7$ Hz, 2H), 4.97 (t, $J = 19.0$ Hz, 1H), 2.42 (s, 3H). ^{31}P NMR (162 MHz, D_2O) δ 13.70 (s). HRMS [ESI^+] calculated for $\text{C}_{20}\text{H}_{18}\text{N}_4\text{Na}_3\text{O}_8\text{P}_2\text{S}_2$ m/z , 636.9729; found 636.9725 [$\text{M} + 3 \text{Na}$] $^+$

Inhibitor 5.28h:

Corresponding bisphosphonate ester: Tetraethyl (((2-(3-(phenylsulfonamido)phenyl)thieno[2,3-d]pyrimidin-4-yl)amino)methylene)bis(phosphonate). Isolated as a cream solid. ^1H NMR (500 MHz, $\text{DMSO}-d_6$) δ 10.61 (s, -NH), 8.58 (d, $J = 9.7$ Hz, -NH), 8.22 (d, $J = 8.8$ Hz, 2H), 8.05 (d, $J = 6.0$ Hz, 1H), 7.84 - 7.82 (m, 2H), 7.63 - 7.55 (m, 4H), 7.24 (d, $J = 8.8$ Hz, 2H), 5.94 (td, $J = 23.3, 9.4$ Hz, 1H), 4.13 - 4.04 (m, 8H), 1.16 - 1.08 (m, 12H). ^{31}P NMR (203 MHz, DMSO) δ 17.12 (s).

Final Inhibitor: (((2-(3-(phenylsulfonamido)phenyl)thieno[2,3-d]pyrimidin-4-yl)amino)methylene)bis(phosphonic acid) (**5.28h**). Isolated as cream solid. ^1H NMR (500 MHz, D_2O) δ 8.20 (d, $J = 8.3$ Hz, 2H), 7.87 (d, $J = 7.6$ Hz, 2H), 7.68 - 7.63 (m, 1H), 7.59 - 7.56 (m, 3H), 7.45 (d, $J = 5.8$ Hz, 1H), 7.22 (d, $J = 8.4$ Hz, 2H), 5.15 (t, $J = 17.0$ Hz, 1H). ^{31}P NMR (203 MHz, D_2O) δ 13.87 (s). ^{13}C NMR (101 MHz, D_2O) δ 165.7, 159.7, 156.9, 140.4, 138.2, 133.4 (two carbons), 129.4 (two carbons), 129.3, 129.2, 126.8, 122.8, 121.3, 118.8, 115.5. C- α to the bisphosphonate was observed by HSQC. HSQC (^1H - ^{13}C): ^1H at δ 5.15 correlates to ^{13}C - α at δ 47.0. HRMS [ESI^+] calculated for $\text{C}_{19}\text{H}_{16}\text{N}_4\text{Na}_3\text{O}_8\text{P}_2\text{S}_2$ m/z , 622.95724; found 622.95769 [$\text{M} + 3 \text{Na}$] $^+$

Inhibitor 5.28i:

Corresponding bisphosphonate ester: Tetraethyl (((2-(3-benzamidophenyl)thieno[2,3-d]pyrimidin-4-yl)amino)methylene)bis(phosphonate). Isolated as a beige solid. ^1H NMR (500 MHz, DMSO- d_6) δ 10.43 (s, -NH), 8.86 (t, $J = 1.7$ Hz, 1H), 8.65 (d, $J = 9.7$ Hz, -NH), 8.12 (d, $J = 7.9$ Hz, 1H), 8.10 (d, $J = 6.0$ Hz, 1H), 8.01 (d, $J = 7.1$ Hz, 2H), 7.91 (dd, $J = 8.1, 1.1$ Hz, 1H), 7.64 (d, $J = 6.0$ Hz, 1H), 7.63 – 7.59 (m, 1H), 7.57 – 7.53 (m, 2H), 7.51 (t, $J = 7.9$ Hz, 1H), 6.06 (td, $J = 23.3, 9.5$ Hz, 1H), 4.18 – 4.07 (m, 8H), 1.19 – 1.10 (m, 12H). ^{31}P NMR (203 MHz, DMSO- d_6) δ 17.01 (s).

Final Inhibitor: (((2-(3-benzamidophenyl)thieno[2,3-d]pyrimidin-4-yl)amino)methylene)bis(phosphonic acid) (**5.28i**). Isolated as cream solid. ^1H NMR (400 MHz, D_2O) δ 8.36 (s, 1H), 8.18 (d, $J = 7.9$ Hz, 1H), 7.95 (d, $J = 7.3$ Hz, 2H), 7.89 (d, $J = 8.2$ Hz, 1H), 7.70 – 7.57 (m, 5H), 7.49 (d, $J = 6.0$ Hz, 1H), 5.13 (t, $J = 18.6$ Hz, 1H). ^{31}P NMR (162 MHz, D_2O) δ 13.79 (s). ^{13}C NMR (101 MHz, D_2O) δ 169.8, 165.5, 159.8, 157.0, 138.7, 137.5, 133.9, 132.4, 129.5, 128.8, 127.4, 125.3, 124.3, 123.1, 122.0, 119.0, 115.9. C- α to the bisphosphonate was observed by HSQC. HSQC (^1H - ^{13}C): ^1H at δ 5.13 correlates to ^{13}C - α at δ 49.5. HRMS [ESI $^+$] calculated for $\text{C}_{20}\text{H}_{16}\text{N}_4\text{Na}_3\text{O}_7\text{P}_2\text{S}$ m/z , 586.9903; found 586.9898 [M + 3 Na] $^+$

Inhibitor 5.28j:

Corresponding bisphosphonate ester: Tetraethyl (((2-(3-(thiophene-2-carboxamido)phenyl)thieno[2,3-d]pyrimidin-4-yl)amino)methylene)bis(phosphonate). Isolated as a yellow solid. ^1H NMR (500 MHz, DMSO- d_6) δ 10.41 (s, -NH), 8.80 (t, $J = 1.8$ Hz, 1H), 8.66 (d, $J = 9.7$ Hz, -NH), 8.12 (d, $J = 7.9$ Hz, 1H), 8.10 - 8.09 (m, 2H), 7.89 - 7.87 (m, 2H), 7.64 (d, $J = 6.0$ Hz, 1H), 7.51 (t, $J = 7.9$ Hz, 1H), 7.25 (dd, $J = 4.9, 3.8$ Hz, 1H), 6.06 (td, $J = 23.4, 9.7$

Hz, 1H), 4.18 - 4.06 (m, 8H), 1.20 – 1.10 (m, 12H). ³¹P NMR (203 MHz, DMSO-d₆) δ 16.97 (s).

MS [ESI⁺] m/z: 639.1 [M + H⁺]⁺

Final Inhibitor: (((2-(3-(thiophene-2-carboxamido)phenyl)thieno[2,3-d]pyrimidin-4-yl)amino)methylene)bis(phosphonic acid) (**5.28j**). Isolated as a yellow solid. ¹H NMR (400 MHz, D₂O) δ 8.35 (s, 1H), 8.17 (d, *J* = 7.9 Hz, 1H), 7.94 (dd, *J* = 3.7, 0.8 Hz, 1H), 7.86 (dd, *J* = 8.0, 1.2 Hz, 1H), 7.80 (dd, *J* = 5.0, 0.9 Hz, 1H), 7.64 - 7.60 (m, 2H), 7.49 (d, *J* = 6.0 Hz, 1H), 7.27 (dd, *J* = 4.9, 3.9 Hz, 1H), 5.14 (t, *J* = 18.8 Hz, 1H). ³¹P NMR (203 MHz, D₂O) δ 13.81 (s). ¹³C NMR (101 MHz, D₂O) δ 165.5, 163.3, 159.8, 156.7, 138.7, 137.6, 137.2, 132.2, 130.4, 129.5, 128.4, 125.2, 124.3, 123.0, 121.9, 119.0, 115.9. C-α to the bisphosphonate was observed by HSQC. HSQC (¹H-¹³C): ¹H at δ 5.14 correlates to ¹³C-α at δ 49.5. HRMS [ESI⁺] calculated for C₁₈H₁₄N₄Na₃O₇P₂S₂ m/z, 592.94667; found 592.94813 [M + 3 Na]⁺

Inhibitor 5.28k:

Corresponding bisphosphonate ester: Tetraethyl (((2-(3-(picolinamido)phenyl)thieno[2,3-d]pyrimidin-4-yl)amino)methylene)bis(phosphonate). Isolated as a yellow solid. ¹H NMR (500 MHz, DMSO-d₆) δ 10.77 (s, -NH), 9.02 (t, *J* = 1.8 Hz, 1H), 8.77 (ddd, *J* = 4.8, 1.5, 0.9 Hz, 1H), 8.65 (d, *J* = 9.7 Hz, -NH), 8.18 (d, *J* = 7.8 Hz, 1H), 8.15 (d, *J* = 7.9 Hz, 1H), 8.12 - 8.08 (m, 2H), 7.93 (ddd, *J* = 8.1, 2.0, 0.8 Hz, 1H), 7.70 (ddd, *J* = 7.5, 4.8, 1.2 Hz, 1H), 7.64 (d, *J* = 6.0 Hz, 1H), 7.51 (t, *J* = 7.9 Hz, 1H), 6.08 (td, *J* = 23.4, 9.7 Hz, 1H), 4.20 – 4.07 (m, 8H), 1.20 – 1.10 (m, 12H). ³¹P NMR (203 MHz, DMSO-d₆) δ 17.00 (s). MS [ESI⁺] m/z: 634.3 [M + H⁺]⁺

Final Inhibitor: (((2-(3-(picolinamido)phenyl)thieno[2,3-d]pyrimidin-4-yl)amino)methylene)bis(phosphonic acid) (**5.28k**). Isolated as a yellow solid. ¹H NMR (500 MHz, D₂O) δ 8.72 (d, *J* = 4.7 Hz, 1H), 8.48 (s, 1H), 8.17 (d, *J* = 7.9 Hz, 2H), 8.07 (td, *J* = 7.8,

1.5 Hz, 1H), 7.98 (d, $J = 9.1$ Hz, 1H), 7.68 - 7.63 (m, 2H), 7.60 (d, $J = 5.9$ Hz, 1H), 7.46 (d, $J = 5.9$ Hz, 1H), 5.06 (t, $J = 19.1$ Hz, 1H). ^{31}P NMR (203 MHz, D_2O) δ 13.68 (s). ^{13}C NMR (101 MHz, D_2O) δ 165.5, 165.3, 159.7, 156.9, 148.9, 148.7, 138.6, 138.4, 137.0, 129.5, 127.3, 125.2, 123.5, 123.1, 122.7, 121.2, 118.9, 115.8, 49.3 (t, $J = 121.8$ Hz). HRMS [ESI⁺] calculated for $\text{C}_{19}\text{H}_{15}\text{N}_5\text{Na}_3\text{O}_7\text{P}_2\text{S}$ m/z , 587.98550; found 587.98657 [M + 3 Na]⁺

Inhibitor 5.28I:

Corresponding bisphosphonate ester: Tetraethyl (((2-(3-(cyclopropanecarboxamido)phenyl)thieno[2,3-d]pyrimidin-4-yl)amino)methylene)bis(phosphonate). Isolated as a yellow solid. ^1H NMR (400 MHz, DMSO-d_6) δ 10.36 (s, -NH), 8.66 (s, 1H), 8.62 (d, $J = 9.7$ Hz, -NH), 8.09 (d, $J = 6.0$ Hz, 1H), 8.04 (d, $J = 7.8$ Hz, 1H), 7.72 (d, $J = 9.0$ Hz, 1H), 7.63 (d, $J = 6.0$ Hz, 1H), 7.43 (t, $J = 7.9$ Hz, 1H), 6.03 (td, $J = 23.4, 9.7$ Hz, 1H), 4.17 - 4.05 (m, 8H), 1.85 - 1.79 (m, 1H), 1.19 - 1.09 (m, 12H), 0.82 - 0.79 (m, 4H). ^{31}P NMR (203 MHz, DMSO-d_6) δ 16.98 (s). MS [ESI⁺] m/z : 597.16 [M + H]⁺

Final Inhibitor: (((2-(3-(cyclopropanecarboxamido)phenyl)thieno[2,3-d]pyrimidin-4-yl)amino)methylene)bis(phosphonic acid) (**5.28I**). Isolated as yellow solid. ^1H NMR (500 MHz, D_2O) δ 8.27 (s, 1H), 8.12 (d, $J = 7.7$ Hz, 1H), 7.82 (d, $J = 8.1$ Hz, 1H), 7.63 (d, $J = 5.9$ Hz, 1H), 7.59 (t, $J = 8.0$ Hz, 1H), 7.51 (d, $J = 6.0$ Hz, 1H), 5.13 (t, $J = 19.0$ Hz, 1H), 1.90 - 1.85 (m, 1H), 1.04 - 0.98 (m, 4H). ^{31}P NMR (203 MHz) δ 13.81 (s). ^{13}C NMR (126 MHz, D_2O) δ 176.2, 165.2, 159.9, 156.8, 138.6, 137.7, 129.4, 124.5, 123.3, 122.7, 120.9, 119.1, 115.9, 50.5 (t, $J = 125.0$ Hz), 14.8, 7.4. HRMS [ESI⁺] calculated for $\text{C}_{17}\text{H}_{16}\text{N}_4\text{Na}_3\text{O}_7\text{P}_2\text{S}$ m/z , 550.99025; found 550.99190 [M + 3 Na]⁺

Inhibitor 5.28m:

Corresponding bisphosphonate ester: Tetraethyl (((2-(3-(cyclohexanecarboxamido)phenyl)thieno[2,3-d]pyrimidin-4-yl)amino)methylene)bis(phosphonate). Isolated as a yellow solid. ¹H NMR (500 MHz, DMSO-d₆) δ 9.97 (s, -NH), 8.68 (t, *J* = 1.8 Hz, 1H), 8.62 (d, *J* = 9.7 Hz, -NH), 8.09 (d, *J* = 6.0 Hz, 1H), 8.03 (d, *J* = 7.9 Hz, 1H), 7.71 (ddd, *J* = 8.1, 2.0, 0.9 Hz, 1H), 7.62 (d, *J* = 6.0 Hz, 1H), 7.42 (t, *J* = 7.9 Hz, 1H), 6.04 (td, *J* = 23.4, 9.7 Hz, 1H), 4.18 – 4.06 (m, 8H), 2.37 (tt, *J* = 11.6, 3.4 Hz, 1H), 1.78 - 1.65 (m, 5H), 1.48 – 1.20 (m, 5H), 1.19 – 1.09 (m, 12H). ³¹P NMR (203 MHz, DMSO-d₆) δ 16.98 (s). MS [ESI⁺] *m/z*: 639.2 [M + H⁺]⁺

Final Inhibitor: (((2-(3-(cyclohexanecarboxamido)phenyl)thieno[2,3-d]pyrimidin-4-yl)amino)methylene)bis(phosphonic acid) (**5.28m**). Isolated as a yellow solid. ¹H NMR (500 MHz, D₂O) δ 8.25 (s, 1H), 8.14 (d, *J* = 7.9 Hz, 1H), 7.82 (d, *J* = 8.1 Hz, 1H), 7.64 – 7.59 (m, 2H), 7.50 (d, *J* = 5.9 Hz, 1H), 5.11 (t, *J* = 19.1 Hz, 1H), 2.49 (tt, *J* = 11.8, 3.3 Hz, 1H), 1.99 - 1.73 (m, 5H), 1.56 - 1.27 (m, 5H). ³¹P NMR (203 MHz, D₂O) δ 13.77 (s). ¹³C NMR (101 MHz, D₂O) δ 179.1, 165.6, 159.9, 157.0, 138.6, 137.5, 129.5, 124.9, 123.8, 123.1, 121.4, 118.9, 115.8, 45.8, 29.1, 25.3, 25.2. C-α to the bisphosphonate was observed by HSQC. HSQC (¹H-¹³C): ¹H at δ 5.11 correlates to ¹³C-α at δ 49.0. HRMS [ESI⁺] calculated for C₂₀H₂₂N₄Na₃O₇P₂S *m/z*, 593.03720; found 593.03804 [M + 3 Na]⁺

Inhibitor 5.28n:

Corresponding bisphosphonate ester: Tetraethyl (((2-([1,1'-biphenyl]-3-yl)thieno[2,3-d]pyrimidin-4-yl)amino)methylene)bis(phosphonate). Prepared *via* Suzuki cross-coupling between tetraethyl (((2-(3-bromophenyl)thieno[2,3-d]pyrimidin-4-

yl)amino)methylene)bis(phosphonate) **5.29b-1** and phenyl boronic acid. Isolated as a light yellow solid. ^1H NMR (500 MHz, CDCl_3) δ 8.74 (s, 1H), 8.45 (d, $J = 7.8$ Hz, 1H), 7.73 – 7.69 (m, 3H), 7.57 (t, $J = 7.7$ Hz, 1H), 7.48 (t, $J = 7.6$ Hz, 2H), 7.40 – 7.36 (m, 3H), 6.02 – 5.91 (m, 2H; -NH and α -CH to the bisphosphonate), 4.30 – 4.13 (m, 8H), 1.29 – 1.22 (m, 12H). ^{31}P NMR (203 MHz, CDCl_3) δ 16.76.

Final Inhibitor: (((2-([1,1'-biphenyl]-3-yl)thieno[2,3-d]pyrimidin-4-yl)amino)methylene)bis(phosphonic acid) (**5.28n**). Isolated as a pale brown solid. ^1H NMR (500 MHz, D_2O) δ 8.52 (s, 1H), 8.31 (d, $J = 7.7$ Hz, 1H), 7.88 – 7.76 (m, 3H), 7.66 (t, $J = 7.8$ Hz, 1H), 7.60 (d, $J = 5.9$ Hz, 1H), 7.55 (t, $J = 7.7$ Hz, 2H), 7.48 (d, $J = 6.0$ Hz, 1H), 7.44 (d, $J = 7.4$ Hz, 1H), 5.19 (t, $J = 17.7$ Hz, 1H). ^{13}C NMR (125 MHz, D_2O): δ 165.7 160.4, 157.0, 141.0, 140.3, 138.3, 129.4, 129.1, 129.0, 127.8, 127.5, 127.1, 126.4, 123.2, 118.8, 115.7. $\text{C}\alpha$ observed by HSQC. HSQC (^1H - ^{13}C): ^1H δ 5.19 correlates with ^{13}C δ 49.0. ^{31}P NMR (203 MHz, D_2O): δ 13.9. MS (ESI⁺) m/z : 478.2 [$\text{M} + \text{H}^+$]⁺.

Inhibitor 5.28o:

Corresponding bisphosphonate ester: Tetraethyl (((2-(3-(2-methylbenzamido)phenyl)thieno[2,3-d]pyrimidin-4-yl)amino)methylene)bis(phosphonate). Isolated as a yellow solid. ^1H NMR (500 MHz, DMSO-d_6) δ 10.47 (s, -NH), 8.88 (s, 1H), 8.63 (d, $J = 9.7$ Hz, -NH), 8.14 - 8.11 (m, 2H), 7.82 (d, $J = 7.9$ Hz, 1H), 7.64 (d, $J = 6.0$ Hz, 1H), 7.51 – 7.47 (m, 2H), 7.43 – 7.38 (m, 1H), 7.34 - 7.31 (m, 2H), 6.07 (td, $J = 23.4, 9.7$ Hz, 1H), 4.19 – 4.07 (m, 8H), 2.43 (s, 3H), 1.18 – 1.10 (m, 12H). ^{31}P NMR (203 MHz, DMSO-d_6) δ 17.01 (s). MS [ESI⁺] m/z : 647.2 [$\text{M} + \text{H}^+$]⁺

Final Inhibitor: (((2-(3-(2-methylbenzamido)phenyl)thieno[2,3-d]pyrimidin-4-yl)amino)methylene)bis(phosphonic acid) (**5.28o**). Isolated as a yellow solid. ^1H NMR (500

MHz, D₂O) δ 8.35 (s, 1H), 8.22 (d, $J = 7.9$ Hz, 1H), 7.98 (dd, $J = 8.0, 1.2$ Hz, 1H), 7.68 (t, $J = 8.0$ Hz, 1H), 7.64 (d, $J = 6.0$ Hz, 1H), 7.62 (d, $J = 8.1$ Hz, 1H), 7.53 - 7.50 (m, 2H), 7.44 - 7.39 (m, 2H), 5.11 (t, $J = 19.0$ Hz, 1H), 2.50 (s, 3H). ³¹P NMR (203 MHz, D₂O) δ 13.77 (s). ¹³C NMR (101 MHz, D₂O) δ 171.9, 165.5, 159.9, 157.0, 138.8, 137.3, 135.7, 135.5, 130.9, 130.6, 129.6, 126.9, 125.9, 125.4, 123.8, 123.0, 121.5, 119.0, 115.9, 18.6. C- α to the bisphosphonate was observed by HSQC. HSQC (¹H-¹³C): ¹H at δ 5.11 correlates to ¹³C- α at δ 49.8. HRMS [ESI⁺] calculated for C₂₁H₁₈N₄Na₃O₇P₂S m/z , 601.00590; found 601.00705 [M + 3 Na]⁺

Inhibitor 5.28p:

Corresponding bisphosphonate ester: Tetraethyl (((2-(3-(3-methylbenzamido)phenyl)thieno[2,3-d]pyrimidin-4-yl)amino)methylene)bis(phosphonate). Isolated as a yellow solid. ¹H NMR (500 MHz, DMSO-d₆) δ 10.38 (br_s, -NH), 8.85 (t, $J = 1.8$ Hz, 1H), 8.65 (d, $J = 9.7$ Hz, -NH), 8.12 (d, $J = 7.9$ Hz, 1H), 8.10 (d, $J = 6.0$ Hz, 1H), 7.92 (dd, $J = 8.1, 1.1$ Hz, 1H), 7.84 (s, 1H), 7.80 (d, $J = 6.6$ Hz, 1H), 7.64 (d, $J = 6.0$ Hz, 1H), 7.50 (t, $J = 7.9$ Hz, 1H), 7.45 - 7.41 (m, 2H), 6.06 (td, $J = 23.4, 9.7$ Hz, 1H), 4.18 - 4.07 (m, 8H), 2.42 (s, 3H), 1.19 - 1.10 (m, 12H). ³¹P NMR (203 MHz, DMSO-d₆) δ 17.00 (s). MS [ESI⁺] m/z : 647.2 [M + H]⁺

Final Inhibitor: (((2-(3-(3-methylbenzamido)phenyl)thieno[2,3-d]pyrimidin-4-yl)amino)methylene)bis(phosphonic acid) (**5.28p**). Isolated as a light brown solid. ¹H NMR (500 MHz, D₂O) δ 8.39 (s, 1H), 8.21 (d, $J = 7.9$ Hz, 1H), 7.95 (d, $J = 8.0$ Hz, 1H), 7.82 (s, 1H), 7.78 (d, $J = 7.3$ Hz, 1H), 7.67 (t, $J = 8.0$ Hz, 1H), 7.64 (d, $J = 6.0$ Hz, 1H), 7.56 - 7.52 (m, 2H), 7.51 (d, $J = 5.9$ Hz, 1H), 5.11 (t, $J = 19.0$ Hz, 1H), 2.48 (s, 3H). ³¹P NMR (203 MHz, D₂O) δ 13.80 (s). ¹³C NMR (101 MHz, D₂O) δ 169.9, 165.3, 159.9, 157.0, 139.2, 138.7, 137.5, 134.0, 133.1, 129.6, 128.8, 127.9, 125.3, 124.5, 124.4, 122.9, 122.0, 119.1, 116.0, 20.5. C- α to the

bisphosphonate was observed by HSQC. HSQC (^1H - ^{13}C): ^1H at δ 5.11 correlates to ^{13}C - α at δ 50.1. HRMS [ESI $^+$] calculated for $\text{C}_{21}\text{H}_{18}\text{N}_4\text{Na}_3\text{O}_7\text{P}_2\text{S}$ m/z , 601.00590; found 601.00727 [M + 3 Na] $^+$

Inhibitor 5.28q:

Corresponding bisphosphonate ester: Tetraethyl (((2-(3-(4-methylbenzamido)phenyl)thieno[2,3-d]pyrimidin-4-yl)amino)methylene)bis(phosphonate). Isolated as a yellow solid. ^1H NMR (500 MHz, DMSO- d_6) δ 10.34 (s, -NH), 8.85 (t, $J = 1.8$ Hz, 1H), 8.65 (d, $J = 9.7$ Hz, -NH), 8.12 -8.09 (m, 2H), 7.93 (d, $J = 8.2$ Hz, 2H), 7.91 (ddd, $J = 8.1, 2.1, 1.0$ Hz, 1H), 7.64 (d, $J = 6.0$ Hz, 1H), 7.50 (t, $J = 7.9$ Hz, 1H), 7.35 (d, $J = 7.9$ Hz, 2H), 6.06 (td, $J = 23.4, 9.7$ Hz, 1H), 4.18 – 4.05 (m, 8H), 2.40 (s, 3H), 1.19 – 1.10 (m, 12H). ^{31}P NMR (203 MHz, DMSO- d_6) δ 17.00 (s). MS [ESI $^+$] m/z : 647.2 [M + H] $^+$

Final Inhibitor: (((2-(3-(4-methylbenzamido)phenyl)thieno[2,3-d]pyrimidin-4-yl)amino)methylene)bis(phosphonic acid) (**5.28q**). Isolated as a cream solid. ^1H NMR (500 MHz, D_2O) δ 8.38 (s, 1H), 8.20 (d, $J = 7.6$ Hz, 1H), 7.93 (d, $J = 7.1$ Hz, 1H), 7.89 (d, $J = 7.9$ Hz, 2H), 7.68 - 7.63 (m, 2H), 7.51 (d, $J = 5.9$ Hz, 1H), 7.46 (d, $J = 7.9$ Hz, 2H), 5.15 (t, $J = 18.9$ Hz, 1H), 2.47 (s, 3H). ^{31}P NMR (203 MHz, D_2O) δ 13.82 (s). ^{13}C NMR (101 MHz, D_2O) δ 169.3, 165.6, 159.5, 156.8, 143.5, 138.3, 137.5, 130.7, 129.4, 129.3, 127.5, 125.0, 124.1, 123.3, 121.6, 118.8, 115.8, 48.9 (t, $J = 124.8$ Hz), 20.6. HRMS [ESI $^+$] calculated for $\text{C}_{21}\text{H}_{18}\text{N}_4\text{Na}_3\text{O}_7\text{P}_2\text{S}$ m/z , 601.00590; found 601.00773 [M + 3 Na] $^+$

Inhibitor 5.28r:

Corresponding bisphosphonate ester: Tetraethyl (((2-(3-(4-ethylbenzamido)phenyl)thieno[2,3-d]pyrimidin-4-yl)amino)methylene)bis(phosphonate). Isolated as a light brown solid. ^1H NMR

(500 MHz, DMSO-d₆) δ 10.36 (s, -NH), 8.86 (s, 1H), 8.66 (d, $J = 9.7$ Hz, -NH), 8.13 - 8.10 (m, 2H), 7.95 (d, $J = 8.1$ Hz, 2H), 7.91 (d, $J = 9.1$ Hz, 1H), 7.64 (d, $J = 6.0$ Hz, 1H), 7.50 (t, $J = 7.9$ Hz, 1H), 7.38 (d, $J = 8.1$ Hz, 2H), 6.07 (td, $J = 23.4, 9.7$ Hz, 1H), 4.18 - 4.09 (m, 8H), 2.69 (q, $J = 7.6$ Hz, 2H), 1.22 (t, $J = 7.6$ Hz, 3H), 1.19 - 1.10 (m, 12H). ³¹P NMR (203 MHz, DMSO-d₆) δ 17.00 (s). MS [ESI⁺] m/z : 661.2 [M + H⁺]⁺

Final Inhibitor: (((2-(3-(4-ethylbenzamido)phenyl)thieno[2,3-d]pyrimidin-4-

yl)amino)methylene)bis(phosphonic acid) (**5.28r**). Isolated as a beige solid. ¹H NMR (500 MHz, D₂O) δ 8.39 (s, 1H), 8.21 (d, $J = 7.9$ Hz, 1H), 7.95 - 7.92 (m, 3H), 7.68 - 7.63 (m, 2H), 7.52 - 7.50 (m, 3H), 5.12 (t, $J = 19.1$ Hz, 2H), 2.79 (q, $J = 7.6$ Hz, 2H), 1.29 (t, $J = 7.6$ Hz, 3H). ³¹P NMR (203 MHz, D₂O) δ 13.78 (s). ¹³C NMR (126 MHz, D₂O) δ 169.6, 165.2, 160.0, 156.9, 149.8, 138.7, 137.5, 131.2, 129.5, 128.3, 127.7, 125.2, 124.4, 122.8, 122.0, 119.1, 115.9, 28.3, 14.6. C- α to the bisphosphonate was observed by HSQC. HSQC (¹H-¹³C): ¹H at δ 5.12 correlates to ¹³C- α at δ 50.5. HRMS [ESI⁺] calculated for C₂₂H₂₀N₄Na₃O₇P₂S m/z , 615.02155; found 615.02296 [M + 3 Na]⁺

Inhibitor 5.28s:

Corresponding bisphosphonate ester: Tetraethyl (((2-(3-(4-

methoxybenzamido)phenyl)thieno[2,3-d]pyrimidin-4-yl)amino)methylene)bis(phosphonate).

Isolated as a yellow solid. ¹H NMR (500 MHz, DMSO-d₆) δ 10.27 (s, -NH), 8.84 (t, $J = 1.7$ Hz, 1H), 8.65 (d, $J = 9.7$ Hz, -NH), 8.11 - 8.09 (m, 2H), 8.02 (d, $J = 8.8$ Hz, 2H), 7.90 (dd, $J = 6.9, 1.2$ Hz, 1H), 7.64 (d, $J = 6.0$ Hz, 1H), 7.49 (t, $J = 7.9$ Hz, 1H), 7.08 (d, $J = 8.9$ Hz, 2H), 6.06 (td, $J = 23.4, 9.7$ Hz, 1H), 4.18 - 4.07 (m, 8H), 3.85 (s, 3H), 1.19 - 1.10 (m, 12H). ³¹P NMR (203 MHz, DMSO-d₆) δ 17.01 (s). MS [ESI⁺] m/z : 663.2 [M + H⁺]⁺

Final Inhibitor: (((2-(3-(4-methoxybenzamido)phenyl)thieno[2,3-d]pyrimidin-4-yl)amino)methylene)bis(phosphonic acid) (**5.28s**). Isolated as beige solid. ^1H NMR (400 MHz, D_2O) δ 8.36 (s, 1H), 8.19 (d, $J = 7.8$ Hz, 1H), 7.98 (d, $J = 8.8$ Hz, 2H), 7.91 (d, $J = 8.1$ Hz, 1H), 7.68 - 7.60 (m, 2H), 7.50 (d, $J = 6.0$ Hz, 1H), 7.17 (d, $J = 8.9$ Hz, 2H), 5.11 (t, $J = 19.0$ Hz, 1H), 3.94 (s, 3H). ^{31}P NMR (162 MHz, D_2O) δ 13.78 (s). ^{13}C NMR (126 MHz, D_2O) δ 169.1, 165.0, 162.2, 160.0, 156.8, 138.7, 137.6, 129.6, 129.5, 126.3, 125.1, 124.4, 122.6, 122.0, 119.2, 116.0, 114.1, 55.5. C- α to the bisphosphonate was observed by HSQC. HSQC (^1H - ^{13}C): ^1H at δ 5.11 correlates to ^{13}C - α at δ 50.0. HRMS [ESI $^+$] calculated for $\text{C}_{21}\text{H}_{18}\text{N}_4\text{Na}_3\text{O}_8\text{P}_2\text{S}$ m/z , 617.00082; found 617.00181 [$\text{M} + 3 \text{Na}$] $^+$

Inhibitor 5.28t:

Corresponding bisphosphonate ester: Tetraethyl (((2-(3-(phenylcarbamoyl)phenyl)thieno[2,3-d]pyrimidin-4-yl)amino)methylene)bis(phosphonate). Prepared *via* **Method A** using tetraethyl (((2-(methylthio)thieno[2,3-d]pyrimidin-4-yl)amino)methylene)bis(phosphonate) **5.27a-1** and (3-(phenylcarbamoyl)phenyl)boronic acid⁵⁹ as coupling partners. Isolated as a light yellow solid. ^1H NMR (400 MHz, DMSO-d_6) δ 10.47 (s, -NH), 8.95 (s, 1H), 8.75 (d, $J = 9.6$ Hz, -NH), 8.57 (d, $J = 7.9$ Hz, 1H), 8.10 (d, $J = 5.7$ Hz, 1H), 8.07 (d, $J = 7.9$ Hz, 1H), 7.82 (d, $J = 7.7$ Hz, 2H), 7.71 - 7.66 (m, 2H), 7.39 - 7.35 (m, 2H), 7.12 (t, $J = 7.4$ Hz, 1H), 6.03 (br, 1H), 4.18 - 4.00 (m, 8H), 1.19 - 1.08 (m, 12H). ^{31}P NMR (162 MHz, DMSO-d_6) δ 17.05 (s). ^{13}C NMR (126 MHz, DMSO-d_6) δ 167.6, 165.5, 157.5, 156.0 (t, $J = 3.7$ Hz), 139.2, 137.7, 135.5, 130.4, 129.4, 128.7, 128.6, 127.1, 123.8, 123.7, 120.3, 120.2, 115.5, 62.9 - 62.7 (m), 16.2 - 16.1 (m). C- α to the bisphosphonate was observed by HSQC. HSQC (^1H - ^{13}C): ^1H at δ 6.03 correlates to ^{13}C - α at δ 45.1. MS [ESI $^+$] m/z : 633.2 [$\text{M} + \text{H}^+$] $^+$

Final Inhibitor: (((2-(3-(phenylcarbamoyl)phenyl)thieno[2,3-d]pyrimidin-4-yl)amino)methylene)bis(phosphonic acid) (**5.28t**). Isolated as off-white solid. ^1H NMR (400 MHz, D_2O) δ 8.81 (s, 1H), 8.58 (d, $J = 7.9$ Hz, 1H), 8.06 (d, $J = 7.8$ Hz, 1H), 7.76 (t, $J = 7.8$ Hz, 1H), 7.66 – 7.63 (m, 3H), 7.56 – 7.52 (m, 3H), 7.36 (t, $J = 7.4$ Hz, 1H), 5.20 (t, $J = 19.0$ Hz, 1H). ^{31}P NMR (203 MHz, D_2O) δ 13.91 (s). ^{13}C NMR (126 MHz, D_2O) δ 169.4, 165.5, 159.7, 157.0, 138.3, 136.9, 134.4, 132.0, 129.4, 129.3, 129.2, 126.9, 126.0, 123.2, 123.0, 119.0, 115.9, 49.3. HRMS [ESI $^+$] calculated for $\text{C}_{20}\text{H}_{16}\text{N}_4\text{Na}_3\text{O}_7\text{P}_2\text{S}$ m/z , 586.9903; found 586.9903 [M + 3 Na] $^+$

Inhibitor 5.28w:

Corresponding bisphosphonate ester: Tetraethyl (((6-(3-benzamidophenyl)thieno[2,3-d]pyrimidin-4-yl)amino)methylene)bis(phosphonate). Prepared *via* Suzuki cross-coupling between tetraethyl (((6-bromothieno[2,3-d]pyrimidin-4-yl)amino)methylene)bis(phosphonate)²³ and (3-benzamidophenyl)boronic acid⁶⁰ as coupling partners. Isolated as a cream solid. ^1H NMR (400 MHz, DMSO-d_6) δ 10.43 (s, -NH), 8.71 (d, $J = 9.7$ Hz, -NH), 8.54 (s, 1H), 8.45 (s, 1H), 8.31 (d, $J = 2.3$ Hz, 1H), 8.03 – 7.99 (m, 2H), 7.77 (d, $J = 7.5$ Hz, 1H), 7.64 – 7.44 (m, 5H), 5.81 (td, $J = 23.5, 9.1$ Hz, 1H), 4.16 – 4.02 (m, 8H), 1.23 – 1.11 (m, 12H). ^{31}P NMR (162 MHz, DMSO-d_6) δ 16.88 (s). MS [ESI $^+$] m/z : 633.2 [M + H] $^+$

Final Inhibitor: (((6-(3-benzamidophenyl)thieno[2,3-d]pyrimidin-4-yl)amino)methylene)bis(phosphonic acid) (**5.28w**). Isolated as a beige solid. ^1H NMR (500 MHz, D_2O) δ 8.27 (s, 1H), 7.92 – 7.89 (m, 4H), 7.67 - 7.63 (m, 2H), 7.59 - 7.56 (m, 3H), 7.52 (t, $J = 7.9$ Hz, 1H). α -CH to the bisphosphonate overlaps with the solvent peak. ^{31}P NMR (203 MHz, D_2O) δ 13.53 (s). ^{13}C NMR (126 MHz, D_2O) δ 169.3, 163.2, 156.2, 153.5, 138.7, 137.9, 133.9, 133.5, 132.4, 129.9, 128.7, 127.3, 122.8, 121.8, 119.0, 118.6, 115.1, 50.8 (t, $J = 125.7$ Hz). HRMS [ESI $^+$] calculated for $\text{C}_{20}\text{H}_{16}\text{N}_4\text{Na}_3\text{O}_7\text{P}_2\text{S}$ m/z , 586.9903; found 586.9906 [M + 3 Na] $^+$

Inhibitor 5.28x:

Corresponding bisphosphonate ester: Prepared *via* Suzuki cross-coupling between tetraethyl (((6-bromo-2-phenylthieno[2,3-d]pyrimidin-4-yl)amino)methylene)bis(phosphonate) **5.27b-1** and phenylboronic acid. Isolated as a yellow solid. ¹H NMR (500 MHz, CDCl₃) δ 8.50 (m, 2H), 7.74 (d, *J* = 7.4 Hz, 2H), 7.57 (s, 1H), 7.52 – 7.45 (m, 5H), 7.39 (t, *J* = 7.4 Hz, 1H), 6.09 – 5.97 (m, 2H; -NH and α-CH to the bisphosphonate), 4.34 – 4.19 (m, 8H), 1.30 – 1.22 (m, 12H). ¹³C NMR (125 MHz, CDCl₃) δ 167.9, 159.1, 154.9 (t, *J* = 3.6 Hz), 141.6, 137.7, 133.6, 130.3, 129.1, 128.7, 128.4, 128.1, 126.3, 116.6, 112.4, 63.9 – 63.6 (m), 44.5 (t, *J* = 147.1 Hz), 16.4 – 16.3 (m). ³¹P NMR (203 MHz, CDCl₃) δ 16.89.

Final Inhibitor: (((2,6-diphenylthieno[2,3-d]pyrimidin-4-yl)amino)methylene)bis(phosphonic acid) (**5.28x**). Isolated as a yellow solid. ¹H NMR (400 MHz, D₂O): δ 8.22 - 8.20 (m, 2H), 7.83 (s, 1H), 7.68 (d, *J* = 7.4 Hz, 2H), 7.58 - 7.55 (m, 3H), 7.37 (t, *J* = 7.7 Hz, 2H), 7.25 (t, *J* = 7.4 Hz, 1H), 5.27 (t, *J* = 19.4 Hz, 1H). ¹³C NMR (100 MHz, D₂O): δ 164.9, 159.9, 156.3, 139.7, 137.3, 132.8, 130.5, 129.1, 128.7, 128.4, 128.2, 125.6, 117.0, 114.3. C_α observed by HSQC. HSQC (¹H -¹³C): 1H δ 5.27 correlates with ¹³C δ 49.0. ³¹P NMR (162 MHz, D₂O): δ 13.8. MS (ESI⁺) *m/z*: 478.2 [M + H⁺]⁺.

Inhibitor 5.28y:

Corresponding bisphosphonate ester: Tetraethyl (((2-(3-benzamidophenyl)-6-methylthieno[2,3-d]pyrimidin-4-yl)amino)methylene)bis(phosphonate). Prepared *via* **Method A** using tetraethyl (((6-methyl-2-(methylthio)thieno[2,3-d]pyrimidin-4-yl)amino)methylene)bis(phosphonate) **5.27a-2** and (3-benzamidophenyl)boronic acid⁶⁰ as coupling partners. Isolated as a yellow solid. ¹H NMR (400 MHz, DMSO-d₆) δ 10.45 (s, -NH), 8.83 (t, *J* = 1.8 Hz, 1H), 8.45 (d, *J* = 9.7 Hz, -

NH), 8.09 (d, $J = 7.9$ Hz, 1H), 8.03 – 7.98 (m, 2H), 7.94 – 7.88 (m, 1H), 7.79 (d, $J = 1.2$ Hz, 1H), 7.63 – 7.58 (m, 1H), 7.57 – 7.52 (m, 2H), 7.49 (t, $J = 7.9$ Hz, 1H), 6.03 (td, $J = 23.4, 9.5$ Hz, 1H), 4.18 – 4.05 (m, 8H), 2.57 (d, $J = 1.1$ Hz, 3H), 1.18 – 1.10 (m, 12H). ^{31}P NMR (162 MHz, DMSO-d₆) δ 17.08 (s). ^{13}C NMR (126 MHz, DMSO-d₆) δ 167.0, 165.6, 157.3, 154.8, 139.4, 138.0, 136.6, 134.8, 131.6, 128.7, 128.4, 127.7, 122.9, 122.2, 119.7, 117.8, 115.9, 62.9 - 62.7 (m), 44.0 (t, $J = 146.5$ Hz), 16.3 - 16.1. R-6 CH₃ was observed by HSQC. HSQC (^1H - ^{13}C): ^1H at δ 2.57 correlates to ^{13}C - α at δ 16.0. MS [ESI⁺] m/z : 647.2 [M + H⁺]⁺

Final Inhibitor: (((2-(3-benzamidophenyl)-6-methylthieno[2,3-d]pyrimidin-4-

yl)amino)methylene)bis(phosphonic acid) (**5.28y**). Isolated as a light yellow solid. ^1H NMR (500 MHz, D₂O) δ 8.32 (s, 1H), 8.15 (d, $J = 7.9$ Hz, 1H), 7.95 (d, $J = 7.5$ Hz, 2H), 7.91 (d, $J = 7.8$ Hz, 1H), 7.68 (t, $J = 7.4$ Hz, 1H), 7.61 (dt, $J = 15.2, 7.8$ Hz, 3H), 7.25 (s, 1H), 5.00 (t, $J = 19.3$ Hz, 1H), 2.60 (s, 3H). ^{31}P NMR (203 MHz, D₂O) δ 13.87 (s). HRMS [ESI⁺] calculated for C₂₁H₁₈N₄Na₃O₇P₂S m/z , 601.0059; found 601.0067 [M + 3 Na]⁺

Expression and Purification of Recombinant hGGPPS:

The hGGPPS enzyme was expressed and purified *via* a slightly modified protocol as described by Kavanagh and coworkers.⁶¹ The plasmid containing N-terminally hexahistidine-tagged human GGPPS was transformed into *E. coli* BL21 (DE3) competent cells containing kanamycin in Luria-Bertani (LB) medium and was grown overnight at 37°C. Terrific broth medium (1L) containing 1 mL of 50 mM kanamycin was inoculated with 10 mL overnight seed culture and grown at 37°C until optical density (OD)₆₀₀ equals 1 at which point the temperature was reduced to 18°C. The culture was induced with 0.5 mM isopropyl 1-thio- β -D-galactopyranoside and allowed to shake overnight. Cells were pelleted *via* centrifugation and were incubated in the freezer (-20°C) overnight or at -80°C until frozen. The frozen cell pellet was subjected to the addition of protease

inhibitor, Complete Mini-EDTA free pellet (Roche Life Science), and 20mL of binding buffer (50 mM HEPES, 500 mM NaCl, 5 mM imidazole, 5% glycerol, 10 mM β -mercaptoethanol, pH adjusted to 7.5). The cells were then sonicated, centrifuged and filtered. The His-tagged protein was loaded onto Ni-NTA agarose column, washed with binding buffer and eluted with buffer containing (50 mM HEPES, 500mM NaCl, 250 mM imidazole, 5% glycerol, 10 mM β -mercaptoethanol, pH was adjusted to 7.5). The collected protein was further purified by gel filtration chromatography using a Superdex 200 gel column with buffer containing 10 mM HEPES, 500 mM NaCl, 5%-20% glycerol, 2 mM β -mercaptoethanol, pH adjusted to 7.5. The protein was concentrated with spin-column concentrator.

***In vitro* hGGPPS Inhibition Assay:**

The assay was based on the method by Kavanagh *et. al.*⁶¹ with minor modifications. All assays were run in triplicate using recombinant human GGPPS (80 ng), FPP (10 μ M), IPP (8.3 μ M; ³H-IPP, 40 mCi/mmoL) in a final volume of 100 μ L buffer containing 50 mM Tris pH 7.7, 2 mM MgCl₂, 1 mM TCEP, 5 μ g/mL BSA and 0.2% (w/v) Tween 20. The enzyme and inhibitor were pre-incubated in the assay buffer in a volume of 80 μ L at 37°C for 10 min. Afterwards, the substrates (FPP, IPP) were added to start the reaction, which also bring the inhibitor, substrate, and buffer contents to the desired final concentrations as indicated above. The assay mixture was then incubated at 37°C for 15 min (Note: the incubation time is based from the time curve determined each time a new batch of enzyme is produced). Assays were terminated by the addition of 200 μ L of HCl/MeOH (1:4) and incubated for 10 min at 37°C. The mixture was then extracted with 700 μ L of petroleum ether, dried through a plug of anhydrous MgSO₄ and 300 μ L of the dried ligroin phase was combined with 8 mL of scintillation cocktail. Finally, the radioactivity was counted using a Beckman Coulter LS6500 liquid scintillation counter.

Reagents for the Enzymatic Assay:

Petroleum ether (high boiling point, 60° - 80°C) was purchased from Sigma Aldrich, liquid scintillation cocktail was purchased from MP Biomedicals (Ecolite Cat #: 882475), ³H-IPP was obtained from American Radiolabeled Chemicals (ART 0377A; 1 mCi/mL), and unlabeled IPP and FPP were purchased from Isoprenoids, Lc. as their tri-ammonium salts.

hGGPPS wild-type enzyme: The wild-type hGGPPS enzyme was stored at -80°C as a 1 µg/µL stock solution in the eluent buffer (10 mM HEPES, pH 7.5, 500 mM NaCl, 5%-20% glycerol, 2.0 mM β-mercaptoethanol).

IPP solution: ³H-IPP was diluted with unlabeled IPP (or cold IPP) to a specific activity of 40 mCi/mmol and 82.7 µM concentration (radiolabeled + unlabeled IPP) in 10 mM Tris pH 7.7. It was stored at -10°C, warmed to 0°C and kept on ice during the assay.

FPP solution: FPP was dissolved and diluted to a 100 µM concentration in 10 mM Tris pH 7.7. It was stored at -10°C, warmed to 0°C and kept on ice during the assay.

Inhibitor solution: 10 mM stock solution in deionized H₂O was prepared from the tri-sodium salt of the corresponding bisphosphonate inhibitor.

In vitro hFPPS assay was carried out based on Method 2 (M2) as previously described.²³ Cell culture and viability assays and apoptosis in human myeloma cell lines were also based on previous procedures with some modifications.^{23, 62} Determination of total Tau and phosphorylated Tau levels in AD brain in the presence of test compounds at different concentrations and LDH assays were also conducted based on previously described procedures.²⁴

5.8. Associated Content

Supporting Information

NMR spectra and homogeneity data of key inhibitors **5.28i**, **5.28q**, **5.28s**, and **5.28t** are provided.

5.9. Author Information

Corresponding Author

*Phone 514-398-3638. Fax 514-398-3797. Email : youla.tsantrizos@mcgill.ca

5.10. Acknowledgments

Financial support for this work was provided by NSERC and FQRNT research grants to Y. S. Tsantrizos and the Canadian Institute of Health Research (CIHR) research grants to A. M. Berghuis, J. Poirier, M. Sebag and Y. S. Tsantrizos.

5.11. References

1. Arrowsmith, C. H.; Audia, J. E.; Austin, C.; Baell, J.; Bennett, J.; Blagg, J.; Bountra, C.; Brennan, P. E.; Brown, P. J.; Bunnage, M. E.; Buser-Doepner, C.; Campbell, R. M.; Carter, A. J.; Cohen, P.; Copeland, R. A.; Cravatt, B.; Dahlin, J. L.; Dhanak, D.; Edwards, A. M.; Frederiksen, M.; Frye, S. V.; Gray, N.; Grimshaw, C. E.; Hepworth, D.; Howe, T.; Huber, K. V. M.; Jin, J.; Knapp, S.; Kotz, J. D.; Kruger, R. G.; Lowe, D.; Mader, M. M.; Marsden, B.; Mueller-Fahrnow, A.; Muller, S.; O'Hagan, R. C.; Overington, J. P.; Owen, D. R.; Rosenberg, S. H.; Ross, R.; Roth, B.; Schapira, M.; Schreiber, S. L.; Shoichet, B.; Sundstrom, M.; Superti-Furga, G.; Taunton, J.; Toledo-Sherman, L.; Walpole, C.; Walters, M. A.; Willson, T. M.; Workman, P.; Young, R. N.; Zuercher, W. J. The promise and peril of chemical probes. *Nat. Chem. Biol.* **2015**, 11, 536-541.
2. Garbaccio, Robert M.; Parmee, Emma R. The impact of chemical probes in drug discovery: A pharmaceutical industry perspective. *Cell Chem. Biol.* **2016**, 23, 10-17.

3. Baell, J. B.; Holloway, G. A. New substructure filters for removal of pan assay interference compounds (PAINS) from screening libraries and for their exclusion in bioassays. *J. Med. Chem.* **2010**, *53*, 2719-2740.
4. Baell, J.; Walters, M. A. Chemical con artists foil drug discovery. *Nature* **2014**, *513*, 481-483.
5. Lipinski, C. A. Lead- and drug-like compounds: the rule-of-five revolution. *Drug Discov. Today Technol.* **2004**, *1*, 337-341.
6. Lipinski, C. A.; Lombardo, F.; Dominy, B. W.; Feeney, P. J. Experimental and computational approaches to estimate solubility and permeability in drug discovery and development settings¹. *Adv. Drug Deliv. Rev.* **2001**, *46*, 3-26.
7. Gleeson, M. P. Generation of a set of simple, interpretable ADMET rules of thumb. *J. Med. Chem.* **2008**, *51*, 817-834.
8. Johnson, T. W.; Dress, K. R.; Edwards, M. Using the Golden Triangle to optimize clearance and oral absorption. *Bioorg. Med. Chem. Lett.* **2009**, *19*, 5560-5564.
9. Leeson, P. D.; Springthorpe, B. The influence of drug-like concepts on decision-making in medicinal chemistry. *Nat. Rev. Drug Discov.* **2007**, *6*, 881-890.
10. Meanwell, N. A. Improving drug candidates by design: A focus on physicochemical properties as a means of improving compound disposition and safety. *Chem. Res. Toxicol.* **2011**, *24*, 1420-1456.
11. Gleeson, M. P.; Hersey, A.; Montanari, D.; Overington, J. Probing the links between in vitro potency, ADMET and physicochemical parameters. *Nat. Rev. Drug Discov.* **2011**, *10*, 197-208.
12. Dahlin, J. L.; Nissink, J. W. M.; Strasser, J. M.; Francis, S.; Higgins, L.; Zhou, H.; Zhang, Z.; Walters, M. A. PAINS in the assay: Chemical mechanisms of assay interference and promiscuous enzymatic inhibition observed during a sulfhydryl-scavenging HTS. *J. Med. Chem.* **2015**, *58*, 2091-2113.
13. Litvinov, V. P. Thienopyrimidines: synthesis, properties, and biological activity. *Russ. Chem. Bull., Int. Ed.* **2004**, *53*, 487-516.
14. Babu, Y. S.; Chand, P.; Wu, M.; Kotian, P. L.; Kumar, V. S.; Lin, T. H.; El-Kattan, Y.; Ghosh, A. K. Therapeutic fuopyrimidines and thienopyrimidines. WO 2006/050161 A3.

15. Tani, N.; Rahnasto-Rilla, M.; Wittekindt, C.; Salminen, K. A.; Ritvanen, A.; Ollakka, R.; Koskiranta, J.; Raunio, H.; Juvonen, R. O. Antifungal activities of novel non-azole molecules against *S. cerevisiae* and *C. albicans*. *Eur. J. Med. Chem.* **2012**, *47*, 270-277.
16. Kanawade, S. B.; Toche, R. B.; Rajani, D. P. Synthetic tactics of new class of 4-aminothieno[2,3-d]pyrimidine-6-carbonitrile derivatives acting as antimicrobial agents. *Eur. J. Med. Chem.* **2013**, *64*, 314-320.
17. Jang, M.-Y.; Jonghe, S. D.; Belle, K. V.; Louat, T.; Waer, M.; Herdewijn, P. Synthesis, immunosuppressive activity and structure–activity relationship study of a new series of 4-N-piperazinyl-thieno[2,3-d]pyrimidine analogues. *Bioorg. Med. Chem. Lett.* **2010**, *20*, 844-847.
18. Heffron, T. P.; Wei, B.; Olivero, A.; Staben, S. T.; Tsui, V.; Do, S.; Dotson, J.; Folkes, A. J.; Goldsmith, P.; Goldsmith, R.; Gunzner, J.; Lesnick, J.; Lewis, C.; Mathieu, S.; Nonomiya, J.; Shuttleworth, S.; Sutherlin, D. P.; Wan, N. C.; Wang, S.; Wiesmann, C.; Zhu, B.-Y. Rational design of phosphoinositide 3-kinase α inhibitors that exhibit selectivity over the phosphoinositide 3-kinase β isoform. *J. Med. Chem.* **2011**, *54*, 7815-7833.
19. Axten, J. M.; Grant, S. W.; Heerding, D. A.; Medina, J. R.; Romeril, S. P.; Tang, J. Chemical compounds. WO 2011/119663 A1.
20. Shook, B. C.; Charavarty, D.; Barbay, J. K.; Wang, A.; Leonard, K.; Alford, V.; Powell, M.; Beauchamp, D. A.; Rassnick, S.; Scannevin, R.; Carroll, K.; Wallace, N.; Croke, J.; Ault, M.; Lampron, L.; Westover, L.; Rhodes, K.; Jackson, P. F. Aminomethyl substituted thieno[2,3-d]pyrimidines as adenosine A2A receptor antagonists. *Med. Chem. Commun.* **2011**, *2*, 950-965.
21. Shook, B. C.; Chakravarty, D.; Barbay, J. K.; Wang, A.; Leonard, K.; Alford, V.; Powell, M. T.; Rassnick, S.; Scannevin, R. H.; Carroll, K.; Wallace, N.; Croke, J.; Ault, M.; Lampron, L.; Westover, L.; Rhodes, K.; Jackson, P. F. Substituted thieno[2,3-d]pyrimidines as adenosine A2A receptor antagonists. *Bioorg. Med. Chem. Lett.* **2013**, *23*, 2688-2691.
22. Fischer, C.; Shah, S.; Hughes, B. L.; Nikov, G. N.; Crispino, J. L.; Middleton, R. E.; Szewczak, A. A.; Munoz, B.; Shearman, M. S. Quinazolinones as γ -secretase modulators. *Bioorg. Med. Chem. Lett.* **2011**, *21*, 773-776.

23. Leung, C. Y.; Park, J.; De Schutter, J. W.; Sebag, M.; Berghuis, A. M.; Tsantrizos, Y. S. Thienopyrimidine bisphosphonate (ThPBP) inhibitors of the human farnesyl pyrophosphate synthase: Optimization and characterization of the mode of inhibition. *J. Med. Chem.* **2013**, *56*, 7939-7950.
24. De Schutter, J. W.; Park, J.; Leung, C. Y.; Gormley, P.; Lin, Y.-S.; Hu, Z.; Berghuis, A. M.; Poirier, J.; Tsantrizos, Y. S. Multistage screening reveals chameleon ligands of the human farnesyl pyrophosphate synthase: Implications to drug discovery for neurodegenerative diseases. *J. Med. Chem.* **2014**, *57*, 5764-5776.
25. Sakamoto, T.; Kondo, Y.; Yamanaka, H. Studies on pyrimidine derivatives. XXIX. Synthesis of pyrimidines fused with five-membered heterocycles by cross-coupling of 5-iodopyrimidines with phenylacetylene and styrene. *Chem. Pharm. Bull.* **1982**, *30*, 2417-2420.
26. Sakamoto, T.; Kondo, Y.; Watanabe, R. Y. O.; Yamanaka, H. Condensed heteroaromatic ring systems. VII : Synthesis of thienopyridines, thienopyrimidines, and furopyridines from o-substituted N-heteroarycetylenes. *Chem. Pharm. Bull.* **1986**, *34*, 2719-2724.
27. Litvinov, V. P. The chemistry of thienopyrimidines. In *Adv. Heterocycl. Chem.*, Alan, R. K., Ed. Academic Press: 2006; Vol. Volume 92, pp 83-143.
28. Bozorov, K.; Zhao, J.-Y.; Elmuradov, B.; Pataer, A.; Aisa, H. A. Recent developments regarding the use of thieno[2,3-d]pyrimidin-4-one derivatives in medicinal chemistry, with a focus on their synthesis and anticancer properties. *Eur. J. Med. Chem.* **2015**, *102*, 552-573.
29. Gewalt, K.; Schinke, E.; Böttcher, H. Heterocyclen aus CH-aciden Nitrilen, VIII. 2-Amino-thiophene aus methylenaktiven Nitrilen, Carbonylverbindungen und Schwefel. *Chem. Ber.* **1966**, *99*, 94-100.
30. Sabnis, R. W.; Rangnekar, D. W.; Sonawane, N. D. 2-aminothiophenes by the gewald reaction. *J. Heterocyclic Chem.* **1999**, *36*, 333-345.
31. Puterová, Z.; Krutošíková, A.; Végh, D. Gewald reaction: Synthesis, properties and applications of substituted 2-aminothiophenes. *Arkivoc* **2010**, *1*, 209-246.
32. Leung, C.-Y.; Langille, A. M.; Mancuso, J.; Tsantrizos, Y. S. Discovery of thienopyrimidine-based inhibitors of the human farnesyl pyrophosphate synthase—

- Parallel synthesis of analogs via a trimethylsilyl ylidene intermediate. *Bioorg. Med. Chem.* **2013**, 21, 2229-2240.
33. Liebeskind, L. S.; Srogl, J. Heteroaromatic thioether–boronic acid cross-coupling under neutral reaction conditions. *Org. Lett.* **2002**, 4, 979-981.
 34. Prokopcová, H.; Kappe, C. O. The Liebeskind–Srogl C-C Cross-Coupling Reaction. *Angew. Chem. Int. Ed.* **2009**, 48, 2276-2286.
 35. Liebeskind, L. S.; Srogl, J. Thiol ester–boronic acid coupling. A mechanistically unprecedented and general ketone synthesis. *J. Am. Chem. Soc.* **2000**, 122, 11260-11261.
 36. Goffinet, M.; Thoulouzan, M.; Pradines, A.; Lajoie-Mazenc, I.; Weinbaum, C.; Faye, J.; Séronie-Vivien, S. Zoledronic acid treatment impairs protein geranyl-geranylation for biological effects in prostatic cells. *BMC Cancer* **2006**, 6, 1-10.
 37. Roelofs, A. J.; Hulley, P. A.; Meijer, A.; Ebetino, F. H.; Russell, R. G. G.; Shipman, C. M. Selective inhibition of Rab prenylation by a phosphonocarboxylate analogue of risedronate induces apoptosis, but not S-phase arrest, in human myeloma cells. *Int. J. Cancer* **2006**, 119, 1254-1261.
 38. Van Beek, E.; Löwik, C.; Van Der Pluijm, G.; Papapoulos, S. The role of geranylgeranylation in bone resorption and its suppression by bisphosphonates in fetal bone explants in vitro: A clue to the mechanism of action of nitrogen-containing bisphosphonates. *J. Bone Miner. Res.* **1999**, 14, 722-729.
 39. Agabiti, S. S.; Liang, Y.; Wiemer, A. J. Molecular mechanisms linking geranylgeranyl diphosphate synthase to cell survival and proliferation. *Mol. Membr. Biol.* **2016**, 1-11.
 40. Fisher, J. E.; Rogers, M. J.; Halasy, J. M.; Luckman, S. P.; Hughes, D. E.; Masarachia, P. J.; Wesolowski, G.; Russell, R. G. G.; Rodan, G. A.; Reszka, A. A. Alendronate mechanism of action: geranylgeraniol, an intermediate in the mevalonate pathway, prevents inhibition of osteoclast formation, bone resorption, and kinase activation in vitro. *Proc. Natl. Acad. Sci.* **1999**, 96, 133-138.
 41. Mosmann, T. Rapid colorimetric assay for cellular growth and survival: Application to proliferation and cytotoxicity assays. *J. Immunol. Methods* **1983**, 65, 55-63.
 42. Kavanagh, K. L.; Guo, K.; Dunford, J. E.; Wu, X.; Knapp, S.; Ebetino, F. H.; Rogers, M. J.; Russell, R. G. G.; Oppermann, U. The molecular mechanism of nitrogen-containing bisphosphonates as antiosteoporosis drugs. *Proc. Natl. Acad. Sci.* **2006**, 103, 7829-7834.

43. Szabo, C. M.; Matsumura, Y.; Fukura, S.; Martin, M. B.; Sanders, J. M.; Sengupta, S.; Cieslak, J. A.; Loftus, T. C.; Lea, C. R.; Lee, H.-J.; Koohang, A.; Coates, R. M.; Sagami, H.; Oldfield, E. Inhibition of geranylgeranyl diphosphate synthase by bisphosphonates and diphosphates: A potential route to new bone antiresorption and antiparasitic agents. *J. Med. Chem.* **2002**, *45*, 2185-2196.
44. Vermes, I.; Haanen, C.; Reutelingsperger, C. Flow cytometry of apoptotic cell death. *J. Immunol. Methods* **2000**, *243*, 167-190.
45. Koopman, G.; Reutelingsperger, C.; Kuijten, G.; Keehnen, R.; Pals, S.; van Oers, M. Annexin V for flow cytometric detection of phosphatidylserine expression on B cells undergoing apoptosis. *Blood* **1994**, *84*, 1415-1420.
46. Vermes, I.; Haanen, C.; Steffens-Nakken, H.; Reutellingsperger, C. A novel assay for apoptosis flow cytometric detection of phosphatidylserine expression on early apoptotic cells using fluorescein labelled Annexin V. *J. Immunol. Methods* **1995**, *184*, 39-51.
47. Brown, M.; Wittwer, C. Flow cytometry: Principles and clinical applications in hematology. *Clin. Chem.* **2000**, *46*, 1221-1229.
48. Adan, A.; Alizada, G.; Kiraz, Y.; Baran, Y.; Nalbant, A. Flow cytometry: basic principles and applications. *Crit. Rev. Biotechnol.* **2016**, 1-14.
49. Chilosi, M.; Adami, F.; Lestani, M.; Montagna, L.; Cimarosto, L.; Semenzato, G.; Pizzolo, G.; Menestrina, F. CD138/syndecan-1: a useful immunohistochemical marker of normal and neoplastic plasma cells on routine trephine bone marrow biopsies. *Mod. Pathol.* **1999**, *12*, 1101-1106.
50. Wills, V. S.; Allen, C.; Holstein, S. A.; Wiemer, D. F. Potent triazole bisphosphonate inhibitor of geranylgeranyl diphosphate synthase. *ACS Med. Chem. Lett.* **2015**, *6*, 1195-1198.
51. Holstein, S. A.; Tong, H.; Hohl, R. J. Differential activities of thalidomide and isoprenoid biosynthetic pathway inhibitors in multiple myeloma cells. *Leuk. Res.* **2010**, *34*, 344-351.
52. Dudakovic, A.; Wiemer, A. J.; Lamb, K. M.; Vonnahme, L. A.; Dietz, S. E.; Hohl, R. J. Inhibition of geranylgeranyl diphosphate synthase induces apoptosis through multiple mechanisms and displays synergy with inhibition of other isoprenoid biosynthetic enzymes. *J. Pharm. Exp. Ther.* **2008**, *324*, 1028-1036.

53. Beffert, U.; Cohn, J. S.; Petit-Turcotte, C.; Tremblay, M.; Aumont, N.; Ramassamy, C.; Davignon, J.; Poirier, J. Apolipoprotein E and β -amyloid levels in the hippocampus and frontal cortex of Alzheimer's disease subjects are disease-related and apolipoprotein E genotype dependent. *Brain Res.* **1999**, 843, 87-94.
54. Tsantrizos, Y. S.; Poirier, J.; Sebag, M.; Berghuis, A.; Park, J.; De Schutter, J. Thienopyrimidine inhibitors of farnesyl and/or geranylgeranyl pyrophosphate synthase. WO **2014/078957** A1.
55. Gao, M.; Shi, Z.; Wang, M.; Zheng, Q.-H. [11C]Olanzapine, radiosynthesis and lipophilicity of a new potential PET 5-HT₂ and D₂ receptor radioligand. *Bioorg. Med. Chem. Lett.* **2013**, 23, 1953-1956.
56. Barbay, J. K.; Chakravarty, D.; Shook, B. C.; Wang, A. Methylene amines of thieno [2,3-d] pyrimidine and their use as adenosine a_{2a} receptor antagonists. WO **2010/045006** A1.
57. Chen, B.; Perspicace, E.; Hesse, S.; Kirsch, G. Microwave-assisted synthesis of 4-amino-2-arylthieno[2,3-d]pyrimidines and their subsequent functionalization. *Synthesis* **2010**, 2010, 2413-2418.
58. Wydysh, E. A.; Medghalchi, S. M.; Vadlamudi, A.; Townsend, C. A. Design and synthesis of small molecule glycerol 3-phosphate acyltransferase inhibitors. *J. Med. Chem.* **2009**, 52, 3317-3327.
59. Zhao, X.; Xin, M.; Wang, Y.; Huang, W.; Jin, Q.; Tang, F.; Wu, G.; Zhao, Y.; Xiang, H. Discovery of thieno[3,2-c]pyridin-4-amines as novel Bruton's tyrosine kinase (BTK) inhibitors. *Bioorg. Med. Chem.* **2015**, 23, 6059-6068.
60. Wetzal, M.; Marchais-Oberwinkler, S.; Hartmann, R. W. 17 β -HSD2 inhibitors for the treatment of osteoporosis: Identification of a promising scaffold. *Bioorg. Med. Chem.* **2011**, 19, 807-815.
61. Kavanagh, K. L.; Dunford, J. E.; Bunkoczi, G.; Russell, R. G. G.; Oppermann, U. The crystal structure of human geranylgeranyl pyrophosphate synthase reveals a novel hexameric arrangement and inhibitory product binding. *J. Biol. Chem.* **2006**, 281, 22004-22012.
62. Lin, Y.-S.; Park, J.; De Schutter, J. W.; Huang, X. F.; Berghuis, A. M.; Sebag, M.; Tsantrizos, Y. S. Design and synthesis of active site inhibitors of the human farnesyl

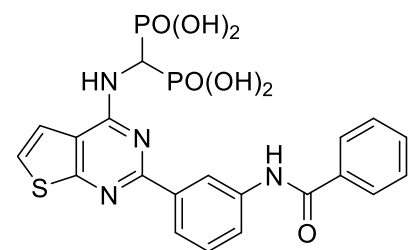
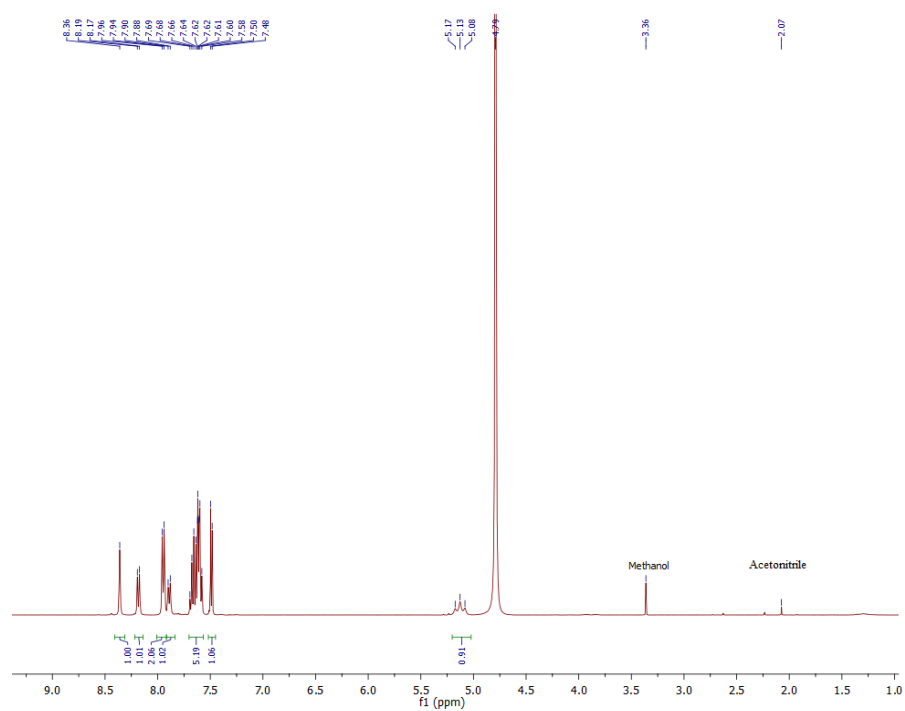
pyrophosphate synthase: Apoptosis and inhibition of ERK phosphorylation in multiple myeloma cells. *J. Med. Chem.* **2012**, 55, 3201-3215.

Chapter 5: Supporting Information

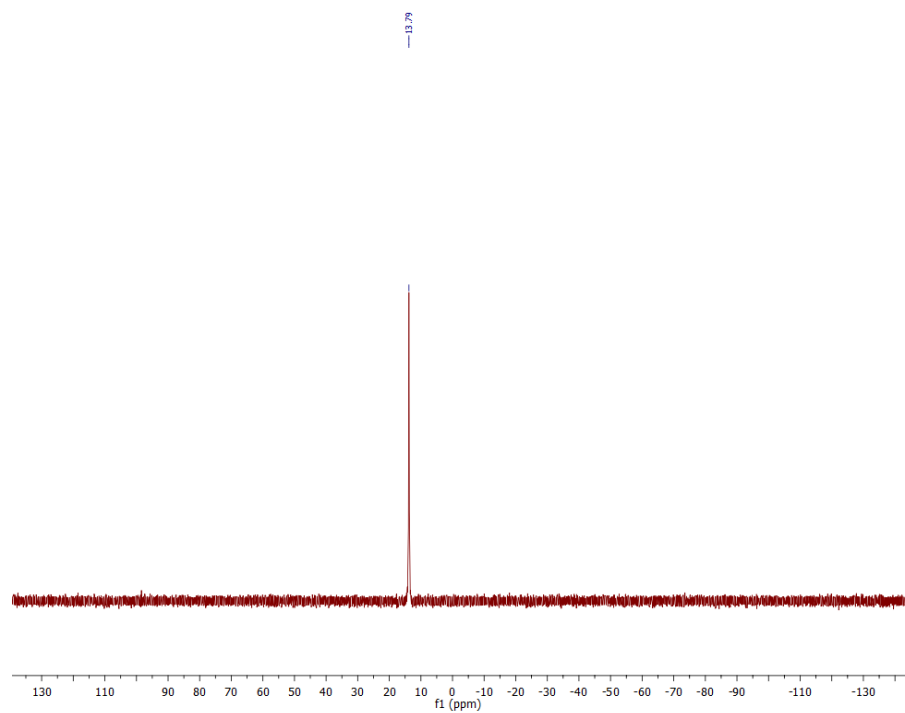
Potent and Selective Thieno[2,3-*d*]pyrimidine-Based Inhibitors of the Human Geranylgeranyl Pyrophosphate Synthase (hGGPPS): Implications for Drug Discovery

Inhibitor **5.28i**:

^1H NMR (400 MHz, D_2O)

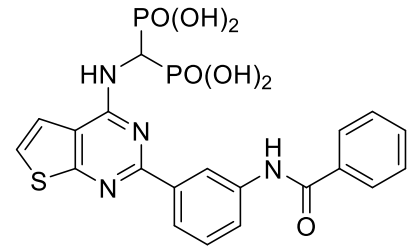
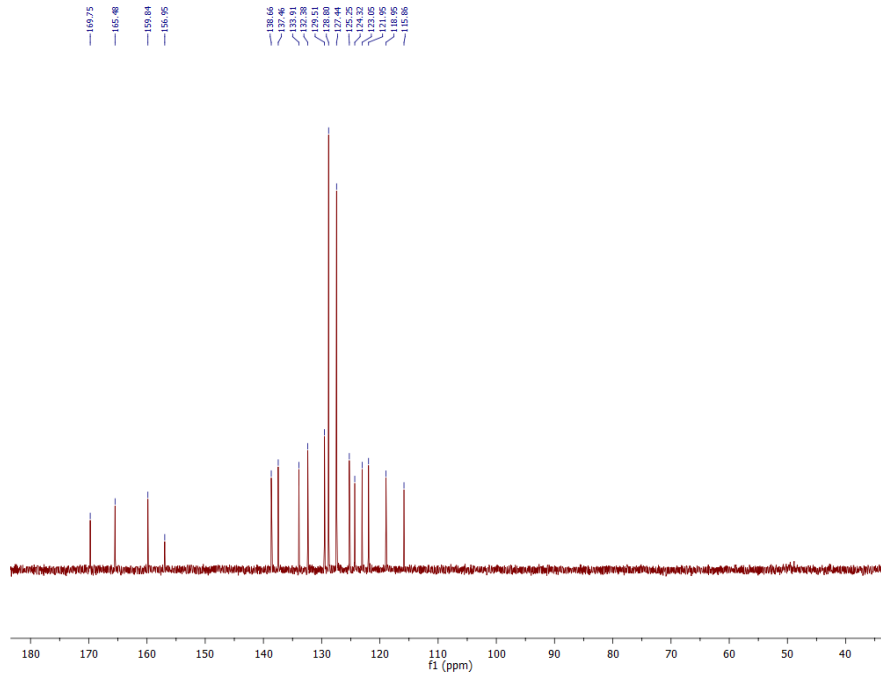


^{31}P NMR (162 MHz, D_2O)

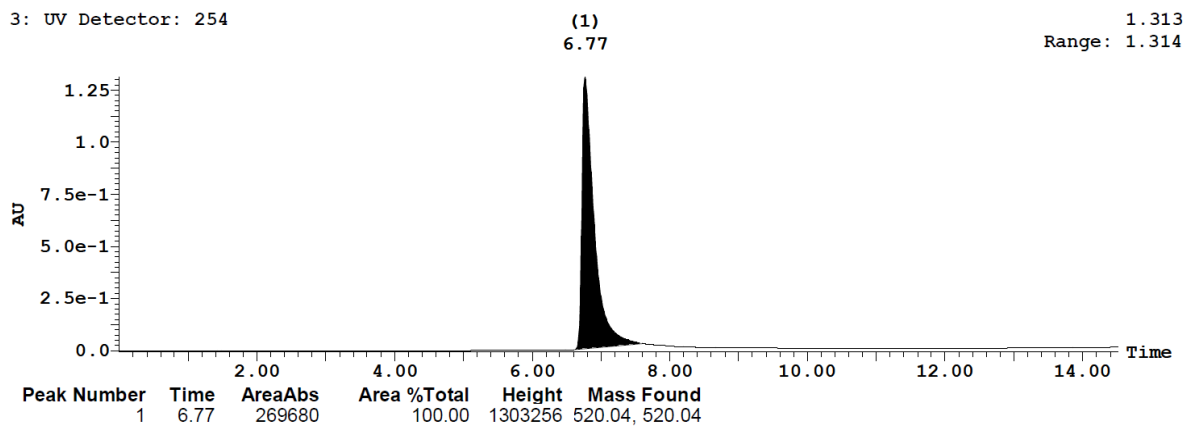


Inhibitor 5.28i:

^{13}C NMR (101 MHz, D_2O)

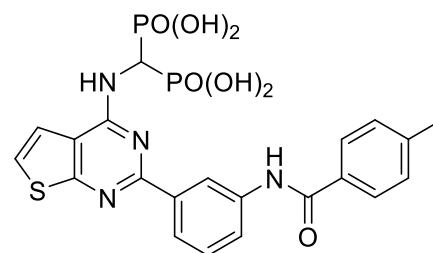
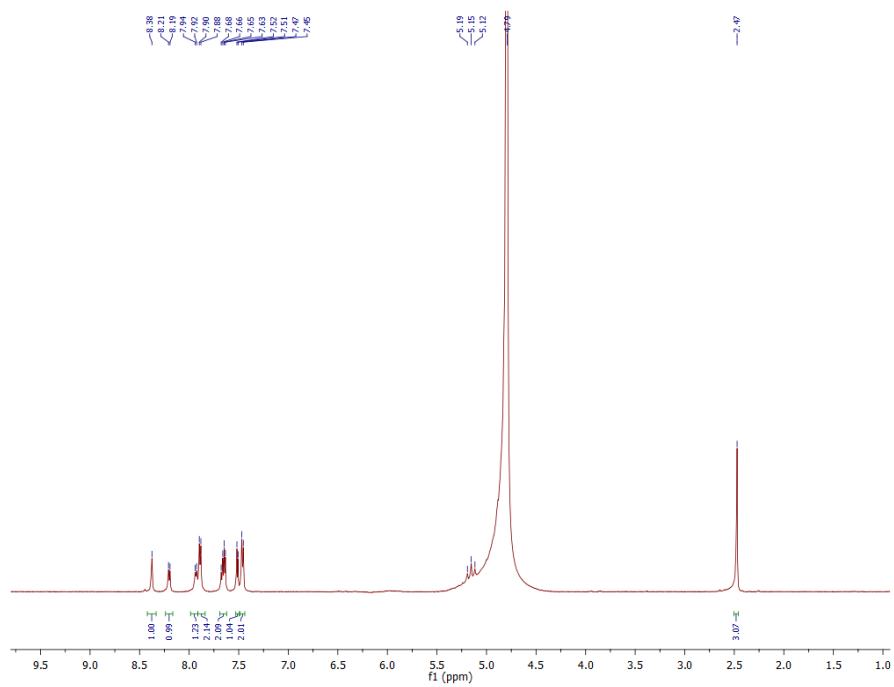


HPLC Chromatogram:

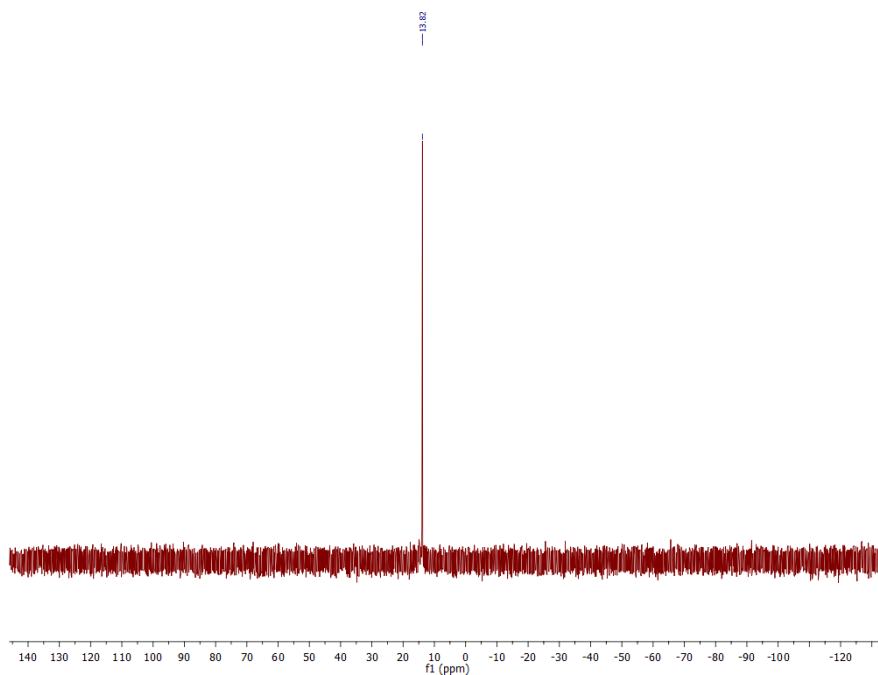


Inhibitor **5.28q**:

^1H NMR (500 MHz, D_2O)

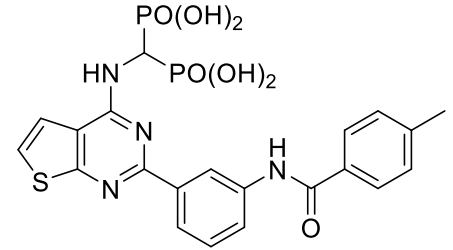
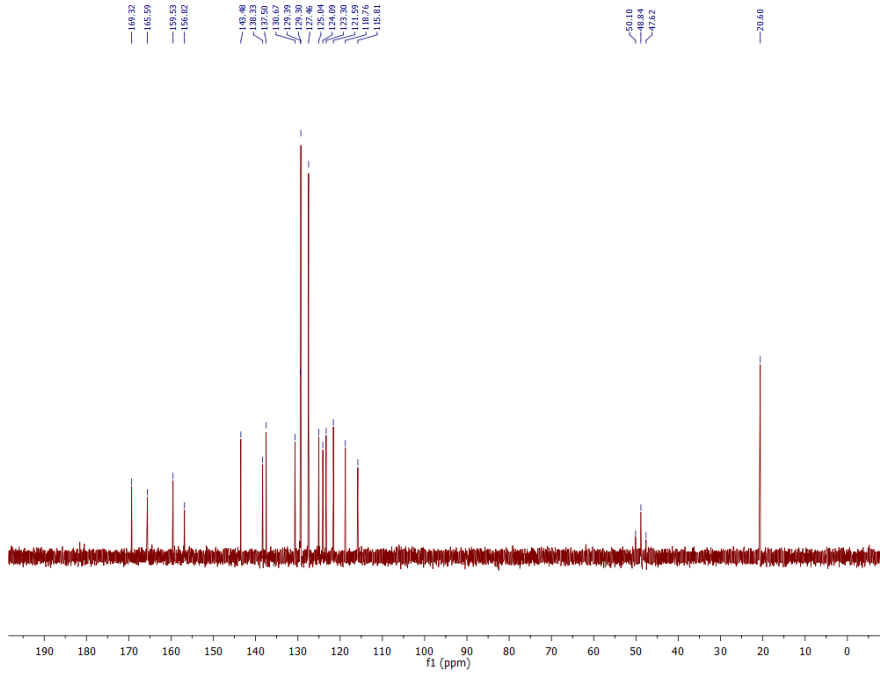


^{31}P NMR (203 MHz, D_2O)



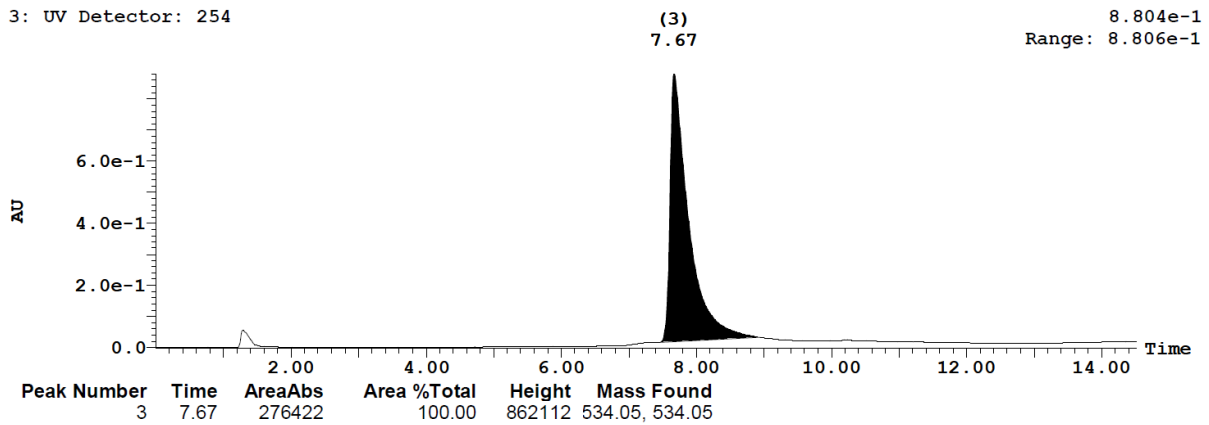
Inhibitor **5.28q**:

^{13}C NMR (101 MHz, D_2O)



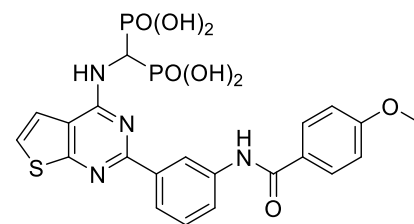
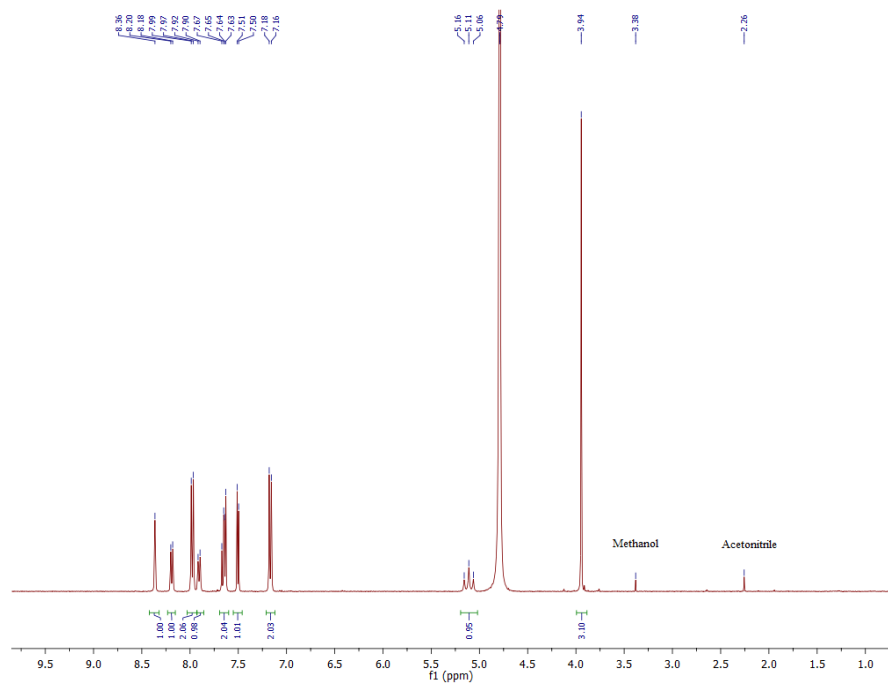
HPLC Chromatogram:

3: UV Detector: 254

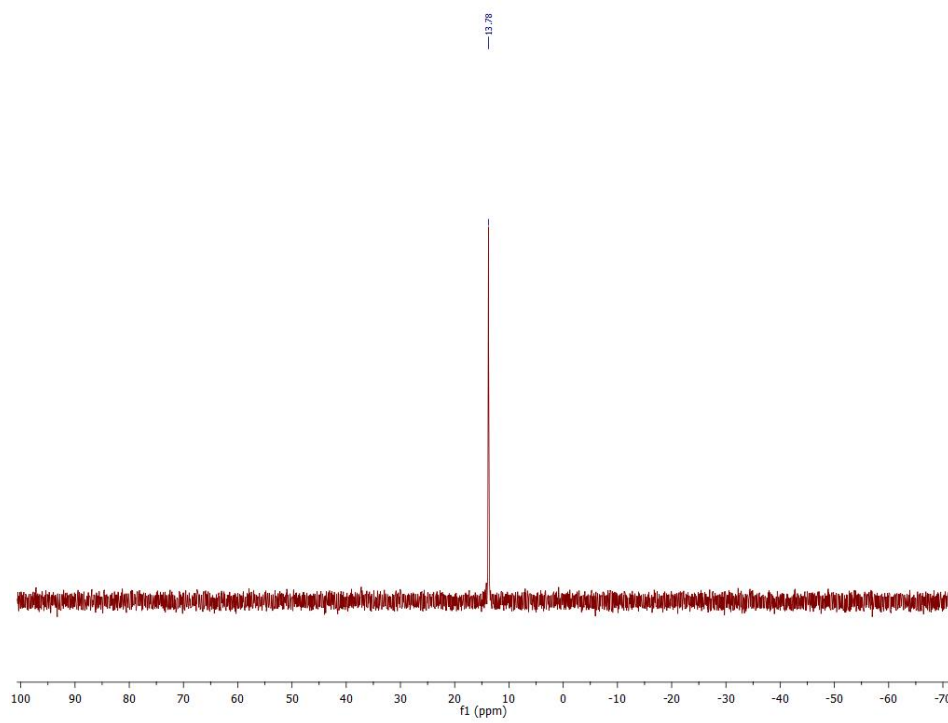


Inhibitor **5.28s**:

^1H NMR (400 MHz, D_2O)

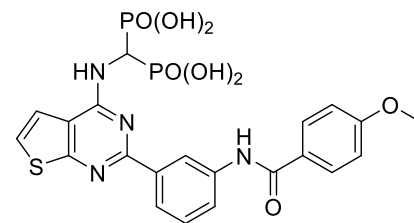
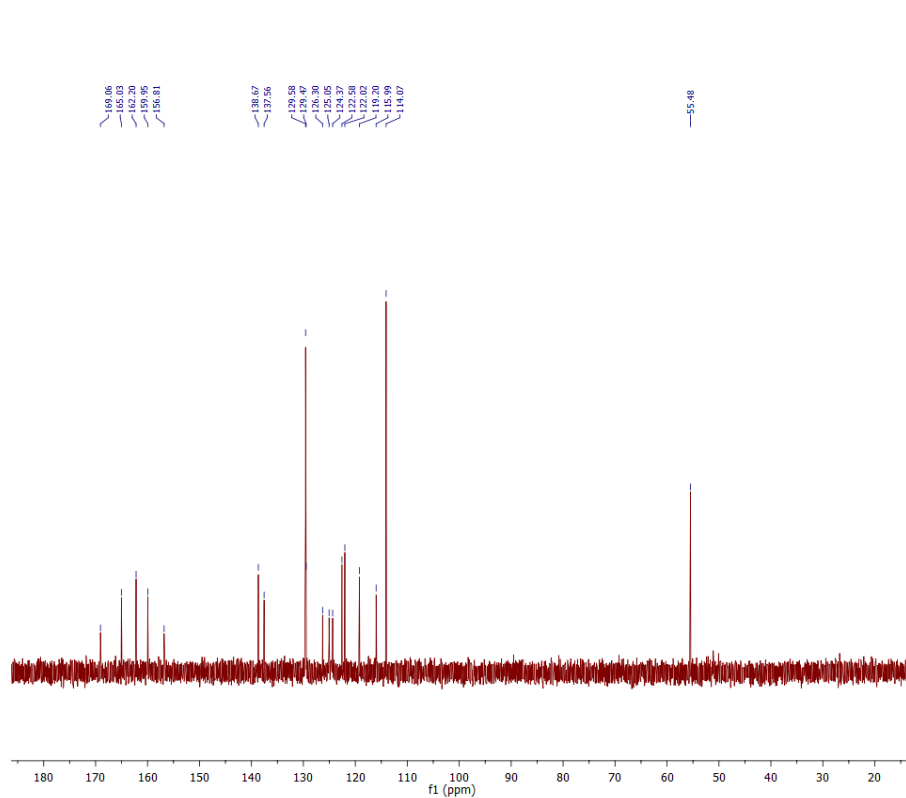


^{31}P NMR (162 MHz, D_2O)



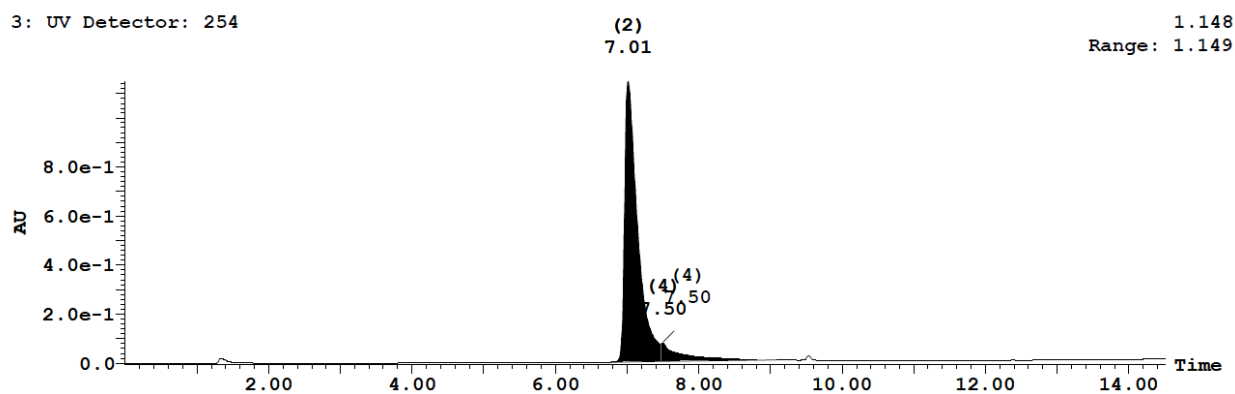
Inhibitor **5.28s**:

^{13}C NMR (126 MHz, D_2O)



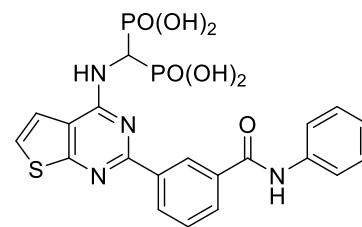
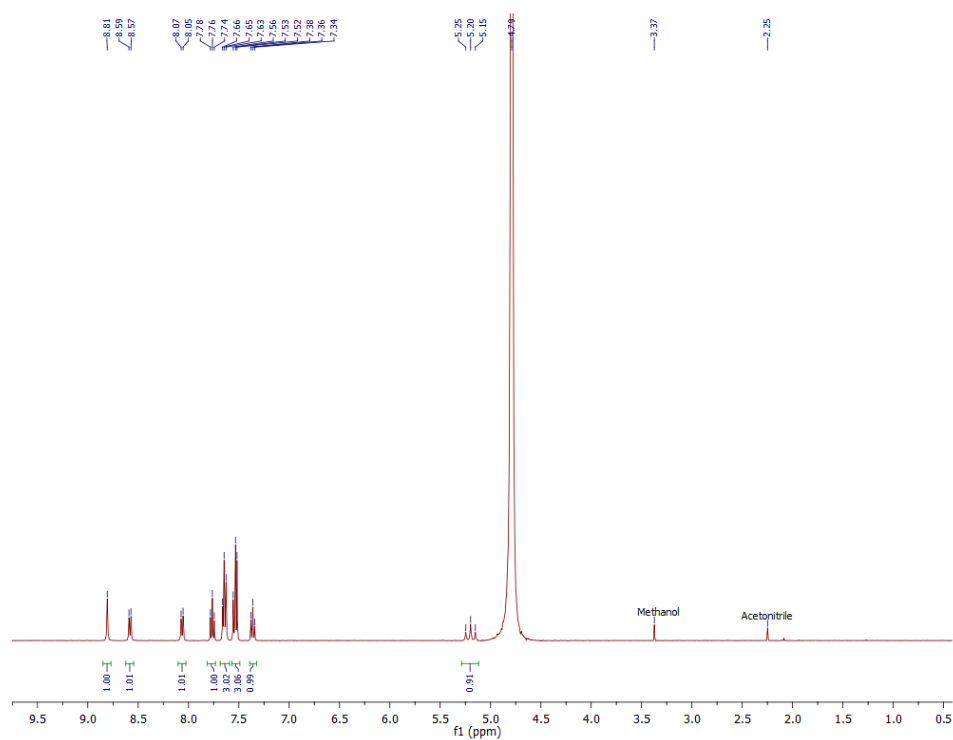
HPLC Chromatogram:

3: UV Detector: 254

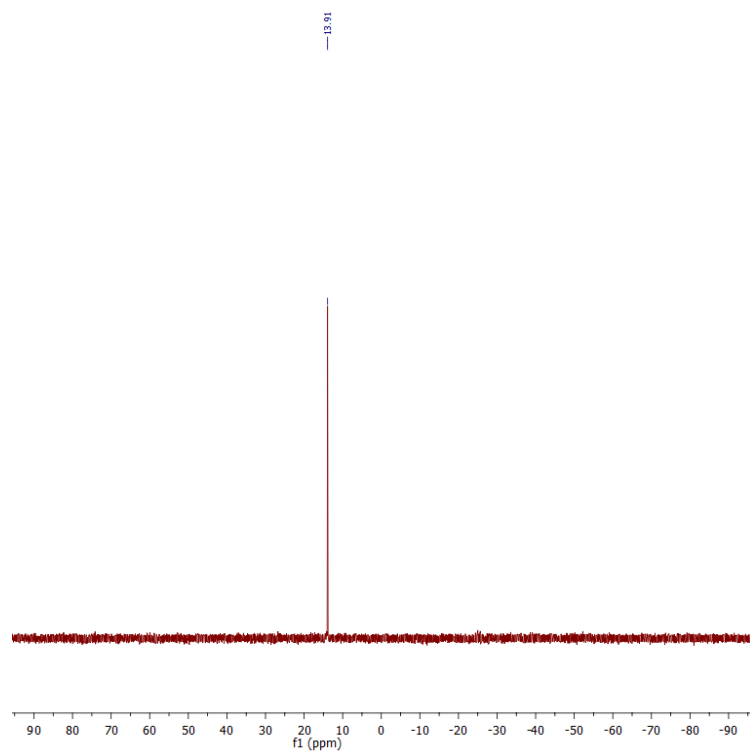


Inhibitor **5.28t**:

^1H NMR (400 MHz, D_2O)

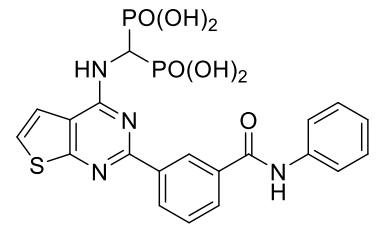
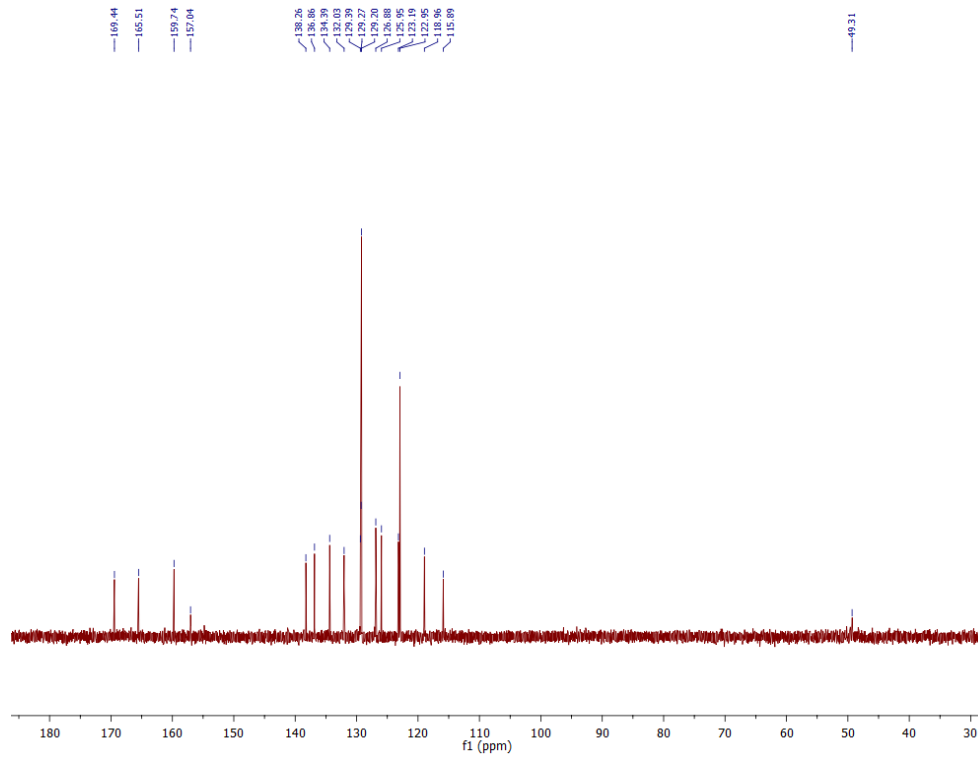


^{31}P NMR (203 MHz, D_2O)



Inhibitor 5.28t:

^{13}C NMR (126 MHz, D_2O)

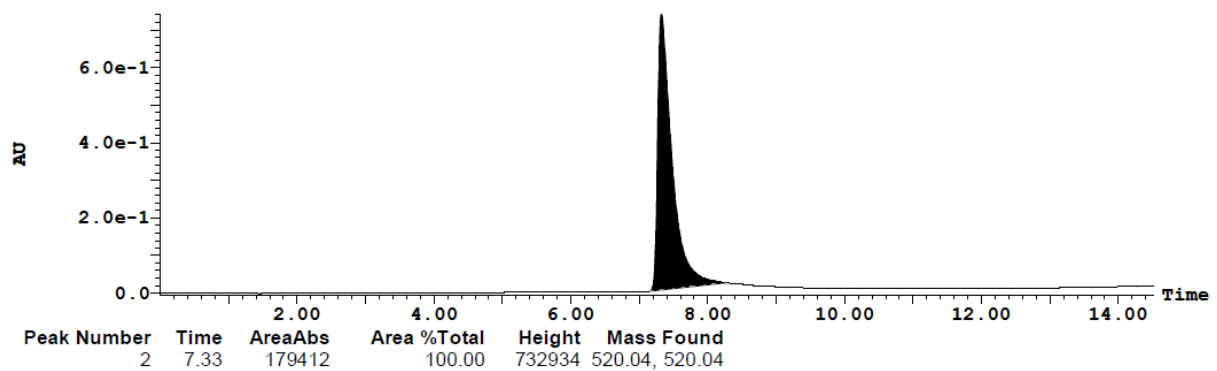


HPLC Chromatogram:

3: UV Detector: 254

(2)
7.33

7.405e-1
Range: 7.425e-1



CHAPTER 6: Contributions to Knowledge

6.1 Claims to Original Knowledge

- a. A modular approach in the synthesis of C-6 and C-7 substituted pyrido[2,3-*d*]pyrimidines was developed. A mini library of compounds containing the bisphosphonate metal anchor was prepared and analogs with low digit micromolar potency in inhibiting the HIV-1 RT-catalyzed DNA polymerization were discovered. The key compounds were also found to generally retain potency against RT variants that are typically associated with resistance to current nucleoside drugs (e.g. K65R and M184V). These pyridopyrimidine-based compounds represent a new chemotype of RT inhibitors for further optimization into novel antiviral agents.

- b. Derivatives of pyrimidinol carboxylic acids were shown to stabilize the untranslocated state of HIV-1 RT, a mode of inhibition that is distinct from the currently known anti-HIV/AIDS drugs. Our preliminary SAR studies also provided insights on the structural requirements ideal in targeting RT pre-translocation. Clinically-validated active site inhibitors of HIV-1 RT polymerase that are not nucleoside or nucleotide analogs are unknown and our studies may provide a venue toward identification of such inhibitors.

- c. Novel inhibitors of HIV-1 RT associated RNase H bearing the pyridopyrimidine scaffold were identified. These compounds can serve as starting points in the design of more potent and selective compounds with antiviral activity that may also help in the validation of the RNase-H enzyme as an alternative target for antiretroviral therapy.

- d. A synthetic protocol to access a structurally diverse library of C-2 substituted thieno[2,3-*d*]pyrimidine bisphosphonate inhibitors of hGGPPS was developed. On the basis of intrinsic potency, selectivity, and “drug-like” physicochemical properties, these compounds can be considered as the best inhibitors of hGGPPS known to date. Our preliminary biological studies also provided evidence on the potential of the hGGPPS enzyme as the target of new therapeutic agents for cancer and neurodegenerative diseases.

6.2 Papers and Conference Presentations

6.2.1 Papers Published

Gritzalis, D.; Park, J.; Chiu, W.; Cho, H.; Lin, Y.-S.; De Schutter, J.W.; **Lacbay, C.M.**; Zielinski, M.; Berghuis, A.M.; Tsantrizos, Y.S. Probing the molecular and structural elements of ligands binding to the active site versus an allosteric pocket of the human farnesyl pyrophosphate synthase. *Bioorg. Med. Chem. Lett.* **2015**, 25, 1117-1123.

Lacbay, C.M.; Mancuso, J.; Lin, Y.-S.; Bennett, N.; Götte, M.; Tsantrizos, Y.S. Modular assembly of purine-like bisphosphonates as inhibitors of HIV-1 reverse transcriptase. *J. Med. Chem.* **2014**, 57, 7435-7449.

6.2.2 Manuscripts in Preparation

Park, J.; Leung, C.Y.; Matralis, A.; **Lacbay, C.M.**; Tsakos, M.; Berghuis, A.M.; Tsantrizos, Y.S. Pharmacophore mapping of thienopyrimidine-based monophosphonate (ThP-MP) inhibitors of the human farnesyl pyrophosphate synthase.

Lacbay, C.M.; Menni, M.; Bernatchez, J.; Götte M.; Tsantrizos, Y.S. Pharmacophore requirements for HIV-1 reverse transcriptase inhibitors that selectively “freeze” the pre-translocation complex during the polymerization catalytic cycle.

Lacbay, C.M.; Vincent, F.; Ta, V.; Do, L.; Waller, D.D.; Huang, X.-F.; Sebag, M.; Tsantrizos, Y.S. Blocking geranylgeranylation of Rap 1A for the treatment of hematological cancers.

Pelleieux, S.; **Lacbay, C.M.**; Tsantrizos, Y.S.; Thérroux, L.; Dea, D.; Poirier, J. Brain isoprenoids and Alzheimer’s disease.

6.2.3 Conference Proceedings

The presenting author is underlined.

Pelleieux, S., Lacbay, C.M., Tsantrizos, Y.S., Thérroux, L., Dea, D., and Poirier, J. Brain isoprenoids and Alzheimer’s disease. *Poster paper presentation*, Alzheimer’s Association International Conference (AAIC), Toronto, Canada, July 2016.

Tchesnokov, E.P., Lacbay, C.M., Tsantrizos, Y.S., and Götte, M. Bisphosphonate-based active site inhibitors of norovirus RNA-dependent RNA polymerase. *Oral presentation*, Bridging the Sciences (BTS) Workshop 2015, Florida, USA, September 2015.

Lacbay, C.M., Mancuso, J., Lin, Y.-S., Bennett, N., Menni, M., Götte, M., and Tsantrizos, Y.S. Development of pyridopyrimidine-based inhibitors of HIV-1 reverse transcriptase. *Oral presentation*, 249th ACS National Meeting and Exposition, Denver, Colorado, USA, March 2015.

Lacbay, C.M., Lin, Y.-S., Mancuso, J., Bennett, N., Götte, M., and Tsantrizos, Y.S. Modular assembly of pyridopyrimidine bisphosphonate inhibitors of HIV-1 reverse transcriptase. *Oral presentation*, 97th Canadian Chemistry Conference and Exhibition, Vancouver, British Columbia, June 2014.

Lacbay, C.M., Bernatchez, J., Götte, M., and Tsantrizos, Y.S. Studies toward the development of a new class of HIV-1 reverse transcriptase inhibitors. *Oral presentation*, 24th Quebec-Ontario Mini-Symposium on Bioorganic and Organic Chemistry (QOMSBOC), Sherbrooke, Quebec, November 2013.

Lacbay, C.M., Lin, Y.-S., and Tsantrizos, Y.S. Synthesis and biological evaluation of pyrido[2,3-*d*]pyrimidine analogs as prenylation inhibitors. *Oral presentation*, 96th Canadian Chemistry Conference and Exhibition, Quebec, Canada, May 2013.